Universiteit
Leiden
The Netherlands

Systems pharmacology of the endocannabinoid system

Kantae, V.

Citation
Kantae, V. (2018, September 6). *Systems pharmacology of the endocannabinoid system*. Retrieved from https://hdl.handle.net/1887/65054

Version:	Not Applicable (or Unknown)
License:	Licence agreement concerning inclusion of doctoral thesis in the Institutional Repository of the University of Leiden
Downloaded from:	https://hdl.handle.net/1887/65054

Note: To cite this publication please use the final published version (if applicable).

Cover Page

Universiteit Leiden

The handle http://hdl.handle.net/1887/65054 holds various files of this Leiden University dissertation.

Author: Kantae, V.
Title: Systems pharmacology of the endocannabinoid system
Issue Date: 2018-09-06

Systems Pharmacology of the Endocannabinoid System

Vasudev Kantae

Publication of this thesis was financially sponsored by:

SCIEX

Leiden Academic Centre for Drug Research (LACDR)

ISBN: 978-94-92679-53-6

© Vasudev Kantae, Leiden, the Netherlands

Cover design: Fred Frij & Vasudev Kantae

Printed by: Print Service Ede

Systems Pharmacology of the Endocannabinoid System

PROEFSCHRIFT

ter verkrijging van
de graad van Doctor aan de Universiteit Leiden,
op gezag van Rector Magnificus Prof. Mr. C.J.J.M. Stolker,
volgens besluit van het college voor Promoties
te verdedigen op donderdag 6 September 2018
Klokke 10:00 uur.

door

Vasudev Kantae

geboren te Vetlapalem, Indië in 1986

PROMOTOR

Prof. dr. Thomas Hankemeier

Prof. dr. Piet H van der Graaf

CO-PROMOTOR

Dr. Amy C Harms

PROMOTIECOMMISSIE

Prof. dr. Hubertus Irth (Chair)
Leiden University, the Netherlands

Prof. dr. Joke Bouwstra (Secretary)
Leiden University, the Netherlands

Prof. dr. Renger Witkamp
Wageningen University, the Netherlands

Prof. dr. Catherijne Knibbe
Leiden University, the Netherlands

Prof. dr. Mario van der Stelt
Leiden University, the Netherlands

Prof. dr. Patrick Rensen
Leiden University Medical Center (LUMC), the Netherlands

The research received support from the Faculty of Science ("Profiling Programme: Endocannabinoids"), Leiden University, the Netherlands.

Contents

Chapter 1
Introduction: Systems pharmacology of the endocannabinoid system **1**

Chapter 2
Pharmacometabolomics informs pharmacokinetics and pharmacodynamics: toward personalized drug therapy **17**

Chapter 3
Quantitative profiling of endocannabinoids and related N-acylethanolamines in human CSF using nano LC-MS/MS **37**

Chapter 4
Investigating the players of 2-arachidonyl glycerol biosynthesis in cellular system **65**

Chapter 5
Activity-based protein profiling reveals off-target proteins of the FAAH inhibitor BIA 10-2474 **81**

Chapter 6
Pharmacokinetic Modeling of Paracetamol Uptake and Clearance in Zebrafish Larvae: Expanding the Allometric Scale in Vertebrates with Five Orders of Magnitude **135**

Chapter 7
System pharmacology of an endocannabinoid system modulator in zebrafish larva **155**

Chapter 8
Endocannabinoid tone is higher in healthy lean South Asian than white Caucasian men **177**

Chapter 9
Conclusion and future prospects **197**

Appendix
Summary **212**
Nederlandse Samenvatting **216**
Dankwoord / Acknowledgements **221**
Curriculum Vitae **223**
List of publications **224**

Chapter 1

General Introduction

Systems thinking in modern drug discovery

Over the last century, the nature of health and disease are increasingly being studied by applying system-based approaches [1]. System-based approaches allow us to overcome the difficulties in predicting the functional state of an intact organism from the functional state of its parts in isolation. This paradigm shift towards more systems-thinking could transform drug discovery and development in a cost-effective manner to produce the right treatment to right patient [2,3]. It has been realized that the current drug discovery approach based on the assumption that a single compound modulates a single target has limitations for the multifactorial abnormalities such as cardiovascular disease, type 2 diabetes, neurological disorders. Furthermore, compounds designed to modulate only the target in a target-based approaches, can have unanticipated effects on "off-target" biochemical mechanisms, and the safety implications of those unwanted effects might not be revealed in early drug development or until a drug candidate is evaluated in large clinical trials. Therefore, it is essential to generate comprehensive molecular descriptions of a disease or the effect of drugs (i.e. drug response) that take into account the breath of biochemical perturbations of an organism [2,4]. Systems pharmacology is a concept that attempts to characterize the molecular network changes due to a disease state and its changes due to a drug: this includes studying drug-perturbed states relative to unperturbed state. The molecular network changes due to diseases are often also referred to as systems pathophysiology or systems biology of diseases.

The concept of having system fingerprints to describe states of complex systems integrating different biochemical components such as genes, transcripts, proteins and endogenous metabolites allows to create system-wide response profiles and study system-state differences [2]. The topological connections between these molecular components define the organization of a given biological system and its function reflects how the system evolves with regards to metabolic fluxes or environmental stimuli [5]. To capture the initial loss of homeostasis within the body, system response profiles can be generated either using blood plasma levels which reflect interactions between organs or by studying cells, complex cellular in-vitro models or tissues in case of multi-factorial diseases. The system response profiles integrate the molecular phenome (different omics), drug response phenotype (Pharmacokinetics-Pharmacodynamics, PK-PD),exposure to environmental factors ranging from toxic substances, drugs to diet (exposome), and the clinical phenome (clinical features and clinical metrics) (**Fig. 1**). System fingerprints, based on biomolecular profiles, to stratify patient populations and to differentiate between responders and non-responders to drugs and

to fine-tune drug interventions are emerging concepts to improve and personalize healthcare approach [6]. In addition, a key tool to achieve inter-species translation of findings in drug development is to have biological networks (gens, proteins and metabolites) that can be comparable between species [7]. To this end metabolomics can serve as an powerful phenotyping platform complementary to other "omics" as it can yield uniform information about disease biochemistry and drug action in both pre-clinical and clinical studies, and helps in improving inter-species translational research [7–9].

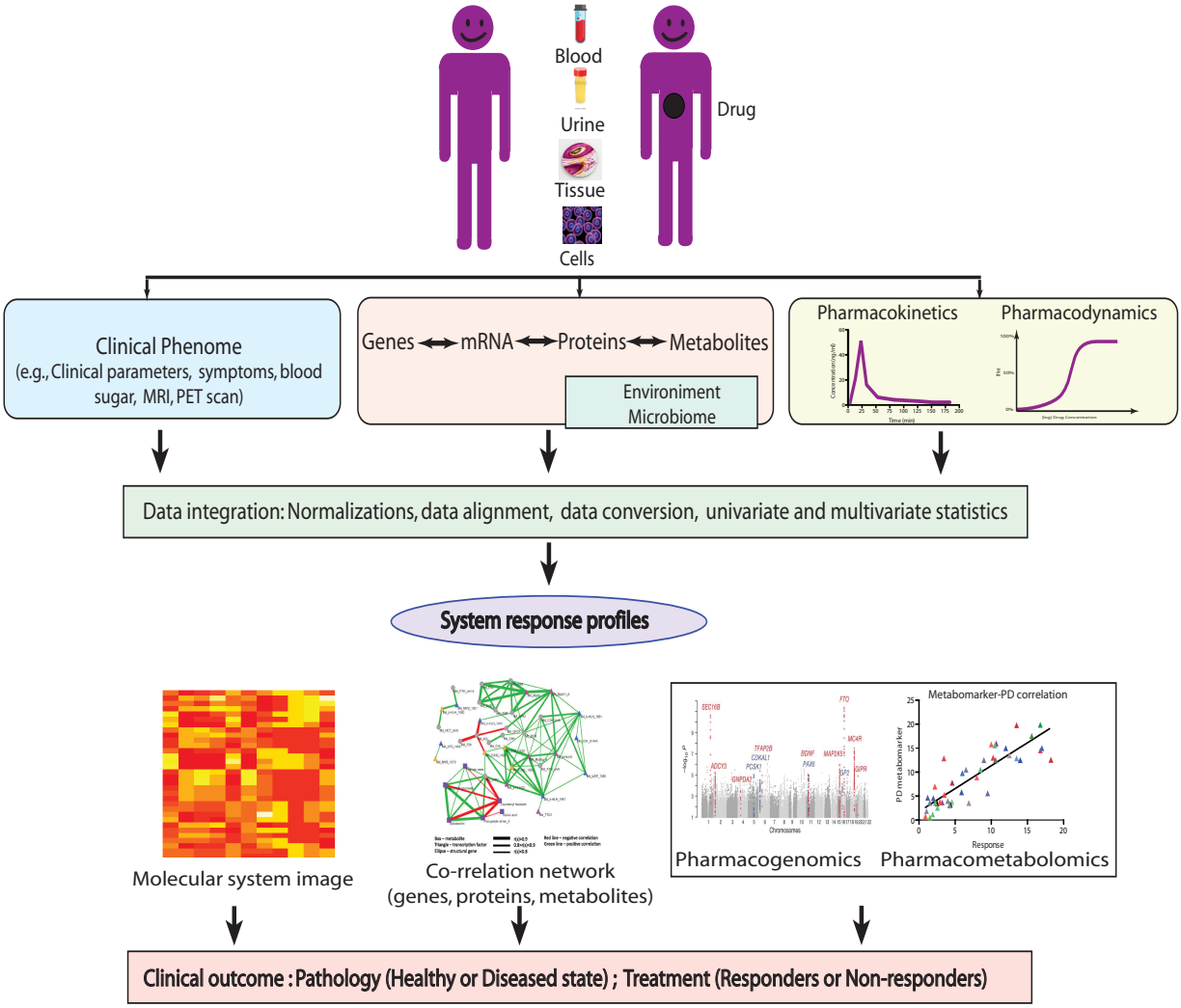

Figure 1: Flowchart for systems pharmacology. An overview of the materials, information and methods that constitute the workflows and outputs of systems pharmacology**.** These different biological, pharmacological and clinical measurements should be studied in a multi-dimensional fashion by taking the inherent spatial and temporal scales of both measurements technology platforms and disease and drug dynamics from the molecular to the population level into account.

Metabolomics and pharmacometabolomics

Metabolomics is a molecular phenotyping tool which provides the comprehensive quantitative and qualitative analysis of metabolites under a given (patho)physiological condition of an individual [10]. Significant progress in genomics and proteomics have increased our understanding of altered genes and protein under a variety of perturbations, including disease conditions and drug effect (**Fig. 2**). Metabolomics serves as an alternative molecular approach to help understand altered metabolic pathways in various perturbations. Metabolomics is especially attractive: subtle changes in genes, transcripts or protein levels can result in substantial changes in the levels and dynamics of metabolite and closely resembles the organism phenotype. In addition, metabolomics is attractive in translational studies, as metabolites have to a major extent identical structures and comparable functions in different species, and localized perturbations in organs due to disease or drug can be measured in blood as metabolites are excreted from the cells and organs, and often reach ultimately the blood stream [7]. The endogenous metabolite profile of an individual is a snapshot of the phenotypic status of an individual resulting from, for instance, age, environmental interactions, and genotype, and inform on an individual's health or disease status [11,12]. Metabolomics or endogenous metabolite profiling may be therefore used as a phenotypic tool to provide new predictive biomarkers and mechanistic markers for individualizing drug treatment [13].

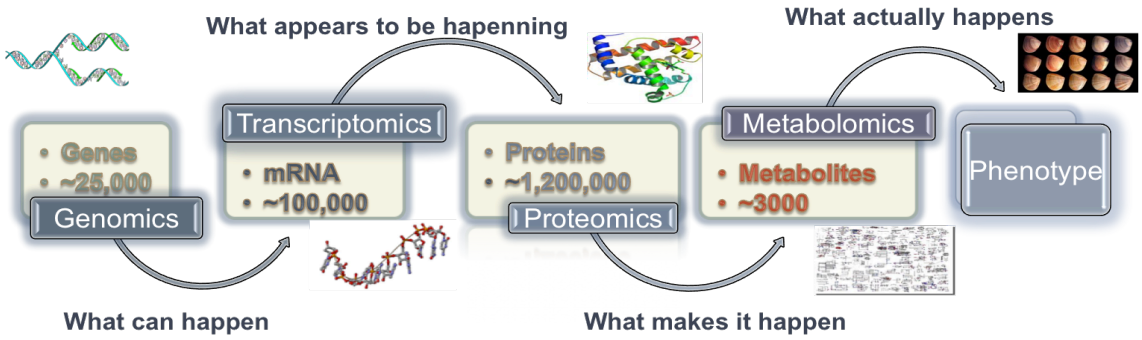

Figure 2: Schematic of 'omic' hierarchy: Genomics, Transcriptomics, Proteomics and Metabolomics. The general flow of information is from genes to transcripts to proteins to metabolites to phenotype (or function). Furthermore, as a feedback mechanisms, metabolites can also regulate enzyme activities and gene expression. The integration of all these 'omic' approaches is the main aim in systems biology.

Pharmacometabolomics is emerging as a sub-discipline of metabolomics that studies the interplay between drug pharmacology and the patients' (patho)physiology, by measuring endogenous metabolites that inform on drug effects and variation in drug response [14–17]. Pharmacokinetics (PK) is the study of the time-course of the drugs in bio fluids and tissues (i.e., what the body does to the drug). Pharmacodynamics (PD) is the study of the biological effects of drugs and their mechanisms of action (i.e., what a drug does to the body). PK-PD plays a key role in drug research, informing about *in vivo* drug and system properties under physiological and pathological conditions [18]. Metabolomics and pharmacometabolomics have the potential to prospectively inform about PK and PD processes, and by that, can take us one step closer to personalized medicine [19]. The systems pharmacology approach we applied in this thesis integrates concepts of metabolomics with PK-PD, in order to gain more insights in disease biochemistry and drug pharmacology.

Evolution of interest in the endocannabinoid system

Cannabis sativa has been used for medicinal and recreational purposes throughout the past millennium; actually, marijuana is still one of the most wide-spread illicit drugs of abuse in the world. It was during the second half of the twentieth century that research finally cast light onto some of its mechanisms of action [20], first with the identification of its major pharmacologically active components, the cannabinoids, and later their molecular targets. (–)-Δ9-Tetrahydrocannabinol (THC) is the most well-known active compound from cannabis and is generally held responsible for the well-known effects such as 'the munchies', a term used for hunger pangs after cannabis use, and central effects on consciousness, such as feeling high and altered time perception [21]. Cannabis also contains many other cannabinoids such as cannabidiol, but for most of these compounds, the pharmacological activity is currently still being investigated (for review on early phytocannabinoid chemistry, refer [22]).

The first guanine-nucleotide-binding protein (G protein)-coupled receptor (GPCR) activated by THC, cannabinoid receptor 1 (CB1; encoded by gene CNR1), was discovered in the brain in 1988 [23] and cloned in 1990 [24], and the crystal structure of human CB1 determined in 2016 [25]and the second GPCR, CB2, was identified in immune cells in 1993 [26]. The tissue distribution of CB1 and CB2 receptors accounts for the well-known psychotropic and peripheral effects of THC. CB1, most abundant GPCR, is distributed in central nervous system (CNS) and also present in the peripheral nervous system [27] and in peripheral metabolic organs (white adipose tissue (WAT), brown adipose tissue (BAT), liver, pancreas, muscle and Gut).

By contrast, CB2 is sparsely present in brain but more abundant in immune tissues and cells [28]. In addition to cannabinoid receptors, the endocannabinoid system (ECS) comprises endogenous ligands, the endocannabinoids and the enzymes responsible for the synthesis and hydrolysis of endocannabinoids.

Pharmacology of the endocannabinoid system

Endocannabinoids are highly lipophilic compounds that are not stored in vesicles after production. They are substantially synthesized "on demand" from membrane phospholipids, and released immediately. The most-studied endocannabinoids are anandamide (N-arachidonoyl ethanolamine, AEA) and 2-arachidonoylglycerol (2-AG). Anandamide is a high-affinity, low-efficacy CB1 agonist, with even lower efficacy at CB2 receptors, whereas 2-AG has lower affinity, but is a fully effective agonist at both CB1 and CB2 [29]. Both AEA and 2-AG are produced at post-synaptic neurons. Although they both derive from cell membrane arachidonic acid derivatives, the levels of these endocannabinoids are differentially regulated (**Fig. 3**). AEA levels depend on synthesis via hydrolysis of N-acyl-phosphatidylethanolamines (NAPE) by a NAPE-specific phospholipase D (NAPE-PLD) [30] and degradation is primarily regulated by fatty acid amide hydrolase (FAAH) [31]. 2-AG levels are regulated by the synthesis enzymes diacylglycerol lipase α and β (DAGL-α and β) [32] and degradation enzyme mono-acylglycerol lipase (MAGL) [33] although ABHD6 (an abbreviation of α,β hydrolase 6) [34] and ABHD12, as well as FAAH [35], are also capable of hydrolysing 2-AG. Both anandamide and 2-AG are also oxidized by the enzyme cyclooxygenase-2 (COX-2; also known as prostaglandin G/H synthase 2), cytochrome p450 and lipooxygenases (LOX) [36]. AEA belongs to a family of bioactive N-acylethanolamines (NAEs), which include N-linoleoylethanolamine (LEA), N-palmitoylethanolamine (PEA), N-oleoylethanolamine (OEA) and N-stearoylethanolamine (SEA), N-docosatetraenylethanolamide (DHEA). These NAEs arise from the same biosynthetic pathway as AEA and are capable to indirectly modulate cannabinoid receptor activity by interfering with endocannabinoid metabolism, known as an "entourage effect" [37]. PEA which acts as a body-own anti-inflammatory agent [38] and, specifically, OEA interacts with nuclear receptor peroxisome proliferator-activated receptor α (PPAR-α), stimulates lipolysis in the liver and adipocytes and acts as a satiety factor [39,40].

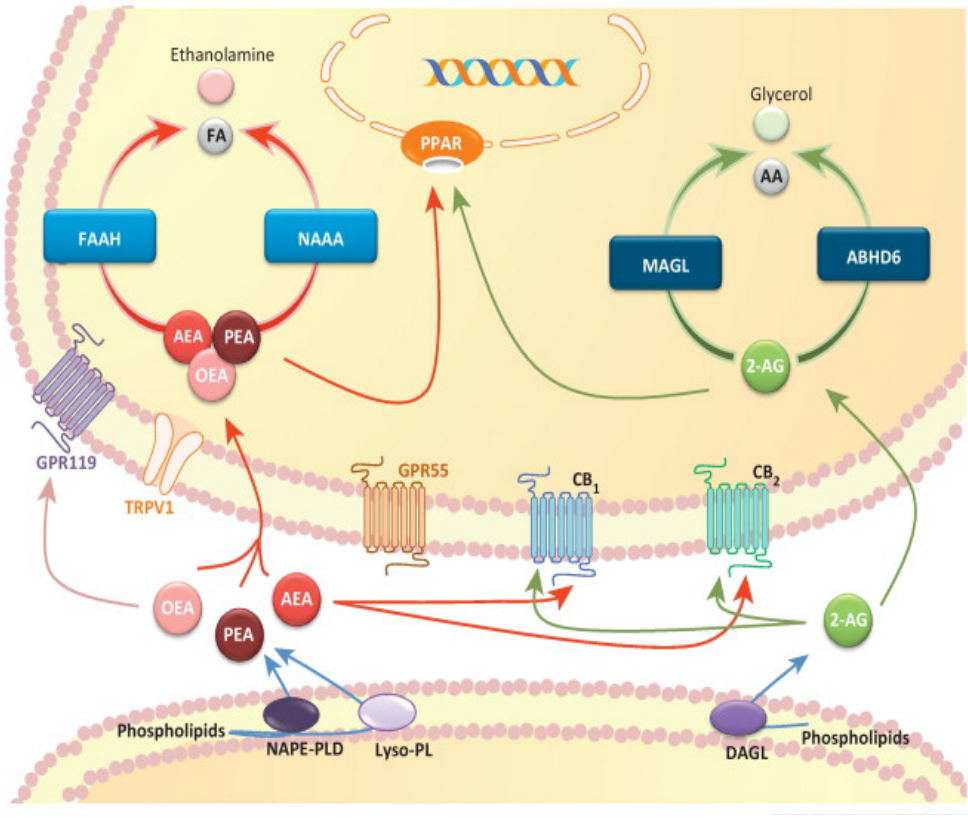

Figure 3: The endocannabinoid system in a nutshell. The figure illustrates the interactions between components of the endocannabinoid system including, receptors (cannabinoid CB1&CB2 and other GPCR relates), biosynthetic &hydrolytic enzymes and ligands (endocannabinoids and N-acylethanolamines). *Adapted from M Alhouayek Trends Mol Med 2012* [41].

Complexity of endocannabinoid system

Endocannabinoids are involved in complex physiological processes that play an important role in a huge number of diseases in almost all areas of medicine. In principle, this makes them appealing targets for drug development, but at the same time challenging. However, because of this complexity and the relatively recent discovery of the endocannabinoid system, its research is still in a premature stage. The endocannabinoid research and drug development is complicated further by a huge number of factors. Firstly, when compared with other pharmacological systems, the endocannabinoid system is one of the most widely distributed systems through the body. This complicates systemic or organ-specific targeting as when aiming to target a specific location, the ubiquitous presence of the system leads to undesirable "side" effects elsewhere in the body, limiting the development of therapeutically tissue-specific drugs. Secondly, the lipophilic nature of the endogenous and exogenous cannabinoids (e.g. Log P values for anandamide and 2-AG are 6.31 and 8.01) respectively leads to difficulties in

optimizing the pharmacokinetic properties and in distributing between blood and organs. Thirdly, the complex physiological network with other pharmacological signaling systems with many layers of regulation and feedback mechanisms makes it difficult to target a specific signaling pathway. This could be one of the reasons why there are so many discrepancies in the results obtained and why it is difficult to draw conclusions on the precise role of endocannabinoid system in various pathophysiological conditions. Fourthly, in case of multicascadic physiological mechanisms, the integration of endocannabinoid system at subcellular levels and the wide range of effects makes it challenging for measurement of changes in their activity, which is essential in drug development.

Endocannabinoid system as a therapeutic drug target

One of the functions of CB1 is to control whole body energy hemostasis [28]. Induction of CB1 receptor stimulates feeding by increasing appetite, whereas blocking CB1 signaling induces hypophagia by an appetite-suppressant effect [42,43]. Since the beginning of the 1990s, the endocannabinoid system has been considered an attractive therapeutic target in numerous diseases. Modulating ECS activity holds therapeutic promise for a broad range of diseases, including neurodegenerative, cardiovascular and inflammatory disorders, obesity/metabolic syndrome, cachexia, chemotherapy-induced nausea and pain, among others [44,45]. An early strategy to treat obesity was to target the cannabinoid receptors directly with exogenous antagonists, like rimonabant or dronabinol. Rimonabant, a CB1 receptor antagonist, was launched as an anti-obesity drug. It showed promise in decreasing appetite and body weight and improved cardio-metabolic risk factors, but was withdrawn from the market due to unwanted side effects on the central nervous system, namely psychiatric effects [46,47] . The most promising alternative strategy to overcome the side effects caused by directly blocking the receptor is to indirectly tune the endogenous ligand concentrations (endocannabinoids) by modulating their synthetic and hydrolysis enzymes [48]. Since the endocannabinoids are produced on demand (in a stimulus-dependent manner), modulating endocannabinoid signaling offers advantages in regulating their biochemistry, thus CB receptor activation, in a tissue-specific manner. Furthermore, the biochemical pathways associated with synthesis and degradation of the endocannabinoids in different tissues have been well elucidated [49], which makes it relatively attractive to chemically synthesize small molecule inhibitors and use them to study the enzyme activities. There are several examples showing the use of covalent enzyme inhibitors, which can be potential drug candidates, for tuning the endogenous endocannabinoid

levels for a beneficial effect. For instance, PF-04457845 is a clinically tested FAAH inhibitor used to increase endocannabinoid tone for beneficial effects such as pain and inflammation [50]. Similarly, LEI105, DH376 has been recently developed to regulate 2-AG levels by inhibiting DAGL enzyme [51,52].

To screen for target engagement, downstream effects, including also to screen for possible off-target effects of drugs, profiling platforms are required. In this regard, Activity based protein profiling (ABPP) can serve as a versatile chemoproteomic method to assess the functional state of entire enzyme classes directly in native biological systems [51,53]. ABPP is unique in its ability to rapidly identify inhibitor interaction and selectivity within large enzyme families in complex proteome samples either by analysis on SDS–polyacrylamide gel electrophoresis (SDS-PAGE) using fluorescent probes or by mass spectrometry (MS)–based analysis for target identification using biotinylated probes. Lipidomics or Metabolomics can be used as another powerful phenotypic platform to identify the target engagement of enzyme substrates or products or to identify the off-target effects of drugs on boarder molecular network [54].

Aim and Scope of Thesis

The overall aim of the research described in this thesis is to develop and apply systems pharmacology approaches to understand and modulate the endocannabinoid system across different models such as in cells, zebrafish, mice and humans (**Fig. 4**). First, the goal is to achieve deeper insights in the functional role of endocannabinoid system in healthy and diseased states. In addition, this research seeks to modulate the endocannabinoid system with newly synthesized drug molecules to understand the drug pharmacology and whether such new compounds may modify the disease biochemistry; this includes the study of target engagement, downstream effects and the off-target effects of new compounds. Furthermore, this research aims to integrate PK and PD concepts and metabolomics to determine the effective and safe drug dosing and drug-response phenotypes in cell and animal models. Finally, this work attempts to translate the findings from humans to animal models, and translate back from animal models to humans in order to improve our understanding of disease biochemistry and to support the discovery and development of novel therapeutic drugs.

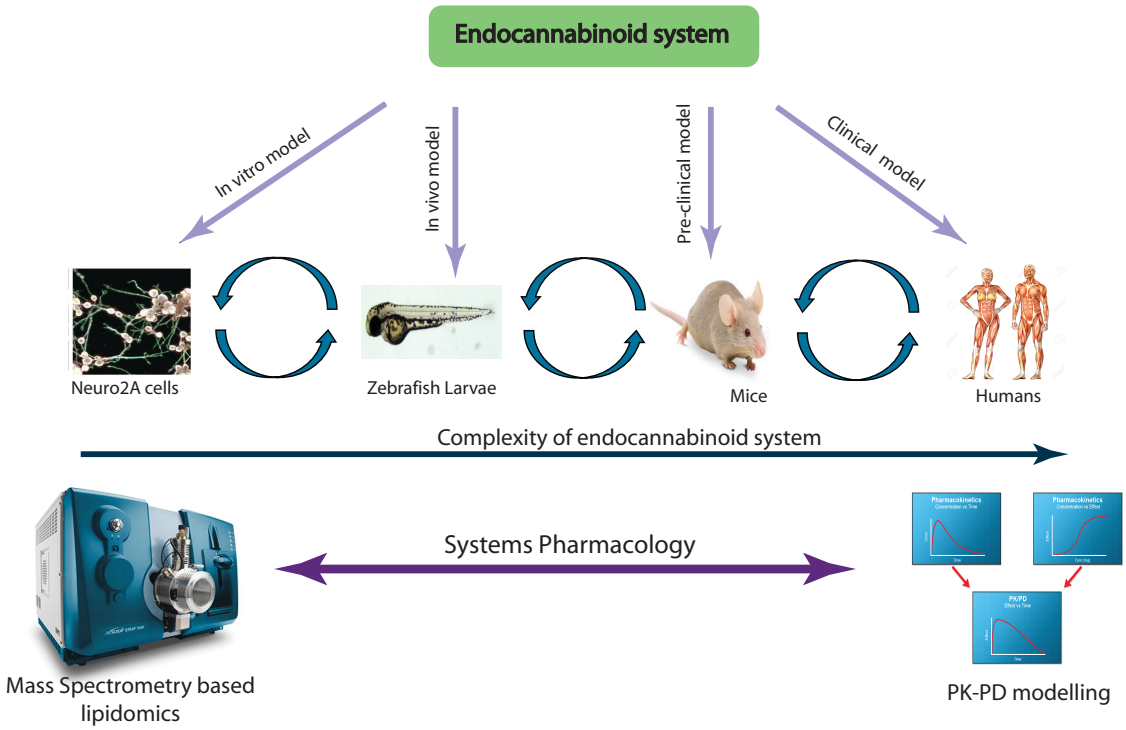

Figure 4: System pharmacology of the endocannabinoid system. This figure illustrates the schematic of overall studies performed in my PhD thesis

In **chapter 2**, the concept of system pharmacology is introduced: the combination of metabolomics with pharmacology is described in order to support the development of personalized medicine. It was highlighted how (pharmaco)metabolomics can predict pharmacokinetic (PK) and pharmacodynamics (PD) processes. In this regard, endogenous biomarkers are therefore indispensable to predict PK-PD.

To study endocannabinoid signaling system, endocannabinoids and their related lipids that are present at very low concentrations (nanomole to picomole range) have to be measured in various biological matrices. Since sensitivity is the key factor, in **Chapter 3** the development of a highly-sensitive nano LC-MS/MS analytical platform is described to quantify endocannabinoids and their congeners in human cerebrospinal fluid (CSF) and later extended to measure in other biological matrices like, cells, zebrafish larvae, plasma (mice and human).

To understand the physiological role of endocannabinoids, especially of 2-AG and AEA, selective inhibitors for their synthetic and hydrolytic enzymes are required. **Chapter 4** describes the use of DH376, a potent *in vivo* active DAGL inhibitor, to investigate which isoform of diacylglycerol lipase (DAGL-α and -β) takes lead in 2-AG biosynthesis in a cellular model. Lipidomics and ABPP were employed to vehicle or DH376 treated wild type and knock-out Neuro2A populations (DAGL-α KO, DAGL-β KO, DAGL-α, -β double KO). These data revelled presence of additional enzymes responsible for 2-AG synthesis. In **chapter 5**, the reason behind the failure of the phase1 clinical trial of the fatty acid amide hydrolase (FAAH) inhibitor BIA 10-2474 was investigated. ABPP and lipidomics profiling platforms were used to measure on-target engagement and off-target effects of this compound. This analysis revealed that the compound interacts with several other lipases and produced substantial alterations in lipid network in human cortical neurons.

In order to gain better understanding of the *in vivo* pharmacology of the endocannabinoid system and to evaluate the systemic effect of drugs, proper *in vivo* model systems are required and need to be properly validated. In this regard, zebrafish larvae were tested as an attractive pre-clinical model system in **chapter 6** which characterizes the pharmacokinetics of paracetamol as a paradigm compound. The zebrafish drug clearance scales reasonably well with the clearance rates in higher vertebrates, including humans, and expanded the current allometric scale by 5 orders of magnitude. To further expand the applicability of zebrafish model in drug research, the pharmacodynamics of an endocannabinoid modulator PF04457845 was evaluated in **chapter 7**. In this chapter, ABPP and lipidomics tools were used to investigate the on-target engagement of PF04457845 on the protein landscape and its

downstream effects on the lipid networks. The results show the *in vivo* exposure of PF04457845 completely inhibited FAAH2 and increased the levels of NAEs, substrates of FAAH, while no cross-reactivity was observed with other serine hydrolases or alterations in lipid networks.

To expand our findings from models to clinical studies, **chapter 8** investigates a possible reason that underlies the disadvantageous metabolic phenotype of South Asians later in life. Quantification endocannabinoids in plasma showed that the South Asian men who have not yet developed a disadvantageous metabolic phenotype have a higher endocannabinoid tone compared to white Caucasian men.

Chapter 9 summarizes the work described in this thesis and its impact on the future researchers studying endocannabinoid system.

References

1. Kitano, H. Computational systems biology. *Nature* **420,** 206–210 (2002).
2. van der Greef, J. & McBurney, R. N. Rescuing drug discovery: in vivo systems pathology and systems pharmacology. *Nat. Rev. Drug Discov.* **4,** 961–967 (2005).
3. Vicini, P. & van der Graaf, P. H. Systems pharmacology for drug discovery and development: paradigm shift or flash in the pan? *Clin. Pharmacol. Ther.* **93,** 379–81 (2013).
4. van der Greef, J. Systems biology, connectivity and the future of medicine. *Syst. Biol. (Stevenage).* **152,** 174–8 (2005).
5. Kitano, H. Systems biology: a brief overview. *Science (80-.).* **295,** 1662–1664 (2002).
6. van der Greef, J., Hankemeier, T. & McBurney, R. N. Metabolomics-based systems biology and personalized medicine: moving towards n = 1 clinical trials? *Pharmacogenomics* **7,** 1087–94 (2006).
7. van der Greef, J., Adourian, A., Muntendam, P. & McBurney, R. N. Lost in translation? Role of metabolomics in solving translational problems in drug discovery and development. *Drug Discov. Today Technol.* **3,** 205–211 (2006).
8. Watkins, S. M. & German, J. B. Metabolomics and biochemical profiling in drug discovery and development. *Curr. Opin. Mol. Ther.* **4,** 224–8 (2002).
9. Kaddurah-Daouk, R., Kristal, B. S. & Weinshilboum, R. M. Metabolomics: a global biochemical approach to drug response and disease. *Annu. Rev. Pharmacol. Toxicol.* **48,** 653–83 (2008).
10. Rabinowitz, J. D., Purdy, J. G., Vastag, L., Shenk, T. & Koyuncu, E. Metabolomics in drug target discovery. *Cold Spring Harb Symp Quant Biol* **76,** 235–246 (2011).
11. Fernie, A. R., Trethewey, R. N., Krotzky, A. J. & Willmitzer, L. Metabolite profiling: from diagnostics to systems biology. *Nat. Rev. Mol. Cell Biol.* **5,** 763–9 (2004).
12. Suhre, K. *et al.* Human metabolic individuality in biomedical and pharmaceutical research. *Nature* **477,** 54–60 (2011).
13. van der Greef, J., Hankemeier, T. & McBurney, R. N. Metabolomics-based systems biology and personalized medicine: moving towards n = 1 clinical trials? *Pharmacogenomics* **7,** 1087–1094 (2006).
14. Clayton, T. A. *et al.* Pharmaco-metabonomic phenotyping and personalized drug treatment. *Nature* **440,** 1073–7 (2006).
15. Kaddurah-Daouk, R. & Weinshilboum, R. Metabolomic Signatures for Drug Response Phenotypes: Pharmacometabolomics Enables Precision Medicine. *Clin. Pharmacol. Ther.* **98,** 71–5 (2015).
16. Nicholson, J. K., Wilson, I. D. & Lindon, J. C. Pharmacometabonomics as an effector for personalized medicine. *Pharmacogenomics* **12,** 103–11 (2011).
17. Ellero-Simatos, S. *et al.* Oxylipid Profile of Low-Dose Aspirin Exposure: A Pharmacometabolomics Study. *J. Am. Heart Assoc.* **4,** e002203 (2015).
18. Gabrielsson, J., Fjellström, O., Ulander, J., Rowley, M. & Van Der Graaf, P. H. Pharmacodynamic-pharmacokinetic integration as a guide to medicinal chemistry. *Curr. Top. Med. Chem.* **11,** 404–418 (2011).
19. Kantae, V. *et al.* Integration of pharmacometabolomics with pharmacokinetics and pharmacodynamics: towards personalized drug therapy. *Metabolomics* **13,** 9 (2017).
20. Mechoulam, R., McCallum, N. K. & Burstein, S. Recent advances in the chemistry and biochemistry of cannabis. *Chem. Rev.* **76,** 75–112 (1976).
21. Foltin, R. W., Fischman, M. W. & Byrne, M. F. Effects of smoked marijuana on food intake and body weight of humans living in a residential laboratory. *Appetite* **11,** 1–14 (1988).

22. Mechoulam, R., Hanuš, L. O., Pertwee, R. & Howlett, A. C. Early phytocannabinoid chemistry to endocannabinoids and beyond. *Nat. Rev. Neurosci.* **15,** 757–764 (2014).
23. Devane, W. A., Dysarz, F. A., Johnson, M. R., Melvin, L. S. & Howlett, A. C. Determination and characterization of a cannabinoid receptor in rat brain. *Mol. Pharmacol.* **34,** 605–13 (1988).
24. Matsuda, L. A., Lolait, S. J., Brownstein, M. J., Young, A. C. & Bonner, T. I. Structure of a cannabinoid receptor and functional expression of the cloned cDNA. *Nature* **346,** 561–4 (1990).
25. Hua, T. *et al.* Crystal Structure of the Human Cannabinoid Receptor CB 1. *Cell* **167,** 750–762.e14 (2016).
26. Munro, S., Thomas, K. L. & Abu-Shaar, M. Molecular characterization of a peripheral receptor for cannabinoids. *Nature* **365,** 61–65 (1993).
27. Mackie, K. Distribution of cannabinoid receptors in the central and peripheral nervous system. *Handb. Exp. Pharmacol.* 299–325 (2005).
28. Silvestri, C. & Di Marzo, V. The Endocannabinoid System in Energy Homeostasis and the Etiopathology of Metabolic Disorders. *Cell Metab.* **17,** 475–490 (2013).
29. Gonsiorek, W. *et al.* Endocannabinoid 2-arachidonyl glycerol is a full agonist through human type 2 cannabinoid receptor: antagonism by anandamide. *Mol. Pharmacol.* **57,** 1045–50 (2000).
30. Okamoto, Y., Morishita, J., Tsuboi, K., Tonai, T. & Ueda, N. Molecular characterization of a phospholipase D generating anandamide and its congeners. *J. Biol. Chem.* **279,** 5298–305 (2004).
31. Cravatt, B. F. *et al.* Molecular characterization of an enzyme that degrades neuromodulatory fatty-acid amides. *Nature* **384,** 83–7 (1996).
32. Bisogno, T. *et al.* Cloning of the first sn1-DAG lipases points to the spatial and temporal regulation of endocannabinoid signaling in the brain. *J. Cell Biol.* **163,** 463–8 (2003).
33. Dinh, T. P. *et al.* Brain monoglyceride lipase participating in endocannabinoid inactivation. *Proc. Natl. Acad. Sci.* **99,** 10819–10824 (2002).
34. Marrs, W. R. *et al.* The serine hydrolase ABHD6 controls the accumulation and efficacy of 2-AG at cannabinoid receptors. *Nat. Neurosci.* **13,** 951–7 (2010).
35. Blankman, J. L., Simon, G. M. & Cravatt, B. F. A comprehensive profile of brain enzymes that hydrolyze the endocannabinoid 2-arachidonoylglycerol. *Chem. Biol.* **14,** 1347–56 (2007).
36. Urquhart, P., Nicolaou, A. & Woodward, D. F. Endocannabinoids and their oxygenation by cyclo-oxygenases, lipoxygenases and other oxygenases. *Biochimica et Biophysica Acta - Molecular and Cell Biology of Lipids* **1851,** 366–376 (2015).
37. Ho, W.-S. V, Barrett, D. A. & Randall, M. D. "Entourage" effects of N-palmitoylethanolamide and N-oleoylethanolamide on vasorelaxation to anandamide occur through TRPV1 receptors. *Br. J. Pharmacol.* **155,** 837–46 (2008).
38. Keppel Hesselink, J. M., de Boer, T. & Witkamp, R. F. Palmitoylethanolamide: A Natural Body-Own Anti-Inflammatory Agent, Effective and Safe against Influenza and Common Cold. *Int. J. Inflam.* **2013,** 151028 (2013).
39. Guzmán, M. *et al.* Oleoylethanolamide stimulates lipolysis by activating the nuclear receptor peroxisome proliferator-activated receptor alpha (PPAR-alpha). *J. Biol. Chem.* **279,** 27849–27854 (2004).
40. Schwartz, G. J. *et al.* The Lipid Messenger OEA Links Dietary Fat Intake to Satiety. *Cell Metab.* **8,** 281–288 (2008).
41. Alhouayek, M. & Muccioli, G. G. The endocannabinoid system in inflammatory bowel diseases: from pathophysiology to therapeutic opportunity. *Trends Mol. Med.* **18,** 615–25 (2012).

42. Koch, M. Cannabinoid Receptor Signaling in Central Regulation of Feeding Behavior: A Mini-Review. *Front. Neurosci.* **11,** 293 (2017).
43. Jager, G. & Witkamp, R. F. The endocannabinoid system and appetite: relevance for food reward. *Nutr. Res. Rev.* **27,** 172–185 (2014).
44. Pacher, P. & Kunos, G. Modulating the endocannabinoid system in human health and disease--successes and failures. *FEBS J.* **280,** 1918–43 (2013).
45. Pacher, P. The Endocannabinoid System as an Emerging Target of Pharmacotherapy. *Pharmacol. Rev.* **58,** 389–462 (2006).
46. Després, J.-P., Golay, A. & Sjöström, L. Effects of Rimonabant on Metabolic Risk Factors in Overweight Patients with Dyslipidemia. *N. Engl. J. Med.* **353,** 2121–2134 (2005).
47. Sam, A. H., Salem, V. & Ghatei, M. A. Rimonabant: From RIO to Ban. *J. Obes.* **2011,** 432607 (2011).
48. Marzo, V. Di. Targeting the endocannabinoid system: to enhance or reduce? *Nat. Rev. Drug Discov.* **7,** 438–455 (2008).
49. Basavarajappa, B. S. Critical enzymes involved in endocannabinoid metabolism. *Protein Pept. Lett.* **14,** 237–46 (2007).
50. Li, G. L. *et al.* Assessment of the pharmacology and tolerability of PF-04457845, an irreversible inhibitor of fatty acid amide hydrolase-1, in healthy subjects. *Br. J. Clin. Pharmacol.* **73,** 706–716 (2012).
51. Baggelaar, M. P. *et al.* Highly Selective, Reversible Inhibitor Identified by Comparative Chemoproteomics Modulates Diacylglycerol Lipase Activity in Neurons. *J. Am. Chem. Soc.* **137,** (2015).
52. Ogasawara, D. *et al.* Rapid and profound rewiring of brain lipid signaling networks by acute diacylglycerol lipase inhibition. *Proc. Natl. Acad. Sci.* **113,** 26–33 (2016).
53. Niphakis, M. J. & Cravatt, B. F. Enzyme Inhibitor Discovery by Activity-Based Protein Profiling. *Annu. Rev. Biochem.* **83,** 341–377 (2014).
54. van Esbroeck, A. C. M. *et al.* Activity-based protein profiling reveals off-target proteins of the FAAH inhibitor BIA 10-2474. *Science (80-.).* **356,** 1084–1087 (2017).

Chapter 2

Integration of pharmacometabolomics with pharmacokinetics and pharmacodynamics: Towards personalized drug therapy

Vasudev Kantae*, Elke H J Krekels*, Michiel J Van Esdonk, Peter Lindenburg, Amy C Harms, Catherijne A J Knibbe, Piet H Van der Graaf, Thomas Hankemeier

* *Authors contributed equally*

Metabolomics. 2017;13(1):9

Abstract

Personalized medicine, in modern drug therapy, aims at a tailored drug treatment accounting for inter-individual variations in drug pharmacology to treat individuals effectively and safely. The inter-individual variability in drug response upon drug administration is caused by the interplay between drug pharmacology and the patients' (patho)physiological status. Individual variations in (patho)physiological status may result from genetic polymorphisms, environmental factors (including current/past treatments), demographic characteristics, and disease related factors. Identification and quantification of predictors of inter-individual variability in drug pharmacology is necessary to achieve personalized medicine. Here, we highlight the potential of pharmacometabolomics in prospectively informing on the inter-individual differences in drug pharmacology, including both pharmacokinetic (PK) and pharmacodynamic (PD) processes, and thereby guiding drug selection and drug dosing. This review focusses on the pharmacometabolomics studies that have additional value on top of the conventional covariates in predicting drug PK. Additionally, employing pharmacometabolomics to predict drug PD is highlighted, and we suggest not only considering the endogenous metabolites as static variables but to include also drug dose and temporal changes in drug concentration in these studies. Although there are many endogenous metabolite biomarkers identified to predict PK and more often to predict PD, validation of these biomarkers in terms of specificity, sensitivity, reproducibility and clinical relevance is highly important. Furthermore, the application of these identified biomarkers in routine clinical practice deserves notable attention to truly personalize drug treatment in the near future.

1. Introduction

One of the main challenges in modern drug therapy is that a single compound with one fixed dose does not optimally treat all individuals in a population that suffer from a specific disease in a population. Knowledge about inter-individual differences in drug pharmacology and descriptors of these differences is essential to treat all individuals in a population effectively and safely. Individual variations in the response to drug treatment may result from genetic polymorphisms [1] or other epigenetic factors, environmental factors including diet, life style, earlier/current drug treatments, and microbiome [2]. Furthermore, demographic characteristics like age, sex, and bodyweight, or disease related factors like disease status and treatment-related factors [3] may cause variation. It is not known *a priori* which of these factors will best predict the clinical outcome of a treatment in an individual.

Personalized medicine, also sometimes referred to as precision medicine, aims to offer a tailored drug treatment to achieve the most optimal therapeutic effects with the least amount of adverse effects for each individual [4]. Information provided by predictors of expected individual responses to a particular drug, can inform clinicians in the decision making process for drug selection and drug dosing regimen [5]. And we are convinced that pharmacometabolomics will allow to find metabolic predictors for drug selection and drug dosing as will be elaborated in this paper.

2. Interplay between drug pharmacology and patients' (patho)physiology

For optimal pharmacotherapy, the interplay between drug pharmacology and patients' (patho)physiology needs to be understood [6,7]. As illustrated in Fig.1, important aspects regarding drug pharmacology are target exposure, target binding, and target activation, these processes are governed by drug-specific properties and patient characteristics. Modulating (patho)physiological biochemistry networks on a cellular level and, more importantly, on a tissue or organ level, or systemic level, will eventually determine the treatment outcome for a patient. The target activation triggers modulation of the (patho)physiological system including self-regulatory feedback mechanisms of the patient, also called downstream effects, and these modulations can vary between patients. When studying the effects of pharmacotherapy, none of the processes in the chain from drug administration to patient outcome (Fig.1) should be studied in isolation. Rather, all aspects need to be considered in the context of their causal and temporal interactions. Moreover, in order to achieve truly

personalized medicine, inter-individual variability throughout these processes need to be quantified and predictors for inter-individual difference identified.

Biomarkers are important tools to study the complex interplay between drug pharmacology and the patients' (patho)physiology, both on a population level and on an individual level. In this context, biomarkers are "a measure that characterizes, in a strictly quantitative manner, a process, which is on the causal path between drug administration and effect" [8]. A variety of biomarkers currently exist and endogenous metabolites, or more probably metabolite fingerprints [6,9], are promising for providing novel biomarkers for all processes on the causal chain between drug dose and patient outcome as outlined in **Fig. 1**.

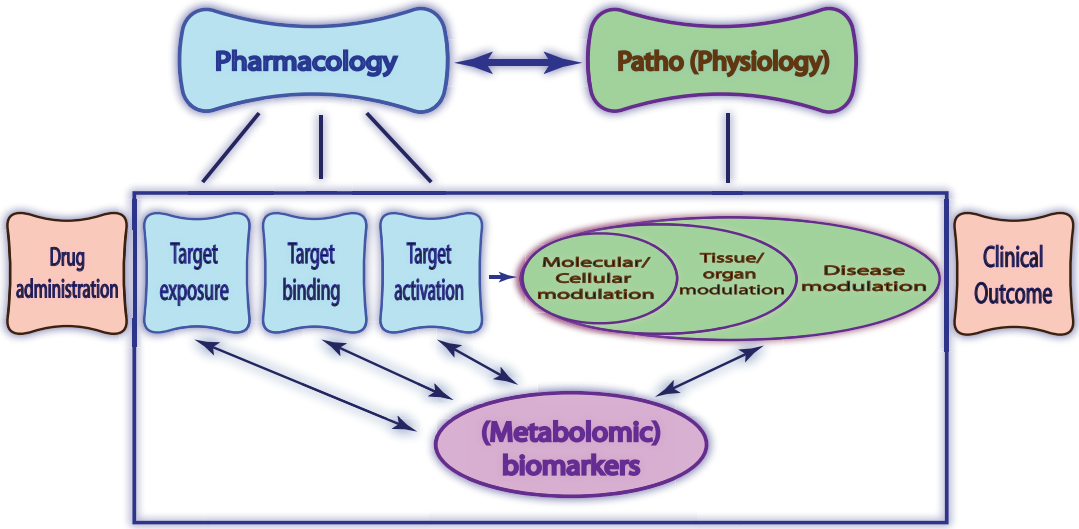

Figure 1: Potential of metabolomics in the interplay between drug pharmacology and patients (patho)physiology

If a drug does not reach its target, it cannot elicit its effect. Thus, drug concentration in blood is a biomarker for target exposure. Because drug concentrations at the target site may be difficult to measure, drug concentration in plasma is often used as a convenient surrogate measure for target exposure. However, in some cases where a compound has a peripheral target site (e.g. in brain), drug concentrations in blood cannot fully predict the target exposure.

Pharmacokinetics (PK) is the study of drug absorption, distribution, metabolism and excretion. Pharmacokinetic profiles describe the time course of drug concentrations in plasma or other tissues or biological matrices. Total drug exposure in a certain tissue is represented by the area under the concentration curve (AUC). The processes underlying drug PK are

quantified using primary parameters like clearance (CL) and distribution volume (V), or secondary parameters like absorption or distribution rate constants. Inter-individual variability in biological processes results in variability in the drug PK profiles between individuals. The ability to predict individual variations in the PK of drugs prior to drug administration is of interest in order to avoid over-dosing (e.g. adverse effects) and under-dosing (e.g. therapeutic failure). Currently, demographic, disease-related or treatment-related factors including for instance age, bodyweight, disease state, drug formulation, and concomitant drug therapy, are used as predictors of quantitative inter-individual differences in the PK of drugs. These predictive factors of variability are called covariates.

Current methodologies using conventional covariates alone can often explain a large part of the inter-individual variability in the PK of a drug [10]. However, this may not be sufficient for drugs with a narrow therapeutic window and relatively high unexplained inter-individual variability. In these cases, therapeutic drug monitoring (TDM) provides a viable option to improve an individuals' pharmacotherapy. With TDM, dose adjustments are made based on additional information on the individual PK parameter values, derived from relevant exposure measures after one or multiple drug doses have been administered.

There are, however, situations where the use of conventional covariates, even in combination with TDM, is not sufficient to guide drug dosing for target exposure attainment. In critically-ill patients, patients with organ failure, or in the end-of-life stages of terminal patients, many (patho)physiological changes and drug-drug interactions occur in quick succession, and all or a number of these factors may influence the PK of administered drugs. In these vulnerable patients, the exact clinical status is difficult to assess using conventional measures, but this information may be essential to predict the individual PK parameter values needed to provide personalized drug dosing.

To elicit an effect, a drug should not just reach a target, it should also bind to the target and activate the target to initiate the desired biosignal that will for instance lead to changes in enzyme activity or changes a (patho)physiological pathway. Factors that influence these interactions include both the physicochemical properties of the drug and the phenotype of the patient. Inter-individual differences in the target phenotype may influence target binding and activation and thereby the eventual treatment outcome in individual patients.

The biosignal initiated by target activation is subsequently potentiated into the (patho)physiological system of the patient. Potentiation of this signal may involve relatively simple molecular pathways, but often involves complex interacting networks related both to

healthy physiology and disease-related pathophysiology, that will yield modulations on cellular, tissue and organ levels, and on the disease state level. A wide range of these factors related to (epi)genetic factors and patient phenotype may result in inter-individual variability in signal potentiation and thereby patient outcome.

Drug pharmacodynamics (PD) is related to the effect of drugs and in PK-PD analysis the relationship between drug concentration, usually in blood, and treatment outcome is defined. Usually, inter-individual variability in PD processes exceeds the inter-individual variability in PK. Failure to properly account for the variability in the PD of a drug may cause therapy failure or toxicity for individual patients [11].

As indicated in **Fig. 1**, drug effects, either desired or unwanted side-effects, can be described on different levels (from target exposure, to target binding and target activation, to ultimately disease modulation leading to clinical outcome) and the relationships between drug concentration and effect will become less direct and potentially more complex when moving downstream in signal potentiation, and ultimately to clinical outcome. Especially in complex diseases of which the mechanism is not yet fully understood, for instance psychological and neurological diseases, there is a strong need for validated biomarkers to assess disease progression. In addition, such a biomarker can be informative about the impact of pharmacotherapy on various levels of the (patho)physiological system.

Similar to PK, conventional covariates can be used as predictors for inter-individual variability in drug effects, but, similar to TDM, in PD they may not always be sufficient. Moreover, also similar to TDM, dose adjustments and even drug selection should be guided based on prediction of individual patient outcome, particularly for drugs in which the drug effects are difficult to quantify or delayed (e.g. psychoactive drugs, cytostatics, antidepressants, etc.). Another example where we need proper PD prediction is the use of drugs in vulnerable or critical patients. In these cases, validated biomarkers that can predict long-term outcome based on short-term changes are needed to facilitate individual optimization of pharmacotherapy.

As outlined above, optimal pharmacotherapy requires information on the current (patho)physiological status of an individual patient. Conventional covariates may be useful in this respect and may even be sufficient in predicting individual deviations from population responses, but when these don't suffice, other methods for the establishment of phenotypic profiles may be required. Such methods are preferably prospective and minimally invasive.

One way of PK phenotyping involves the administration of a probe drug or drug cocktail to assess the phenotype of several drug-metabolizing enzymes[12]. However, this is not always feasible, especially in vulnerable populations, and this involves prolonged clinical visits and increases time and cost of treatment. An alternative phenotyping approach would be using endogenous biomarkers that could predict enzyme activity without risk, time, and cost of exogenous drug administration. Another advantage of endogenous biomarkers is that retrospective analysis of banked samples can be conducted. Identified predictive endogenous biomarkers can be used as covariates to guide clinicians in decision making regarding treatment options by using minimal amounts of biological fluids. In this regard, the application of metabolomics can serve as an alternative or additional method to the current clinical practices to achieve personalized treatment [13–18].

Metabolomics or endogenous metabolite profiling may be used as a phenotypic tool to provide accurate information on the current (patho)physiological status of patients to prospectively inform on individual differences in both PK and PD processes and thereby guide drug selection and drug dosing. Furthermore, in cases where the exact mechanism of a disease or drug effect is unknown, endogenous metabolites and their change after administration of a drug can provide mechanistic insight in disease status and drug response of an individual [19].

3. Metabolomics and pharmacometabolomics

Pharmacogenomics (PG), which uses genetic polymorphisms to predict individual variations in responses to drugs, for instance to classify patients as poor or rapid drug metabolizers, or drug responders or non-responders [20–22] has been increasingly used to inform personalized medicine. However, studying a patient's genotype does not always allow for a clear definition of a phenotype, nor does it give information about the current (patho)physiological state of an individual [23], as the genotype does not capture time-varying processes influenced by environmental factors and/or disease-related factors.

Metabolomics offers an advantage over PG in explaining the inter-individual variability in drug PK or PD, as it provides a direct readout of the current metabolic state of an individual. The endogenous metabolite profile is a snapshot of the phenotypic status of an individual resulting from, for instance, demographic factors, environmental interactions, microbiota, or disease status. Pharmacometabolomics is emerging as a discipline of metabolomics that studies the interplay between drug pharmacology and the patients'

(patho)physiology, by measuring endogenous metabolites that inform on variability in the drug PK or PD phenotype [24–27]. This concept has first been illustrated in rats, in a study that showed that metabolomic information in pre-dose urine samples is predictive of both drug metabolism (PK) and toxicity (PD) of paracetamol [24].

So far, pharmacometabolomic research addresses:

1. the identification of endogenous metabolites for predicting individual drug PK characteristics [28–33].
2. the identification of endogenous metabolites and their metabolic pathways for predicting individual drug PD characteristics [34–42].
3. the identification of endogenous metabolite biomarkers for monitoring disease progression and pharmacotherapy in individual patients [43–45].

The analytical methods applied to discover metabolic biomarkers use advanced and sensitive analytical instruments such as NMR, LC-MS and GC-MS [46–49]. Metabolomics research can be conducted either in a targeted or un-targeted fashion. In targeted approaches, pre-selected endogenous metabolites, which belong either to defined chemical classes or to particular metabolic pathways, are quantified. In an untargeted approach or a global profiling approach, endogenous metabolites are quantified in an unbiased fashion without any pre-selection of metabolites. This mode is advantageous in exploratory studies, which can generate hypotheses as well as generate data for biomarker discovery. However, in an untargeted metabolomic analysis, the physicochemical properties of the metabolites determine whether they can be in principle extracted and detected, and quantitative information on endogenous metabolite concentration is often less precise than in targeted analysis, and comparability between studies and labs is less straightforward than in targeted analysis, where absolute concentrations are reported for targeted metabolites for which a calibration model is available.

For the discovery of metabolite biomarkers to identify predictors of PK and/or PD variability or for monitoring the disease progression and the modulation of the disease progression by pharmacotherapy, disease metabolic phenotypes or pre- and post-dose metabolic phenotypes are often established. These metabolic phenotypes offer unique read-outs that contain information about the (patho)physiological state of an individual at particular time points. The optimal design of the metabolomic biomarker discovery study, will depend on the intended use of the biomarker, which could include for instance identification of responders and non-responders to drug treatment, predict individual PK

variability or assess drug-drug interactions. The statistical models of the metabolomics data will then integrate both causal and temporal information. Ultimately, the metabolite biomarkers may be used in routine clinical practice, either prospectively to guide drug selection and drug dose selection based on pre-dose metabolite biomarker profiles, or retrospectively to monitor the effects of pharmacotherapy.

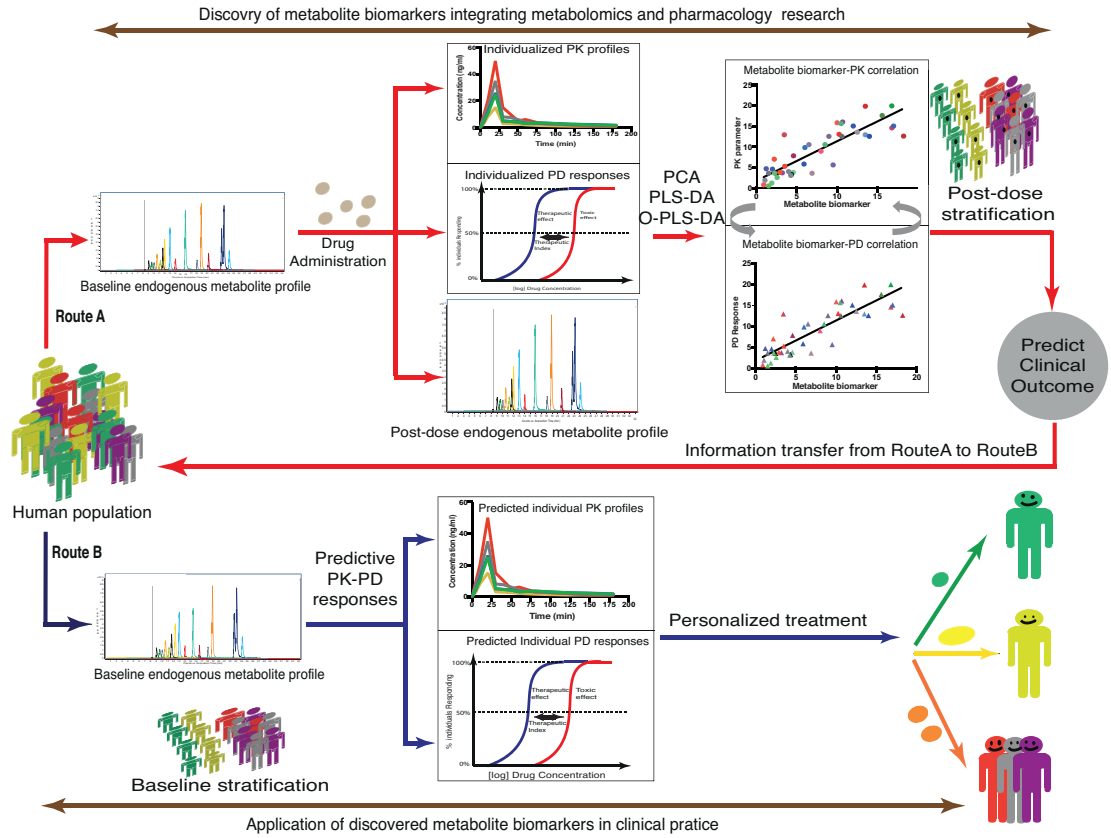

Figure 2: Pharmacometabolomics in research (*route A*) and clinical practice (*route B*). ***Route A (red):*** Discovery of metabolite biomarkers to predict pharmacological treatment outcome using statistical methods that couple data from metabolomics profiling to PK and / or PD variables of an individual. ***Route B (blue):*** Prospective application of metabolite biomarkers in routine clinical practice, using information from *route A* for personalized treatment.

Fig. 2 illustrates the use of pharmacometabolomics in both research (route A) and clinical practice (route B)**.** Route A illustrates how pharmacometabolomics can be coupled to the clinical outcome variables of pharmacotherapy to investigate and identify metabolomic biomarkers for drug pharmacology and the interaction with patients' (patho)physiology. In this route, pre-dose and post-dose endogenous metabolite profiles are obtained together with individual PK and PD variables. Using a range of multivariate statistical methods such as for

instance principal component analysis (PCA), partial least squares discriminant analysis (PLS-DA) and orthogonal partial least squares discriminant analysis (O-PLS-DA), correlations between endogenous metabolites and pharmacological characteristics can be investigated [50]. Further research is then focused on identifying the role of the biomarker in the causal chain between drug administration and patient outcome, for instance using network analysis [51] and/or population models that quantify the time course of drug concentration and drug effect [52,53]. Route B illustrates how the pharmacometabolomic information obtained in route A is prospectively applied in clinical practice to personalize drug treatment. Using pre-dose samples and the quantitative knowledge on the relationships between endogenous metabolites and pharmacological outcome, pharmacotherapy, in terms of drug selection and dose selection, can be tailored to an individual.

4. Pharmacometabolomics informs pharmacokinetics

Target exposure is one of the first steps on the causal chain linking drug dosing to patient outcome. Knowledge on the sources and extent of inter-individual variability and the availability of descriptors for variability, will allow clinicians to prospectively adjust drug doses for individual patients.

The main aim of pharmacometabolomic studies related to drug PK is to identify endogenous metabolite markers that allow for the stratification of patients into exposure groups, which is needed to individualize drug dosing regimens. Factors that are known to have marked impact on the PK of drugs include, for instance, expression and activity of drug metabolizing enzymes, tissue composition including the expression of drug binding plasma proteins and tissue proteins, drug transporters, and gut microbiome.

One of the first reported human studies linking pre-dose metabolomics information in urine to drug exposure measures was performed in healthy volunteers taking tacrolimus [28]. Tacrolimus is an immunosuppressant used during organ transplantation and has a narrow therapeutic index with a high degree of inter-individual variability in its PK. As dose adjustments of this drug are futile by the time over-dosing (e.g. organ toxicity) or under-dosing (e.g. organ rejection) become apparent, accurate exposure monitoring or prediction is important. In the study, the authors used first untargeted metabolomic profiling and multivariate statistics to correlate endogenous urine metabolites to the AUC of tacrolimus. Then a hypothetical molecular network was developed that included the obtained metabolic biomarkers, and findings on important modules in this network were linked to mechanistic

knowledge of the underlying PK processes for tacrolimus to select possibly causal biomarkers. From this, a metabolomic phenotype based on pre-dose urine concentrations of four endogenous metabolites was derived that can predict a patients' exposure to tacrolimus, thereby allowing a prospective individual dose selection.

Another report linked pre-dose plasma metabolomic profiles to exposure measures of atorvastatin in healthy volunteers [29]. Atorvastatin is an HMG-CoA reductase inhibitor for which considerable inter-individual variability in drug metabolism leads to up to 45-fold differences in plasma concentrations leading to therapy failure in some and adverse effects in others. In this study, the authors first applied untargeted profiling of metabolites with GC-MS and PLS analysis to establish a model that predicts endogenous metabolites and pharmacokinetic parameters (C_{max} and AUC). Using selected metabolites, hypothetical metabolic networks were constructed to visualize the role of metabolite pathways explaining the variability. Later, an O-PLS model was used to stratify the individuals into subgroups based on the pre-dose metabolite behavior. For atorvastatin, conventional covariates have proven to be suboptimal in predicting individual exposure measures and this study showed a combination of endogenous metabolite biomarkers to have increased predictive value for this drug.

As drug metabolizing enzyme activity is an important contributor to drug clearance, and as drug clearance is a major determinant for exposure, some (pharmaco)metabolomic studies investigate endogenous metabolomic predictors for drug metabolizing enzyme activity in general. It is, however, important to note that other factors, including hepatic blood flow, plasma protein binding, and hepatic transporters, also influence drug metabolic clearance. These factors may limit the direct translation of findings regarding drug metabolism of one probe compound to other compounds that are substrates for the same enzymes.

When focusing on the metabolism, CYP3A enzymes are responsible for the metabolism of the majority of prescribed drugs. These enzymes have multiple functional alleles and they are subject to induction and inhibition by various exogenous compounds. The interaction processes are highly variable between individuals and become especially relevant in patients taking multiple drugs. To investigate the applicability of pharmacometabolomics in prospectively informing on induction of CYP3A4 metabolism, Rahmioglu et al. performed a study correlating pre-dose metabolomic urine measures to quinidine metabolite ratios after CYP3A4 induction with Hypericum perforatum, known as St. John's Wort [32]. Endogenous

urinary metabolite measures were identified that were predictive of the quinidine metabolite ratio (3-hydroxyquinine to quinine (3OH-Q:Q)), but they all remained empirical predictors as none of these could be mechanistically linked to CYP3A4 activity. A potential explanation for this is that ratios in drug metabolite concentrations are dependent on both formation and elimination rates of metabolites, making this measure not very specific for enzyme activity alone.

A more recent study in healthy male volunteers used a more direct measure for CYP3A activity by investigating the clearance of midazolam, a drug that is known to be predominantly cleared through CYP3A-mediated metabolism. Moreover, this study not only investigated scenarios after CYP3A induction using ketoconazole, but also included situations without drug interactions or with inhibition using rifampicin [31]. The authors were able to identify an endogenous steroid metabolomic profile in urine which could accurately predict midazolam clearance under all investigated conditions. A link between steroid metabolism and CYP3A activity had already been established, but this study defined a more predictive biomarker profile. Moreover, the authors showed that timing of urine collection in each treatment phase did not influence the predictive value of the biomarker, suggesting that it can be reliably used to establish current midazolam clearance in patients that are already receiving drug therapy.

In the pediatric population, on top of genetic, environmental and disease-related factors that are also present in adults, growth and development results in continuous changes in physiological processes underlying drug PK and PD. Much research efforts have focused on quantifying the influence of these changes on the PK, and to a lesser extent PD, of drugs in children. A recent study by Tay-Sontheimer et al. [33], illustrated a first attempt to use pharmacometabolomic approaches to prospectively and non-invasively predict drug clearance of a CYP2D6 substrate in this population as well. Strong conclusions cannot yet be made based on this study, since parent and drug metabolite ratios were used to define enzyme activity. Other limitation in this study were encountered as the identified endogenous metabolite biomarker Ml, could not be structurally identified based on its fragmentation spectra, and most importantly the concentration of the endogenous metabolite biomarker was below the detection limits in samples of poor metabolizers. However, the idea of using pre-dose pharmacometabolomic measures to prospectively determine drug doses in the pediatric population is appealing.

As most drug metabolism occurs in the hepatocytes of the liver, influx and efflux transporters in these cells may influence the metabolic clearance of their substrates. Moreover, efflux transporters in hepatocytes may offer an alternative clearance route by transporting drugs directly into the bile. Also within nephrons of the kidneys, active transporters may facilitate drug excretion or reuptake. Finally, intestinal drug uptake and tissue distribution of drugs may be influenced by transporters. As with enzymes, genetic polymorphisms in drug transporters may influence their activity [54] and interactions with endogenous or exogenous compounds may induce or inhibit the transporters in a time-dependent manner [55].

In a recent study using an untargeted metabolomics approach, a pre-dose urinary metabolomic profile based on 28 endogenous metabolites was identified that was predictive of the clearance of high-dose methotrexate in patients with lymphoid malignancies [30]. Inter-individual and inter-occasion variability in the clearance of methotrexate is large, leading to regular toxicity events in patients. Many of the 28 identified endogenous metabolites are substrates for organic anion transporters in the kidney, transporters that are also known to play a major role in the elimination of methotrexate, suggesting that metabolomic profiles may also provide information on the function of transporters at a given time-point.

Recently it has been recognized that the human gut microbiome may contribute to variations in the response to drug treatment, for instance by the bacterial synthesis of unique metabolites from administered drugs or their metabolites. In a study of paracetamol, Clayton et al., demonstrated that formation of *p*-cresol by the gut microbiome results in a competitive interaction for the systemic sulphation of paracetamol, causing a decreased relative sulphation of the drug [56]. Given that the therapeutic window of paracetamol is wide, this finding may not be of big relevance for this specific drug, but it may have important implications for other drugs that have a narrow therapeutic window and large inter-individual differences in drug metabolism. Also for simvastatin, a relationship between pre-dose levels of secondary bile acids produced in the gut and drug effect has been identified [57], although the exact mechanism underlying this finding is not yet known. The identified secondary bile acids correlated with the concentration of simvastatin, and interactions of these bile acids with (patho)physiological mechanisms are also proposed to influence patients' responses to simvastatin treatment. As the microbiome of individuals may vary over time, the results of these studies suggest that pharmacometabolomics may provide relevant information on the

status of the microbiome of a patient at a given time and the expected effect this has on pharmacotherapy.

4. Pharmacometabolomics informs pharmacodynamics

The majority of pharmacometabolomic studies are focused on drug PD and changes in (patho)physiology upon drug exposure. The potential of this type of pharmacometabolomic research has been highlighted for instance in neuropsychiatric diseases [37,39,58–61], neurodegenerative disorders[62], cardiovascular diseases [35,36,40,57], cancer [34,45,63], chronic kidney disease [64] and hematology [38,65].

Most pharmacometabolomic studies in PD set out to investigate the effects of pharmacotherapy by investigating differences in pre and post-dose endogenous metabolomic profiles and identifying patterns that can explain inter-individual differences in treatment outcome. However, as is illustrated in Fig. 1, changes in various levels of the (patho)physiological system induced by pharmacotherapy should not be regarded as static or be studied in isolation, as they only form one link in the context of their causal and temporal interaction in all the processes between drug administration and patient outcome. The studies establishing a link between a specific endogenous metabolite or metabolite profile and treatment outcome of pharmacotherapy should therefore be followed up by extensive studies into the behavior of the new metabolite biomarker under various pharmacological interventions of the (patho)physiological system to validate the specificity, sensitivity, reproducibility, and clinical relevance of the new metabolite biomarker. These validation studies should focus on the influence of different drug doses or drug concentrations on the newly identified metabolite biomarker to establish a concentration-effect relationship, on understanding the causal and temporal relationships of changes in the new metabolite biomarker and other biomarkers or measurements of treatment outcome, and on the response of the new metabolite biomarker to pharmacotherapy with both agonist and antagonist agents. Population modeling approaches can provide a useful tool in quantitatively integrating all the information obtained in the various investigations.

5. Pharmacometabolomics informs the clinician

Although metabolomics studies have identified a number of metabolite biomarkers that can describe and predict inter-individual variability in the PK or PD of drugs, the application of the obtained knowledge in clinical practice remain relatively limited. Validation of promising

metabolite biomarkers is therefore urgently required to prove their specificity, sensitivity, reproducibility and clinical relevance. Once the understanding of causal and temporal relationships and inter-individual variability is there, the obtained knowledge needs to be taken to the clinic to optimize drug therapy.

It is worth to mention that pharmacogenomics studies have played an important role in predicting drug PK in the last decade, but pharmacogenomics does not provide information about the current (patho)physiological state of an individual, and take environmental factors into account. As one's individual genome will be soon available for many persons, pharmacogenomics is very attractive for PK prediction. However, there are many cases where pharmacogenomics was not able to predict PK, and where pharmacometabolomics is an attractive alternative. The reason is that pharmacometabolomics provides a snapshot of the phenotypic status of an individual resulting from, for instance, demographic factors, environmental interactions, microbiota, or disease(s) status. We anticipate that pharmacometabolomics and pharmacogenomics are very complementary techniques, which we expect will be often combined ultimately in clinical decision support for PK (and PD) prediction.

For the implementation of metabolic biomarkers in the clinical lab there are different requirements: (i) metabolites should be reported as absolute concentrations, (ii) the analysis should be cost-effective and (iii) results should be available to the clinicians in a timely manner. Implementation can occur in two different ways, via targeted analysis, specific cost-efficient assays covering only a limited number of required metabolites, or a broader panel allowing for a general metabolomics assay covering hundred or more (identified) metabolites that inform about the general health state including the prediction of treatment outcome. For the targeted assay, we can expect that small analyzers will be developed. This might be based on aptamers, miniaturized NMR or mass spectrometers, and might be even handheld. For the broader clinical metabolic profile most probably a lab-based metabolite analyzer using a cost-efficient mass spectrometer will be used. The more metabolite biomarkers will become validated, the more attractive it will be to implement metabolite profiling in the clinical lab for clinical decision support, and we are convinced that with the significant increase of metabolomics studies reporting metabolic biomarkers for PK/PD this will become routine over some years.

It is worth mentioning that pharmacometabolomics can also inform the drug researcher on variation of PK or PD in early clinical studies, especially whether (i) a drug is

exposed to the target, (ii) whether the drug engages with the target and (iii) whether the drug modulates the target in the desired manner. However, this aspects were not the subject of this review.

6. Conclusion and Future recommendations

An interplay between many factors related both to drug pharmacology and a patients' (patho)physiology is responsible for the drug treatment outcome for the patient. Variability in all these processes can yield variability in treatment outcome. While conventional covariates are often sufficient in prospectively informing treating physicians on the PK of individuals, pharmacometabolomics has proven to have additional value in prospectively informing PK and aiding in prospective drug dose individualization when conventional covariates cannot explain inter-individual variability sufficiently. Compared to pharmacogenomics, pharmacometabolomics takes the actual health state into account. This is especially important in critically-ill patients, the elderly or terminal patients where many drug-drug interaction occurs, and also for drugs with a narrow therapeutic window and relatively high unexplained inter-individual variability, and where you want to predict outcome before starting any treatment rather than using therapeutic drug monitoring to modify the treatment regime. This may be particularly relevant in patient populations taking multiple drugs or which rapidly change their health state, such as patients with organ failure or organ transplants, but also in pediatric or elderly patients or pregnant women.

Pharmacometabolomics can aid in predicting pharmacodynamics and ultimately clinical treatment outcome. As (patho)physiology changes during disease and pharmacotherapy, it is important to not consider the endogenous metabolites as static variables in isolation. The influence of drug dose and temporal changes in drug concentrations and metabolite network interactions should be part of these investigations as well, before endogenous metabolite markers can be considered for informing drug selection or drug dose selection in patients. Therefore, both PK and PD, should be included in pharmacometabolomics studies, where currently often PK is not considered in many PD pharmacometabolomic studies.

In conclusion, pharmacometabolomics is very promising for predicting pharmacokinetics and pharmacodynamics, and if we can manage to incorporate findings in this field in clinical practice, we are able to realize personalized medicine.

References

1. Weinshilboum, R. Inheritance and drug response. *N. Engl. J. Med.* **348,** 529–37 (2003).
2. Li, H. & Jia, W. Cometabolism of microbes and host: implications for drug metabolism and drug-induced toxicity. *Clin. Pharmacol. Ther.* **94,** 574–81 (2013).
3. Alomar, M. J. Factors affecting the development of adverse drug reactions (Review article). *Saudi Pharm. J. SPJ Off. Publ. Saudi Pharm. Soc.* **22,** 83–94 (2014).
4. Schork, N. J. Personalized medicine: Time for one-person trials. *Nature* **520,** 609–611 (2015).
5. Kitsios, G. D. & Kent, D. M. Personalised medicine: not just in our genes. *BMJ* **344,** e2161 (2012).
6. van der Greef, J. & McBurney, R. N. Rescuing drug discovery: in vivo systems pathology and systems pharmacology. *Nat. Rev. Drug Discov.* **4,** 961–967 (2005).
7. Vicini, P. & van der Graaf, P. H. Systems pharmacology for drug discovery and development: paradigm shift or flash in the pan? *Clin. Pharmacol. Ther.* **93,** 379–81 (2013).
8. Danhof, M., Alvan, G., Dahl, S. G., Kuhlmann, J. & Paintaud, G. Mechanism-based pharmacokinetic-pharmacodynamic modeling-a new classification of biomarkers. *Pharm. Res.* **22,** 1432–7 (2005).
9. Adourian, A. *et al.* Correlation network analysis for data integration and biomarker selection. *Mol. Biosyst.* **4,** 249–259 (2008).
10. Joerger, M. Covariate pharmacokinetic model building in oncology and its potential clinical relevance. *AAPS J.* **14,** 119–32 (2012).
11. Levy, G. Predicting effective drug concentrations for individual patients. Determinants of pharmacodynamic variability. *Clin. Pharmacokinet.* **34,** 323–33 (1998).
12. Sharma, A., Pilote, S., Bélanger, P. M., Arsenault, M. & Hamelin, B. A. A convenient five-drug cocktail for the assessment of major drug metabolizing enzymes: a pilot study. *Br. J. Clin. Pharmacol.* **58,** 288–97 (2004).
13. van der Greef, J., Hankemeier, T. & McBurney, R. N. Metabolomics-based systems biology and personalized medicine: moving towards n = 1 clinical trials? *Pharmacogenomics* **7,** 1087–94 (2006).
14. Bernini, P. *et al.* Individual human phenotypes in metabolic space and time. *J. Proteome Res.* **8,** 4264–71 (2009).
15. Fernie, A. R., Trethewey, R. N., Krotzky, A. J. & Willmitzer, L. Metabolite profiling: from diagnostics to systems biology. *Nat. Rev. Mol. Cell Biol.* **5,** 763–9 (2004).
16. Schnackenberg, L. K. Global metabolic profiling and its role in systems biology to advance personalized medicine in the 21st century. *Expert Rev. Mol. Diagn.* **7,** 247–59 (2007).
17. Guo, L. *et al.* Plasma metabolomic profiles enhance precision medicine for volunteers of normal health. *Proc. Natl. Acad. Sci. U. S. A.* **112,** E4901-10 (2015).
18. Suhre, K. *et al.* Human metabolic individuality in biomedical and pharmaceutical research. *Nature* **477,** 54–60 (2011).
19. Kaddurah-Daouk, R., Kristal, B. S. & Weinshilboum, R. M. Metabolomics: a global biochemical approach to drug response and disease. *Annu. Rev. Pharmacol. Toxicol.* **48,** 653–83 (2008).
20. Evans, W. E. & Relling, M. V. Moving towards individualized medicine with pharmacogenomics. *Nature* **429,** 464–468 (2004).
21. Evans, W. E. & McLeod, H. L. Pharmacogenomics--drug disposition, drug targets, and side effects. *N. Engl. J. Med.* **348,** 538–49 (2003).

22. Pirmohamed, M. Personalized pharmacogenomics: predicting efficacy and adverse drug reactions. *Annu. Rev. Genomics Hum. Genet.* **15,** 349–70 (2014).
23. Carr, D. F., Alfirevic, A. & Pirmohamed, M. Pharmacogenomics: Current State-of-the-Art. *Genes (Basel).* **5,** 430–43 (2014).
24. Clayton, T. A. *et al.* Pharmaco-metabonomic phenotyping and personalized drug treatment. *Nature* **440,** 1073–7 (2006).
25. Kaddurah-Daouk, R. & Weinshilboum, R. Metabolomic Signatures for Drug Response Phenotypes: Pharmacometabolomics Enables Precision Medicine. *Clin. Pharmacol. Ther.* **98,** 71–5 (2015).
26. Nicholson, J. K., Wilson, I. D. & Lindon, J. C. Pharmacometabonomics as an effector for personalized medicine. *Pharmacogenomics* **12,** 103–11 (2011).
27. Lindon, J. C., Holmes, E. & Nicholson, J. K. Metabonomics techniques and applications to pharmaceutical research & development. *Pharmaceutical Research* **23,** 1075–1088 (2006).
28. Phapale, P. B. *et al.* An integrative approach for identifying a metabolic phenotype predictive of individualized pharmacokinetics of tacrolimus. *Clin. Pharmacol. Ther.* **87,** 426–36 (2010).
29. Huang, Q. *et al.* A Pharmacometabonomic Approach To Predicting Metabolic Phenotypes and Pharmacokinetic Parameters of Atorvastatin in Healthy Volunteers. **14**, 3970-81 (2015).
30. Kienana, M. *et al.* Endogenous metabolites that are substrates of Organic Anion Transporter's (OATs) predict methotrexate clearance. *Pharmacol. Res.* **118**, 121-132 (2016).
31. Shin, K.-H. *et al.* Evaluation of endogenous metabolic markers of hepatic CYP3A activity using metabolic profiling and midazolam clearance. *Clin. Pharmacol. Ther.* **94,** 601–9 (2013).
32. Rahmioglu, N. *et al.* Prediction of variability in CYP3A4 induction using a combined 1H NMR metabonomics and targeted UPLC-MS approach. *J. Proteome Res.* **10,** 2807–16 (2011).
33. Tay-Sontheimer, J. *et al.* Detection of an endogenous urinary biomarker associated with CYP2D6 activity using global metabolomics. *Pharmacogenomics* **15,** 1947–62 (2014).
34. Keun, H. C. *et al.* Serum molecular signatures of weight change during early breast cancer chemotherapy. *Clin. Cancer Res.* **15,** 6716–23 (2009).
35. Kaddurah-Daouk, R. *et al.* Lipidomic analysis of variation in response to simvastatin in the Cholesterol and Pharmacogenetics Study. *Metabolomics* **6,** 191–201 (2010).
36. Krauss, R. M., Zhu, H. & Kaddurah-Daouk, R. Pharmacometabolomics of statin response. *Clin. Pharmacol. Ther.* **94,** 562–5 (2013).
37. Kaddurah-Daouk, R. *et al.* Pretreatment metabotype as a predictor of response to sertraline or placebo in depressed outpatients: a proof of concept. *Transl. Psychiatry* **1,** e26- (2011).
38. Yerges-Armstrong, L. M. *et al.* Purine pathway implicated in mechanism of resistance to aspirin therapy: pharmacometabolomics-informed pharmacogenomics. *Clin. Pharmacol. Ther.* **94,** 525–32 (2013).
39. Zhu, H. *et al.* Pharmacometabolomics of response to sertraline and to placebo in major depressive disorder - possible role for methoxyindole pathway. *PLoS One* **8,** e68283 (2013).
40. Trupp, M. *et al.* Metabolomics reveals amino acids contribute to variation in response to simvastatin treatment. *PLoS One* **7,** e38386 (2012).
41. Kaddurah-Daouk, R. & Weinshilboum, R. M. Pharmacometabolomics: implications

for clinical pharmacology and systems pharmacology. *Clin. Pharmacol. Ther.* **95,** 154–67 (2014).
42. Condray, R. *et al.* 3-Hydroxykynurenine and clinical symptoms in first-episode neuroleptic-naive patients with schizophrenia. *Int. J. Neuropsychopharmacol.* **14,** 756–67 (2011).
43. Kinross, J. M., Holmes, E., Darzi, A. W. & Nicholson, J. K. Metabolic phenotyping for monitoring surgical patients. *Lancet (London, England)* **377,** 1817–9 (2011).
44. Nicholson, J. K., Everett, J. R. & Lindon, J. C. Longitudinal pharmacometabonomics for predicting patient responses to therapy: drug metabolism, toxicity and efficacy. *Expert Opin. Drug Metab. Toxicol.* **8,** 135–9 (2012).
45. Backshall, A., Sharma, R., Clarke, S. J. & Keun, H. C. Pharmacometabonomic profiling as a predictor of toxicity in patients with inoperable colorectal cancer treated with capecitabine. *Clin. Cancer Res.* **17,** 3019–28 (2011).
46. Dona, A. C. *et al.* Precision high-throughput proton NMR spectroscopy of human urine, serum, and plasma for large-scale metabolic phenotyping. *Anal. Chem.* **86,** 9887–94 (2014).
47. Emwas, A.-H. M., Salek, R. M., Griffin, J. L. & Merzaban, J. NMR-based metabolomics in human disease diagnosis: applications, limitations, and recommendations. *Metabolomics* **9,** 1048–1072 (2013).
48. Chen, C., Gonzalez, F. J. & Idle, J. R. LC-MS-based metabolomics in drug metabolism. *Drug Metab. Rev.* **39,** 581–97 (2007).
49. Garcia, A. & Barbas, C. Gas chromatography-mass spectrometry (GC-MS)-based metabolomics. *Methods Mol. Biol.* **708,** 191–204 (2011).
50. Bartel, J., Krumsiek, J. & Theis, F. J. Statistical methods for the analysis of high-throughput metabolomics data. *Comput. Struct. Biotechnol. J.* **4,** e201301009 (2013).
51. Kotze, H. L. *et al.* A novel untargeted metabolomics correlation-based network analysis incorporating human metabolic reconstructions. *BMC Syst. Biol.* **7,** 107 (2013).
52. Wright, D. F. B., Winter, H. R. & Duffull, S. B. Understanding the time course of pharmacological effect: a PKPD approach. *Br. J. Clin. Pharmacol.* **71,** 815–23 (2011).
53. Gabrielsson, J., Fjellström, O., Ulander, J., Rowley, M. & Van Der Graaf, P. H. Pharmacodynamic-pharmacokinetic integration as a guide to medicinal chemistry. *Curr. Top. Med. Chem.* **11,** 404–418 (2011).
54. Kerb, R. Implications of genetic polymorphisms in drug transporters for pharmacotherapy. *Cancer Lett.* **234,** 4–33 (2006).
55. Konig, J., Muller, F. & Fromm, M. F. Transporters and Drug-Drug Interactions: Important Determinants of Drug Disposition and Effects. *Pharmacol. Rev.* **65,** 944–966 (2013).
56. Clayton, T. A., Baker, D., Lindon, J. C., Everett, J. R. & Nicholson, J. K. Pharmacometabonomic identification of a significant host-microbiome metabolic interaction affecting human drug metabolism. *Proc. Natl. Acad. Sci. U. S. A.* **106,** 14728–33 (2009).
57. Kaddurah-Daouk, R. *et al.* Enteric microbiome metabolites correlate with response to simvastatin treatment. *PLoS One* **6,** e25482 (2011).
58. Quinones, M. P. & Kaddurah-Daouk, R. Metabolomics tools for identifying biomarkers for neuropsychiatric diseases. *Neurobiol. Dis.* **35,** 165–76 (2009).
59. Kaddurah-Daouk, R. *et al.* Pharmacometabolomic mapping of early biochemical changes induced by sertraline and placebo. *Transl. Psychiatry* **3,** e223 (2013).
60. Kaddurah-Daouk, R. *et al.* Metabolomic mapping of atypical antipsychotic effects in schizophrenia. *Mol. Psychiatry* **12,** 934–45 (2007).

61. Yao, J. K. *et al*. Altered interactions of tryptophan metabolites in first-episode neuroleptic-naive patients with schizophrenia. *Mol. Psychiatry* **15,** 938–53 (2010).
62. Kaddurah-Daouk, R. *et al*. Alterations in metabolic pathways and networks in Alzheimer's disease. *Transl. Psychiatry* **3,** e244 (2013).
63. Dang, L. *et al*. Cancer-associated IDH1 mutations produce 2-hydroxyglutarate. *Nature* **462,** 739–744 (2009).
64. Zhao, Y.-Y. *et al*. A pharmaco-metabonomic study on chronic kidney disease and therapeutic effect of ergone by UPLC-QTOF/HDMS. *PLoS One* **9,** e115467 (2014).
65. Ellero-Simatos, S. *et al*. Pharmacometabolomics reveals that serotonin is implicated in aspirin response variability. *CPT pharmacometrics Syst. Pharmacol.* **3,** e125 (2014).

Acknowledgements

This project received support from the Faculty of Science ("Profiling programme: Endocannabinoids"), Leiden University (VK, TH). This project has been supported by SysMedPD (www.sysmedpd.eu) within the European Union's Horizon 2020 research and innovation programme under grant agreement No 668738.

Chapter 3

Quantitative profiling of endocannabinoids and related *N*-acylethanolamines in human CSF using nano LC-MS/MS

Vasudev Kantae*, Shinji Ogino*, Marek Noga, Amy C Harms, Robin M van Dongen, Gerrit LJ Onderwater, Arn MJM van den Maagdenberg, Gisela M Terwindt, Mario van der Stelt, Michel D Ferrari, Thomas Hankemeier

* *Authors contributed equally*

Journal of Lipid Research. 2017; 58(3): 615-624

Abstract

Endocannabinoids, a class of lipid messengers, have emerged as crucial regulators of synaptic communication in the central nervous system (CNS). Dysregulation of these compounds has been implicated in many brain disorders. Although some studies have identified and quantified a limited number of target compounds, a method that provides comprehensive quantitative information on endocannabinoids and related *N*-acylethanolamines (NAEs) in CSF is currently lacking as measurements are challenging due to low concentrations under normal physiological conditions. Here we developed and validated a high-throughput nano liquid chromatography-electrospray ionization mass spectrometry (nano LC-ESI-MS/MS) platform for the simultaneous quantification of endocannabinoids (anandamide (AEA), 2-arachidonoyl glycerol (2-AG)), ten related NAEs and eight additional putatively annotated NAEs in human CSF. Requiring only 200 μL of CSF, our method has limits of detection from 0.28 to 61.2 pM with precisions of RSD <15% for most compounds. We applied our method to CSF from 45 healthy humans and demonstrated potential age and gender effects on concentrations of endocannabinoids and NAEs. Notably, our results show that docosahexaenoyl ethanolamide (DHEA) concentrations increase with age in males. Our method may offer new opportunities to gain insight into regulatory functions of endocannabinoids in the context of (ab)normal brain function.

Introduction

The endocannabinoid system has emerged as a crucial regulator of synaptic communication in the central nervous system (CNS)[1–3]. Dysregulation of this system is implicated in various neurological and psychiatric disorders, such as neuroinflammation, stroke, brain trauma, anxiety and depression[4–8]. The endocannabinoid system consists of endogenous lipid messengers (endocannabinoids) that activate two distinct cannabinoid (CB_1 and CB_2) receptors and the enzymes responsible for the synthesis and degradation of the endocannabinoids. Anandamide (*N*-arachidonoyl ethanolamine; AEA) and 2-arachidonoylglycerol (2-AG) are the two best studied endocannabinoids[9]. They are synthesized on demand from membrane lipids in a stimulus-dependent manner and are degraded by fatty acid amide hydrolase (FAAH) and monoacyl glycerol lipase (MAGL), respectively[10,11].

In addition to AEA & 2-AG, there are endogenous lipid compounds capable of activating the cannabinoid CB_1 and CB_2 receptors, i.e. virodhamine (*O*-arachidonoyl ethanolamine; O-AEA), *N*-arachidonoyldopamine (NADA) and noladinether (2-arachidonylglycerol ether; 2-AGE), but their physiological relevance is largely unknown. Related bioactive lipids, such as *N*-linoleoylethanolamine (LEA), *N*-palmitoylethanolamine (PEA), *N*-oleoylethanolamine (OEA) and *N*-stearoylethanolamine (SEA) are produced through the same biosynthetic pathway as anandamide. These *N*-acylethanolamines (NAEs) have negligible or only weak affinity for the cannabinoid CB_1 and CB_2 receptors, but are able to indirectly modulate cannabinoid receptor activity by interfering with endocannabinoid metabolism, the so-called 'entourage effect'[12]. Of note, some of the NAEs may exert biological activities through other proteins, such as transient receptor potential cation channel, subfamily V, member 1 (TRPV1), G-coupled protein receptors (GPR55, GPR18 and GPR119) or nuclear receptors (peroxisome proliferator-activated receptor α and γ[13,14]. It is worth mentioning that the endocannabinoids, arachidonoyl glycerol's and fatty acid ethanolamides, are not only metabolized by FAAH or MAGL but are oxidized by several other enzymes such as cyclo-oxygenase-2 (COX-2), cytochrome P450 and lipoxygenase (LOX) enzymes. These enzymes convert endocannabinoids into a new array of oxygenated intermediates such as prostaglandin ethanolamides (called as prostamides) and prostaglandin glycerol esters or the lipids can be lipooxegenated to many hydroxylated end-products. However, these intermediates are pharmacologically distinct from their parent endocannabinoids and possess different biological functions [15,16].

Quantification of endocannabinoid levels in the CNS is important to understand their role in human brain disease. Since the cerebrospinal fluid (CSF) is exchanged with brain interstitium, it is regarded as the most relevant accessible body fluid that reflects free endocannabinoid and NAE levels in the CNS[17]. However, limited information is currently available on endocannabinoid and NAE levels in the CSF from healthy humans or patients. Previous studies have quantified the endocannabinoids 2-AG and AEA[18–21] and two NAEs (OEA and PEA)[22–24], but not the related lipid messengers.

Under normal physiological conditions, endocannabinoid concentrations are very low (in the nanomolar to femtomolar range) in CSF compared to their levels in blood and tissues. This puts extra demands on the sensitivity of the quantification method. Advanced powerful techniques such as UHPLC (ultra –high performance liquid chromatography) coupled to MS have been employed to quantify endocannabinoids in blood[25–27] and other tissue extracts[28] but these techniques are less suitable for endocannabinoid quantification in CSF due to its limited availability. We envisioned that nano LC would offer the opportunity to increase the sensitivity of the analytical system; a microfluidic chip-based approach would provide the sensitivity by allowing injection of a larger sample volume by coupling an on-line enrichment column with small internal diameter (ID) analytical column, resulting in a higher concentration in the eluting peak. In addition, the reduced flow rate of nano LC compared with conventional LC can improve sensitivity through an increase in the ionization efficiency[29]. Using microfluidic chip-based technology, incorporating an enrichment column, a six-port valve, a separation column and a nano electrospray tip, allows the coupling of miniaturized separation with a nano electrospray ionization source[30]. This design results in lower dead volumes and fewer connections compared to classical nano LC equipment, thereby leading to increased sensitivity and robustness by less peak broadening and dilution effects during transfer of the sample to LC column and later to LC-MS interface[31].

By making use of these advantages, we developed and validated a nano LC-ESI-MS/MS method for the simultaneous quantification of endocannabinoid and related NAEs in clinical (human) CSF. By combining a simple Liquid-Liquid Extraction (LLE) method for sample preparation, a nano LC separation and Multiple Reaction Monitoring (MRM) for detection, we could show that an extended range of endocannabinoids and related molecules can be measured. To show the applicability of this novel method, CSF samples of 45 healthy volunteers were measured to study variation in endocannabinoid levels in relation to gender and age.

Material and methods

Materials

Ultra-performance liquid chromatography (UPLC)-grade acetonitrile (ACN) and methanol (MeOH) were purchased from Actu-All Chemicals (Oss, The Netherlands). Formic acid was purchased from Acros Organics (Morris Plains, NJ, USA). Toluene was obtained from Biosolve (Valkenswaard, The Netherlands). EDTA disodium salt was obtained from Sigma-Aldrich Chemie B.V. (Zwijndrecht, The Netherlands). Purified Millipore H_2O was obtained from a Milli-Q PF Plus system (Merck Millipore). NADA, 1-AG, 2-AG, DEA (*N*-docosatetraenoylethanolamide), DHEA (*N*-docosahexaenoylethanolamide), 2-AGE, DGLEA (N-dihomo-γ-Linolenoylethanolamide), AEA, SEA, OEA, LEA, PEA, O-AEA, and deuterated standards, NADA-d8, 2-AG-d8, DHEA-d4, AEA-d8, SEA-d3, OEA-d4, LEA-d4, PEA-d4 were purchased from Cayman Chemical (Ann Arbor, MI, USA).

Preparation of standards and internal standards

Pure standards (>98% purity) in ethanol or acetonitrile at different stock concentrations were provided from the manufacturer. The standard stock solutions (STD) were diluted to a concentration of 1 mM using acetonitrile. A final mix of working solution at 100 nM for compounds in group A (NADA, AEA, DEA, DHEA, DGLEA, 2-AGE, LEA, O-AEA) and at 1 µM for compounds in group B (2-AG, 1-AG, SEA, OEA, PEA) were prepared. The deuterated internal standard solutions (ISTDs) were diluted to 100 µM except for 2-AG-d8 at 259 µM. A final working solution was prepared with 100 nM AEA-d8, NADA-d8, DHEA-d4 and 1000 nM 2-AG-d8, SEA-d3, PEA-d4, LEA-d3 and OEA-d4.

Calibration curve preparation

On the day of analysis, the STD working solution was further diluted to seven additional calibration levels as shown in **Table. 1**. Each calibration point was mixed with ISTD-mix at 1:1. The concentrations of ISTDs were chosen to be near the endogenous concentrations of the analytes in CSF.

Table. 1: Stock concentrations of endocannabinoids and related NAEs standards in the calibration line

Compound group	Concentrations (nM)[a]							
	C0	C1	C2 (low)	C3	C4 (medium)	C5	C6 (high)	C7
A	0	0.01	0.03	0.1	0.3	1	3	10
B	0	0.1	0.3	1	3	10	30	100

[a]Seven levels of standard solutions (C1 to C7) are spiked to build the calibration line. These standards will be diluted 21 times in CSF matrix for their final concentrations.

Sampling protocol for clinical CSF samples, used for method development and validation

CSF was sampled via lumbar puncture between L3/L4, L4/L5, or L5/S1. CSF was collected in 12-mL polystyrene tubes (no. 160172; no. 160172; Greiner Bio-One B.V., Alphen aan den Rijn, The Netherlands) and processed within 30 minutes. A small portion was used for cell count, and the remaining CSF was centrifuged at 21°C for 5 minutes (500 g). A portion of the supernatant was used for clinical measurements (i.e. glucose, total protein), and the remaining CSF was stored in 2.0-mL polyethylene cryotubes (Micro tube, no. 72609; Sarstedt AG & C0, Nümbrecht, Germany) and stored at -20 °C. All samples remained at -20 °C until they were pooled in a 50-mL polypropylene tube (no. 210261; Greiner Bio-One B.V). The pooled sample was aliquoted into 2-mL Eppendorf tubes (no. 211-2120; VWR, Amsterdam, The Netherlands) and stored at -80 °C. These clinical CSF samples were used for method validation purpose and termed “pooled CSF samples”. On the day of analysis, 1000 µL of ethanol was added to each aliquot (0.5 mL CSF) to model conditions of study samples and mixed thoroughly and placed on ice.

Sampling of healthy subjects

CSF study samples were collected for an ongoing biochemical study, which was approved by the local medical ethics committee (LUMC). All subjects provided written informed consent before sampling. Prior to CSF sampling, 6 mL of cold ethanol (ethanol absolute, no. 8098; J.T.Baker, Phillipsburg, NJ, USA) was added to a 15 mL-polypropylene sampling tube (no. 188271; Greiner Bio-One B.V.) and placed on ice. Ethanol was added for denaturation of enzymes present in CSF upon sampling. Subsequently, 3 mL of CSF was sampled directly into the tube and inverted several times to mix CSF and ethanol thoroughly. Immediately

after sampling, the CSF/ethanol mixture was divided in 1.5 mL-aliquots into 7 x 1.8 mL-cryotubes (no. 368632; Nunc, Hardenberg, The Netherlands), and placed on dry ice within 30 minutes from sampling. All aliquots were stored at -80°C within 60 minutes from sampling. No extra freeze-thaw cycles were allowed before sample preparation.

Sample extraction

Sample extraction was performed on ice. For CSF samples, 600 µL of the CSF/EtOH mixture (200 µL/400 µL) was transferred into 2-mL Eppendorf tubes and 100 µL of 100 mM citrate buffer (pH 5.0) with 25 mM EDTA and 10 µL of deuterated internal standard mixture was added. After adding 550 µL of ice-cold toluene, the tubes were thoroughly mixed for 3 min using a bullet blender (Next Advance, Inc., Averill park, NY, USA), followed by a centrifugation step (4°C / 5000 g / 5 min). Then 475 µL of the upper layer (toluene) was aspirated and transferred into 500 µL Eppendorf tubes. Samples were dried under gentle stream of nitrogen placed on ice followed by reconstitution with 10 µL of water/MeOH (50/50). The reconstituted samples were centrifuged (4°C / 14000 rpm / 5 min) before transferring into vials for LC-MS.

Chip-based nano LC-MS/MS analysis

Endocannabinoids and related NAEs were measured using a targeted method on an Agilent 6460 triple quadrupole MS system in conjunction with Agilent 1100/1200 series nano-LC system consisting of a G1375 capillary pump, G2226 nano pump and a G1376 uWPS autosampler with thermostat (Agilent Technologies, Waldbron, Germany). Separation was carried out with an Agilent Polaris-HR-Chip 3C18 (G4240-62030, Waldbronn, Germany), which was inserted in the HPLC-Chip Cube MS interface (Agilent Technologies, Waldbron, Germany) operated at ambient temperatures. This chip has a 360-nL enrichment column with a 150 mm (lenght) x 75 µm (width) separation column and a particle size of 3 µm. The mobile phase was 10 mM formic acid/Water (A) and ACN (B). The analytical gradient was performed in two steps: first, 8 µL of sample was loaded on the enrichment column using the capillary pump delivering a mobile phase in isocratic mode composed of 40% B at a flow rate of 2 µL/min. After the sample was trapped on the enrichment column, it was switched in line with the analytical column. The nano pump gradient started at 45% B and linearly increased up to 80% B in 12 minutes at a flow rate of 400 nL/min. The column was then held at 95% B for 2 minutes before returning to 45% B. The column was re-equilibrated for 5

minutes prior to the next injection giving a total analysis time of 20 minutes. During the analytical gradient, the enrichment column was flushed with 16 µL of 100% B for 8 minutes. At the same time, the injection needle was washed with ACN/H2O (1/1, v/v) using an injection program. The temperature in the autosampler was maintained at 8°C. Electrospray ionization was operated in positive ion mode with a capillary spray voltage set at 1800 V and nitrogen nebulizer gas flow rate of 4 L/min and a temperature of 365°C. For endocannabinoids and related NAEs, individually optimized MRM parameters were determined for each transition for target compounds and ISTDs. The detailed list of MRM parameters and transitions is shown in **Table. S1**.

To maximize the potential of the platform, MRM transitions for other *N*-acylethanolamines (NAEs) were also included. Targets were selected based on: 1) combinations of major fatty acids and ethanolamine (general structure of NAEs) and 2) measurements of CSF by precursor ion scan mode for the characteristic product ion of NAEs, which is the protonated ethanolamine ion at m/z 62 (data not shown). These putatively annotated NAEs are listed as EA (from ethanolamine) followed by molecular mass (m/z) value. Details of MRM transitions included in the method are listed in **Table. S1**.

Data preprocessing

Peak area integration was performed with Mass Hunter Quantitative analysis (Version B.05.01; Agilent, Santa Clara, CA, USA) and manually inspected. Peak areas of analytes were corrected by the appropriate ISTD and response ratios were calculated and used throughout the analysis.

Method validation

An in-house 3-day validation protocol was used to determine linearity, LOD and LOQ, precision (intra- and inter-batch effect), recovery and matrix effect[32].

Linearity, LOD and LOQ Purchased standards were spiked to both pooled CSF ('matrix calibration line') and water as blank matrix ('academic calibration line') in seven different concentrations (Table 1) to determine the linearity, limit of detection (LOD) and limit of quantification (LOQ). For method validation, each calibration level was prepared using the sample extraction method explained above four times and injected once from each sample.

Responses in the calibration levels were compared by means of *t*-tests going from low-level to high level. If there was no significance difference between two adjacent levels, then the lower level was excluded from the calibration curve. Regression lines for both matrix and academic line were calculated with $1/X^2$ weighting. If the differences in slopes of the regression lines between matrix and academic lines were less than 10%, LOD and LOQ values were calculated from academic lines. When the slopes differed, the matrix line was used for these calculations. Each LOD and LOQ was calculated by 3.3 x [standard deviation of y-estimate in the regression line]/[slope], and 3 x LOD, respectively.

Precision The intra-batch and inter-batch effects were evaluated using the quadruplicate analysis of the pooled CSF samples spiked at three different concentrations (lower level (C2), medium (C4), and high level (C6)) over the three different days of the validation protocol. The pooled CSF was spiked with ISTDs, which behave like the endogenous compounds and are therefore perfectly suited to determine analytical characteristics. Precision was calculated as the relative standard deviation (RSD) of the ratio of target to ISTD. An RSD less than 15% for medium and high levels and less than 20% for the low level was considered acceptable.

Recovery and matrix effect Recovery and matrix effects were evaluated using ISTDs spiked to the pooled CSF samples. Recovery was assessed by determining the ratio of the peak areas obtained by spiking ISTDs to the sample before and after extraction. The matrix effect was assessed by determining the ratio of the peak areas obtained by spiking ISTDs to pooled CSF and to water after extraction.

Biological application in CSF of healthy subjects

A small study was performed to understand the changes in endocannabinoid levels in the CSF of healthy subjects due to gender and age. The experimental design included 45 individual study samples plus performance indicators. Duplicate samples were prepared and analyzed for 5 samples (15% of total samples). Additionally, 20 quality control (QC) samples were prepared by pooling individual study samples. A calibration curve was prepared by spiking the calibrations standards along with internal standards to the QC samples. All samples were randomized and each batch includes calibration samples and an even distribution of duplicates, QC samples and blanks.

Data pre-treatment

To detect outliers among QC samples, a principle component analysis (PCA) was used and QCs outside the 95% confidence region were detected and removed as statistical outliers: Two QC samples showed high concentrations for LEA, OEA, PEA and SEA and were detected as statistical outliers. These concentrations were possibly caused by (an) exogenous source(s)[33]. After removal of the outliers, the final QC set was used to determine optimal ISTDs for compounds without an isotopically labeled equivalent as an ISTD, as previously described[34]. Values from QC samples were used for monitoring data quality and correcting for shifts in MS sensitivity over time[34]. After correction with QC samples, relative standard deviations (RSD) of study QC samples were calculated for all compounds. Next, corrected data of biological samples (identified compounds only) were analyzed with PCA to detect outliers. In the current data set, one outlier was detected and was removed from further statistical analysis. Finally, RSDs of duplicates were calculated and afterwards one of two samples was randomly selected from remaining duplicate pairs to analyze variability. One duplicate pair was identified as an outlier due to contamination and was excluded.

Statistical analysis

Prior to statistical analysis, study QC corrected data were log-transformed for data normalization. To study whether endocannabinoid and related NAEs concentrations depend on gender or age, multiple linear regression analysis was applied. For each compound, its concentration was set as the dependent variable with gender and age as predictors. To study whether potential age effects are gender-specific, linear regression was repeated after splitting data by gender. Statistical analysis was performed with R software (version 3.0.3, function *lm*). All reported p-values are without multiple testing corrections. P-values <0.05 were considered significant

Result & Discussion

Method development

Although some analytical methods for profiling endocannabinoids and related NAEs in human plasma have been reported[25,27], methods for CSF are limited to anandamide, 2-AG, PEA and OEA[22,23]. To achieve a high-throughput and sensitive method for detection and quantification of these compounds, two important parameters were optimized. First, liquid chromatography conditions, including gradient and solvent composition, were optimized to obtain an adequate separation of molecules, especially isomers which are indistinguishable by fragmentation pattern, while at the same time maintaining a short chromatographic run time (**Fig.1**).

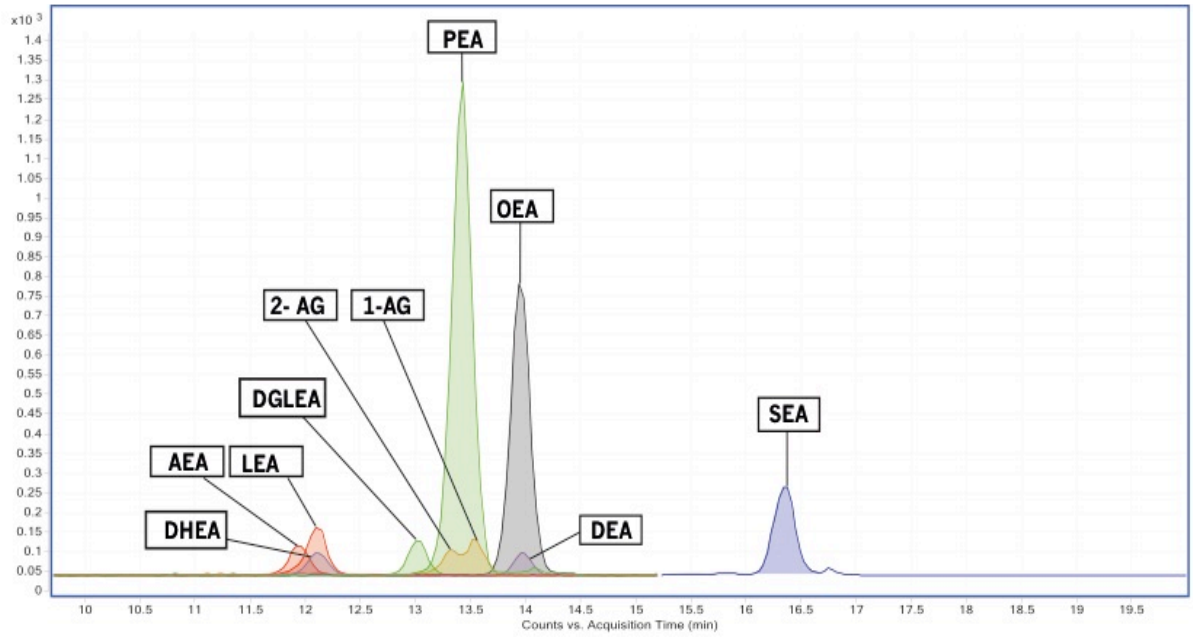

Figure 1: Overlay of MS/MS chromatograms of endocannabinoids and related NAEs in standard mix.

For example, DGLEA and EA350 are structural isomers, but are chromatographically separated (**Fig.2**). Next, optimal transitions were determined for each compound to maximize sensitivity, and for each MS/MS transition it was confirmed with standards that there is no cross-talk between compounds. This method uses dynamic MRM, which calculates optimal MRM parameters for multiple analytes using user inputs of retention times windows (delta RT) and cycle time and these parameters remain constant throughout all runs. The individual MRM dwell time is adjusted to maintain constant cycle

time which is selected to provide adequate sampling speed for quantitation of narrow LC peaks. When compared to traditional time segmented methods, dynamic MRM methods include fewer ion transitions per unit time during a typical MS scan, which results in longer dwell times for individual ion transitions. The MRM was operated in positive mode as the analytes were more efficiently ionized in that mode. For selective detection and quantification of co-eluting metabolites, specific precursor and fragment ions were used for their separation. For selective detection and quantification of co-eluting metabolites, specific precursor and fragment ions were used for their separation. The fragmentation pattern for *N*-acylethanolamine derivatives included the characteristic loss of m/z 62.1 resulting from the fragmentation of the amide bond (**Fig. S3A**). Our chip-based nano LC-MS/MS method allowed quantification of 12 endocannabinoids and related NAEs, along with eight putatively identified NAEs in CSF (**Table. S1**).

Table 2: Difference in %RSD (Relative Standard Deviation) expressed in percentage between 2-AG alone and combined 2-AG and 1-AG

Calibration levels	RSD (%)	
	2-AG	1-AG + 2-AG
C0	27	5
C1	38	8
C2	20	3
C3	15	11
C4	19	6
C5	16	8
C6	8	5
C7	3	4

The isomerisation from 2-AG to 1-AG due to acyl migration complicates the measurements of the two regio-isomers. As shown in **Table. 2**, the sum of 2-AG and 1-AG showed a superior RSD (5-11%) during batch measurement compared with 2-AG only (3-38%), which indicated that acyl migration might have occurred during sample preparation and measurement. Another contribution to that error could be problems with peak integration, as the two isomers are not separated at baseline. Based on this result, the sum of 1-AG and 2-AG was used for further data analysis in this paper. In LLE, toluene was previously reported to suppress acyl migration during the evaporation step to a large extent[35]. However,

moderate levels of acyl migration were observed in the current study and this is likely due to difference in matrices and sample handling procedures compared to previous studies. Moreover, this is the first study to use toluene extraction method for CSF whereas the previous studies were demonstrated in plasma [25,35]. Furthermore, it has been reported that elevated temperatures, presence of serum albumin in the sample, and high pH values accelerate acyl migration[35,36]. Interestingly, a recent study reports that in plasma 1-AG is not an endogenous compound but rather the result of chemical isomerization during sample storage, and therefore summing the concentrations of both the isomers will provide meaningful data for biological interpretation[27].

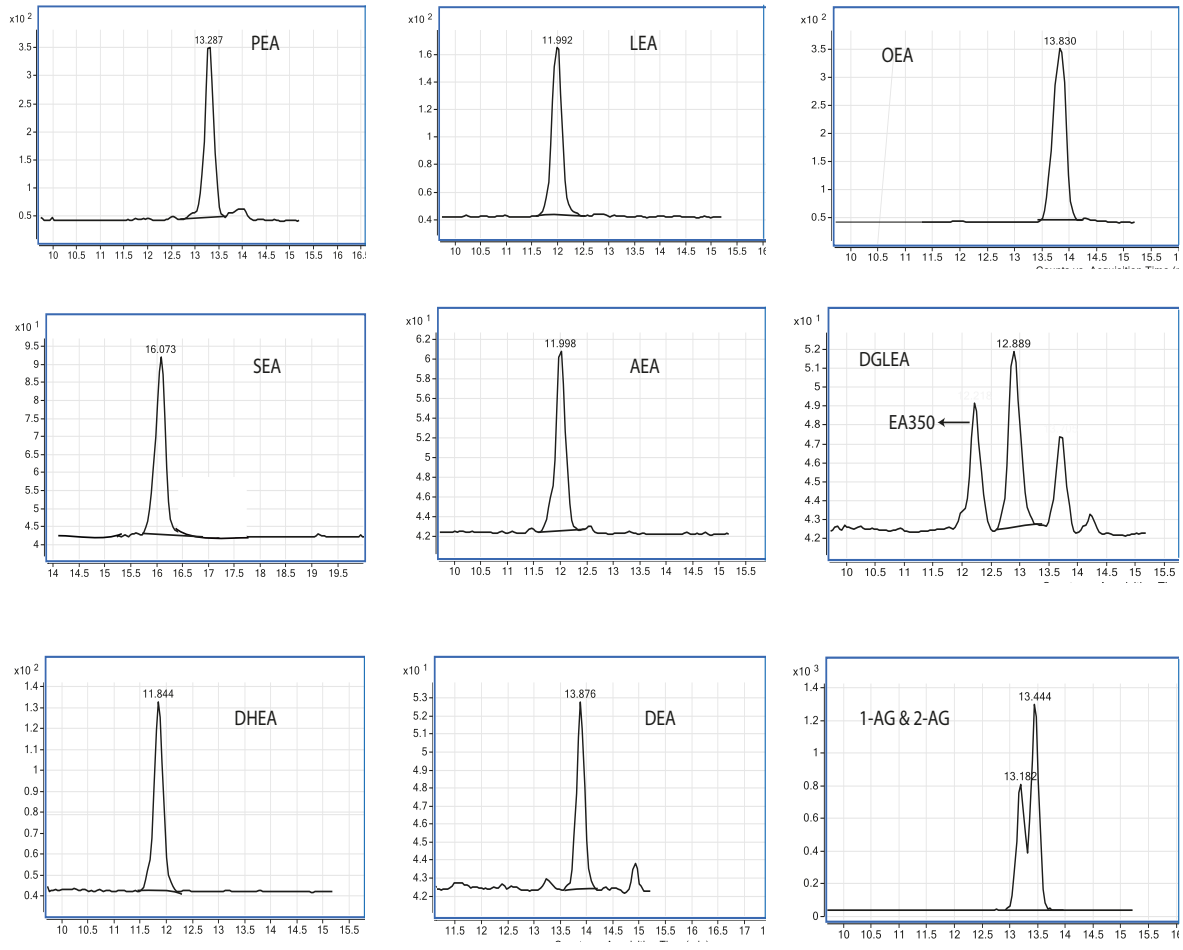

Figure 2. Endogenous peaks of endocannabinoids and related NAEs in CSF. The x-axis is retention time and the y-axis is response signal. X-axis is retention time and Y-axis is response signal.

The stability of endocannabinoids and NAEs and their ex-vivo generation, i.e. during and after sampling needs greater attention to avoid variability and inaccuracy of the

measurements. To date, the stability of endocannabinoids in CSF was not reported, but in blood NAEs concentrations dramatically increase when withdrawn blood samples are improperly stored. 2AG, 1AG levels were shown to be stable for 2h but a gradual reduction of 2AG was detected after 4h[25]. Here, the pooled CSF used for validation was not stored immediately at cold conditions after withdrawal, which might cause increased NAE and 2AG-1AG levels. This has no negative consequences for this study because these pooled samples were only used to assess the validation parameters by spiking the internal standards, and no biological conclusions were drawn from this pooled sample. The study samples, on the other hand, were processed and stored within 30min after sample collection to improve the stability and accuracy of the measurements.

Method validation

Validation was performed using pooled CSF samples. Linearity and sensitivity (LOD and LOQ) are summarized in Table 3. Precision (Intra and Inter-day) values are summarized in Table 4. Recovery and matrix effect are summarized in **Fig. 3.**

Table 3: **Validation parameters: Calibration range, Retention time, LOD (limits of detection), LOQ (limits of quantification)**

Compound (abbr.)	C	C=C	m/z	Calibration ranges (pM)	Retention time (min)	R^2	LOD (pM)	LOQ (pM)
PEA	16	0	299.5	4.7-4761	13.29	0.996	35.4	107.4
LEA	18	2	323.5	0.47-476	11.99	0.996	3.2	9.6
OEA	18	1	325.5	4.7-4761	13.83	0.997	14.4	43.7
SEA[a]	18	0	327.6	4.7-4761	16.07	0.976	146.9	445
AEA	20	4	347.5	0.47-476	12.00	0.997	0.28	0.86
DGLEA	20	3	349.6	0.47-476	12.89	0.996	0.53	1.6
DHEA	22	6	371.6	0.47-476	11.84	0.996	0.9	2.8
DEA	22	4	375.6	0.47-476	13.88	0.995	0.31	0.94
1-AG+ 2-AG	20	4	378.6	4.7-4761	13.44(1-AG) 13.18(2-AG)	0.997	20.2	61.2

"C" and "C=C" = number of carbon atoms and number of double bonds in the fatty acid chain of the molecule, respectively; m/z = mass-to-charge ratio; R^2= correlation coefficient; LOD= limit of detection; LOQ= limit of quantification. [a] The LOD and LOQ values of SEA are high due to the contaminant peak present in ethanol used during sample collection.

Linearity and sensitivity: Pooled CSF samples were spiked with 7 levels of calibration standards (**Table. 3**) to determine linearity, LOD, and LOQ for each compound (9 targets). The goodness-of-fit, R^2, ranges from 0.995 to 0.999 for all compounds [with the exception of SEA (R^2 0.976)], demonstrating that the method is linear in the selected calibration range (**Fig. S4**). The LOQs are between 0.9 and 61.2 pM for most of the compounds except for those with a contamination problem (PEA and SEA), which shows that the method is suitable for measuring endogenous levels in CSF (**Table. 5**).

Precision: The intra- and inter-batch variability were assessed using the standards spiked at three different concentrations (Low (C2), medium (C4) and high (C6)) in pooled CSF samples (**Table. 4**). Quadruplicate sample preparations were performed in each batch, and a total of three batches were processed. The intra-batch RSDs ranged from 1 to 23%. Possible batch-to-batch effects were calculated using the three calibration levels (C2, C4, and C6) measured on three different days. Inter-batch effects ranged from 3 to 21%.

Table 4: Analysis of pooled CSF samples showing precision (Intra- & inter-batch effect)

	Intra-batch precision (%)			Inter-batch precision (%)		
Compound	**Low (C2)**	**Middle (C4)**	**High (C6)**	**Low (C2)**	**Middle (C4)**	**High (C6)**
PEA	9	8	3	14	13	4
LEA	23	12	11	21	18	7
OEA	9	8	5	13	12	5
SEA	14	7	9	15	17	7
AEA	6	5	6	6	6	5
DGLEA	14	5	10	13	5	8
DHEA	5	1	3	4	5	3
DEA	9	3	5	10	7	4
1-AG+2-AG	11	5	2	14	9	11

The precision values are expressed in RSD (relative standard deviation). Low, Middle, High are three different concentration (for concentrations refer **Table.1**) used to show intra- and inter-batch precision.

Recovery, matrix effect. Recovery and Matrix effect were evaluated using deuterated compounds otherwise used as ISTDs (**Fig. 3**). Recovery was calculated as the ratio of the response of the ISTD of samples spiked before extraction versus samples spiked after extraction. If possible losses of organic phase during sample extraction were compensated by

using one of the deuterated ISTDs as ISTD (DHEA-d4), the recoveries were 81% to 119%. Matrix effect (ion suppression) was calculated as the ratio of the response of the ISTD spiked after extraction in matrix versus water. The matrix effect ranged from 38% to 81%. The ion suppression for these compounds most probably is due to co-eluting phospholipids. SEA-d3 was removed from **Fig. 3** due to ion suppression by the presence of a high concentration of unlabeled SEA contamination in the sample collection solvents (see above). The compounds had good recovery after correction by an ISTD added prior to extraction. The matrix effects differed between compounds. This does not present a problem as long as an isotopically labelled compound is available as an ISTD; fortunately, for those compounds for which isotopically ISTDs were not available, the matrix effects were reproducible. For target compounds with matching internal standards, the ISTD corrected concentrations were shown to have acceptable reproducibility. Among the detected compounds in the current method, seven compounds have their respective deuterated ISTD for analytical corrections, but for DGLEA and DEA, deuterated standards were not available. For these compounds, LEA-d4 and AEA-d4 respectively were chosen as their ISTDs due to their chemical similarly and their similar elution times.

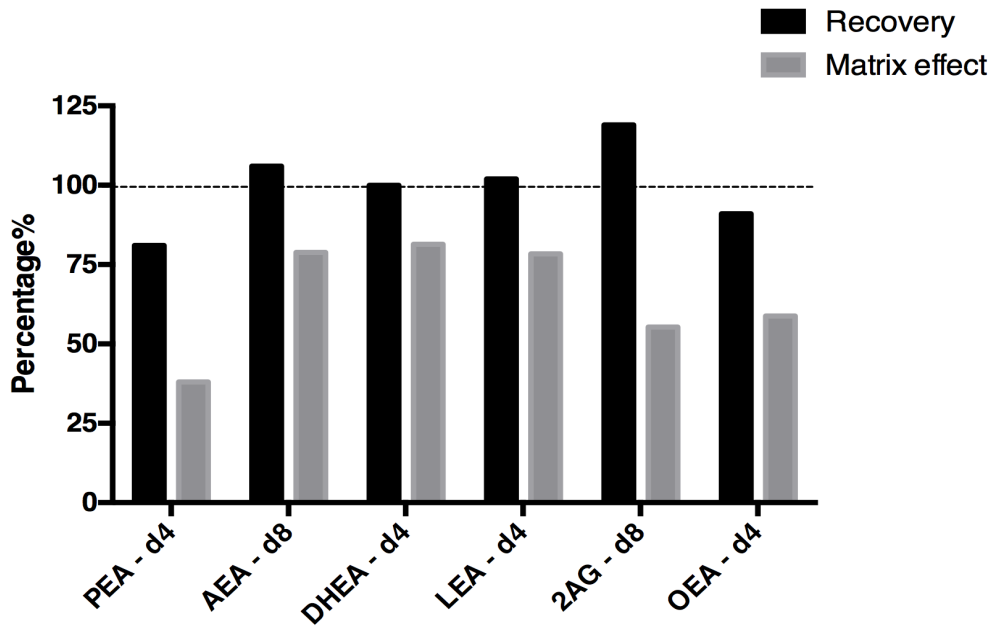

Figure 3: Recovery and matrix effect of deuterated internal standards in CSF. Recover and matrix effect values are expressed in percentages. Recovery: Higher values indicate better recoveries. Matrix effect: Values above 100% implies ion enhancement and below 100% implies ion suppression.

CSF endocannabinoids and related NAEs in healthy subjects

To demonstrate the applicability of the method, we measured 45 human CSF samples from 22 healthy females (mean age 30.9 years ± 12.8 years SD) and 23 healthy males (mean age 39.3 ± 16.5 SD). Nine compounds were detected and quantified (**Fig. 2**).

Table. 5: Concentrations of endocannabinoids and related NAEs quantified in 45 CSF samples of healthy subjects

Compound Name	Concentration (pM)				QC_ RSD (%) (n = 18)	Duplicate_ RSD (%) (n = 4 pairs)
	Min	Max	Median	SD		
PEA	41.4	270.4	83.7	48.7	10	48
LEA	3.6	28.8	9.6	6.2	10	33
OEA	22.0	116.6	44.4	19.0	15	20
SEA	67.0	310.3	108.4	54.5	13	57
AEA	0.5	2.7	1.6	0.5	10	14
DGLEA	0.4	2.2	1.0	0.4	5	6
DHEA	3.61	24.89	8.48	3.92	4	2
DEA	1.2	5.6	2.9	0.9	5	6
1-AG +2-AG	36.5	235.3	82.6	44.7	11	6

The RSD (relative standard deviation) expressed in percentage of QC (quality controls) and duplicates used during the analysis of healthy subjects. SD: Standard deviation

Endogenous concentrations and ranges of endocannabinoids measured in healthy subjects are listed in **Table. 5**. The concentrations of AEA and 2-AG are in line with the previous studies[37]. In addition to the compounds shown in Table 3, several putatively annotated NAEs were observed in human CSF (**Fig. S2**). Of note, an interesting observation in the current CSF samples is the ratio of DHEA/AEA being around 10, which is contrary to plasma, where the ratio is almost equal to 1(27). This could be because the availability of DHA is greater in CSF than arachidonic acid, precursors for DHEA and AEA, which are then processed downstream at equal rates. If this is not the case, this could indicate that the synthesizing enzymes have a preference for DHA to generate DHEA or, alternatively, it could be that AEA is a better substrate for FAAH than DHEA. However, further investigation is required to elucidate the exact reason, but this was not the main aim of this study.

The he identity of one of the putatively annotated NAEs, EA350 peak, was assigned as 5(Z),8(Z),11(Z)-eicosatrienoic acid ethanolamide using a commercially available authentic standard and the identity was further confirmed by comparing *m/z*, retention time and fragmentation pattern of the authentic standard. The MS/MS fragmentation is shown in **Fig. S3B**. In similar manner, the identities of all the remaining putatively annotated NAEs should be confirmed by purchasing authentic standards, however these standards are still not commercially available. Although further work needs to be done for annotating all metabolites and understanding the biological implications, this highly sensitive method clearly shows the applicability in measuring a broad range of endocannabinoids and related NAEs.

Although we could not confirm the identity for most of the putatively identified compounds and observed some matrix effect due to ion suppression, we believe that our method with this broader coverage of endocannabinoids and their congeners will help us to understand the biological insights of the endocannabinoid system as a "whole" in future studies, and to possibly understand the biological role of these putatively identified compounds. Moreover, this method depicted acceptable reproducibility and sensitivity of these molecules in the application to clinical samples such as the migraine samples.

Gender and age differences in healthy controls

It is important for designing large case-control studies to know whether endocannabinoids and related NAEs concentrations show a gender or age dependence. In our study, these factors were analyzed using data from healthy subjects using multiple linear regression analysis. Significant effects of age were present for DHEA. DHEA concentrations were higher in older males (**Fig. 4**). In blood, higher concentrations of docosahexaenoic acid (DHA), the fatty acid of DHEA, were reported in elderly (≥65 years, gender not reported)[38]. Intake of DHA can alter DHEA concentrations in blood and brain[39]. Additionally, age-related changes in DHA metabolism could play important roles as well[40]. There were no significant gender differences in endocannabinoids or related NAEs when corrected for the age imbalance (**Table. S2**). This study proves the importance of proper age and sex matching of cases and controls to obtain significant results in studies directed at discovery of endocannabinoid related biomarkers and/or to obtain novel insights in health and disease.

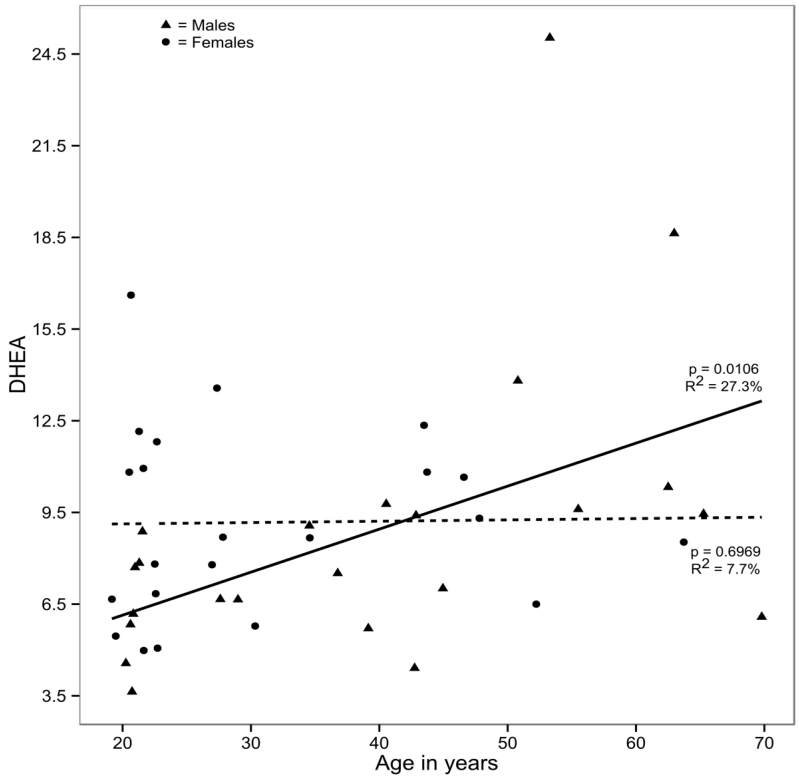

Figure 4: Relationships between DHEA concentrations and age . Linear regression lines are plotted separately for males (solid line) and females (dotted line). Solid circles represent males and solid triangles represent females. The y-axis shows relative concentrations (in picomoles) before log transformation.

Conclusion

A nano LC-ESI-MS/MS method for the simultaneous quantification of classical endocannabinoids and the related NAEs was developed and validated in human (clinical) CSF. We measured AEA, 2-AG, ten annotated NAEs and eight putatively annotated NAEs, whereas previously only four endocannabinoids had been measured in CSF [22,23]. Requiring only 200 µL of CSF per sample, this sensitive method has LODs reaching pM-fM levels while maintaining good linearity and precision. Application of this method in CSF from healthy humans resulted in novel insights on gender and age effects, i.e. concentrations of DHEA increased with age in males, illustrating the possibilities of this method to study the regulatory functions of endocannabinoids in the context of brain (dys)function.

Acknowledgement

This project received support from the Faculty of science ("Profiling Programme: Endocannabinoids"), Leiden University (VK, MvdS, TH). This project was financed by The Netherlands Metabolomics Centre, The Netherlands Genomics Initiative and The Netherlands Organization for Scientific Research (NWO). This work was supported by grants of the Netherlands Organization for Scientific Research (NWO) [VIDI 91711319 to G.M.T. & VICI 91856601 to M.D.F.] and the European Community (EC) [FP7-EUROHEADPAIN - no. 602633 to G.M.T., A.M.J.M.vdM. & M.D.F.]. This project has received funding from CoSTREAM project (http://www.costream.eu) within the European Union's Horizon 2020 research and innovation programme under grant agreement No 667375. SO was supported by Astellas. The authors acknowledge Agilent Technologies for their advice regarding the Chip Cube system. All organizations had no role in the design or conduct of the study.

References

1. Wilson, R. I. & Nicoll, R. a. Endocannabinoid signaling in the brain. *Science* **296,** 678–682 (2002).
2. Di Marzo, V. Endocannabinoid signaling in the brain: biosynthetic mechanisms in the limelight. *Nat. Neurosci.* **14,** 9–15 (2011).
3. Freund, T. F., Katona, I. & Piomelli, D. Role of endogenous cannabinoids in synaptic signaling. *Physiol. Rev.* **83,** 1017–66 (2003).
4. Di Marzo, V., Stella, N. & Zimmer, A. Endocannabinoid signalling and the deteriorating brain. *Nat. Rev. Neurosci.* **16,** 30–42 (2014).
5. Lutz, B., Marsicano, G., Maldonado, R. & Hillard, C. J. The endocannabinoid system in guarding against fear, anxiety and stress. *Nat. Rev. Neurosci.* **16,** 705–718 (2015).
6. Fernández-Ruiz, J., Moro, M. A. & Martínez-Orgado, J. Cannabinoids in Neurodegenerative Disorders and Stroke/Brain Trauma: From Preclinical Models to Clinical Applications. *Neurotherapeutics* **12,** 793–806 (2015).
7. Soltesz, I. *et al*. Weeding out bad waves: towards selective cannabinoid circuit control in epilepsy. *Nat. Rev. Neurosci.* **16,** 264–277 (2015).
8. Katona, I. & Freund, T. F. Endocannabinoid signaling as a synaptic circuit breaker in neurological disease. *Nat. Med.* **14,** 923–930 (2008).
9. Mechoulam, R., Hanuš, L. O., Pertwee, R. & Howlett, A. C. Early phytocannabinoid chemistry to endocannabinoids and beyond. *Nat. Rev. Neurosci.* **15,** 757–764 (2014).
10. Di Marzo, V. Targeting the endocannabinoid system: to enhance or reduce? *Nat. Rev. Drug Discov.* **7,** 438–55 (2008).
11. Fowler, C. J. Transport of endocannabinoids across the plasma membrane and within the cell. *FEBS J.* **280,** 1895–1904 (2013).
12. Ho, W.-S. V, Barrett, D. A. & Randall, M. D. "Entourage" effects of N-palmitoylethanolamide and N-oleoylethanolamide on vasorelaxation to anandamide occur through TRPV1 receptors. *Br. J. Pharmacol.* **155,** 837–46 (2008).
13. Bradshaw, H. B. & Walker, J. M. The expanding field of cannabimimetic and related lipid mediators. *Br. J. Pharmacol.* **144,** 459–65 (2005).
14. Tsuboi, K. *et al*. Biosynthetic pathways of bioactive N-acylethanolamines in brain. *CNS Neurol. Disord. Drug Targets* **12,** 7–16 (2013).
15. Urquhart, P., Nicolaou, A. & Woodward, D. F. Endocannabinoids and their oxygenation by cyclo-oxygenases, lipoxygenases and other oxygenases. *Biochimica et Biophysica Acta - Molecular and Cell Biology of Lipids* **1851,** 366–376 (2015).
16. Rouzer, C. A. & Marnett, L. J. Endocannabinoid oxygenation by cyclooxygenases, lipoxygenases, and cytochromes P450: cross-talk between the eicosanoid and endocannabinoid signaling pathways. *Chem. Rev.* **111,** 5899–921 (2011).
17. Brown, P. D., Davies, S. L., Speake, T. & Millar, I. D. Molecular mechanisms of cerebrospinal fluid production. *Neuroscience* **129,** 957–970 (2012).
18. Koppel, J. *et al*. Endocannabinoids in Alzheimer's disease and their impact on normative cognitive performance: a case-control and cohort study. *Lipids Health Dis.* **8,** (2009).
19. Romigi, A. *et al*. Cerebrospinal fluid levels of the endocannabinoid anandamide are reduced in patients with untreated newly diagnosed temporal lobe epilepsy. *Epilepsia* **51,** 768–72 (2010).
20. Leweke, F. M. *et al*. Anandamide levels in cerebrospinal fluid of first-episode schizophrenic patients: impact of cannabis use. *Schizophr. Res.* **94,** 29–36 (2007).
21. Morgan, C. J. a *et al*. Cerebrospinal fluid anandamide levels, cannabis use and psychotic-like symptoms. *Br. J. Psychiatry* **202,** 381–2 (2013).

22. Jumpertz, R., Guijarro, A., Pratley, R. E., Piomelli, D. & Krakoff, J. Central and peripheral endocannabinoids and cognate acylethanolamides in humans: association with race, adiposity, and energy expenditure. *J. Clin. Endocrinol. Metab.* **96,** 787–91 (2011).
23. Di Filippo, M., Pini, L. A., Pelliccioli, G. P., Calabresi, P. & Sarchielli, P. Abnormalities in the cerebrospinal fluid levels of endocannabinoids in multiple sclerosis. *J. Neurol. Neurosurg. Psychiatry* **79,** 1224–9 (2008).
24. Giuffrida, A. *et al.* Cerebrospinal anandamide levels are elevated in acute schizophrenia and are inversely correlated with psychotic symptoms. *Neuropsychopharmacology* **29,** 2108–14 (2004).
25. Fanelli, F. *et al.* Estimation of reference intervals of five endocannabinoids and endocannabinoid related compounds in human plasma by two dimensional-LC/MS/MS. *J. Lipid Res.* **53,** 481–493 (2012).
26. Balvers, M. G. J., Wortelboer, H. M., Witkamp, R. F. & Verhoeckx, K. C. M. Liquid chromatography-tandem mass spectrometry analysis of free and esterified fatty acid N-acyl ethanolamines in plasma and blood cells. *Anal. Biochem.* **434,** 275–83 (2013).
27. Pastor, A., Farré, M., Fitó, M., Fernandez-Aranda, F. & de la Torre, R. Analysis of ECs and related compounds in plasma: artifactual isomerization and ex vivo enzymatic generation of 2-MGs. *J. Lipid Res.* **55,** 966–77 (2014).
28. Iannotti, F. A. *et al.* Analysis of the "endocannabinoidome" in peripheral tissues of obese Zucker rats. *Prostaglandins. Leukot. Essent. Fatty Acids* **89,** 127–35 (2013).
29. Saz, J. M. & Marina, M. L. Application of micro- and nano-HPLC to the determination and characterization of bioactive and biomarker peptides. *J. Sep. Sci.* **31,** 446–58 (2008).
30. Houbart, V. *et al.* A validated microfluidics-based LC-chip-MS/MS method for the quantitation of fluoxetine and norfluoxetine in rat serum. *Electrophoresis* **33,** 3370–9 (2012).
31. Houbart, V. *et al.* Development of a nano-liquid chromatography on chip tandem mass spectrometry method for high-sensitivity hepcidin quantitation. *J. Chromatogr. A* **1218,** 9046–54 (2011).
32. Strassburg, K. *et al.* Quantitative profiling of oxylipins through comprehensive LC-MS/MS analysis: application in cardiac surgery. *Anal. Bioanal. Chem.* **404,** 1413–26 (2012).
33. Skonberg, C., Artmann, A., Cornett, C., Hansen, S. H. & Hansen, H. S. Pitfalls in the sample preparation and analysis of N-acylethanolamines. *J. Lipid Res.* **51,** 3062–73 (2010).
34. van der Kloet, F. M., Bobeldijk, I., Verheij, E. R. & Jellema, R. H. Analytical Error Reduction Using Single Point Calibration for Accurate and Precise Metabolomic Phenotyping. *J. Proteome Res.* **8,** 5132–5141 (2009).
35. Zoerner, A. A. *et al.* Simultaneous UPLC-MS/MS quantification of the endocannabinoids 2-arachidonoyl glycerol (2AG), 1-arachidonoyl glycerol (1AG), and anandamide in human plasma: minimization of matrix-effects, 2AG/1AG isomerization and degradation by toluene solvent extractio. *J. Chromatogr. B. Analyt. Technol. Biomed. Life Sci.* **883–884,** 161–71 (2012).
36. Rouzer, C. A., Ghebreselasie, K. & Marnett, L. J. Chemical stability of 2-arachidonylglycerol under biological conditions. *Chem. Phys. Lipids* **119,** 69–82 (2002).
37. Nicholson, J. *et al.* Leptin levels are negatively correlated with 2-arachidonoylglycerol in the cerebrospinal fluid of patients with osteoarthritis. *PLoS One* **10,** e0123132 (2015).

38. Fortier, M. *et al*. Higher plasma n-3 fatty acid status in the moderately healthy elderly in southern Québec: higher fish intake or aging-related change in n-3 fatty acid metabolism? *Prostaglandins. Leukot. Essent. Fatty Acids* **82,** 277–80 (2010).
39. Meijerink, J., Balvers, M. & Witkamp, R. N-Acyl amines of docosahexaenoic acid and other n-3 polyunsatured fatty acids - from fishy endocannabinoids to potential leads. *Br. J. Pharmacol*. **169,** 772–83 (2013).
40. Plourde, M. *et al*. Plasma incorporation, apparent retroconversion and β-oxidation of 13C-docosahexaenoic acid in the elderly. *Nutr. Metab. (Lond)*. **8,** 5 (2011).

Supplementary information

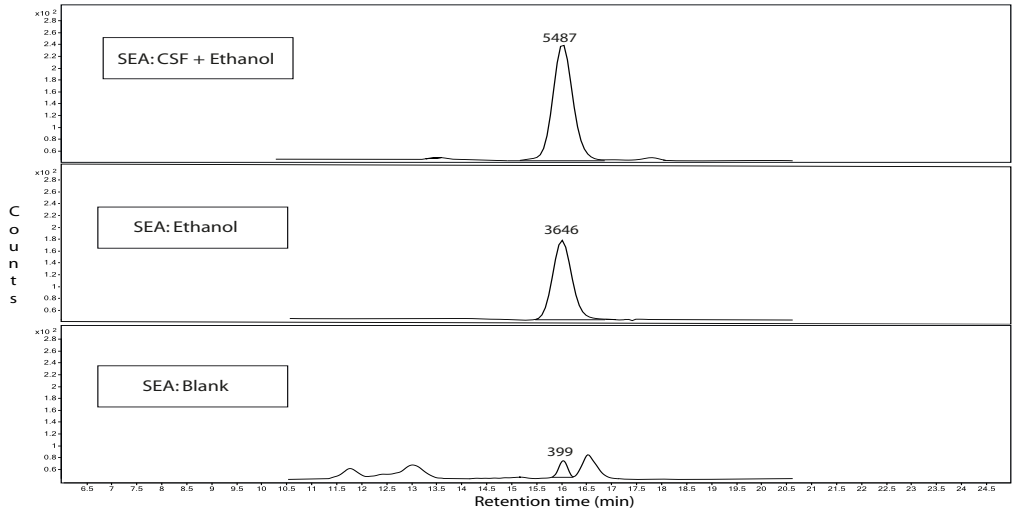

Figure S1: Contaminant of SEA from ethanol and blank(MeOH/H2O). Top window: chromatogram of SEA in sample with ethanol. Middle window: chromatogram of background SEA in pure ethanol. Bottom window: Chromatogram of background SEA in blank. X-axis is retention time and Y-axis is response signal.

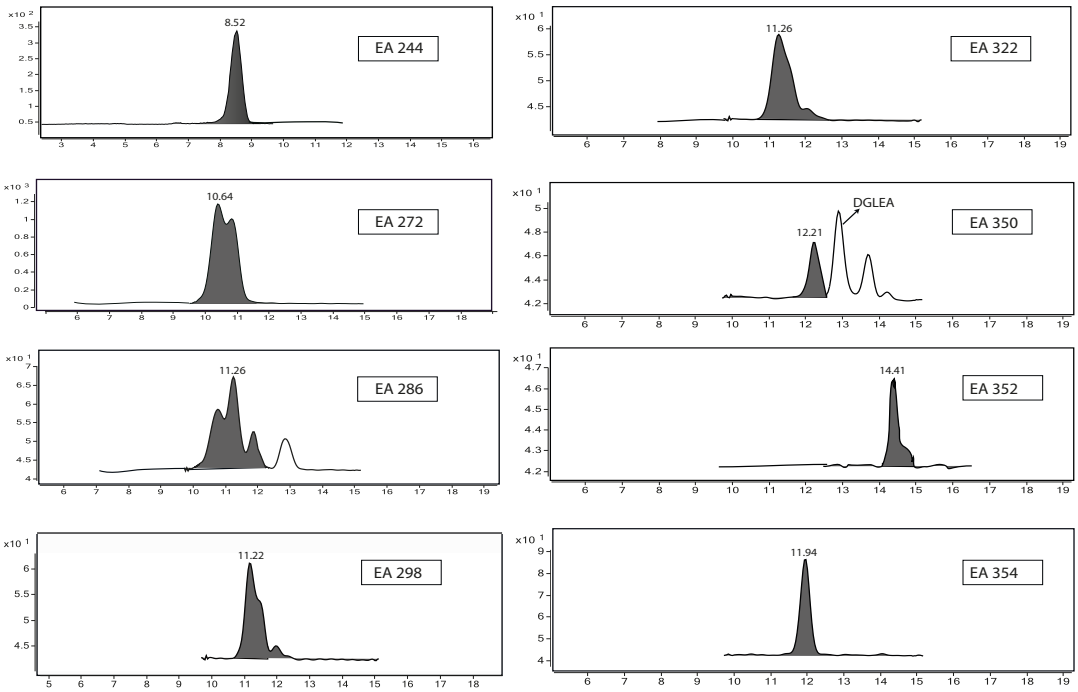

Figure S2: Chromatograms of putatively annotated NAEs in CSF. Putatively annotated NAEs are labeled as EA (from ethanolamine) followed by molecular mass (*m/z*) value. X-axis is retention time and Y-axis is response signal.

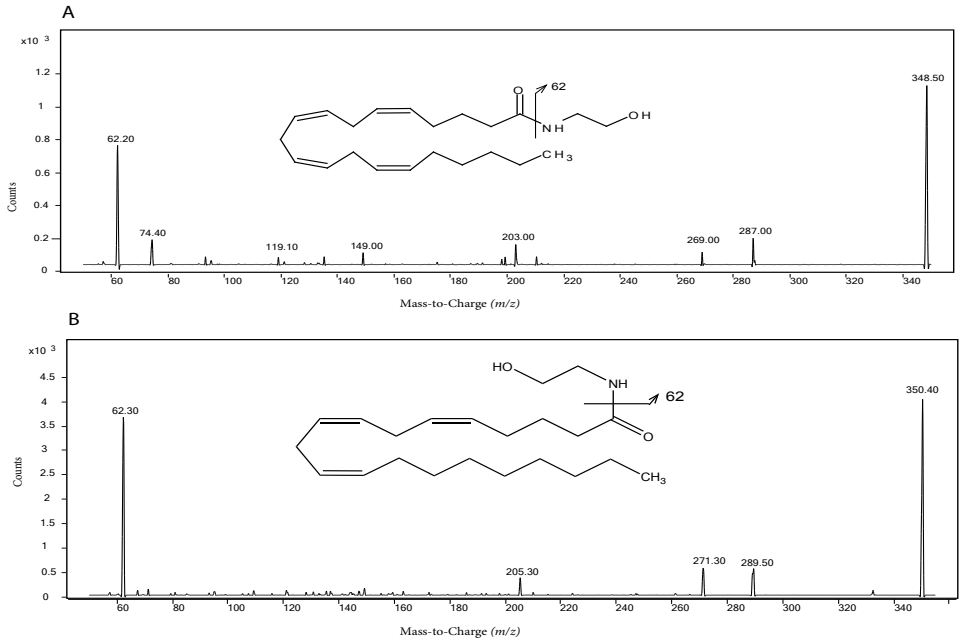

Figure S3: MS/MS fragmentation mass spectra of anandamide and EA350 Fragmentation pattern of (A) anadamide (384.2>62.3) and putatively annotated NAE, (B) EA350 (350.4>62.3) in positive mode at a collision energy of 10V. X-axis is m/z and Y-axis is response signal.

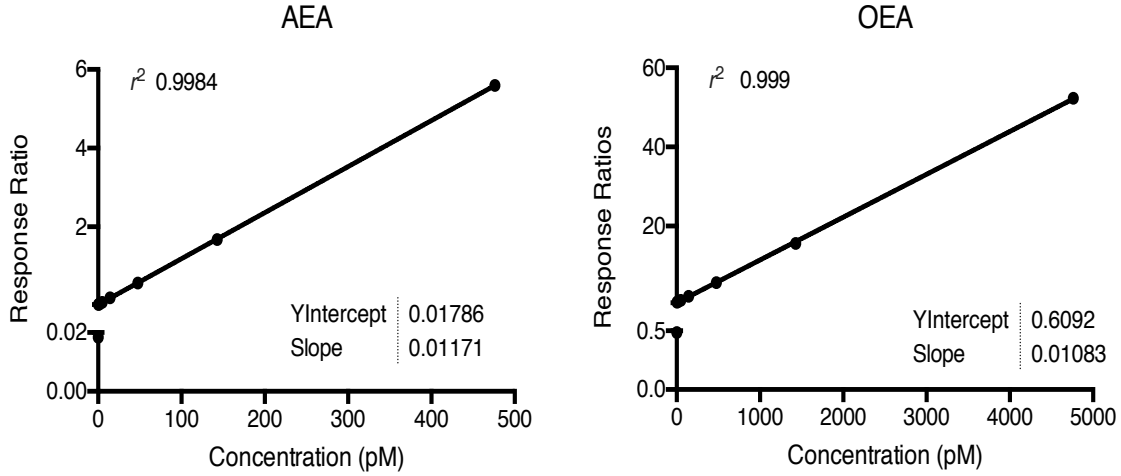

Figure S4: Calibration curves for AEA and OEA compounds. The displayed calibration curves are constructed in matrix (standard-addition method) in their respective dynamic ranges and the y-intercept of the curve represents the endogenous concentrations.

Table S1: MRM (Multiple reaction monitoring) parameters of the target list

Compound Name	C	C = C	MW g/mole	Compound name	Precursor Ion (m/z)	Product Ion (m/z)	Dwell time (msec)	CE
Identified								
PEA	16	0	299.5	*N*-palmitoylethanolamide	300.3	62.1	20	10
LEA	18	2	323.5	*N*-linoleoylethanolamide	324.3	62.1	50	10
OEA	18	1	325.5	*N*-oleoylethanolamide	326.3	62.1	50	10
SEA	18	0	327.6	*N*-stearoylethanolamide	328.3	62.1	300	10
AEA	20	4	347.5	*N*-arachidonoyl ethanolamide	348.3	62.1	200	10
DGLEA	20	3	349.6	*N*-dihomo-γ-linol enoylethanolamide	350.3	62.1	400	10
DHEA	22	6	371.6	*N*-docosahexaenoyl ethanolamide	372.3	62.1	100	10
DEA	22	4	375.6	*N*-docosatetraenoyl ethanolamide	376.3	62.1	400	10
1&2-A[a]	20	4	378.6	*N*-arachidonoylglycerol	379.3	287.1	100	5
Internal Standards								
PEA - d4	16	0	303.5	*N*-palmitoylethanolamide - d4	304.3	62.1	20	10
LEA - d4	18	2	327.5	*N*-linoleoylethanolamide - d4	328.3	66.1	20	10
OEA - d4	18	1	329.6	*N*-oleoylethanolamide - d4	330.3	66.1	20	10
SEA - d3	18	0	330.6	*N*-stearoylethanolamide - d3	331.3	62.1	100	10
AEA - d8	20	4	355.6	*N*-arachidonoylethanolamide - d8	356.3	62.1	20	10
DHEA - d4	22	6	375.6	*N*-docosahexaenoylethanolamide- d4	376.3	66.1	20	10
2-AG - d8	20	4	386.6	*N*-arachidonoylglycerol - d8	387.3	294.1	100	10
Putatively annotated								
EA244	12	0	243.5	*N*-laurylethanolamide	244.3	62.1	800	10
EA272	14	0	271.5	*N*-myristylethanolamide	272.3	62.1	400	10
EA286	15	0	285.5	*N*-pentadecanoyl ethanolamide	286.3	62.1	800	10

EA298	16	1	297.5	*N*-palmitoleoyl ethanolamide	298.3	62.1	50	10
EA322	18	3	321.5	*N*-α-linolenyl ethanolamide	322.3	62.1	100	10
EA350	20	3	349.5	*N*-eicosatrienoyl ethanolamide	350.3	62.1	150	10
EA352	20	2	351.5	*N*-eicosadienoyl ethanolamide	352.3	62.1	150	10
EA354	20	1	353.5	*N*-eicosenoyl ethanolamide	354.3	62.1	50	10

Not detected in CSF

O-AEA	20	4	347.5	*O*-arachidonoyl ethanolamine	348.3	62.1	200	10
NADA	20	4	439.6	*N*-arachidonoyldopamine	440.4	137	50	25
2-AGE	20	4	364.6	2-arachidonyl glyceryl ether	365.2	273.1	50	13

The target list includes identified compounds, deuterated ISTDs, putatively annotated compounds and compounds which are included in the list but are not detected in the sample. All compounds are analyzed in positive mode. The fragmentor voltage is at 100V for all transitions. "C" and "C=C" = number of carbon atoms and number of double bonds in the fatty acid chain of the molecule, respectively; MW= molecular weight (g/mole); m/z = mass-to-charge ratio; CE= Collision energy (volts); [a] Parameters are same for 1-AG and 2-AG.

Table S2: Results from linear regression analysis (n=45 healthy controls)

(A)

Compound	Gender			Age			R^2
	Coefficient	*95% C.I.*	*P-value*	*Coefficient*	*95% C.I.*	*P-value*	
DHEA	**1.1795**	**[0.9351; 1.4878]**	**0.1588**	**1.0097**	**[1.0020; 1.0175]**	***0.015**	14.4%
DEA	0.9857	[0.7902; 1.2296]	0.8960	1.0004	[0.9931; 1.0077]	0.919	0.1%
DGLEA	1.1698	[0.9230; 1.4826]	0.1889	1.0018	[0.9939; 1.0097]	0.653	4.1%
AEA	0.9270	[0.7483; 1.1484]	0.4790	1.0040	[0.9969; 1.0111]	0.267	5.4%
1&2-AG	1.0694	[0.8331; 1.3726]	0.5906	1.0044	[0.9961; 1.0127]	0.295	2.8%
LEA	1.0738	[0.7618; 1.5137]	0.6776	1.0009	[0.9896; 1.0123]	0.876	0.4%
PEA	0.9989	[0.7705; 1.2950]	0.9932	1.0000	[0.9915; 1.0087]	0.991	0.0%
OEA	1.0917	[0.8712; 1.3680]	0.4368	1.0016	[0.9942; 1.0091]	0.663	1.6%
SEA	1.0338	[0.8182; 1.3063]	0.7755	0.9981	[0.9904; 1.0058]	0.615	1.1%
EA354	0.9867	[0.9509; 1.0238]	0.4672	0.9994	[0.9982; 1.0006]	0.322	2.8%
EA350	0.9667	[0.7446; 1.2552]	0.7951	1.0052	[0.9966; 1.0139]	0.232	4.2%
EA352	1.0897	[0.8656; 1.3716]	0.4557	1.0039	[0.9963; 1.0116]	0.309	3.0%
EA298	1.1462	[0.8317; 1.5796]	0.3956	1.0116	[1.0009; 1.0224]	*0.034	10.4%
EA286	1.1764	[0.8131; 1.7021]	0.3798	1.0066	[0.9944; 1.0190]	0.284	3.6%
EA244	0.9283	[0.5816; 1.4816]	0.7496	0.9982	[0.9829; 1.0138]	0.817	0.3%
EA272	0.9624	[0.6535; 1.4172]	0.8425	0.9969	[0.9842; 1.0097]	0.623	0.6%
EA322	1.0782	[0.6364; 1.8266]	0.7747	0.9961	[0.9788; 1.0136]	0.651	0.9%

(B)

		Age			R^2
		Coefficient	*95% C.I.*	*P-value*	
Males	DHEA	1.0141	[1.0036; 1.0246]	0.0106	27.3%
Females	DHEA	1.0023	[0.9902; 1.0146]	0.6969	7.7%

(A) For each compound, its relative concentration was set as dependent variable with gender and age as predictors. Regression coefficients were exponentiated because the dependent variable was log-transformed. **(B)** Regression analysis split by gender for DHEA.

Chapter 4

Investigating the players of 2-arachidonyl glycerol biosynthesis in cellular system

Vasudev Kantae*, Annelot C. M. van Esbroeck*, Juan Zhou, Amy C Harms, Thomas Hankemeier*, Mario van der Stelt*

* *Authors contributed equally*

Manuscript in preparation

Abstract

The endocannabinoid 2-AG is an important signaling lipid, which interacts with the cannabinoid CB1 and CB2 receptors. 2-AG is synthesized by diacylglycerol lipase-α (DAGL-α) and DAGL-β, but their respective contribution to 2-AG synthesis remains unclear. In this study, we investigate which isoform of DAGLs takes lead in the biosynthesis of 2-AG using Neuro2A cellular model, a DAGL expressing murine neuroblastoma cell line. Activity based protein profiling (ABPP) was employed to assess DAGL activity and lipidomics to quantify downstream effects. We confirmed *in situ* DAGL-β inhibition by DH376, a potent *in vivo* active DAGL inhibitor, while DAGL-α could not be detected. Lipidomics revealed a dose-dependent reduction of 2-AG levels upon DH376 treatment, thereby confirming a functional effect of the inhibitor. Next, DAGL knock-out populations (DAGL-α KO, DAGL-β KO, DAGL-α, -β double KO) were generated in Neuro2A cells using CRISPR/Cas9-technology. The KO of DAGL-β was confirmed in the gel-based ABPP assay, whereas DAGL-α could not be detected in either WT or KO populations. Lipidomics, however, revealed no significant reduction of 2-AG levels in any of these DAGL KOs, whereas DH376 substantially suppressed 2-AG levels in these cells. These data suggest the presence of additional enzymes responsible for 2-AG synthesis, which can be targeted by DH376. Identification, validation and characterization of these additional enzymes is currently ongoing.

Introduction

2-Arachidonylglycerol (2-AG) is an important signaling lipid and an intermediate in lipid metabolism [1,2]. 2-AG and anandamide (AEA) are well-studied ligands in the endocannabinoid class, that interact with the cannabinoid CB1 and CB2 receptors. Endocannabinoids and cannabinoid receptors are part of an endogenous signaling system, the endocannabinoid system (ECS) [3]. ECS is involved in plethora of physiological and pathological processes and is emerging as a therapeutic drug target [4–6]. 2-AG is the most abundant endocannabinoid present in the brain and is the primary mediator in neurogenesis, synaptic transmission, synapse formation thereby mediating synaptic plasticity [7,8]. Several lines of evidence show the involvement of 2-AG in various pathological conditions like obesity [9], neuro-inflammation [10], anxiety [11], addiction [12,13] and pain [14].

2-AG is synthesized primarily by two main different pathways. A signaling pathway via a two-step process starting from sn-2 arachidonoyl phosphatidylinositol 4,5-bisphosphate (PIP2). In the first step, PIP2 is hydrolyzed into arachidonyl-containing diacylglycerol (DAG) species by phospholipase Cβ (PLCβ), which is activated by various G-protein-coupled receptors. The second step is catalyzed by diacylglycerol lipase (DAGL-α and -β), in which DAG is converted into 2-AG in a sn-1 specific manner. A second metabolic pathway starting from PIP2 towards phosphathidyl inositol (PI) by PIP2 phosphatases, followed by hydrolysis of sn-1-ester by phospholipase A1 to generate 2-arachidonyl-LPI. In the final step, phosphate is removed by lysophospholipase C (LysoPLC) to form 2-AG.

2-AG is synthesized "on demand" mainly by DAGL-α (120 kDa) and DAGL-β (70 kDa). Both enzymes belong to the serine hydrolase family and structurally differ by the presence of a long C-terminal tail (~300 amino acids) in DAGL-α [15]. Both enzymes are expressed in developing and adult brain and the localization of both enzymes markedly shift during the brain development [16,17]. Genetic studies using DAGL knockout (KO) mice have shown that DAGL-α and DAGL-β regulate 2-AG production in a tissue-type-dependent manner [18–20]. For instance, 2-AG levels in the CNS of DAGL-α and -β knockout mice were reduced 80% and 50% respectively. However, in the liver of DAGL-β knockout mice 2-AG levels were reduced 90%, while they were reduced only 50% in DAGL-α knockout mice [18]. Previous genetic KO studies suggest that DAGL-α was the predominant 2-AG synthesizing enzyme in neurons and participates in endocannabinoid-mediate plasticity, while DAGL-β is dominant in microglia [21] and in peripheral tissues like liver, [18] and has been implicated in inflammatory response in macrophages [22]. Another study in hippocampal neurons suggest

that DAGL-β is capable of eliciting endocannabinoid-mediated synaptic plasticity under certain conditions and both isoforms of DAGL can cooperatively mediate synaptic transmission at both excitatory and inhibitory synapses [23]. To this end, the above studies indicate that two isoforms of DAGL are responsible for production of 2-AG, but which isoform majorly contributes to 2-AG synthesis still remains to be elucidated.

To study the physiological role of DAGL, highly selective potent inhibitors are required. Selective inhibitors for the DAGL subtypes have not been identified yet. Dual DAGL-α and -β inhibitors were used to study the physiological role of 2-AG in health and disease models [24–26]. Recently, Ogasawara *et al*. reported the first CNS *in vivo* active dual DAGL-α/ β inhibitor DH376. Lipid analysis in brain revealed extensive reorganization of lipid signaling networks (including anandamide signaling) upon DAGL inhibition by DH376, which largely mirrors the myriad lipid changes observed in the brains of DAGLα–/– mice [27]. This indicates the key role of DAGLs in orchestrating the lipid cross-talks in the brain. In addition, the effect of DH376 was assessed in Neuro2A cellular model [28] but which isoform of DAGL is taking lead in 2-AG synthesis is not studied yet.

To investigate the activity and selectivity of the enzyme inhibitors, Activity-based protein profiling (ABPP) can serve as a powerful profiling technique for discovering selective inhibitors acting in their physiological context. ABPP is unique in its ability to rapidly identify inhibitor activity and selectivity within large enzyme families in complex protein samples [29]. To monitor the activity of DAGL, it is also important to quantify the downstream effects, endocannabinoid production in this case. Therefore, an LC-MS/MS platform was developed and applied to quantitatively profile the endocannabinoids, 2-AG and AEA and other related congeners in neuronal cells which allows better understanding of DAGL physiological role at molecular level. Generating specific DAGL subtype knockouts allows to better understand which subtype of DAGL is contributing more for 2-AG synthesis. To this end, CRISPR-Cas9 technology was employed that allows efficient targeted genome editing in all organisms without leaving any foreign DNA. This RNA-guided DNA endonuclease, Cas9 method exhibits higher fidelity and low cell toxicity when compared with traditional gene editing techniques. CRISPR-Cas9 can be used for knocking out specific gene expression, so that the function of that particular gene can be elucidated [30,31].

The objective of this study is to investigate which DAGL isoform takes lead in 2-AG biosynthesis in a cellular system. The functional effect of DAGLs in Neuro2A cell model was assessed using DH376, a dual inhibitor for DAGL-α and-β, by ABPP and lipidomics. CRISPR/Cas9 technology was used to generate DAGL-α and DAGL-β single and double knockout Neuro2A lines to study the role of the two DAGL isoforms in this cellular system.

Materials and Methods

General cell culture

Neuro2A wildtype and knockout cell lines were used as a cell model. Cells were cultured at 37 °C under 7% CO_2 in DMEM containing phenol red, glutamax, 10% (v/v) Newborn Calf Serum (Thermo Fisher), and penicillin and streptomycin (200 μg/mL each; Duchefa). Medium was refreshed every 2-3 days and cells were passaged twice a week at 80-90% confluence by resuspension in fresh medium. In the treatments methods below, the term *in situ* is used to designate experiments in which live cells are treated with inhibitors.

Neuro2A treatment for Lipidomics

2.5 million cells in 4 mL complete DMEM per 6 cm dish were seeded 40-48 h prior to treatment initiation. Cell viability was checked by Trypan Blue staining in a TC20 automated Cell Counter (Bio-Rad) and was 95% or higher at time of cell seeding.

Prior to treatment, culture medium was aspirated and cells were washed carefully (to prevent detachment of the cells) with 2 mL PBS. Subsequently 2 mL treatment medium (serum-free DMEM, 0.1% DMSO (vehicle), 0-10 μM DH376) was added to each dish and cells were incubated (1h or 2 h, 37 °C, 7% CO_2). After incubation, treatment medium was aspirated and cells were carefully washed with 2 mL PBS. Cells were harvested in 1250 μL PBS using a P1000 micropipette. Cell viability was checked for part of the samples by Trypan Blue staining in a TC20 automated Cell Counter (Bio-Rad) and was 90-99%. 1000 μL of the cell suspension was transferred to a low binding Eppendorf tube and cells were pelleted (1000 *g*, 3 min, RT). The supernatant was aspirated and cell pellets were snap frozen in liquid nitrogen and stored at -80 °C until lipidomics analysis.

The remaining cell suspension (250 μL) was transferred to an Eppendorf tube and snap frozen in liquid N_2 immediately. This suspension was thawed on ice and homogenized using a probe sonicator (5 sec/sample, 30% amplitude). Protein concentrations of these lysates were determined by Bradford Protein Assay and used for normalization purposes.

Neuro2A treatment for ABPP

Cells were seeded at 1:6 from an 80% confluent 10cm dish to a 6-well plate 48 hours prior to treatment initiation. Prior to treatment, culture medium was aspirated and cells were carefully washed with 1 mL PBS. Subsequently 1 mL treatment medium (serum-free DMEM, 0.1% DMSO (vehicle), 0/100 nM DH376) was added to each dish and cells were incubated (2 h, 37 °C, 7% CO_2). After incubation, treatment medium was aspirated and cells were carefully

washed with 1 mL PBS. Cells were harvested in 1 mL PBS using a P1000 micropipette. The cell suspension was transferred to a low binding Eppendorf tube and cells were pelleted (1000 *g*, 3 min, RT). The supernatant was aspirated and cell pellets were snap frozen in liquid nitrogen and stored at -80 °C until whole lysate preparation and ABPP analysis.

ABPP

Whole cell lysate preparation

Cell pellets were thawed on ice, resuspended in cold lysis buffer (20 mM HEPES pH 7.2, 250 mM sucrose, 1 mM $MgCl_2$, 2.5 U/mL benzonase) and incubated on ice (~15 min). Protein concentrations were determined by a Bradford Protein Assay (Bio-Rad), samples were diluted to 2.0 mg/mL in buffer (20 mM Hepes, pH 7.2) and are analyzed immediately.

ABPP: Direct activity based probes

Gel-based activity based protein profiling (ABPP) was performed and analyzed with minor adaptations on previously reported procedures [32]. *In situ* treated cells (15 μL whole lysate, 2.0 mg/mL) were directly incubated with the activity based probe (1 µM or 2 µM MB064 [24] or 500 nM FP-TAMRA, 20 min, RT). Reactions were quenched with 4* Laemmli buffer (5 μL, 240 mM Tris (pH 6.8), 8% (w/v) SDS, 40% (v/v) glycerol, 5% (v/v) β-mercaptoethanol, 0.04% (v/v) bromophenol blue). Samples were resolved on a 10% acrylamide SDS-PAGE gel (180 V, 80 min), scanned using Cy3 and Cy5 multichannel settings (605/50 and 695/55, filters respectively) (ChemiDoc MP, Bio-Rad) and subsequently stained with Coomassie as a protein loading control. Fluorescence was normalized to Coomassie staining and quantified with Image Lab (Bio-Rad). IC_{50} curves were fitted with Graphpad Prism® 7.

LC-MS/MS based lipidomics

The endocannabinoid extraction and LC-MS/M analysis was adapted from our previously developed method[32]. The concentration using 2-2.5 million cells of Neuro2A was determined after correction with isotopically labeled internal standards and individual calibration curves and normalized to protein concentrations. A targeted list of 24 endocannabinoids and NAEs were monitored out of which 16 were detected and quantified. The method was validated in terms of precision, recovery and matrix effects (**Fig. S1-S3**). The absolute values of endocannabinoids and NAEs in Neuro2A cells are listed in **Table. S1**.

Results and discussion

Function of DAGLs in cellular system

To investigate whether DAGLs are responsible for 2-AG synthesis in a cellular system, a dual inhibitor for DAGLs, DH376, was used in Neuro2A. Neuro2A is a murine neuroblastoma cell line known to express DAGL-α and -β [33]. Initially we performed a competitive gel-based ABPP to investigate the activity of endogenous DAGLs in Neuro2A cells. These studies were performed using a tailored activity-based probe MB064 which can label active DAGL [24]. *In situ* treatment with DH376 dose-dependently reduced DAGL-β (70 kDa) labelling with a pIC_{50} of 8.4 ± 0.1 (**Fig. 1A, B**), which is similar to that measured in mouse brain membrane proteome [27]. Of note, dose-dependent inhibition of ABHD6, a hydrolyzing enzyme of 2-AG [34], upon DH376 treatment was also observed [27]. It was reported that the mRNA levels of DAGL-α protein were 128 fold lower compared to DAGL-β in Neuro 2A cells [35]. In line with this, DAGL-α activity cannot be monitored as its activity was below the detection limits of our ABPP assay.

We next assessed whether DAGL inhibition reduces 2-AG production in Neuro2A cells. Initially a time dependency curve was generated to select the appropriate time point of DH376 treatment required to achieve full inhibition. LC-MS/MS based lipidomics results showed significant reduction of 2-AG levels after 30 min of treatment **(Fig. 1C**). However, we chose 1hr time point for easy sample handling. Furthermore, we investigated whether longer incubation of DH376 has an effect on 2-AG levels. No further reduction in 2-AG levels were observed up to 24h of inhibitor treatment (**Fig. 1C**). Using 1h incubation, dose-dependence data was generated. Lipidomics results showed a concentration-dependent reduction of 2-AG levels in Neuro2A cells with a pIC_{50} of 8.0 ± 01 (**Fig. 1D**). Taken together these data showed that 2-AG levels in Neuro2A cells can be dose- and time-dependently reduced by DH376.

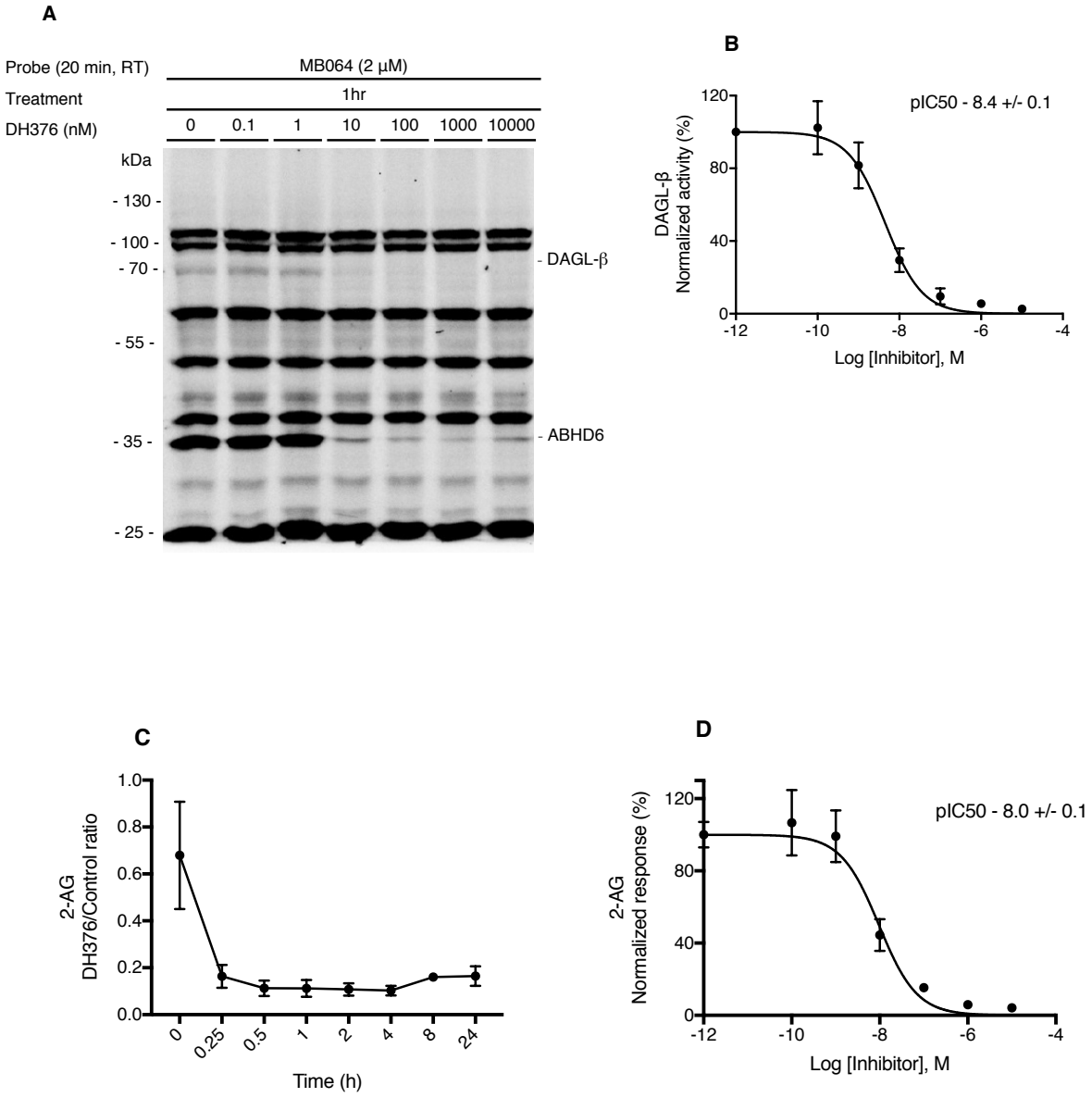

Figure 1: DH376 dose-dependently inhibits DAGL-β and reduces 2-AG levels. (A) Representative gel of concentration dependent inhibition of endogenous DAGL-β inhibition in *in situ* treated Neuro2A cells as determined with ABPP using MB064 **(B)** Dose-response curve of DAGL-β inhibition as determined with ABPP using MB064. **(C)** Time course decrease in the levels of 2-AG in Neuro2A cells treated with vehicle (DMSO) or DH376 (1 µM, 1h, 37°C). The response in **(C)** are expressed as ratio between DH376 treated to vehicle treated (DMSO) to compensate for sample changes over time. **(D)** Dose-dependent decrease in the levels of 2-AG upon DH376 treatment (1h, 37°C). The responses in **(B)** and **(D)** are normalized and expressed in percentages (%). N = 3 independent experiments per group.

Activity of DAGLs in Neuro2A knockout cells

Validation of DAGL KOs in Neuro2A cells

To investigate which isoform of DAGLs is predominantly responsible for 2-AG synthesis, Neuro2A populations lacking either DAGL-α or DAGL-β or both DAGL-α and –β, generated via the CRISPR/Cas9 technology, were used. Genetic modification was confirmed by a T7E-assay for DAGL-α and DAGL-β. ABPP and western blot (WB) were used to check activity and abundance of DAGL-β in the knockout line, showing a decrease of ~80-100% in both assays (**Fig. 2A** for ABPP and data not shown for WB). DAGL-α was not detected by ABPP or western blot in both WT and KO. Other serine hydrolases were not affected by knockout of DAGL and their treatment with DH376, as was shown by ABPP using TAMRA-FP probe which can label a broader range of serine hydrolases (**Fig. 2B**).

DH376 substantially reduced 2-AG levels in DAGL KO's

Next, we evaluated the endogenous levels of 2-AG in Neuro2A DAGL KOs cells using LC-MS/MS based lipidomics. As a control, wildtype cells were treated with DH376. Surprisingly, in DAGLα -/-, DAGLβ -/- and dual DAGLα, β-/- cells, no significant reduction of 2-AG and AEA levels were observed compared to wild-type cells **(Fig. 2C, 2D)**. Importantly, we observed that DH376 was still able to substantially suppress 2-AG levels, but not AEA-levels, in all three DAGL knock-out cell lines (**Fig. 2C, 2D**). These results suggest the presence of additional enzymes targeted by DH376 responsible for the synthesis of 2-AG in Neuro2A cells.

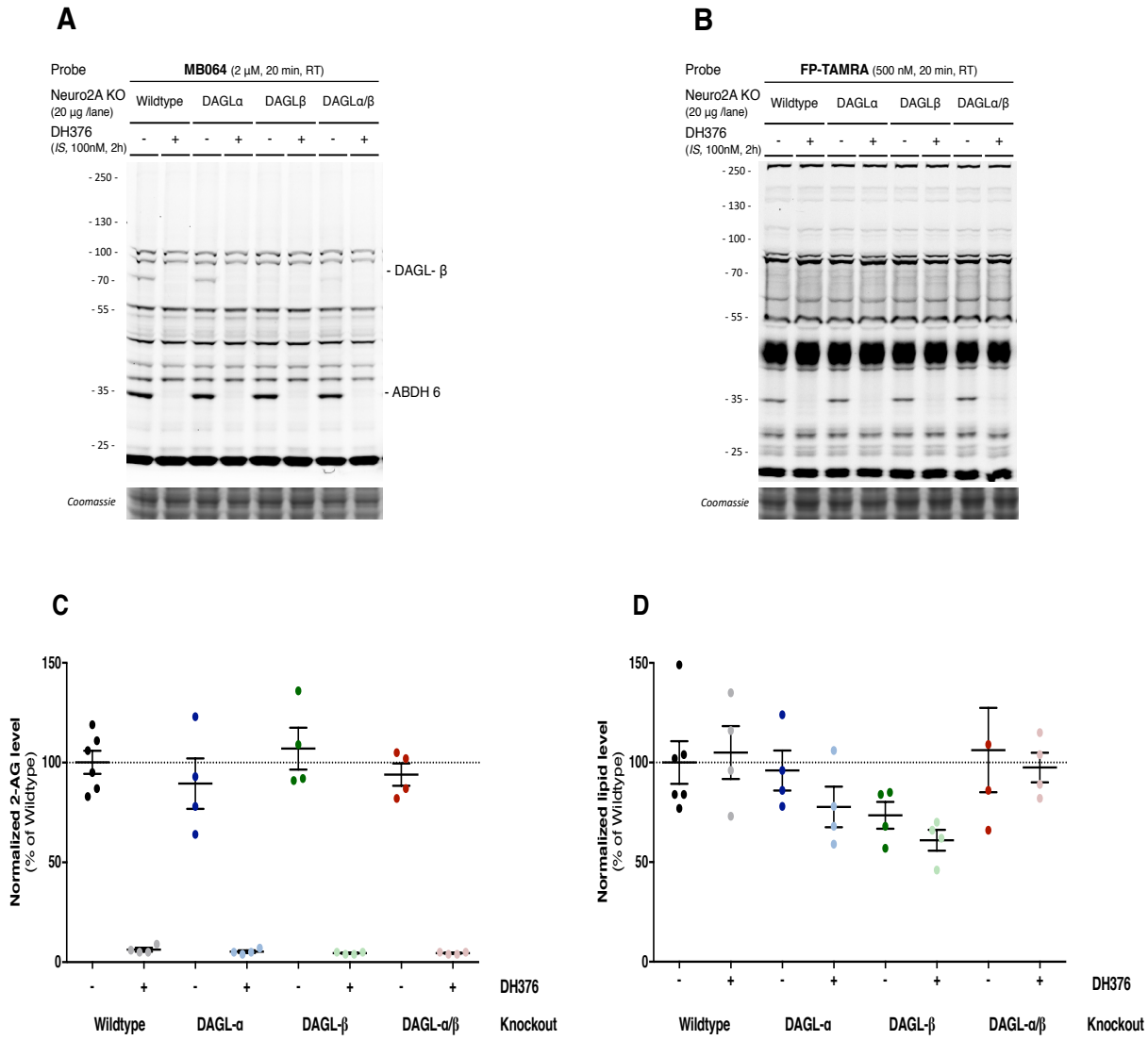

Figure 2: ABPP and lipidomics on DAGL Neuro2A knockouts and the effect of DH376 on KO's. Representative gel-based ABPP on the selectivity and activity of DAGL in Neuro2A KO's and *in situ* treatment of WT and KO's with DMSO (0.1%) or DH376 (100 nM, 2 hours, 37°C) as measured using competitive-ABPP with MB064 **(A)** and FP-TAMRA **(B)** probes. Scatter plot of 2-AG **(C)** and AEA **(D)** levels in WT and Neuro2A KO's and their treatment with DMSO (-) (0.1%) or DH376 (+) (100 nM, 2 hours, 37°C; n=6 for WT; n=4 for others). The values in scatter plots are normalized to wild type and expressed in percentages (%).

Conclusions and future prospects

In summary, the *in vitro* functional activity of DAGLs was evaluated in wildtype and DAGL knockouts in Neuro2A cells using ABPP and lipidomics analysis with DH376 inhibitor. The results of DH376 treatment to DAGL knockouts reveled substantial suppression of endogenous 2-AG levels. This study paves the way to the identification and characterization of new enzyme targets responsible for 2-AG biosynthesis.

One patent has been filed claiming that purified ABHD11 protein extracted from pig brain exhibits similar activity to DAGLs [36], however the endogenous activity of this enzyme remains to be elucidated. In addition, DDHD2 protein has been reported to possess DAGLs activity, however the endogenous activity is not well studied [37]. It was previously reported that two additional enzymes, 1-LPA phosphatases and 2-AG-LPI are also responsible for 2-AG synthesis [2], but these enzymes are not targeted by DH376.

Click chemistry ABPP is a chemoproteomics method which can be used to identify target engagement and potential off-targets of newly developed small molecule inhibitors. Click chemistry ABPP can be performed to discover and identify new targets labelled by DH376 treatment *in vivo* with an Cy5-azide ABPP probe that can detect labeled proteins in whole proteomes by copper(I)-catalyzed ligation (CuAAC) [38]. Since DH376 already contains an alkyne moiety which can be clicked to CY5-azide, it is an ideal inhibitor for performing click chemistry.

After performing click-chemistry ABPP, MS-based chemoproteomics can be used to identify the proteins inhibited by DH376 treatment on wild type and knockouts. This methodology allows for a more accurate quantification avoiding band overlap (as observed in gel-based ABPP) and enables screening over a broader range of particular serine hydrolases. Once the enzyme targets are identified, specific Neuro2A knockouts of identified enzymes can be generated to understand their role and contribution to 2-AG synthesis. Identification of all the players and their contribution to 2-AG synthesis is important to understand the regulatory mechanism of 2-AG signalling and their contribution in different cell types. Targeting specific enzymes in particular cell type to tune endocannabinoid signalling is highly essential to reduce off-target effects and to provide therapeutic solutions for diseases such as metabolic disorders, neurological disorders, where 2-AG levels are upregulated. Overall, ABPP and lipidomics served as versatile techniques that can be used to identify enzyme targets.

References

1. Ahn, K., McKinney, M. K. & Cravatt, B. F. Enzymatic pathways that regulate endocannabinoid signaling in the nervous system. *Chem. Rev.* **108**, 1687–1707 (2008).
2. Murataeva, N., Straiker, A. & MacKie, K. Parsing the players: 2-arachidonoylglycerol synthesis and degradation in the CNS. *Br. J. Pharmacol.* **171,** 1379–1391 (2014).
3. Di Marzo, V. Endocannabinoid signaling in the brain: biosynthetic mechanisms in the limelight. *Nat. Neurosci.* **14,** 9–15 (2011).
4. Pacher, P. & Kunos, G. Modulating the endocannabinoid system in human health and disease--successes and failures. *FEBS J.* **280**, 1918–43 (2013).
5. Di Marzo, V. Targeting the endocannabinoid system: to enhance or reduce? *Nat. Rev. Drug Discov.* **7**, 438–55 (2008).
6. Silvestri, C. & Di Marzo, V. The Endocannabinoid System in Energy Homeostasis and the Etiopathology of Metabolic Disorders. *Cell Metab.* **17**, 475–490 (2013).
7. Alger, B. E. Endocannabinoids at the synapse a decade after the dies mirabilis (29 March 2001): What we still do not know. *J. Physiol.* **590,** 2203–2212 (2012).
8. Soltesz, I. *et al.* Weeding out bad waves: towards selective cannabinoid circuit control in epilepsy. *Nat. Rev. Neurosci.* **16**, 264–277 (2015).
9. Kirkham, T. C., Williams, C. M., Fezza, F. & Di Marzo, V. Endocannabinoid levels in rat limbic forebrain and hypothalamus in relation to fasting, feeding and satiation: Stimulation of eating by 2-arachidonoyl glycerol. *Br. J. Pharmacol.* **136**, 550–557 (2002).
10. Nomura, D. K. *et al.* Endocannabinoid hydrolysis generates brain prostaglandins that promote neuroinflammation. *Science (80-.).* **334**, 809–813 (2011).
11. Shonesy, B. C. *et al.* Genetic Disruption of 2-Arachidonoylglycerol Synthesis Reveals a Key Role for Endocannabinoid Signaling in Anxiety Modulation. *Cell Rep.* **9**, 1644–1653 (2014).
12. Ramesh, D. *et al.* Blockade of Endocannabinoid Hydrolytic Enzymes Attenuates Precipitated Opioid Withdrawal Symptoms in Mice. *J. Pharmacol. Exp. Ther.* **339**, 173–185 (2011).
13. Muldoon, P. P. *et al.* Inhibition of monoacylglycerol lipase reduces nicotine withdrawal. *Br. J. Pharmacol.* **172,** 869–882 (2015).
14. Wilkerson, J. L. *et al.* Diacylglycerol lipase β inhibition reverses nociceptive behaviour in mouse models of inflammatory and neuropathic pain. *Br. J. Pharmacol.* **173**, 1678–1692 (2016).
15. Bisogno, T. *et al.* Cloning of the first sn1-DAG lipases points to the spatial and temporal regulation of endocannabinoid signaling in the brain. *J. Cell Biol.* **163**, 463–8 (2003).
16. Ludányi, A. *et al.* Complementary synaptic distribution of enzymes responsible for synthesis and inactivation of the endocannabinoid 2-arachidonoylglycerol in the human hippocampus. *Neuroscience* **174,** 50–63 (2011).
17. Yoshida, T. *et al.* Unique inhibitory synapse with particularly rich endocannabinoid signaling machinery on pyramidal neurons in basal amygdaloid nucleus. *Proc. Natl. Acad. Sci.* **108,** 3059–3064 (2011).
18. Gao, Y. *et al.* Loss of Retrograde Endocannabinoid Signaling and Reduced Adult Neurogenesis in Diacylglycerol Lipase Knock-out Mice. *J. Neurosci.* **30,** 2017–2024 (2010).

19. Tanimura, A. *et al*. The Endocannabinoid 2-Arachidonoylglycerol Produced by Diacylglycerol Lipase α Mediates Retrograde Suppression of Synaptic Transmission. *Neuron* **65,** 320–327 (2010).
20. Yoshino, H. *et al*. Postsynaptic diacylglycerol lipase α mediates retrograde endocannabinoid suppression of inhibition in mouse prefrontal cortex. *J. Physiol*. **589**, 4857–4884 (2011).
21. Viader, A. *et al*. A chemical proteomic atlas of brain serine hydrolases identifies cell type-specific pathways regulating neuroinflammation. *Elife* **5**, e12345 (2016).
22. Hsu, K. L. *et al*. DAGLβ inhibition perturbs a lipid network involved in macrophage inflammatory responses. *Nat. Chem. Biol*. **8**, 999–1007 (2012).
23. Jain, T., Wager-Miller, J., Mackie, K. & Straiker, A. Diacylglycerol Lipase (DAGL) and DAGL Cooperatively Regulate the Production of 2-Arachidonoyl Glycerol in Autaptic Hippocampal Neurons. *Mol. Pharmacol*. **84**, 296–302 (2013).
24. Baggelaar, M. P. *et al*. Development of an activity-based probe and in silico design reveal highly selective inhibitors for diacylglycerol lipase-α in brain. *Angew. Chem. Int. Ed. Engl*. **52,** 12081–5 (2013).
25. Janssen, F. J. *et al*. Discovery of Glycine Sulfonamides as Dual Inhibitors of sn-1-Diacylglycerol Lipase α and α/β-Hydrolase Domain 6. *J. Med. Chem*. **57**, 6610–22 (2014).
26. Janssen, F. J. & van der Stelt, M. Inhibitors of diacylglycerol lipases in neurodegenerative and metabolic disorders. *Bioorganic Med. Chem. Lett*. **26**, 3831–3837 (2016).
27. Ogasawara, D. *et al*. Rapid and profound rewiring of brain lipid signaling networks by acute diacylglycerol lipase inhibition. *Proc. Natl. Acad. Sci*. **113,** 26–33 (2016).
28. Deng, H. Chemical tools to modulate endocannabinoid biosynthesis. (Leiden University, 2017).
29. Niphakis, M. J. & Cravatt, B. F. Enzyme Inhibitor Discovery by Activity-Based Protein Profiling. *Annu. Rev. Biochem*. **83**, 341–377 (2014).
30. Hsu, P. D., Lander, E. S. & Zhang, F. Development and applications of CRISPR-Cas9 for genome engineering. *Cell* **157**, 1262–1278 (2014).
31. Wang, H., Russa, M. La & Qi, L. S. CRISPR/Cas9 in Genome Editing and Beyond. *Annu. Rev. Biochem*. **85**, 227–264 (2016).
32. Van Esbroeck, A. C. M. *et al*. Activity-based protein profiling reveals off-target proteins of the FAAH inhibitor BIA 10-2474. *Science (**80-**.)*. 356, (2017).
33. Jung, K.-M., Astarita, G., Thongkham, D. & Piomelli, D. Diacylglycerol Lipase-alpha and -beta Control Neurite Outgrowth in Neuro-2a Cells through Distinct Molecular Mechanisms. *Mol. Pharmacol*. **80,** 60–67 (2011).
34. Marrs, W. R. *et al*. The serine hydrolase ABHD6 controls the accumulation and efficacy of 2-AG at cannabinoid receptors. *Nat. Neurosci*. **13,** 951–7 (2010).
35. Baggelaar, M. P. *et al*. Highly Selective, Reversible Inhibitor Identified by Comparative Chemoproteomics Modulates Diacylglycerol Lipase Activity in Neurons. *J. Am. Chem. Soc*. **137**, 8851-7 (2015).
36. Capdevielle, J. et al. Diacylglycerol Lipase and Uses Thereof. International patent number **WO2013068445A1**. Filing date 8 Nov 2012; Publication date 16 May 2013
37. Araki, M. *et al*. Enzymatic characterization of recombinant rat DDHD2: a soluble diacylglycerol lipase. *J. Biochem*. **160**, 269–279 (2016).
38. Speers, A. E., Adam, G. C. & Cravatt, B. F. Activity-based protein profiling in vivo using a copper(I)-catalyzed azide-alkyne [3 + 2] cycloaddition. *J. Am. Chem. Soc*. **125,** 4686–4687 (2003).

Supplementary Information

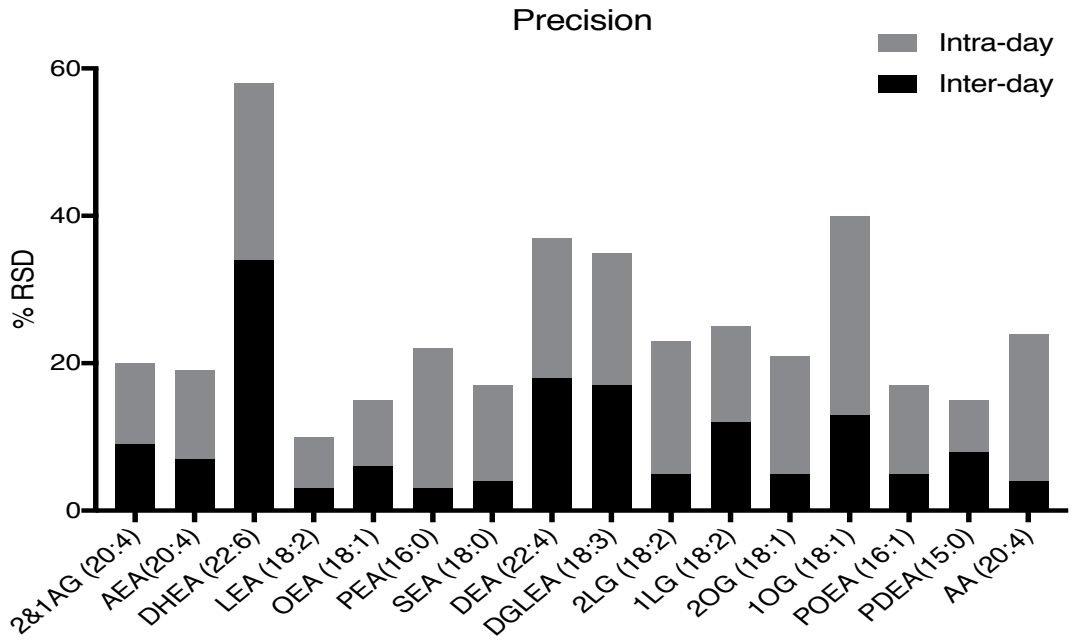

Figure S1: The precision values of endocannabinoids and associated N-acylethanolamines (NAEs). The values are expressed in RSD (relative standard deviation). Intra-day is analysed using 5 biological samples and inter-day is analysed by analysing 5 biological samples in three consecutive days.

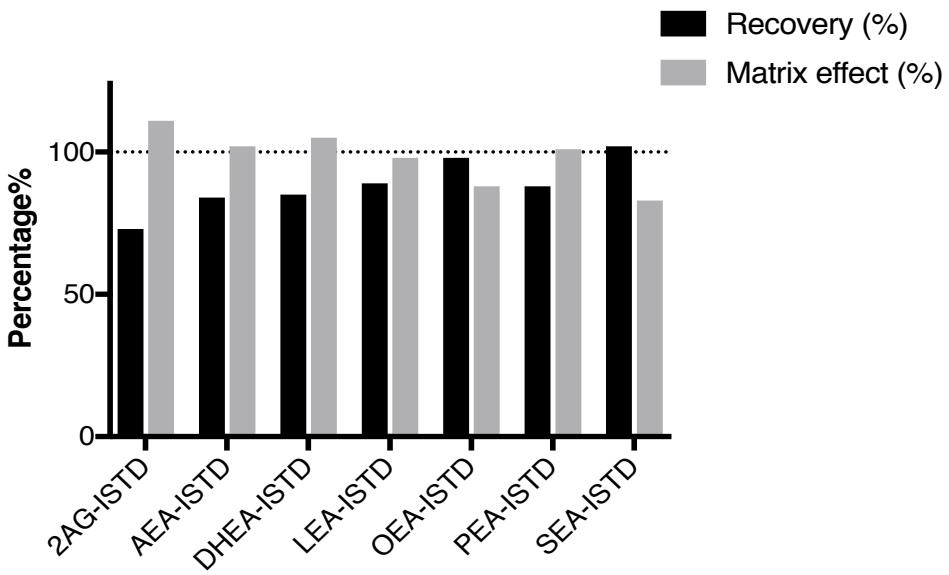

Figure S2: Recovery and matrix effect values are expressed in percentages. Recovery: Higher values indicate better recoveries. Matrix effect: Values above 100% implies ion enhancement and below 100% implies ion suppression.

Table S1: Concentrations of endocannabinoids and related NAEs quantified in Neuro2A cells (n=4)

S. No	Compound	Mean (fM/1M cells)	SEM
1	2&1AG (20:4)	2.3E+04	1.0E+03
2	AEA (20:4)	8.7	0.7
3	DHEA (22:6)	4.8	1.5
4	LEA (18:2)	52.3	1.5
5	OEA (18:1)	39.2	2.1
6	PEA (16:0)	104.3	1.5
7	SEA (18:0)	119.0	2.6
8	DEA (22:4)	22.3	0.5
9	DGLEA (18:3)	4.5	0.5
10	2LG (18:2)	5.1E+04	1.2E+03
11	1LG (18:2)	5.3E+03	3.4E+02
12	2OG (18:1)	1.2E+05	3.0E+03
13	1OG (18:1)	6.8E+03	5.1E+02
14	POEA (16:1)	19.1	0.2
15	PDEA (15:0)	1.6	0.3
16	AA (20:4)	1.1E+05	2.5E+03

The concentrations are determined using individual calibration curves. Labelled internal standards were used to correct for losses. SEM- Standard error of mean

Chapter 5

Activity-based protein profiling reveals off-target proteins of the FAAH inhibitor BIA 10-2474

Annelot C.M. van Esbroeck*, Antonius P.A. Janssen*, Armand B. Cognetta III*, Daisuke Ogasawara* Guy Shpak, Mark van der Kroeg, **Vasudev Kantae**, Marc P. Baggelaar, Femke M.S. de Vrij, Hui Deng, Marco Allarà, Filomena Fezza, Zhanmin Lin, Tom van der Wel, Marjolein Soethoudt, Elliot D. Mock, Hans den Dulk, Ilse L. Baak, Bogdan I. Florea, Giel Hendriks, Luciano De Petrocellis, Herman S. Overkleeft, Thomas Hankemeier, Chris I. De Zeeuw, Vincenzo Di Marzo, Mauro Maccarrone, Benjamin F. Cravatt, Steven A. Kushner, Mario van der Stelt

* *Authors contributed equally*

Science. 2017; 356(6342): 1084-1087

Abstract

A recent phase 1 trial of the fatty acid amide hydrolase (FAAH) inhibitor BIA 10-2474 led to the death of one volunteer and produced mild-to-severe neurological symptoms in four others. Although the cause of the clinical neurotoxicity is unknown, it has been postulated, given the clinical safety profile of other tested FAAH inhibitors, that off-target activities of BIA 10-2474 may have played a role. Here we use activity-based proteomic methods to determine the protein interaction landscape of BIA 10-2474 in human cells and tissues. This analysis revealed that the drug inhibits several lipases that are not targeted by PF04457845, a highly selective and clinically tested FAAH inhibitor. BIA 10-2474, but not PF04457845, produced substantial alterations in lipid networks in human cortical neurons, suggesting that promiscuous lipase inhibitors have the potential to cause metabolic dysregulation in the nervous system.

Main text

In January 2016, a first-in-human study of the fatty acid amide hydrolase (FAAH) inhibitor BIA 10-2474 led to the death of one volunteer and the hospitalization of four others [1–4]. All patients manifested mild-to-severe neurological symptoms [3]. FAAH is a membrane-bound serine hydrolase that degrades the endocannabinoid anandamide and related amidated lipids [5–8]. Three explanations for the clinical neurotoxicity of BIA 10-2474 have been proposed: (i) Errors may have occurred in the clinical trial itself, either in the manufacturing or handling of the compound or in the conduct of the trial; (ii) through its inhibitory effects on FAAH, BIA 10-2474 may have produced high levels of long-chain fatty acid amides (e.g., anandamide) and their oxygenated metabolites, which could potentially overstimulate cannabinoid CB_1 [8], transient receptor potential vanilloid 1 (TRPV1) ion channels [9], and/or N-methyl-D-aspartate (NMDA) receptors [10]; or (iii) BIA 10-2474 and/or its metabolites might have off-target activities. The first hypothesis was dismissed by the French authorities [4]. The second hypothesis is considered unlikely because other FAAH inhibitors, such as PF04457845, have exhibited favorable safety profiles in Phase 1 and 2 clinical trials [11,12]. The third hypothesis has not been directly evaluated, because little or no information is available regarding the protein interaction profile of BIA 10-2474 [1].

BIA 10-2474 (**Fig. 1A**) contains an electrophilic imidazole urea that may react with the nucleophilic serine of FAAH and other serine hydrolases to form covalent and irreversible adducts. We predicted that the serine hydrolase targets of BIA 10-2474 could be identified using chemical proteomic methods [13–15]; this would allow us to compare its selectivity profile to that of PF04457845 (**Fig. 1A**), a FAAH inhibitor that progressed to Phase 2 trials without serious adverse events [11,12,16]. We first synthesized BIA 10-2474, along with BIA 10-2639, a confirmed metabolite in which the *N*-oxide of BIA 10-2474 has been reduced to a pyridine [4] (**Fig. 1A**), in two independent labs and confirmed their structures by ^{1}H- and ^{13}C-NMR and high-resolution mass spectrometry [17]. Both independently generated sets of compounds displayed equivalent activities in the subsequently described biological assays.

Our initial experiments with substrate hydrolysis assays revealed that BIA 10-2474 showed weak *in vitro* inhibitory activity against human and rat FAAH, displaying median inhibitory concentrations (IC_{50}) values ≥ 1 μM (**Fig. 1B, Fig. S1, and Table. 1**). Consistent with previous reports [16], PF04457845 potently inhibited FAAH with IC_{50} values of ~1-10 nM (**Fig. 1B and Table. 1**). By contrast, BIA 10-2474 exhibited greatly improved potency in cellular assays (*in situ*), blocking human FAAH activity in transfected HEK293T (human

embryonic kidney 293T) cells with IC_{50} values of 0.05-0.07 μM (**Fig. 1B**). BIA 10-2474 and PF04457845 did not interact with other proteins of the endocannabinoid system or with the endocannabinoid-binding transient receptor potential (TRP) ion channels (**Tables . S2 and S3**).

Table 1. *In vitro* and *in situ* inhibitory potencies of BIA 10-2474, BIA 10-2639, and PF04457845 against FAAH and representative off-targets.

		IC_{50} (μM)		
Enzyme	Treatment	BIA 10-2474	BIA 10-2639	PF04457845
FAAH	*in vitro*	7.5	4.1	0.0040
FAAH	*in situ* (4 h)	0.049	0.049	0.011
FAAH2	*in situ* (4 h)	0.40	0.10	0.59
ABHD6	*in situ* (4 h)	0.081	0.079	>10
CES2	*in situ* (4 h)	2.0	0.63	>10
ABHD11	*in situ* (4 h)	>10	2.3	>10
PNPLA6	*in situ* (24 h)	11	N.D.	>50

Measurements were made by gel-based ABPP of HEK293T cells recombinantly expressing the indicated human serine hydrolases. Data represent inhibitor treatment of cells for 4 h with the exception of PNPLA6, where data represent inhibitor treatment of cells for 24 h. Data represent average values from three independent experiments per group. See Table S4 for error measurements related to IC_{50} values.

We also created alkynylated analogues of BIA 10-2474 – AJ167, AJ179 and AJ198 – and found that two of these compounds (AJ179 and AJ198) labeled mouse and human FAAH in brain lysates, as detected by coupling to azide fluorescent reporter groups via copper(I)-catalyzed azide-alkyne cycloaddition ("click") chemistry (**Fig. S2**) [18]. This finding, coupled with the time-dependent inhibition of FAAH displayed by BIA 10-2474 (**Table. S1**), provides strong evidence that BIA 10-2474 and related imidazole ureas exhibit an irreversible mode of action.

To investigate the serine hydrolase interaction landscape of BIA 10-2474, we used activity-based protein profiling (ABPP), a chemical proteomic method that uses active site-directed chemical probes (e.g., fluorophosphonates (FPs) or β-lactones for serine hydrolases) to assess the functional state of entire enzyme classes directly in native biological systems [13–15]. When coupled to fluorescent reporter groups, ABPP probes enable visualization of enzyme activities in complex proteomes by SDS–polyacrylamide gel electro- phoresis (SDS-PAGE) and in-gel fluorescence scanning. When coupled to a biotin reporter group, ABPP probes enable affinity enrichment and identification of enzyme activities by mass spectrometry (MS)-based proteomics. In both formats, ABPP serves as a versatile method to assess target

engagement and proteome-wide selectivity for small-molecule inhibitors. Gel-based ABPP with a fluorescent FP probe (FP-TAMRA) confirmed the relative *in vitro* and *in situ* potencies of BIA 10-2474 and PF04457845 for human FAAH in transfected HEK293T cell preparations (**Fig. 1C**). The reason for the increased cellular activity of BIA 10-2474 is unclear but could reflect cellular accumulation of the compound, which has been observed for other types of enzyme inhibitors [19].

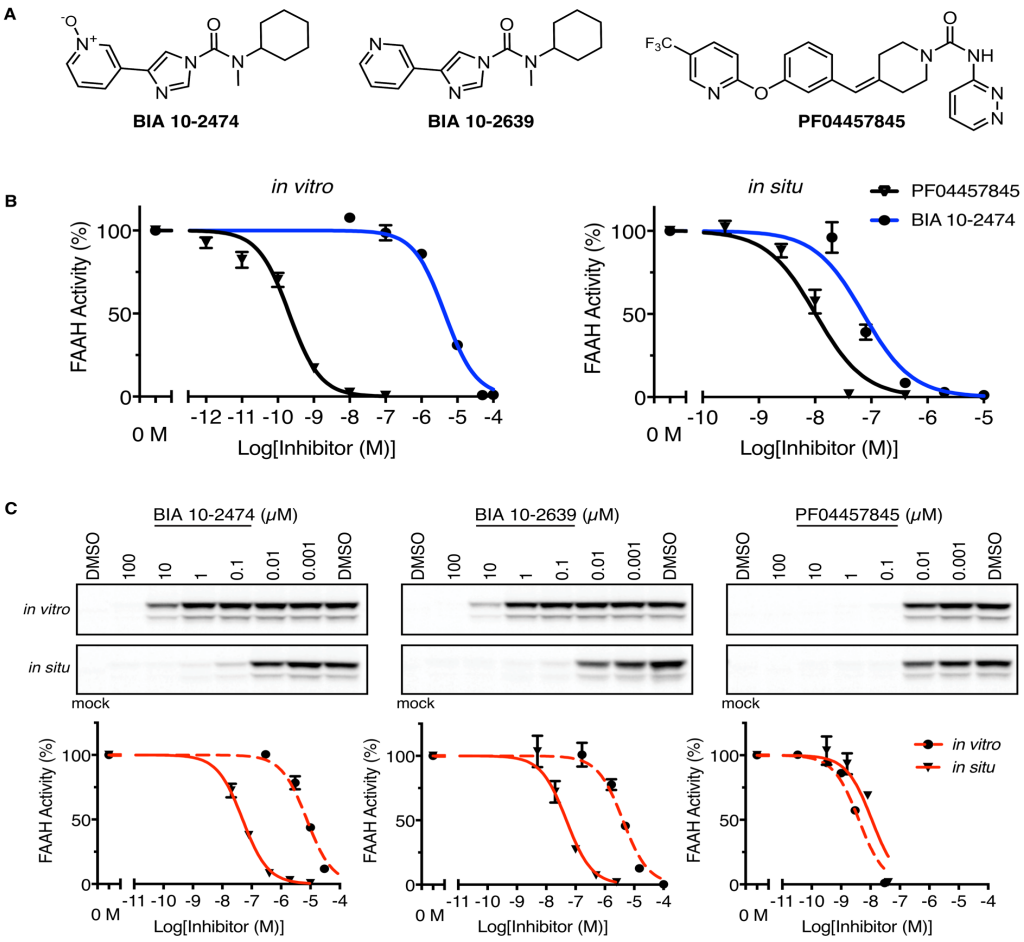

Figure 1: Comparison of human FAAH inhibition by BIA 10-2474, BIA 10-2639, and PF04457845. (A) The structures of BIA 10-2474, the metabolite BIA 10-2639, and PF04457845. **(B)** Inhibition of human FAAH in HEK293T cell lysates (*in vitro*) or intact cells (*in situ*) as measured using an anandamide substrate hydrolysis assay. **(C)** *In vitro and in situ* inhibition of human FAAH as measured by competitive gel-based ABPP. *Top panels*, HEK293T cell lysates (*in vitro*) or intact cells (*in situ*) recombinantly expressing human FAAH were pretreated with compound or DMSO (*in vitro*: 30 min, 37 °C *in situ*: 4 h, 37 °C). FAAH activity was measured by reactivity with the serine hydrolase-directed probe fluorophosponate-rhodamine and visualization of signals by gel-based ABPP. *Bottom panels*, Corresponding IC50 curves for gel-based ABPP data shown in Top Panels. N = 3 independent experiments per group.

Initial ABPP studies were performed in the human colon carcinoma cell line SW620, which expresses a wide diversity of endogenous serine hydrolase activities, including FAAH and FAAH2. Isotopically heavy and light amino acid-labeled SW620 cells were treated with dimethyl sulfoxide (DMSO) or drug (BIA 10-2474 or PF04457845; 0.2 or 10 μM each for 4 h, or 50 μM each for 24 h) and then lysed and treated with a biotinylated FP probe. The samples are then combined, and subjected to streptavidin enrichment and quantitative LC-MS analysis, in which proteins displaying heavy:light ratios of > 2.0 were designated as drug-inhibited targets. We focused on human cell studies and tested a broad range of inhibitor concentrations because the deleterious neurological effects of BIA 10-2474 were observed in humans, but not other mammals, and occurred at drug doses that were 10 to 50 times higher than that required for blockade of FAAH activity in the clinical trial participants [4].

Our MS-based ABPP studies confirmed that both BIA 10-2474 and PF04457845 fully engaged human FAAH at all tested concentrations (0.2, 10, and 50 μM) (**Fig. 2A, B and Fig. S3**). Both drugs showed good selectivity for FAAH at the lowest concentration tested (0.2 μM; **Fig. S3**). PF04457845 maintained this selectivity profile at higher concentrations, displaying only a single major off-target – the homologous enzyme FAAH2 – among ~60 quantified serine hydrolases, consistent with previous studies [16]. By contrast, BIA 10-2474 and its metabolite BIA 10-2639 exhibited numerous off-targets across the tested drug concentration range, including FAAH2 and several lipid hydrolases, such as ABHD6, ABHD11, LIPE, and PNPLA6 and xenobiotic drug-metabolizing enzymes CES1, CES2, and CES3 (**Fig. 2A and B**). Some of these off-targets, such as ABHD6 and CES2, were near-completely inhibited (>90%) at both 10 μM and 50 μM concentrations of BIA 10-2474.

Representative off-targets of BIA 10-2474 were recombinantly expressed in HEK293T cells and verified to engage BIA 10-2474 by gel-based ABPP (**Fig. 2C**). These experiments also confirmed the relative potency of off-targets mapped by MS-based ABPP, with BIA 10-2474 exhibiting greater inhibitory activity against ABHD6 and CES2 compared to PNPLA6. In contrast, none of the recombinantly expressed enzymes were inhibited by PF04457845 except FAAH2 (**Fig. 2C**).

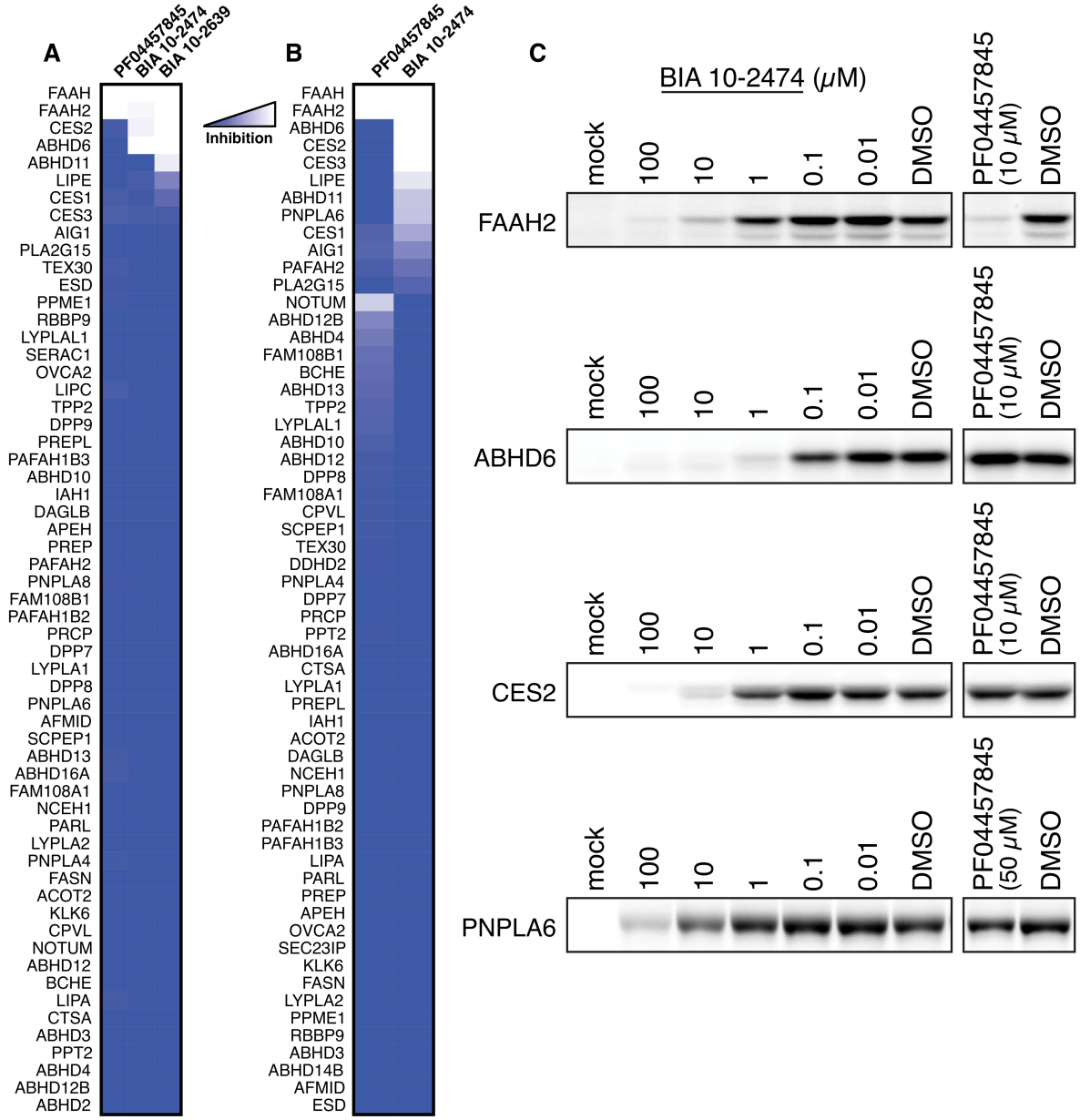

Figure 2: Quantitative proteomic analysis of serine hydrolase targets of FAAH inhibitors in human cells. (A,B) MS-based ABPP of serine hydrolase activities in SW620 cells treated with DMSO or FAAH inhibitor. Shown in (**A**) are BIA 10-2474, BIA 10-2639, and PF04457845 (10 μM, 4 h, 37 °C). Shown in (**B**) are BIA 10-2474 and PF04457845 (50 μM, 24 h, 37 °C). Data are expressed as median SILAC ratio values for all isotopic peptide pairs quantified per protein from two biological replicates. (**C**) Confirmation of representative off-targets of BIA 10-2474 by gel-based ABPP of recombinantly expressed enzymes in HEK293T cells.

Our chemical proteomic data, taken together, demonstrated that both BIA 10-2474 and its major metabolite BIA 10-2639 cross-react with several human serine hydrolases that do not interact with PF04457845 (**Tables. 1 and S4**). One possible contributing factor to this broader

interaction profile is the greater intrinsic reactivity of BIA 10-2474 compared to PF04457845, which is reflected in their respective rates of methanolysis (**Fig. S4**). We also note that human CES2 and ABHD6 were both more potently inhibited by BIA 10-2474 and BIA 10-2639 compared to the mouse orthologs of these enzymes (**Table. S2**), indicating the potential for species differences in the off-target-mediated activities of these compounds.

Many of the off-targets of BIA 10-2474 are involved in cellular lipid metabolism [20,21] and most (with the exception of FAAH2) show substantial expression in human brain tissue (**Fig. S5**). Although the poor *in vitro* activity displayed by BIA 10-2474 limited our ability to identify off-targets in brain tissue lysates, we were able to confirm cross-reactivity of this drug with both FAAH and ABHD6 in human frontal cortex proteome (post-mortem samples acquired from three male donors who were 49, 50, and 80 years of age and who were not associated with the BIA 10-2474 trial) (**Fig. S6**). We also observed several of the off-targets of BIA 10-2474 by ABPP of human cortical neurons derived from induced pluripotent stem cells (**Fig. S7**).

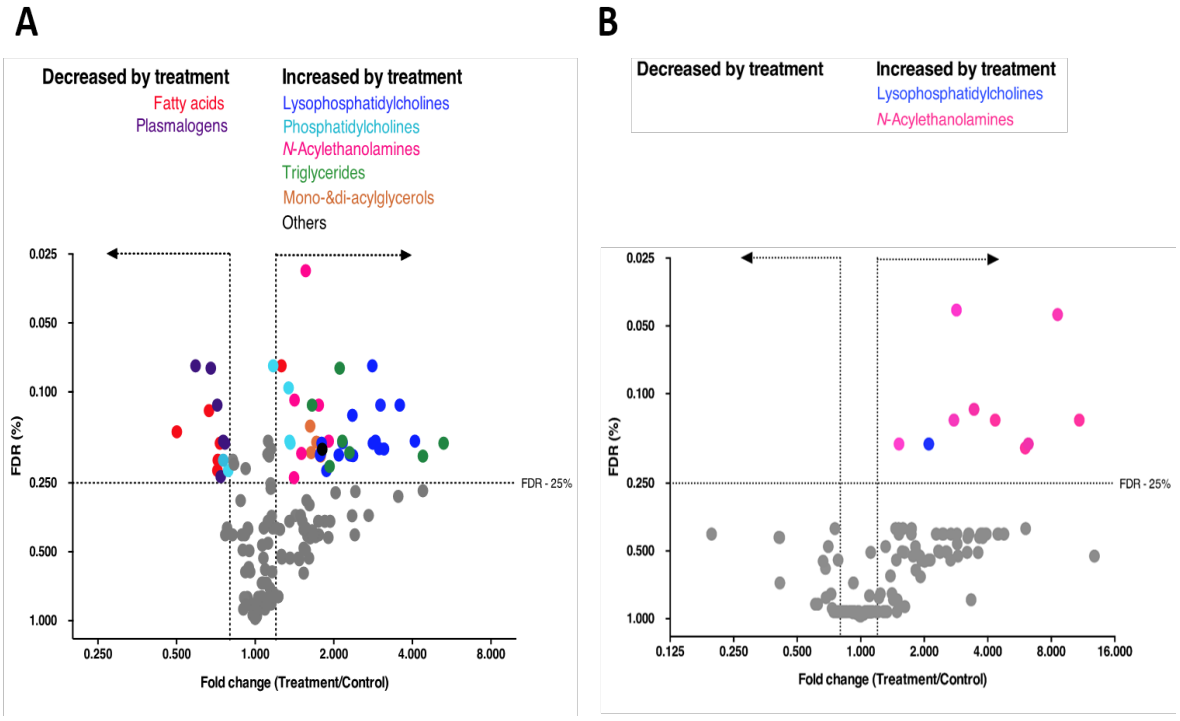

Figure 3: BIA 10-2474, but not PF04457845, causes substantial alterations in lipid metabolism in human cortical neurons. (**A, B**) Cortical neurons were treated with DMSO (**A,B**), BIA 10-2474 (50 μM) (**A**) or with PF04457845 (1 μM) (**B**) and analyzed by MS-based lipidomics after 48 h. X-axis denotes fold change of lipid species in the inhibitor-treated cells vs DMSO-treated cells. Lipidomic data are presented as a volcano plot and lipids with a fold

change (FC) threshold of ≥1.20 or ≤0.80 and Benjamini–Hochberg false discovery rate (FDR) ≤ 25% are represented by colored circles distinguished by lipid class. Data represent average values from at least two independent experiments.

We next tested whether prolonged exposure to BIA 10-2474 altered lipid metabolism in human cortical neurons. We performed targeted lipidomic analysis of human cortical neurons cultures treated with vehicle (DMSO) or BIA 10-2474 (50 μM) at a concentration that was ~20 times greater than the maximum concentration (C_{max}) observed in the human clinical trial [22]. In total, the amounts of 161 lipid species were quantified, of which 54 showed a fold change of ≥ 1.20 or ≤ 0.80 when using a Benjamini–Hochberg false discovery rate ≤ 25% (**Fig. 3A and Table. S5**). The lipids affected by BIA 10-2474 included FAAH substrates (*N*-acylethanolamines), as well as several other lipid classes, including triglycerides, monoacylglycerols, (lyso)phosphatidylcholines, free fatty acids and plasmalogens. By contrast, treatment of human cortical neuron cultures with PF04457845 (1 μM), which was also tested at a concentration that was 20 times greater tham the clinical C_{max} for the drug [11], produced a more restricted profile of lipid changes, predominantly corresponding to the expected elevations of *N*-acylethanolamines (**Fig. 3B**).

Here we have shown that BIA 10-2474 acts as an irreversible inhibitor of FAAH that displays greater cross-reactivity with human serine hydrolases than the clinically tested FAAH inhibitor PF04457845. Many of the off-targets of BIA 10-2474 are lipolytic enzymes, raising the possibility that disruption of cellular lipid networks may have contributed to the compound's neurotoxicity. Notably, disruption of neuronal lipid metabolism by inhibition of PNPLA6, one of the off-target proteins of BIA 10-2474 identified in this study, has previously been linked to organophosphate-based neurotoxicity in humans [21,23–25], and recessive loss-of-function mutations in the *PNPLA6* gene are responsible for a broad spectrum of neurodegenerative disorders [26,27].

Although our data provide information about the selectivity of BIA 10-2474, they do not allow us to conclude that inhibition of one or more of the identified off-target proteins is responsible for the clinical neurotoxicity caused by this drug. Nor can we exclude the possibility that non-covalent interactions of BIA 10-2474 or its metabolites with other proteins might have contributed to the reported clinical effects [28]. Regardless, our study highlights the general utility of ABPP as a versatile chemical proteomic method to assess on-target engagement and off-target activity of covalent drugs to guide therapeutic development.

Materials and Methods

Probes and inhibitors

Activity based probe TAMRA-fluorophosphonate (FP-TAMRA) was purchased from Thermo Fisher, MB064 was synthesized in-house as previously described [29]. PF04457845 was synthesized in house, as well as purchased from Sigma Aldrich. URB597 was purchased from Sigma Aldrich. Inhibitor BIA 10-2474, BIA 10-2639 and activity based probes AJ167, AJ179 and AJ198 were synthesized as described in the synthetic methods *(vide infra)*. All synthesized compounds were at least 95% pure and were analyzed by LC/MS, NMR and HRMS. Other chemicals, reagents, and primers were purchased from Sigma Aldrich unless indicated otherwise.

BIA 10-2639 and PF04457845 used in **Table. S4, Fig. 1, 2, S3, and S4** were generously provided by Pfizer Inc.

Cloning

Full-length human cDNA of ABHD6, FAAH, ABHD11, PNPLA6, CES2 (Source Bioscience) and FAAH2 (BioCat) was cloned into mammalian expression vector pcDNA3.1, containing genes for ampicillin and neomycin resistance. The inserts were cloned in frame with a C-terminal FLAG-tag and site-directed mutagenesis was used to remove restriction by silent point mutations. Plasmids were isolated from transformed XL-10 Z-competent cells (Maxi Prep kit: Qiagen) and sequenced at the Leiden Genome Technology Center. Sequences were analyzed and verified (CLC Main Workbench).

Full-length human and mouse cDNAs used for **Table. S4** and **Fig. 1 and 2** were purchased from Dharmacon and Origene. Sequencing was performed by Eton BioScience.

Cell culture

General

HEK293T (human embryonic kidney) cells were cultured at 37 °C under 7% CO_2 in DMEM containing phenol red, stable glutamine, 10% (v/v) New Born Calf Serum (Thermo Fisher), and penicillin and streptomycin (200 μg/mL each; Duchefa). Medium was refreshed every 2-3 days and cells were passaged twice a week at 80-90% confluence by resuspension in fresh medium. HEK293T and SW620 cells used for **Table. S4 and Fig. 1, 2, S1A and S3** were

cultured at 37 °C under 5% CO_2 in DMEM or RPMI, respectively, containing penicillin, streptomycin, and fetal calf serum.

Cells lines were purchased from ATCC and were regularly tested for mycoplasma contamination. Cultures were discarded after 2-3 months of use.

Human neural cell culture

Human iPSC-dervied cortical neurons were differentiated from neural progenitor cells (NPCs) (Axol Biosciences, line ax0015). Briefly, NPCs were plated on sterile coverslips in 12-well plates, coated with poly-L-ornithin/laminin (Sigma-Aldrich), in neural differentiation medium (Neurobasal medium, 1% N2 supplement, 2% B27-RA supplement, 1% MEM-NEAA, 20 ng/ml BDNF (ProSpec Bio)), 20 ng/ml GDNF (ProSpec Bio), 1 μM db-cAMP (Sigma-Aldrich), 200 μM ascorbic acid (Sigma-Aldrich), 2 µg/ml laminin, and 1% P/S), resulting in neural networks composed of neurons and glia. Cells were refreshed with neural differentiation medium 3 times per week. During weeks 1-4, medium was fully refreshed. After 4 weeks of neural differentiation, only half of the volume of medium per well was refreshed.

Transient transfection

One day prior to transfection HEK293T cells were seeded to 15-cm dishes or 12-well plates (~62.500 cells/cm^2). Prior to transfection, culture medium was aspirated and a minimal amount of medium was added. A 3:1 (m/m) mixture of polyethyleneimine (PEI) (60 µg/dish or 1.875 µg/well) and plasmid DNA (20 µg/dish or 0.625 µg/well) was prepared in serum free culture medium and incubated for 15 min at RT. Transfection was performed by dropwise addition of the PEI/DNA mixture to the cells. Transfection with the empty pcDNA3.1 vector was used to generate control samples. After 24 h, medium was refreshed. Medium was aspirated 48 or 72 h post-transfection and cells were harvested by resuspension in PBS. Cells were pelleted by centrifugation (5 min, 1,000 *g*) and the pellet was washed with PBS. Supernatant was discarded and cell pellets were frozen in liquid nitrogen and stored at -80 °C until sample preparation.

For **Table. S4 and Fig. 1, 2 and S1A**, a slightly altered procedure was used: One day prior to transfection HEK293T cells were seeded in 15-cm dishes or 6-well plates (~62.500 cells/cm^2). After 24 h a mixture of polyethyleneimine (PEI, 1 mg/mL) (45 μL or 3 μL/well) and plasmid DNA (15 μg or 0.5 μg/well) were incubated in serum free DMEM (45 min, RT), and then added dropwise the cells. 48 h post-transfection cells were harvested or used for *in situ* treatments.

In situ treatment

The term *in situ* is used to designate experiments in which live cell cultures are treated with inhibitor, whereas the term *in vitro* refers to experiments in which the inhibitor is incubated with cell lysates/homogenates.

In situ treatment of HEK293T cells

In situ treatment was initiated 24 h (for 24 – 48 h treatment) or 48 h (for 2 h treatment) post-treatment in 12-well plates. Medium was aspirated and medium containing inhibitor or DMSO as vehicle was added (0.1-1.0 % DMSO, DMSO concentration constant within each experiment). Final concentrations for inhibitors are indicated in the main text and figure legends. After 2, 4, 24, or 48 h exposure to treatment medium, medium was aspirated and cells were harvested and stored as described above until sample preparation (whole cell lysate).

In situ treatment of human neural cell culture

Cells were treated with inhibitor *in situ* 7-8 weeks after plating of NPCs. Culture slides were then collected from 6-well culture plates 24 h or 48 h after initiation of *in situ* treatment with BIA 10-2474 (50 μM, 0.25% DMSO) or vehicle (0.25% DMSO). The *in situ* treated cells were harvested in PBS as described above and stored at -80 ˚C until further use.

Sample preparation

Whole cell lysate

Cell pellets were thawed on ice, resuspended in cold lysis buffer (20 mM HEPES pH 7.2, 2 mM DTT, 250 mM sucrose, 1 mM $MgCl_2$, 2.5 U/mL benzonase) and incubated on ice (15-30 min). The cell lysate was used for membrane preparation (below) or was diluted to appropriate concentration in cold storage buffer (20 mM Hepes, pH 7.2, 2 mM DTT) for use as whole lysate (HEK293T: 2.0 mg/mL, human cortical neurons: 0.75 mg/mL, human neural cells: 1.5 mg/mL). Protein concentrations were determined by a Quick Start™ Bradford Protein Assay and diluted samples were flash frozen in liquid nitrogen and stored at -80 ^{0}C until further use.

Cell pellets used for **Table. S4 and Fig. 1** were resuspended in cold PBS, lysed with a probe sonicator, and diluted to 1 mg/mL in PBS. Protein concentrations were determined with the DC Assay (Bio-Rad).

Tissue lysate

Mouse brains (C57Bl/6) were isolated according to guidelines approved by the ethical committee of Leiden University (DEC#13191), frozen in liquid nitrogen, and stored at -80 °C until use. Human Brain Tissue was supplied by the Netherlands Brain Bank and stored at -80 °C until use. Tissues were thawed on ice, dounce homogenized in cold lysis buffer and incubated on ice (15 min), followed by two low-speed spins (3 min, 1,400–2,500 *g*, 4°C) to remove debris. The supernatant fraction was collected for further use.

Membrane preparation from lysate

The membrane and cytosolic fractions of cell or tissue lysates were separated by ultracentrifugation (93,000 *g*, 45 min, 4°C). The supernatant was collected (cytosolic fraction) and the membrane pellet was resuspended in cold storage buffer by thorough pipetting and passage through an insulin needle. Protein concentrations were determined by a Quick Start™ Bradford Protein Assay and samples were diluted to 2.0 mg/mL with cold storage buffer, flash frozen in liquid nitrogen and stored at -80 °C until further use. FAAH and FAAH2 overexpression membranes were mixed in an appropriate ratio for ABPP (0.1 mg/mL: 1.0 mg/mL).

Lysates used for **Table. S4, Fig. S1A and S3** were subjected to ultracentrifugation (100,000 *g*, 45 min) to separate the membrane and soluble fractions. After removal of the soluble fraction, the membrane pellet was washed once with cold PBS, and then resuspended by probe sonication in cold PBS.

Western Blot

Cell lysates, membrane or cytosol fractions (15 μL) were denatured with 4x Laemmli buffer (5 μL, final concentrations: 60 mM Tris (pH 6.8), 2% (w/v) SDS, 10% (v/v) glycerol, 1.25% (v/v) β-mercaptoethanol, 0.01% (v/v) bromophenol blue) and 5-20 µg proteome per sample was resolved on a 10% acrylamide SDS-PAGE gel (180 V, 75 min). Proteins were transferred to 0.2 μm polyvinylidene difluoride membranes by Trans-Blot Turbo™ Transfer system (Bio-Rad). Membranes were washed with TBS (50 mM Tris, 150 mM NaCl) and blocked with 5% milk in TBS-T (50 mM Tris, 150 mM NaCl, 0.05% Tween 20) for 1 h at RT. Membranes were then incubated with primary antibody in 5% milk TBS-T (AMPA, FLAG: O/N, 4°C, α-tubulin, FLAG: 1 h, RT), washed with TBS-T, incubated with matching secondary antibody in 5% milk TBS-T (1 h, RT) and washed with TBS-T and TBS. Imaging solution (10 mL Luminol, 100

μL ECL enhancer, 3 μL H_2O_2) was added to develop membranes and chemiluminescence was detected on the ChemiDoc (Bio-Rad) using standard chemiluminescence settings. The signal was normalized to Coomassie staining and quantified with Image Lab (Bio Rad).

Primary antibodies: monoclonal mouse-anti-FAAH1 (1:1000, Cell Signaling Technology, #2942) polyclonal rat-anti-α-Tubulin (1:1000, GeneTex, GTX76511), monoclonal mouse-anti-FLAG (1:5000, Sigma Aldrich, F3156). Secondary antibodies: HRP-coupled-goat-anti-rabbit (1:5000, Santa Cruz, sc2030), HRP-coupled-goat-anti-rat (1:5000, Santa Cruz, sc2032), HRP-coupled-goat-anti-mouse (1:5000, Santa Cruz, sc2005).

Activity based protein profiling

Gel based: Direct activity based probes

Gel-based activity based protein profiling (ABPP) was performed and analyzed with minor adaptations on previously reported procedures 3. In brief, for *in vitro* inhibition, human or mouse brain proteome or cell lysate (15 μL, 0.75, 1.5 or 2.0 mg/mL, lysate, cytosol or membrane fraction) was pre-incubated with vehicle or inhibitor (0.375 μL 40* inhibitor stock, 30 min, 37 ˚C) followed by an incubation with the activity based probe (250 nM MB064 or 500 nM FP-TAMRA, 20 min, RT). Final concentrations for the inhibitors are indicated in the main text and figure legends. For *in situ* inhibition, the *in situ*-treated cells (15 μL whole lysate) were directly incubated with the activity based probe (250 nM MB064 or 500 nM FP-TAMRA, 20 min, RT). Reactions were quenched with 4x Laemmli buffer (5 μL, 240 mM Tris (pH 6.8), 8% (w/v) SDS, 40% (v/v) glycerol, 5% (v/v) β-mercaptoethanol, 0.04% (v/v) bromophenol blue). 7.5, 15 or 20 µg per reaction was resolved on a 10% acrylamide SDS-PAGE gel (180 V, 75 min). Gels were scanned using Cy3 and Cy5 multichannel settings (605/50 and 695/55, filters respectively) and stained with Coomassie after scanning. Fluorescence was normalized to Coomassie staining and quantified with Image Lab (Bio-Rad). IC_{50} curves were fitted with Graphpad Prism® 7 (Graphpad Software Inc.).

Tissue and cell lysates used for **Table. S4, Fig. 1 and 2** (1 mg/mL, 50 μL) were treated with FP-TAMRA (1 μM, 30 min, 37 °C) Samples were then quenched by adding 4x SDS-PAGE loading buffer (17 μL), resolved by SDS-PAGE, and visualized using ChemiDoc MP (Bio-Rad). Signal intensity was then quantified with ImageJ 1.45s, and IC_{50} curves were fitted with GraphPad Prism 7.

Gel based: Two-step activity based probes

The two-step labeling was adapted from previously developed methods [30]. In brief, human or mouse proteome (40 μL, 2 mg/mL, cytosol or membrane fraction) was pre-incubated with vehicle or inhibitor (50 μM, 30 min, 37 ^{0}C) followed by an incubation with the alkyne probe (50 μM, 30 min, 37 ^{0}C). Click reagent was freshly prepared by mixing copper sulfate (2 μL/reaction, 100 mM in water), THPTA (0.4 μL/reaction, 100 mM in water), sodium ascorbate (1.2 μL/reaction, 1 M in water), and Cyanine 5-Azide (Cy5–N_3, 1.60 μL/reaction, 1 mM in DMSO). Click reagent (5.0 μL) was added to each proteome, mixed by brief vortexing and incubated (60 min, RT). Proteins were precipitated by adding methanol (50 μL), chloroform (15 μL) and water (15 μL), mixed by brief vortexing and pelleted by centrifugation (10 min, 4000 rpm). The supernatant was removed and the pellet was washed twice with methanol (50 μL). The pellet was then redissolved in 40 μL of 2x Laemmli buffer (120 mM (pH 6.8), 4% (w/v) SDS, 20% (v/v) glycerol, 2.5% (v/v) β-mercaptoethanol, 0.02% (v/v) bromophenol blue) by vortexing. Samples were boiled (95˚C, 5 min) and 20 μg proteome per reaction was resolved on a 10% acrylamide SDS-PAGE gel (180 V, 75 min). Gels were scanned using Cy3 and Cy5 multichannel settings (605/50 and 695/55, filters respectively) and stained with Coomassie after scanning. Coomassie staining was performed as a protein loading control.

Activity based proteomics

Activity based proteomics was based on previously described procedures [14]. In summary, human GFi3 proteome or mouse whole brain proteome (250 μL cytosolic or membrane fraction at 1.0 mg/mL) was incubated with vehicle (2% DMSO) or inhibitor (BIA 10-2474**,** BIA 10-2639, or PF04457845, 50 μM, 30 min, 37 ˚C). The proteome of *in situ* treated human neural cells (250 μL whole lysate at 0.35 mg/mL, 24 h treatment) was used without additional inhibitor incubation. The proteomes were then labeled with MB108 or FP-Biotin (10 μM, 60 min, RT). The labeling reaction was quenched and excess probe was removed by chloroform methanol precipitation. Precipitated proteome was resuspended in 6M Urea/25 mM ammonium bicarbonate (250 μL) and incubated (15 min, RT). Subsequently DTT (2.5 μL, 1 mM) was added and the mixture was incubated (15 min, 65˚C). The sample cooled to RT and iodoacetamide (0.5 M, 20 μL) was added to alkylate the sample (30 min, RT, dark). SDS (70 μL, 10% (v/v)) was added and the proteome was heated (5 min, 65^{0}C). The sample was diluted with PBS (3 mL). 50 μL of a 50% slurry of Avidin–Agarose from egg white (Sigma-Aldrich) was washed with PBS and added to the proteome sample. The beads were incubated with the

proteome (3 h, RT, shaking). The beads were isolated by centrifugation (2500 *g*, 2 min) and washed with SDS in PBS (10 mL, 0.5% (w/v)), followed by 3 washes with PBS. The beads were transferred to low-binding Eppendorf tubes and proteins were digested with sequencing grade trypsin (Promega) (500 ng per sample) in 250 µL buffer (100 mM Tris, 100 mM NaCl, 1 mM $CaCl_2$, 2 % acetonitrile) (37 ˚C, O/N, vigorous shaking). The pH was adjusted with formic acid to pH 3 and the beads were removed by filtration.

The peptides were isotopically labeled by on stage tip dimethyl labeling according to literature procedures [14], with the following modification. Dimethyl labeling was performed by the subsequent addition of 20, 20, 30, 30 and 40 µL of Light (vehicle) or Medium (inhibitor) reagent to the stage tips. The centrifugation speed during labeling was adjusted to have a flow through time of approximately 5 min (400-1000 *g*) per labeling step.

For **Fig. 2 and S3**, Stable Isotope Labeling with Amino acids in Cell culture (SILAC) ABPP cell samples were prepared and analyzed on an LTQ-Orbitrap Velos (Thermo Scientific), and searched/quantified based on previously described procedures [31,32].

Targeted lipidomics

Sample extraction

Lipids were extracted from *in situ* treated human neural cells (48 h, 50 µM BIA 10-2474 or vehicle (0.25% DMSO)). The sample extraction was performed on ice. In brief, cell pellets with 1 million cells were transferred to 1.5 mL Eppendorf tubes, spiked with 10 μL each of deuterated labeled internal standard mix for endocannabinoids (*N*-arachidonoyl ethanolamine (AEA)-d8, *N*-arachidonoyldopamine (NADA)-d8, *N*-docosahexaenoylethanolamide (DHEA)-d4, 2-arachidonoylglycerol (2-AG)-d8, *N*-stearoylethanolamine (SEA)-d3, *N*-palmitoylethanolamine(PEA)-d4, *N*-linoleoylethanolamine (LEA)-d3 and *N*-oleoylethanolamine (OEA)-d4), positive apolar lipids (lysophosphatidylcholines (LPC)17:0, phosphatidylethanolamines (PE)17:0/17:0, phosphatidylcholines (PC)17:0/17:0, sphingomyelins (SM) d18:1/17:0, triglycerides (TG) 17:0/17:0/17:0, ceramides (Cer) d18:1/17:0) and negative polar lipids (fatty acid (FA)17:0-d33), followed by the addition of ammonium acetate buffer (100 μL, 0.1 M, pH 4). After extraction with methyl tert-butyl ether (1 mL), the tubes were thoroughly mixed for 4 min using a bullet blender at medium speed (Next Advance, Inc., Averill park, NY, USA), followed by a centrifugation step (5000 *g*, 12 min, 4°C). Then 925 µL of the upper layer methyl tert-butyl ether was transferred into clean

1.5 mL Eppendorf tubes. Samples were dried in a speed-vac followed by reconstitution in acetonitrile/water (50 µL, 90/10, v/v). The reconstituted samples were centrifuged (14000 *g*, 3 min, 4°C) before transferring into LC-MS vials. Each sample was injected on three different lipidomics platforms: endocannabinoids (5 μL), positive apolar lipids (2 μL) and for negative polar lipids (8 μL).

LC-MS/MS Analysis for endocannabinoids

A targeted analysis of 21 endocannabinoids and related NAEs (*N*-acylethanolamines) were measured using an Acquity UPLC I class Binary solvent manager pump (Waters, Milford, USA) in conjugation with AB SCIEX 6500 quadrupole-ion trap (QTRAP) (AB Sciex, Massachusetts, USA). Separation was performed with Acquity HSS T3 column (1.2 x 100 mm, 1.8 μm) maintained at 45 °C. The aqueous mobile phase A consisted of 2 mM ammonium formate and 10 mM formic acid, and the organic mobile phase B was acetonitrile. The flow rate was set to 0.4 ml/min; initial gradient conditions were 55% B held for 2 min and linearly ramped to 100% B over 6 minutes and held for 2min; after 10 s the system returned to initial conditions and held 2 min before next injection. Electrospray ionization-MS was operated in positive mode for measurement of 21 endocannabinoids and NAEs, and a selective Multiple Reaction Mode (sMRM) was used for quantification.

LC-MS/MS analysis for positive apolar and negative polar lipids

Both lipidomics methods are adapted and modified from previously published work [33]. Briefly, these methods are measured on an Acquity UPLC Binary solvent manager pump (Waters) coupled to an Agilent 6530 electrospray ionization quadrupole time-of-flight (ESI-Q-TOF, Agilent, Jose, CA, USA) high resolution mass spectrometer using reference mass correction. The chromatographic separation was achieved on an Acquity HSS T3 column (1.2 x 100 mm, 1.8 μm) maintained at 40°C for both methods. The positive polar lipids that include targets from different lipid classes including (lyso)phosphatidylcholines, triglycerides, ceramides. (lyso)phosphatidylethanolamines and sphingomyelins were separated using a flow of 0.4 mL/min over a 16 min gradient. In positive mode, the aqueous mobile phase A consisted of 60:40 (v/v) acetonitrile:H_2O with 10 mM ammonium formate, and the organic mobile phase B consisted of 10:90 (v/v) Acetonitrile : Isopropanol with 10 mM Ammonium formate. The negative apolar lipids that constitute mainly free fatty acids and (lyso)phosphatidylcholines were separated with a flow of 0.4 mL/min over 15 min gradient. In negative mode, the aqueous

mobile phase A consisted of 5:95 (v/v) acetonitrile:H_2O with 10 mM ammonium formate, and the organic mobile phase B consisted of 99% (v/v) methanol with 10 mM Ammonium formate. The targets in both lipid methods were detected full scan (100-1000 m/z) in their respective ion charge mode.

Activity assays

Natural substrate-based LC-MS assay hFAAH1

FAAH substrate hydrolysis measurements were determined according to the previously reported LC-MS-based assay [8]. hFAAH1-transfected HEK293T proteomes (5 μg) in 70 μL of DPBS was used for measuring substrate hydrolysis activity. 30 μL of 0.167 mM substrate (50 μM final concentration) was incubated with the enzyme solution with DMSO or inhibitor for 30 min at 37 °C. The reactions were quenched by the addition of 300 μL of 2:1 vol/vol $CHCl_3$:MeOH, doped with 1 nmol AA-d8, then the organic phase was subjected to LC-MS analysis.

Radiolabeled natural substrate assay hFAAH and mFAAH

The radiolabeled natural substrate based assay for human and mouse FAAH was performed as reported previously [34]. In brief, chemicals were of the purest analytical grade. Anandamide (AEA) was purchased from Sigma Chemical Co. (St. Louis, MO, USA). URB597 and purified hFAAH were obtained from Cayman Chemical (Ann Arbor, MI, USA). [^{14}C-ethanolamine]-anandamide (60 Ci/mmol) was purchased from ARC (St. Louis, MO). Mouse brain membranes (50 μg per test), prepared as reported [34], or hFAAH (2.5 μg per test) were pre-incubated for 15 min at room temperature with each compound, then they were incubated with 10 μM [^{14}C-ethanolamine]anandamide (15 min, 37 °C, in 500 μL of 50 mM Tris–HCl buffer (pH = 9)). The reaction was stopped by the addition of 0.6 mL of ice-cold methanol/chloroform (2:1, v/v). The mixture was centrifuged (3000 *g*, 5 min), the upper aqueous layer was put in a vial containing liquid scintillation cocktail (Ultima Gold XR, Perkin Elmer Life Sciences), and radioactivity was quantified in a β-counter.

Rat FAAH activity

The radiolabeled natural substrate based assay for FAAH was performed as reported previously using rat brain membranes either co-incubation with radiolabeled substrate and inhibitors, or pre-treated with inhibitors for 20 min prior to incubation with radiolabeled substrate [35].

Natural substrate-based fluorescence assay ABHD6

The natural substrate ABHD6 assay was performed as previously published [36].

Natural substrate-based fluorescence assay DAGLα/β

The natural DAG substrate assay was performed as reported previously [37]. Standard assay conditions: 0.2 U/mL glycerol kinase (GK), glycerol-3-phosphate oxidase (GPO) and horseradish peroxidase (HRP), 0.125 mM ATP, 10 μM Amplifu™ Red, 5% DMSO in a total volume of 200 μL. The assay additionally contained 5 μg/mL MAGL-overexpressing membranes, 100 μM SAG and 0.0075% (w/v) Triton X-100, with a final protein concentration of 50 μg/mL. The mDAGLβ assay was performed as the hDAGLα assay, but assay buffer was supplemented with 5 mM $CaCl_2$ and the SAG concentration was 75 μM.

Natural substrate-based fluorescence assay MAGL

The natural substrate MAGL assay was performed as previously published [37].

Surrogate substrate assay NAPE-PLD

The surrogate substrate assay was based on a previously reported method [38]. The membrane protein fraction HEK293T cells transiently overexpressing NAPE-PLD was diluted to 0.4 mg/mL in assay buffer (50 mM Tris-HCl (pH 7.5), 0.02% Triton X-100, 150 mM NaCl). The substrate PED6 (Invitrogen) stock (10 mM) was consecutively diluted in DMSO (25x) and in assay buffer (10x). Relevant concentrations of compounds are prepared in DMSO. The assay is performed in a dark Greiner 96 wells plate, end volume 100 μL. The membrane protein lysate (final concentration 0.04 mg/ml) is incubated with inhibitor or vehicle (30 min, 37 °C). A sample without membrane protein lysate is incorporated for background subtraction. Subsequently, substrate is added (PED6, final concentration: 1 μM) and the measurement is started immediately on a TECAN infinite M1000 pro (37 °C, scanning at 2 min intervals for 1 h: excitation 485 nm, emission 535 nm).

Radioligand displacement assays CB_1/ CB_2-receptor

[^{3}H]CP55940 displacement assays to determine the affinity for the cannabinoid CB_1 and CB_2 were performed as previously described [39,40], with the following changes: Ligands of interest were incubated (25 °C, 2 h) with membrane aliquots containing 1.5 μg (CHOK1hCB_2_bgal) membrane protein in 100 μL assay buffer (50 mM Tris–HCl, 5 mM $MgCl_2$, 0.1 % BSA, pH 7.4) with ~1.5 nM [^{3}H]CP55940 per assay point. Non-specific binding was determined in the presence of 10 μM AM630. Filtration was performed on 96-well GF/C filters, each well presoaked for 30 min with 25 μL 0.25 % PEI, using a 96-wells Filtermate harvester (PerkinElmer). Filter-bound radioactivity was determined by scintillation spectrometry using a Microbeta® 2450 microplate counter (PerkinElmer).

Fluorescent Ca^{2+} assays for TRP ion channels

HEK293 (human embryonic kidney) cells stably over-expressing recombinant human TRPV1 or rat TRPA1, TRPV2, TRPV3, TRPV4, or TRPM8 were grown on 100 mm diameter Petri dishes as mono-layers in minimum essential medium (MEM) supplemented with non-essential amino acids, 10 % fetal bovine serum, 2 mM glutamine, and maintained at 5 % CO_2 at 37 °C. Quantitative real time analysis was carried out to measure TRP gene over-expression in transfected-cells (data not shown). On the day of the experiment, cells were loaded with the methyl ester Fluo-4 AM in MEM (4 μM in DMSO containing 0.02 % Pluronic F-127, Invitrogen), kept in the dark at room temperature for 1 h, washed twice with Tyrode's buffer (145 mM NaCl, 2.5 mM KCl, 1.5 mM $CaCl_2$, 1.2 mM $MgCl_2$, 10 mM D-glucose, and 10 mM HEPES, pH 7.4), resuspended in the same buffer and transferred (about 100,000 cells) to the quartz cuvette of the spectrofluorimeter (PerkinElmer LS50B equipped with PTP-1 Fluorescence Peltier System; PerkinElmer Life and Analytical Sciences, Waltham, MA, USA) under continuous stirring. The effects on intracellular Ca^{2+} concentration ($[Ca^{2+}]_i$) before and after the addition of various concentrations of test compounds was measured by cell fluorescence (λ_{EX} = 488 nm, λ_{EM} = 516 nm) at 25 °C. The effects of compounds were normalized against the response to ionomycin (4 μM) in each experiment. The increases in fluorescence in wild-type HEK293 cells (i.e. not transfected with any construct) were used as baseline and subtracted from the values obtained from transfected cells. Efficacy was defined as the maximum response elicited by the compounds tested and was determined by comparing their effect with the analogous effect observed with 4 μM ionomycin (Cayman), while the potency of the compounds (EC_{50}) was determined as the concentration required to produce

half-maximal increases in $[Ca^{2+}]_i$. Curve fitting (sigmoidal dose–response variable slope) and parameter estimation were performed with GraphPad Prism® (GraphPad Software Inc., San Diego, CA).

Antagonist/desensitizing behavior was evaluated by adding the test compounds in the quartz cuvette 5 min before stimulation of cells with agonists. In the case of human TRPV1-expressing HEK293 cells the agonist used was capsaicin (0.1 μM, in the case of SR141716A 10 nM was also used), which was able of elevating intracellular Ca^{2+} with a potency of EC_{50} = 5.3 ± 0.4 nM and efficacy = 78.6 ± 0.6 %.

For TRPV2, the rat TRPV2-HEK293 cells exhibited a sharp increase in $[Ca^{2+}]_i$ upon application of lysophosphatidylcholine (LPC) 3 μM. The concentration for half-maximal activation was 3.40 ± 0.02 μM and efficacy was 91.7 ± 0.5 %.

In the case of TRPV3, rat TRPV3-expressing HEK-293 cells were first sensitized with the non-selective agonist 2-aminoethoxydiphenyl borate (100 μM). Antagonist/desensitizing behavior was evaluated against thymol (100 μM), which showed an efficacy of 34.7 ± 0.2 % and a potency of EC_{50} = 84.1 ± 1.6 μM.

In the case of rat TRPV4-expressing HEK-293 cells the agonist used was *N*-((1*S*)-1-{[4-((2*S*)-2-{[(2,4-dichlorophenyl)sulfonyl]amino}-3-hydroxypropanoyl)-1-piperazinyl]carbonyl}-3-methylbutyl)-1-benzothiophene-2-carboxamide (GSK1016790A), (10 nM), which was able of elevating intracellular Ca^{2+} with a potency of EC_{50} = 0.46 ± 0.07 μM, and an efficacy of 51.9 ± 1.7 %.

In the case of rat TRPM8-expressing HEK-293 cells, antagonist/desensitizing behavior was evaluated against icilin at 0.25 μM and 0.10 μM. For icilin, efficacy was 75.1 ± 1.1 and potency EC_{50} = 0.11 ± 0.01 μM.

In the case of HEK-293 cells stably over-expressing recombinant rat TRPA1, the effects of TRPA1 agonists are expressed as a percentage of the effect obtained with 100 μM allyl isothiocyanate (AITC), which showed a potency of EC_{50} = 1.41 ± 0.04 μM and an efficacy of 65.9 ± 0.5.

The effect on $[Ca^{2+}]_i$ exerted by agonist alone was taken as 100%. Data are expressed as the concentration exerting a half-maximal inhibition of agonist-induced $[Ca^{2+}]_i$ elevation (IC_{50}), which was calculated again using GraphPad. All determinations were performed at least in triplicate. Statistical analysis of the data was performed by analysis of variance at each point using ANOVA followed by the Bonferroni's test.

Methanolysis assay

5 mM concentration of BIA 10-2474 and PF04457845 in DMSO (10 μL) were incubated with various concentrations of NaOMe in MeOH (90 μL) for 24 h at 37 °C. The reactions were quenched with corresponding concentration of AcOH in water (90 μL). Methanolysis of the compounds was quantified by LC/UV-Vis monitoring (Agilent Technologies 1200) Liquid chromatography (LC) separation was achieved using a Luna reverse-phase C18 column (150 x 4.6 mm with 5 μm diameter particles, Phenomonex). Percent methanolysis was calculated by product peak area/total peak area multiplied by 100. Data is expressed as mean ± SEM (n=3).

Statistical methods

All statistical measures and methods are included in the respective Figure or Table captions. In brief: all data are shown as the mean ± SEM where applicable. A Student's *t*-test (unpaired, two-tailed) was used to determine differences between two groups. Data that included more than two groups or two factors were analyzed by two-way ANOVA, with post-hoc Tukey HSD test. All statistical analyses were conducted using Excel or GraphPad Prism version 7, and a *p*-value less than 0.05 was considered significant throughout unless indicated otherwise. For the lipid profiling study (**Fig. 3, Table. S5**), a Benjamini Hochberg correction (25 % false discovery rate) was applied.

A sample size of n=3 was sufficient to detect ≥ 50% inhibition of protein labeling with a 20% standard deviation and a power of 80% at a $p < 0.05$. Routinely, a protein is considered to be an off-target, if 50% inhibition of activity is reached at 10 μM. Since, BIA 10-2474 was weakly active on FAAH in in vitro assays (IC50 > 1 μM), the window of the ABPP assays was increased to a concentration of 50 μM to detect off-targets.

Synthetic methods

General remarks

All reactions were performed using oven- or flame-dried glassware and dry solvents. Reagents were purchased from Sigma-Aldrich, Acros, and Merck and used without further purification unless noted otherwise. All moisture sensitive reactions were performed under an argon atmosphere.

^{1}H and ^{13}C NMR spectra were recorded on a Bruker AV 400 MHz spectrometer at 400.2 (^{1}H) and 100.6 (^{13}C) MHz using $CDCl_3$ as solvent, unless stated otherwise. Chemical shift

values are reported in ppm with tetramethylsilane or solvent resonance as the internal standard ($CDCl_3$, δ 7.26 for ^1H, δ 77.16 for ^{13}C). Data are reported as follows: chemical shifts (δ), multiplicity (s = singlet, d = doublet, dd = double doublet, td = triple doublet, t = triplet, q = quartet, quintet = quint, br = broad, m = multiplet), coupling constants *J* (Hz), and integration. High- resolution mass spectra were recorded on a Thermo Scientific LTQ Orbitrap XL. Liquid chromatography was performed on a Finnigan Surveyor LC/MS system, equipped with a C18 column. Flash chromatography was performed using SiliCycle silica gel type SiliaFlash P60 (230–400 mesh). TLC analysis was performed on Merck silica gel 60/Kieselguhr F254, 0.25 mm. Compounds were visualized using $KMnO_4$ stain (K_2CO_3 (40 g), $KMnO_4$ (6 g), and water (600 mL)).

Synthesis of BIA 10-2474 (7) and BIA 10-2639 (6):

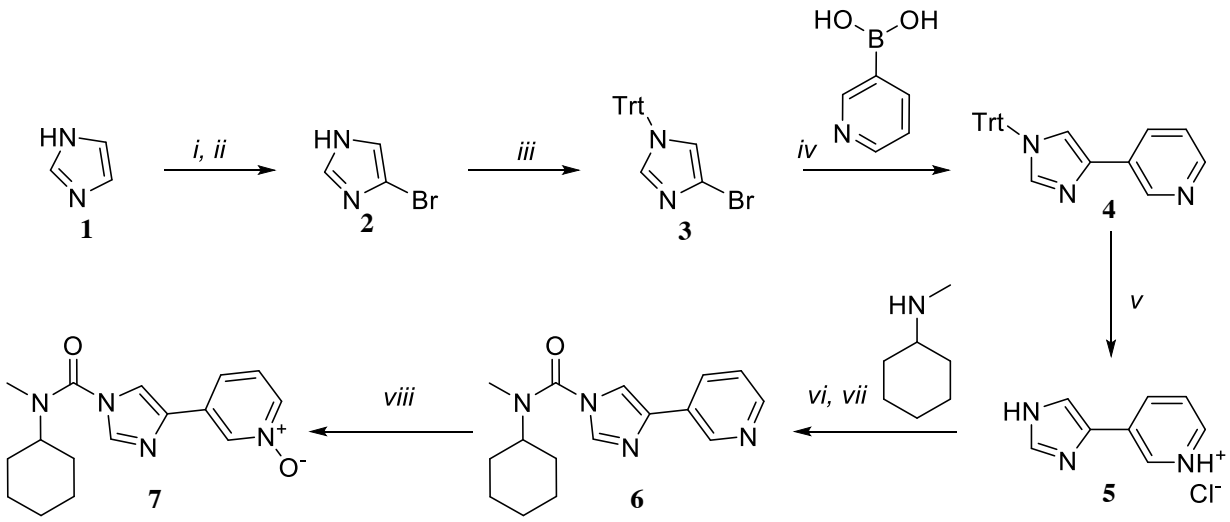

Reagents and conditions: *i)* NBS, DMF, RT; *ii)* 20% Na_2SO_3 (aq), 100°C, 20%; *iii)* TrtCl, DIPEA, DMF, RT, 93%; *iv)* $CsCO_3$, $Pd(PPh_3)_4$, pyridin-3-ylboronic acid, DMF:H_2O (8:1), 95°C, 75%; *v)* 4N HCl in dioxane, MeOH, RT, 69%; *vi)* Na_2CO_3, triphosgene, *N*-methylcyclohexanamine, DCM, 0-20°C; *vii)* cyclohexyl(methyl)carbamic chloride, 3-(1*H*-imidazol-4-yl)pyridine hydrochloride, DMAP, DIPEA, THF, reflux, 74%; *viii)* peracetic acid, DCM, 0-20°C, 97%.

Synthesis of 4-bromo-1H-imidazole (2)

To a solution of 1*H*-imidazole **1** (4 g, 58.8 mmol) in DMF (100 mL) a solution of 1-bromopyrrolidine-2,5-dione (11.50 g, 64.6 mmol) in DMF (100 mL) was added over 1.5 h. Reaction left to stir for 110 h and concentrated to dryness. The residue obtained was taken up

in 20% sodium sulphite solution in water and refluxed for 8 h. Upon cooling a precipitate formed which was filtered and dried to yield **2** (1.735 g, 11.81 mmol, 20% yield) as an off-white solid. ^{1}H NMR (400 MHz, MeOD) δ 7.61 (s, 1H), 7.11 (s, 1H). Spectroscopic data are in accordance with literature values [41].

Synthesis of 4-bromo-1-trityl-1H-imidazole (3)

DIPEA (4.06 mL, 23.27 mmol) was added to a solution of trityl chloride (4.87 g, 17.45 mmol) and 4-bromo-1*H*-imidazole (1.71 g, 11.63 mmol) in DMF (20 mL). The resulting mixture was left to stir for 140 h. The resulting suspension was filtered and the yellowish solid was washed with methanol to yield a fine white solid which was purified by column chromatography to yield **3** (4.2 g, 10.79 mmol, 93% yield) as a white solid. ^{1}H NMR (400 MHz, $CDCl_3$) δ 7.43 – 7.30 (m, 10H), 7.19 – 7.04 (m, 6H), 6.80 (s, 1H). ^{13}C NMR (101 MHz, $CDCl_3$) δ 141.86, 138.71, 129.86, 128.45, 128.33, 120.90. Spectroscopic data are in accordance with literature values [42].

Synthesis of 3-(1-trityl-1H-imidazol-4-yl)pyridine (4)

Cesium carbonate (6.70 g, 20.55 mmol), 4-bromo-1-trityl-1*H*-imidazole (2.00 g, 5.14 mmol) and pyridin-3-ylboronic acid (0.631 g, 5.14 mmol) were suspended in a mixture of DMF (40 mL) and water (5 mL). The resulting mixture was degassed by sonication for 30 min under a flow of argon. Tetrakis(triphenylphosphine)palladium(0) (148 mg, 0.128 mmol) was added and the mixture was heated to 90 degrees for 16 h. The reaction mixture was diluted with 100 mL of EtOAc and washed with water. The organic layer was separated and the water layer extracted twice with 100 mL of EtOAc. The combined organic layers were washed with brine, dried with $MgSO_4$ and concentrated. The oily residue was purified by column chromatography to yield **4** (1.50 g, 3.87 mmol, 75% yield) as a white solid. ^{1}H NMR (400 MHz, $CDCl_3$) δ 8.95 (dd, J = 2.3, 0.8 Hz, 1H), 8.42 (dd, J = 4.9, 1.7 Hz, 1H), 8.03 (dt, J = 8.0, 2.0 Hz, 1H), 7.99 (s, 1H), 7.68 (ddd, J = 12.0, 8.3, 1.4 Hz, 1H), 7.56 (d, J = 1.4 Hz, 1H), 7.47 – 7.40 (m, 1H), 7.34 (p, J = 3.9, 3.5 Hz, 9H), 7.24 (d, J = 1.4 Hz, 1H), 7.24 – 7.16 (m, 7H). ^{13}C NMR (101 MHz, $CDCl_3$) δ 147.70, 146.42, 142.06, 139.66, 137.83, 132.04, 131.90, 129.97, 129.68, 128.15, 123.40, 117.92, 75.60.

Synthesis of 3-(1H-imidazol-4-yl)pyridine hydrochloride (5)

To a solution of 3-(1-trityl-1*H*-imidazol-4-yl)pyridine (1.24 g, 3.20 mmol) in MeOH HCl in dioxane (4 M, 4.0 mL) was added and the mixture was stirred for 1 h at RT. A white precipitate formed which was filtered off. The filtrate was vigorously stirred and pentane was slowly added to the mixture. More precipitate formed which was filtered off. The resulting solids were air dried to yield **5** (401.3 mg, 2.210 mmol) in 69% yield. ^{1}H NMR (400 MHz, D_2O) δ 9.08 (d, J = 2.0 Hz, 1H), 8.84 (d, J = 1.3 Hz, 1H), 8.80 – 8.71 (m, 2H), 8.09 (dd, J = 8.3, 5.8 Hz, 1H), 8.00 (d, J = 1.3 Hz, 1H). ^{13}C NMR (101 MHz, D_2O) δ 143.10, 141.56, 138.96, 136.02, 127.80, 127.33, 127.14, 118.56.

Synthesis of N-cyclohexyl-N-methyl-4-(pyridin-3-yl)-1H-imidazole-1-carboxamide (6)

Triphosgene (0.831 g, 2.80 mmol) was added portionwise to a solution of *N*-methylcyclohexanamine (0.73 mL, 5.6 mmol) in DCM at 0 °C. After addition was complete, dried Na_2CO_3 (1.19 g, 11.2 mmol) was added in one batch and the mixture was allowed to warm to RT and stirred for 2 h. Na_2CO_3 was filtered off and the filtrate was concentrated to yield crude cyclohexyl(methyl)carbamic chloride which was used without further purification.

To a stirred solution of **5** (203 mg, 1.120 mmol), DMAP (68.4 mg, 0.560 mmol) and DIPEA (0.587 mL, 3.36 mmol) in dry THF (40 mL) at 0°C was added a solution of crude cyclohexyl(methyl)carbamic chloride in 5 mL THF. The resulting mixture was refluxed for 6 h under inert atmosphere. After the reaction was completed the cooled mixture was poured into saturated aqueous NH_4Cl solution and extracted three times with EtOAc. The combined organic layers were washed with brine, dried with $MgSO_4$ and concentrated *in vacuo* to yield a white solid. Purification by column chromatography yielded an analytically pure sample of **6** of 234 mg (74% yield). HRMS (ESI+) m/z: calculated for $C_{16}H_{21}N_4O$ ([M+H]): 285.1710; found: 285.1710. ^{1}H NMR (400 MHz, $CDCl_3$) δ 9.03 (dd, J = 2.3, 0.9 Hz, 1H), 8.54 (dd, J = 4.9, 1.6 Hz, 1H), 8.20 (dt, J = 8.0, 1.9 Hz, 1H), 7.94 (d, J = 1.3 Hz, 1H), 7.60 (d, J = 1.3 Hz, 1H), 7.41 (ddd, J = 8.0, 4.9, 0.9 Hz, 1H), 3.95 (t, J = 12.0 Hz, 1H), 3.01 (s, 3H), 1.97 – 1.77 (m, 5H), 1.71 (d, J = 13.3 Hz, 1H), 1.59 (qd, J = 12.7, 12.2, 4.0 Hz, 2H), 1.46 – 1.31 (m, 2H), 1.14 (qt, J = 13.1, 3.5 Hz, 1H). ^{13}C NMR (101 MHz, $CDCl_3$) δ 150.98, 147.35, 145.67, 138.79, 137.47, 133.39, 129.63, 123.99, 114.32, 57.72, 31.42, 30.03, 25.44, 25.24. Spectroscopic data are in accordance with literature values [43].

Synthesis of 3-(1-(cyclohexyl(methyl)carbamoyl)-1H-imidazol-4-yl)pyridine 1-oxide (7)

N-cyclohexyl-*N*-methyl-4-(pyridin-3-yl)-1*H*-imidazole-1-carboxamide **6** (100 mg, 0.352 mmol) was dissolved in dry DCM (25 mL) and cooled to 0°C. Peracetic acid (0.119 mL, 0.703 mmol) as a 39% solution in acetic acid was added in one batch and the resulting mixture was stirred for 16 h. When TLC showed full conversion the reaction mixture was concentrated and purified by column chromatography to yield **7** (102.6 mg, 0.342 mmol, 97% yield) as a white solid. HRMS (ESI+) m/z: calculated for $C_{16}H_{21}N_4O_2$ ([M+H]): 301.1659; found: 301.1659. ^{1}H NMR (400 MHz, $CDCl_3$) δ 8.72 (t, *J* = 1.6 Hz, 1H), 8.18 (ddd, *J* = 6.4, 1.8, 1.0 Hz, 1H), 7.93 (d, *J* = 1.3 Hz, 1H), 7.77 (dt, *J* = 8.1, 1.2 Hz, 1H), 7.60 (d, *J* = 1.3 Hz, 1H), 7.34 (dd, *J* = 8.0, 6.4 Hz, 1H), 3.99 – 3.84 (m, 1H), 3.00 (s, 3H), 1.87 (t, *J* = 13.5 Hz, 4H), 1.71 (d, *J* = 13.4 Hz, 1H), 1.59 (qd, *J* = 12.8, 12.2, 3.9 Hz, 2H), 1.45 – 1.29 (m, 2H), 1.13 (qt, *J* = 13.1, 3.5 Hz, 1H). ^{13}C NMR (101 MHz, $CDCl_3$) δ 150.72, 137.84, 137.66, 136.75, 136.18, 133.22, 126.25, 124.17, 115.75, 57.95, 31.60, 30.13, 25.56, 25.33. Spectroscopic data are in accordance with literature values [17].

Synthesis of PF04457845 (16)

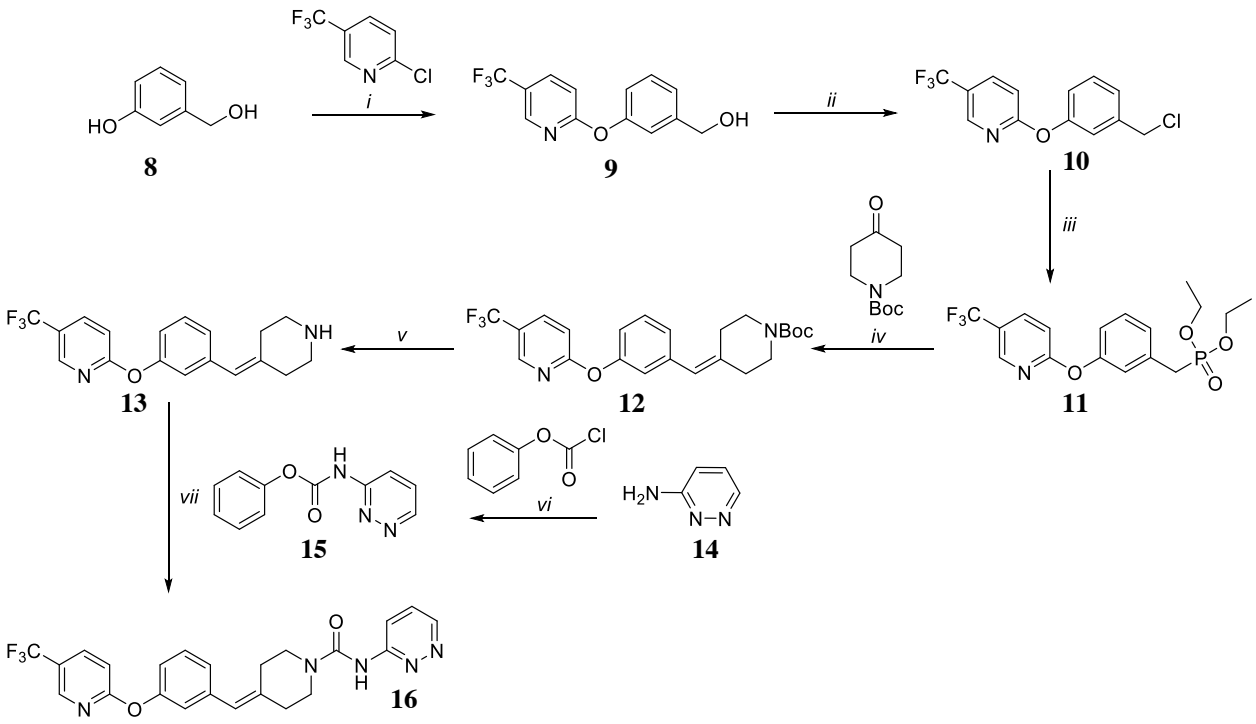

Reagents and conditions: *i)* 2-chloro-5-(trifluoromethyl)pyridine, K_2CO_3, DMF, 95-105°C, 98%; *ii)* $SOCl_2$, DCM, 0-20°C, 96%; *iii)* triethyl phosphite, toluene, 135-140°C, 52%; *iv)* KO^{t}Bu, *tert*-butyl 4-oxopiperidine-1-carboxylate, THF, -10°C, 63%; *v)* HCl, EtOAc, RT; *vi)*

phenyl carbonochloridate, pyridine, ACN, 0-20°C; *vii)* phenyl pyridazin-3-ylcarbamate, DIPEA, ACN, RT, 32%.

(3-((5-(trifluoromethyl)pyridin-2-yl)oxy)phenyl)methanol (9)

To a solution of 2-chloro-5-(trifluoromethyl)pyridine (182 mg, 1.0 mmol) in DMF was added 3-(hydroxymethyl)phenol (137 mg, 1.1 mmol) and K_2CO_3 (207 mg, 1.5 mmol). The solids were washed into the flask with another small amount of DMF. The mixture was heated to 95 - 105°C for 5 h. The reaction mixture was cooled to RT and poured into ice water. The mixture was extracted twice with ether/hexane (2:1). The combined organic layers were dried over $MgSO_4$ and concentrated under reduced pressure. The crude product was purified by flash chromatography using pentane/EtOAc) 5:1) to give the desired product **22** (265 mg, 0.984 mmol, 98% yield). ^{1}H NMR (400 MHz, $CDCl_3$) δ 8.38 – 8.31 (m, 1H), 7.87 (dd, *J* = 8.7, 2.5 Hz, 1H), 7.35 (t, *J* = 7.8 Hz, 1H), 7.17 (d, *J* = 7.6 Hz, 1H), 7.11 (t, *J* = 1.9 Hz, 1H), 7.04 – 6.93 (m, 2H), 4.58 (s, 2H), 3.45 (s, 1H). ^{13}C NMR (101 MHz, $CDCl_3$) δ 165.81, 153.29, 145.34 (q, *J* = 4.0 Hz), 143.48, 136.92, 129.88, 123.86, 123.67 (q, *J* = 271.7 Hz) 121.59 (q, *J* = 34.3 Hz), 120.32, 119.75, 111.45, 64.28. Spectroscopic data are in accordance with literature values [44].

2-(3-(chloromethyl)phenoxy)-5-(trifluoromethyl)pyridine (10)

To a solution of (3-((5-(trifluoromethyl)pyridin-2-yl)oxy)phenyl)methanol (95 mg, 0.353 mmol) in DCM at -5°C was added dropwise $SOCl_2$ (0.031 mL, 0.423 mmol). After that, the reaction was stirred at RT for 1 h until TLC shows the reaction was completed. The reaction mixture was concentrated *in vacuo* to near dryness. 2 mL of toluene was added to the residue and the solution was again concentrated *in vacuo* to near dryness (repeated 3 times). The crude product was purified by flash chromatography pentane/EtOAc (4:1) to give the desired product **10** (97 mg, 0.34 mmol, 96% yield). ^{1}H NMR (400 MHz, $CDCl_3$) δ 8.47 – 8.38 (m, 1H), 7.90 (dd, *J* = 8.7, 2.5 Hz, 1H), 7.41 (t, *J* = 7.9 Hz, 1H), 7.31 – 7.24 (m, 1H), 7.21 (t, *J* = 2.0 Hz, 1H), 7.11 (dd, *J* = 8.2, 2.3 Hz, 1H), 7.02 (d, *J* = 8.7 Hz, 1H), 4.59 (s, 2H).^{13}C NMR (101 MHz, $CDCl_3$) δ 165.66, 153.44, 145.55 (q, *J* = 4.04 Hz), 139.51, 136.84, 130.17, 125.62, 123.77 (q, *J* = 272.7 Hz), 121.86 (q, *J* = 31.3 Hz),121.70, 121.58, 111.61, 45.63. Spectroscopic data are in accordance with literature values [44].

Diethyl (3-((5-(trifluoromethyl)pyridin-2-yl)oxy)benzyl)phosphonate (11)

A solution of 2-(3-(chloromethyl)phenoxy)-5-(trifluoromethyl)pyridine (86 mg, 0.3 mmol) in toluene (2mL) and triethyl phosphite (79 μL, 0.45 mmol) was heated to 135-140°C for 7 h. The reaction was left standing at RT overnight and solidified. The solid was suspended in ether/hexane (1:2) and the suspension was stirred at RT for 3 h and filtered. The solid was rinsed with ether/hexane (1:2) pressed dry under suction and further dried *in vacuo* at 32°C for 7. The white solid **11** (60 mg, 0.154 mmol, 51% yield) was obtained without further purification. ^{1}H NMR (400 MHz, $CDCl_3$) δ 8.43 – 8.40 (m,1H), 7.89 (ddd, *J* = 8.7, 2.6, 0.6 Hz, 1H), 7.41 – 7.34 (m, 1H), 7.20 (ddt, *J* = 7.7, 2.5, 1.1 Hz, 1H), 7.11 (q, *J* = 2.2 Hz, 1H), 7.05 (dtd, *J* = 8.2, 2.3, 0.9 Hz, 1H), 7.00 (dt, *J* = 8.7, 0.8 Hz, 1H), 4.08 – 4.00 (m, 4H), 3.20 (s, 1H), 3.15 (s, 1H), 1.25 (td, *J* = 7.0, 0.4 Hz, 6H).^{13}C NMR (101 MHz, $CDCl_3$) δ 165.29, 152.80, 144.74, 136.51, 133.00, 129.38, 126.49, 123.26 (q, *J* = 271.7 Hz), 122.42, 121.09 (q, *J* = 33.33 Hz),119.62, 111.02, 62.01, 33.34, 31.97, 15.64. Spectroscopic data are in accordance with literature values [44].

tert-Butyl 4-(3-((5-(trifluoromethyl)pyridin-2-yl)oxy)benzylidene)piperidine-1-carboxylate (12)

Potassium *tert*-butoxide (0.578 mL, 0.93 mmol) in THF (1.6 M) was added dropwise in 5 min to a stirred mixture of diethyl (3-((5-(trifluoromethyl)pyridin-2-yl)oxy)benzyl)phosphonate (300 mg, 0.77 mmol) in dried THF at -10°C. The temperature rose to -3°C during the addition. The resulting red mixture was stirred between -6°C and -10°C for 30 min. A solution of *tert*-butyl 4-oxopiperidine-1-carboxylate (169 mg, 0.848 mmol) in THF was added dropwise over a 5 minute period. The temperature rose to 2°C. The resulting mixture was stirred at RT over the next 16h. The mixture was poured into 40 mL ice water. The resulting suspension was stirred at RT for 2.5 h and was then extracted with DCM. The combined extracts were washed with brine and dried over $MgSO_4$. The crude product was purified by flash chromatography using pentane/EtOAc (4:1) to give the desired product **12** (210 mg, 0.483 mmol, 63% yield). ^{1}H NMR (400 MHz, $CDCl_3$) δ 8.44 (d, *J* = 2.5 Hz, 1H), 7.89 (dd, *J* = 8.7, 2.5 Hz, 1H), 7.37 (td, *J* = 7.6, 1.0 Hz, 1H), 7.09 (dd, *J* = 7.8, 1.4 Hz, 1H), 7.04 – 6.95 (m, 3H), 6.35 (s, 1H), 3.46 (dt, *J* = 38.9, 5.8 Hz, 4H), 2.48 (t, *J* = 5.8 Hz, 2H), 2.33 (t, *J* = 5.8 Hz, 2H), 1.48 (s, 9H). ^{13}C NMR (101 MHz, $CDCl_3$) δ 171.28, 154.86, 153.14, 145.72, 139.63, 136.81, 132.77, 129.63, 126.22, 123.85, 123.36 (q, *J* = 272.7 Hz), 121.94, 121.12 (q, *J* = 34.3 Hz), 119.41, 111.50,

79.75, 45.34, 44.33, 36.09, 29.17, 28.41. Spectroscopic data are in accordance with literature values [44].

2-(3-(piperidin-4-ylidenemethyl)phenoxy)-5-(trifluoromethyl)pyridine (13)

To a solution of *tert*-butyl 4-(3-((5-(trifluoromethyl)pyridin-2-yl)oxy)benzylidene)piperidine-1-carboxylate (150 mg, 0.345 mmol) in EtOAc (1 mL) was added HCl (4M in dioxane, 0.432 mL, 1.73 mmol). After TLC indicated complete consumption of the starting material, the mixture was poured into a saturated aqueous solution of $NaHCO_3$ and the product was extracted with DCM (3x). The combined organic layers were dried over Na_2SO_4 and concentrated under reduced pressure to provide the crude product, which was used in the next step without further purification. ^{1}H NMR (400 MHz, $CDCl_3$) δ 9.81 (br, 1H), 8.43 (d, *J* = 2.4 Hz, 1H), 7.92 (dd, *J* = 8.7, 2.5 Hz, 1H), 7.41 (t, *J* = 7.9 Hz, 1H), 7.09 – 6.98 (m, 3H), 6.95 (t, *J* = 1.9 Hz, 1H), 6.47 (s, 1H), 3.23 (d, *J* = 50.3 Hz, 4H), 2.79 (d, *J* = 48.8 Hz, 4H). ^{13}C NMR (101 MHz, $CDCl_3$) δ 153.25, 145.49, 138.10, 136.94, 133.49, 129.96, 126.59, 126.00, 123.63 (q, *J* = 271.2 Hz), 121.91, 121.70, 121.53 (q, *J* = 33.3 Hz), 120.25, 111.70, 45.34, 44.68, 32.64, 25.84. Spectroscopic data are in accordance with literature values [44].

Phenyl pyridazin-3-ylcarbamate (15)

To a stirred suspension of pyridazin-3-amine (100 mg, 1.05 mmol) and pyridine (0.213 mL, 2.63 mmol) in ACN (5 mL) was added phenyl carbonochloridate (198 mg, 1.26 mmol) dropwise at 0°C. The mixture was stirred at 0°C for 1 hour. To the mixture was added water (10 mL) and the mixture was stirred at room temperature for 30 min and 0°C for 1 hour. The solid was collected by filtration and washed with ACN and water (1:2) to give crude product which was used in the next step without further purification. ^{1}H NMR (400 MHz, $CDCl_3$) δ 9.21 (dd, *J* = 4.8, 1.4 Hz, 1H), 7.76 (dd, *J* = 8.6, 1.5 Hz, 1H), 7.65 (dd, *J* = 8.6, 4.8 Hz, 1H), 7.36 (d, *J* = 6.3 Hz, 2H), 7.26 (d, *J* = 1.3 Hz, 1H), 7.19 (d, *J* = 1.4 Hz, 2H). ^{13}C NMR (101 MHz, $CDCl_3$) δ 155.51, 151.36, 150.17, 129.65, 128.75, 126.68, 126.42, 121.20.

N-(pyridazin-3-yl)-4-(3-((5-(trifluoromethyl)pyridin-2-yl)oxy)benzylidene)piperidine-1-carboxamide PF04457845 (16)

To a mixture of 2-(3-(piperidin-4-ylidenemethyl)phenoxy)-5-(trifluoromethyl)pyridine (20 mg, 0.060 mmol) and phenyl pyridazin-3-ylcarbamate (15.5 mg, 0.07 mmol) in acetonitrile (2

mL) DIPEA (0.026 mL, 0.15 mmol) was added dropwise. The solution was stirred at RT for 17 h, after which the reaction mixture was poured into ice-water. The resulting mixture was stirred for 1 hour. The solid was filtered off, rinsed with water and pressed dry. The residue was extracted with DCM (3x) and the combined organic layers were dried over Na_2SO_4 and concentrated under reduced pressure. The crude product was purified by flash chromatography (DCM:MeOH = 50:1) to give the desired product **15** (8.7 mg, 0.019 mmol, 32% yield). HRMS (ESI+) m/z: calculated for $C_{23}H_{21}F_3N_5O_2$ ([M+H]): 455.1636; found: 455.1642. ^{1}H NMR (400 MHz, $CDCl_3$) δ 8.79 (brs, 1H), 8.49 – 8.41 (m, 1H), 8.33 (brs, 1H), 7.91 (dd, *J* = 8.7, 2.5 Hz, 1H), 7.51 – 7.36 (m, 2H), 7.11 (d, *J* = 7.9 Hz, 1H), 7.07 – 6.98 (m, 3H), 6.43 (s, 1H), 3.70 (t, *J* = 5.9 Hz, 2H), 3.60 (t, *J* = 5.9 Hz, 2H), 2.62 (t, *J* = 5.6 Hz, 2H), 2.48 (t, *J* = 5.7 Hz, 2H). Spectroscopic data are in accordance with literature values [44].

Synthesis of three 2-step probes AJ167 (17), AJ179 (18) and AJ198 (19)

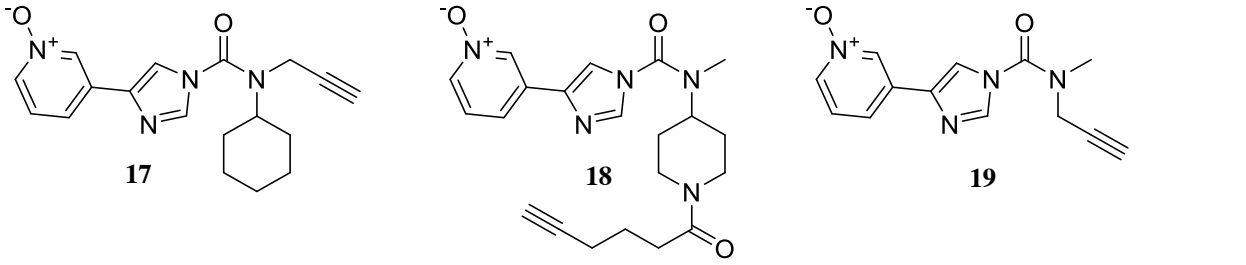

Synthesis of AJ167 (17)

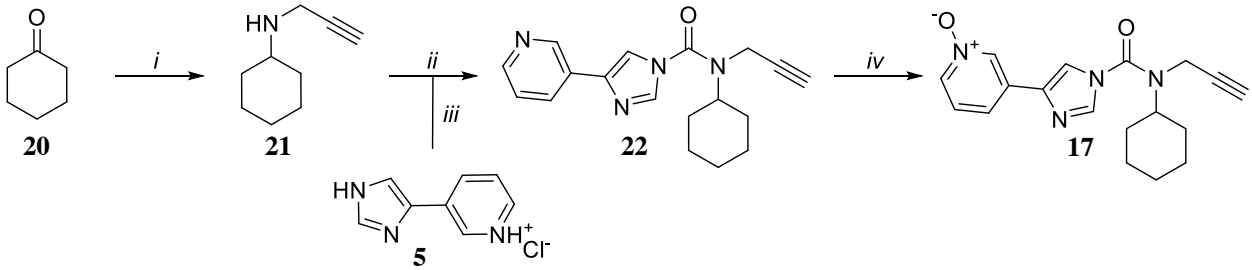

Reagents and conditions: *i)* propargylamine, AcOH, sodium triacetoxyborohydride, DCM, 0-20°C, 97%; *ii)* triphosgene, Na_2CO_3, DCM, 0-20°C; *iv)* 3-(1*H*-imidazol-4-yl)pyridine hydrochloride, DIPEA, DMAP, THF, reflux, 65%; *v)* peracetic acid, DCM, 0-20°C, 55%.

Synthesis of N-(prop-2-yn-1-yl)cyclohexanamine (21)

To a stirred solution of prop-2-yn-1-amine (0.50 mL, 7.8 mmol), cyclohexanone (0.404 mL, 3.90 mmol) and sodium triacetoxyborohydride (1.655 g, 7.81 mmol) in dry THF (40 mL) was

slowly added one equivalent of acetic acid (0.223 mL, 3.90 mmol). The resulting mixture was stirred for 5 hours at room temperature after which the solvent was evaporated off. The crude was purified by column chromatography to yield *N*-(prop-2-yn-1-yl)cyclohexanamine (0.521 g, 3.80 mmol, 97 % yield) as a colourless oil. ^{1}H NMR (400 MHz, $CDCl_3$) δ 3.46 (d, *J* = 2.5 Hz, 2H), 2.74 – 2.59 (m, 1H), 2.21 (t, *J* = 2.4 Hz, 1H), 1.92 – 1.80 (m, 2H), 1.80 – 1.67 (m, 2H), 1.68 – 1.53 (m, 2H), 1.31 – 0.98 (m, 5H). ^{13}C NMR (101 MHz, $CDCl_3$) δ 82.51, 71.04, 54.95, 35.08, 33.01, 26.11, 24.83.

Synthesis of N-cyclohexyl-N-(prop-2-yn-1-yl)-4-(pyridin-3-yl)-1H-imidazole-1-carboxamide (22)

A solution of *N*-(prop-2-yn-1-yl)cyclohexanamine (227 mg, 1.652 mmol) and triphosgene (163 mg, 0.551 mmol) in dry DCM (30 mL) was cooled to 0°C and sodium carbonate (175 mg, 1.652 mmol) was added in one batch. The resulting suspension was stirred for 2 hours at room temperature. Na_2CO_3 was filtered off and the filtrate concentrated *in vacuo*.

To a stirred solution of 3-(1*H*-imidazol-4-yl)pyridine hydrochloride (100 mg, 0.551 mmol), DMAP (67.3 mg, 0.551 mmol) and DIPEA (385 μL, 2.202 mmol) in dry THF (30 mL) at 0°C was added a solution of crude carbamic chloride in 5 mL THF. The resulting mixture was refluxed for 4 hours under inert atmosphere. After the reaction was completed the cooled mixture was poured into saturated aqueous NH_4Cl solution and extracted three times with ethyl acetate. The combined organic layers were washed with brine, dried with $MgSO_4$ and concentrated *in vacuo* to yield a white solid. This was purified by column chromatography to yield an analytically pure sample of 110 mg (65% yield). ^{1}H NMR (500 MHz, $CDCl_3$) δ 9.02 (d, *J* = 2.2 Hz, 1H), 8.53 (dd, *J* = 1.6, 4.9 Hz, 1H), 8.17 (d, *J* = 1.3 Hz, 1H), 8.13 (dt, *J* = 1.9, 7.9 Hz, 1H), 7.82 (d, *J* = 1.3 Hz, 1H), 7.35 (dd, *J* = 4.8, 7.9 Hz, 1H), 4.09 (d, *J* = 2.4 Hz, 2H), 4.00 (tt, *J* = 3.7, 12.1 Hz, 1H), 2.49 (t, *J* = 2.4 Hz, 1H), 1.93 (ddt, *J* = 2.8, 13.7, 41.4 Hz, 4H), 1.70 (qd, *J* = 3.5, 12.4 Hz, 2H), 1.47 – 1.09 (m, 4H). ^{13}C NMR (126 MHz, $CDCl_3$) δ 150.70, 148.50, 146.69, 139.41, 132.62, 129.11, 123.74, 114.03, 79.91, 73.59, 58.82, 35.02, 30.55, 25.70, 25.26.

Synthesis of 3-(1-(cyclohexyl(prop-2-yn-1-yl)carbamoyl)-1H-imidazol-4-yl)pyridine 1-oxide AJ167 (17)

22 (20 mg, 0.065 mmol) is dissolved in dry DCM (10 mL) and cooled to 0°C. Peracetic acid (20 μL, 0.118 mmol) as a 39% solution in acetic acid was added in one batch and the resulting

mixture was stirred for 16 hours, slowly warming up to RT. The reaction mixture was concentrated and purified by column chromatography to yield 3-(1-(cyclohexyl(prop-2-yn-1-yl)carbamoyl)-1*H*-imidazol-4-yl)pyridine 1-oxide (11.5 mg, 0.035 mmol, 55% yield) as a white solid. HRMS (ESI+) m/z: calculated for $C_{18}H_{20}N_4O_2$ ([M+H]): 325.1659; found: 325.1658. ^{1}H NMR (400 MHz, $CDCl_3$) δ 8.68 (s, 1H), 8.16 (d, *J* = 1.1 Hz, 2H), 7.86 – 7.80 (m, 1H), 7.75 (d, *J* = 8.0 Hz, 1H), 7.34 (t, *J* = 7.1 Hz, 1H), 4.07 (d, *J* = 2.4 Hz, 2H), 3.98 (tt, *J* = 12.0, 3.6 Hz, 1H), 2.49 (t, *J* = 2.4 Hz, 1H), 2.01 – 1.85 (m, 4H), 1.70 (qd, *J* = 12.2, 3.5 Hz, 2H), 1.46 – 1.10 (m, 4H). ^{13}C NMR (101 MHz, $CDCl_3$) δ 150.24, 137.87, 137.69, 137.04, 132.80, 126.02, 123.17, 115.26, 79.65, 73.80, 58.89, 35.01, 30.47, 25.64, 25.19.

Synthesis of AJ179 (18)

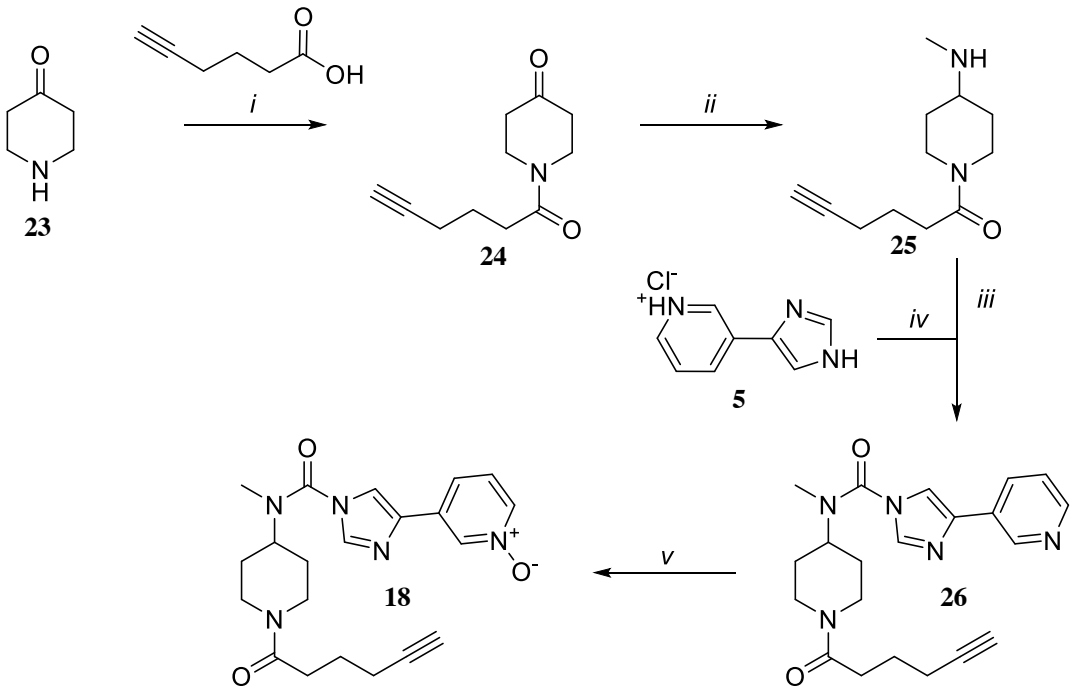

Reagents and conditions*: i)* hex-5-ynoic acid, HBTU, DIPEA, THF:DCM (1:1), RT, 91%; *ii)* $MeNH_3Cl$, AcOH, DIPEA, sodium triacetoxy-borohydride, DCM, 0-20°C, 89%; *iii)* triphosgene, Na_2CO_3, DCM, 0-20°C; *iv)* 3-(1*H*-imidazol-4-yl)pyridine hydrochloride, DIPEA, DMAP, THF, reflux, 43%; *v)* peracetic acid, DCM, 0-20°C, 17%.

Synthesis of 1-(hex-5-ynoyl)piperidin-4-one (24)

To a stirred solution of hex-5-ynoic acid (0.396 mL, 3.58 mmol) in a 1:1 mixture of THF:DCM DIPEA (1.42 mL, 8.14 mmol) and HBTU (2.72 g, 7.16 mmol) were added in one batch. After

the solution became homogenous piperidin-4-one hydrochloride hydrate (0.50 g, 3.26 mmol) was added. The mixture was left to stir for 215 h at room temperature. The reaction was quenched with saturated $NaHCO_3$ (aq) and extracted three times with EtOAc. The combined organic layers were washed with brine, dried over $MgSO_4$ and concentrated under reduced pressure. The residue was purified by column chromatography to yield **24** (572 mg, 2.96 mmol, 91% yield) as a colourless oil. ^{1}H NMR (400 MHz, $CDCl_3$) δ 3.90 (t, *J* = 6.4 Hz, 2H), 3.80 (t, *J* = 6.3 Hz, 2H), 2.58 (t, *J* = 7.3 Hz, 2H), 2.53 – 2.46 (m, 4H), 2.33 (td, *J* = 6.7, 2.7 Hz, 2H), 2.00 (t, *J* = 2.6 Hz, 1H), 1.91 (p, *J* = 7.0 Hz, 2H). ^{13}C NMR (101 MHz, $CDCl_3$) δ 206.91, 171.11, 83.64, 69.32, 44.06, 41.29, 40.90, 38.66, 31.43, 23.68, 17.92.

Synthesis of 1-(4-(methylamino)piperidin-1-yl)hex-5-yn-1-one (25)

1-(hex-5-ynoyl)piperidin-4-one **24** (572 mg, 2.96 mmol) was dissolved in DCM and methanamine hydrochloride (400 mg, 5.92 mmol), acetic acid (0.373 mL, 6.51 mmol) and DIPEA (1.09 mL, 6.22 mmol) were added. When cooled to 0°C sodium triacetoxyborohydride (1.25 g, 5.92 mmol) was added in one portion. The resulting suspension was left to stir for 18 h warming up to RT. The reaction was quenched with a saturated aqueous Na_2CO_3 solution and extracted three times with EtOAc. The combined organic layers were washed with brine, dried over $MgSO_4$ and concentrated *in vacuo*. The residue was purified by column chromatography to yield **25** (549 mg, 2.64 mmol, 89% yield) as a colorless oil. ^{1}H NMR (400 MHz, $CDCl_3$) δ 4.44 (dtd, *J* = 13.4, 4.2, 1.9 Hz, 1H), 3.86 (dtd, *J* = 13.6, 4.1, 1.9 Hz, 1H), 3.09 (ddd, *J* = 14.0, 11.4, 2.9 Hz, 1H), 2.75 (ddd, *J* = 13.9, 11.5, 3.1 Hz, 1H), 2.60 (tt, *J* = 10.0, 3.9 Hz, 1H), 2.46 (t, *J* = 7.3 Hz, 2H), 2.44 (s, 3H), 2.27 (td, *J* = 6.8, 2.7 Hz, 2H), 2.01 (t, *J* = 2.6 Hz, 1H), 1.98 – 1.78 (m, 4H), 1.33 – 1.15 (m, 2H). ^{13}C NMR (101 MHz, $CDCl_3$) δ 170.30, 83.68, 69.02, 56.32, 43.98, 40.19, 33.42, 32.55, 31.72, 31.49, 23.84, 17.88.

Synthesis of N-(1-(hex-5-ynoyl)piperidin-4-yl)-N-methyl-4-(pyridin-3-yl)-1H-imidazole-1-carboxamide (26)

25 (274 mg, 1.32 mmol) was dissolved in DCM (25 mL) and cooled to 0°C. Sodium carbonate (209 mg, 1.97 mmol) and triphosgene (390 mg, 1.32 mmol) were added and the mixture was stirred for 2 hours at RT. The solids were filtered off and the filtrate was concentrated under reduced pressure and redissolved in THF (25 mL). DIPEA (0.459 mL, 2.63 mmol), **5** (59.7 mg, 0.329 mmol) and DMAP (161 mg, 1.32 mmol) were added and the resulting mixture was refluxed for 4 h. The reaction was quenched with saturated aqueous $NaHCO_3$ solution and

extracted three times with EtOAc. The organic layers were combined, washed with brine and dried using $MgSO_4$. The solvent was removed and the crude purified by column chromatography to yield **26** (54.0 mg, 0.142 mmol, 43% yield) as a white solid. ^{1}H NMR (400 MHz, $CDCl_3$) δ 9.07 – 8.98 (m, 1H), 8.58 – 8.51 (m, 1H), 8.14 (dt, *J* = 7.9, 1.9 Hz, 1H), 7.97 (d, *J* = 1.3 Hz, 1H), 7.61 (d, *J* = 1.3 Hz, 1H), 7.37 (dd, *J* = 7.9, 4.8 Hz, 1H), 4.85 (ddt, *J* = 13.4, 4.8, 2.4 Hz, 1H), 4.29 (tt, *J* = 12.2, 4.2 Hz, 1H), 4.13 – 4.00 (m, 1H), 3.22 – 3.09 (m, 1H), 3.02 (s, 3H), 2.63 (td, *J* = 13.0, 2.8 Hz, 1H), 2.51 (t, *J* = 7.4 Hz, 2H), 2.31 (td, *J* = 6.7, 2.7 Hz, 2H), 1.99 (t, *J* = 2.6 Hz, 1H), 2.01 – 1.83 (m, 4H), 1.76 (qt, *J* = 12.2, 3.9 Hz, 2H). ^{13}C NMR (101 MHz, $CDCl_3$) δ 170.67, 151.29, 148.44, 146.52, 139.42, 137.50, 132.79, 129.05, 123.80, 114.03, 83.78, 69.20, 55.57, 44.62, 40.94, 32.15, 31.53, 29.23, 28.53, 23.80, 18.00.

Synthesis of 3-(1-((1-(hex-5-ynoyl)piperidin-4-yl)(methyl)carbamoyl)-1H-imidazol-4-yl)pyridine 1-oxide AJ179 (18)

A solution of **26** (25 mg, 0.066 mmol) in DCM (25 mL) was cooled to 0°C and peracetic acid (50 μL, 0.30 mmol) was added in one batch. The resulting mixture was left to stir for 16 h, after which the solvent was removed *in vacuo*. The resulting crude was purified by column chromatography to yield an analytically pure sample of **18** (4.5 mg, 0.011 mmol, 17% yield) as a white solid. ^{1}H NMR (400 MHz, MeOD) δ 8.82 (d, *J* = 1.7 Hz, 1H), 8.27 (d, *J* = 6.0 Hz, 1H), 8.22 (d, *J* = 1.2 Hz, 1H), 8.17 (d, *J* = 1.2 Hz, 1H), 8.05 (d, *J* = 8.3 Hz, 1H), 7.61 (dd, *J* = 8.1, 6.3 Hz, 1H), 4.73 (d, *J* = 13.3 Hz, 1H), 4.33 – 4.19 (m, 1H), 4.19 – 4.10 (m, 1H), 3.27 – 3.17 (m, 1H), 3.04 (s, 3H), 2.71 (dd, *J* = 14.0, 11.2 Hz, 1H), 2.61 – 2.55 (m, 2H), 2.32 – 2.25 (m, 2H), 2.06 (s, 1H), 2.02 – 1.74 (m, 6H). ^{13}C NMR (101 MHz, MeOD) δ 171.79, 151.05, 138.53, 137.24, 135.78, 135.46, 133.45, 126.77, 125.67, 116.99, 82.89, 68.90, 55.81, 44.57, 40.74, 31.16, 29.34, 28.56, 27.88, 24.03, 17.18.

Synthesis of AJ198 (19)

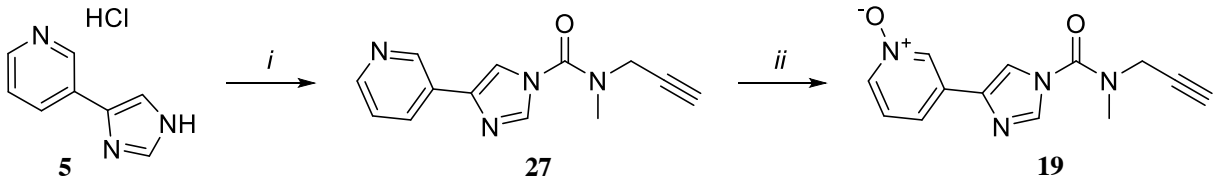

Reagents and conditions: *i)* propargylamine, triphosgene, Na_2CO_3, DCM, 0-20°C, 3-(1*H*-imidazol-4-yl)pyridine hydrochloride, DIPEA, DMAP, THF, reflux, 28%; *ii)* peracetic acid, DCM, 0-20°C, 56%.

Synthesis of N-methyl-N-(prop-2-yn-1-yl)-4-(pyridin-3-yl)-1H-imidazole-1-carboxamide (27)

To a stirred solution of *N*-methylprop-2-yn-1-amine (0.084 ml, 1.0 mmol) in DCM (10 ml) at 0°C sodium carbonate (106 mg, 1.000 mmol) was added. Triphosgene (223 mg, 0.750 mmol) was added and the mixture is stirred at RT for 1 hour. The suspension is then filtered and the filtrate is concentrated *in vacuo* to a yellow oil. This is redissolved in 10 mL of dry THF (molecular sieves) and 3-(1*H*-imidazol-4-yl)pyridine hydrochloride (182 mg, 1.00 mmol) and DIPEA (0.437 ml, 2.50 mmol) are added. The mixture is heated up and refluxed for 16 hours. The reaction is quenched by the addition of saturated aqueous $NaHCO_3$ and is extracted three times with ethyl acetate. This is washed with brine, dried with $MgSO_4$ and concentrated. Purification using column chromatography yields **27** in 28% yield (68 mg, 0.28 mmol). ^{1}H NMR (300 MHz, $CDCl_3$) δ 8.99 (s, 1H), 8.45 (d, *J* = 4.9 Hz, 1H), 8.30 – 8.13 (m, 2H), 8.02 (s, 1H), 7.47 (dd, *J* = 4.9, 8.1 Hz, 1H), 4.29 (d, *J* = 1.3 Hz, 1H), 3.22 (s, 4H), 2.93 (q, *J* = 2.1 Hz, 1H). ^{13}C NMR (75 MHz, $CDCl_3$) δ 148.78, 146.94, 134.57, 125.41, 116.53, 75.23, 40.81, 36.52, 30.74.

Synthesis of 3-(1-(methyl(prop-2-yn-1-yl)carbamoyl)-1H-imidazol-4-yl)pyridine 1-oxide AJ198 (19)

N-methyl-*N*-(prop-2-yn-1-yl)-4-(pyridin-3-yl)-1*H*-imidazole-1-carboxamide (20 mg, 0.083 mmol) is dissolved in DCM (10 mL) and cooled to 0 °C. Peracetic acid (0.092 ml, 0.416 mmol) as 30% solution in acetic acid is added in one batch. The mixture is stirred for 72 hours, slowly warming up to RT. The crude is then concentrated under reduced pressure and purified by column chromatography to yield **19** (12 mg, 0.047 mmol, 56% yield) as a white solid. HRMS (ESI+) m/z: calculated for $C_{13}H_{12}N_4O_2$ ([M+H]): 257.1033; found: 257.1037. ^{1}H NMR (400 MHz, MeOD) δ 8.80 (t, *J* = 1.7 Hz, 1H), 8.25 (dt, *J* = 1.3, 6.5 Hz, 1H), 8.22 (d, *J* = 1.3 Hz, 1H), 8.15 (d, *J* = 1.3 Hz, 1H), 8.02 (dt, *J* = 1.2, 8.1 Hz, 1H), 7.58 (dd, *J* = 6.4, 8.1 Hz, 1H), 4.29 (d, *J* = 2.4 Hz, 2H), 3.22 (s, 3H), 2.92 (t, *J* = 2.5 Hz, 1H).

NMR spectra of tested compounds

3-(1-(cyclohexyl(methyl)carbamoyl)-1H-imidazol-4-yl)pyridine 1-oxide BIA 10-2474 (7)

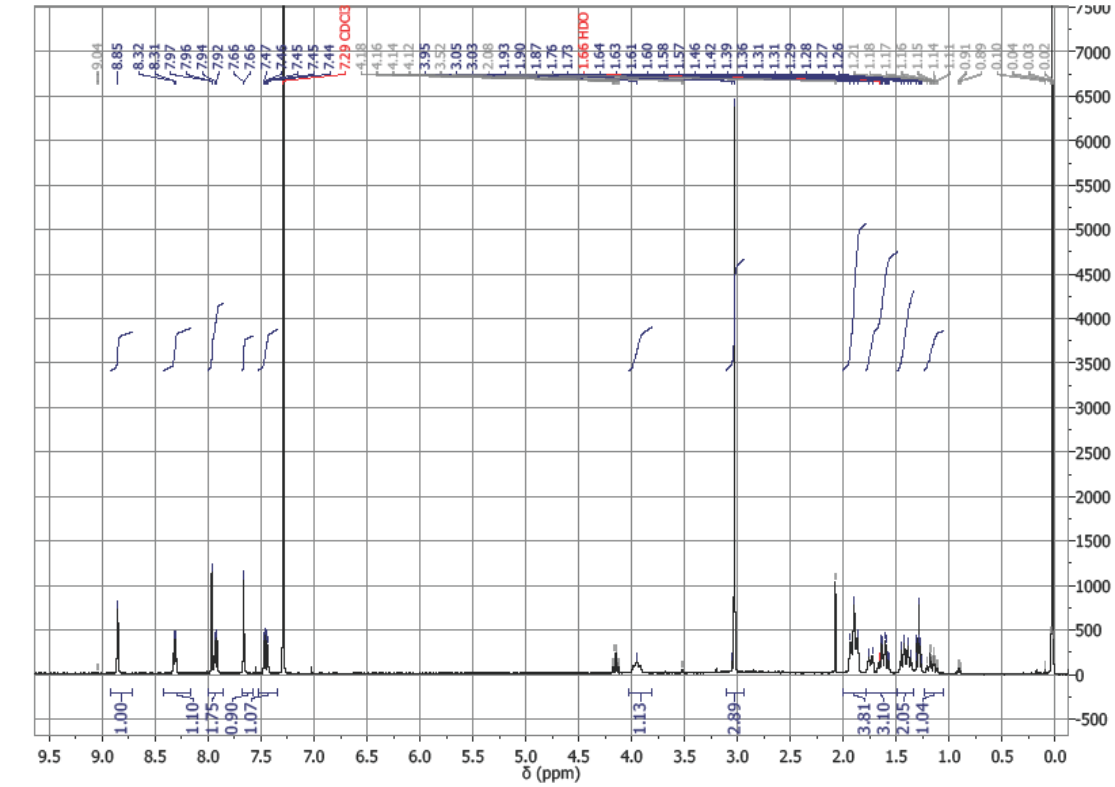

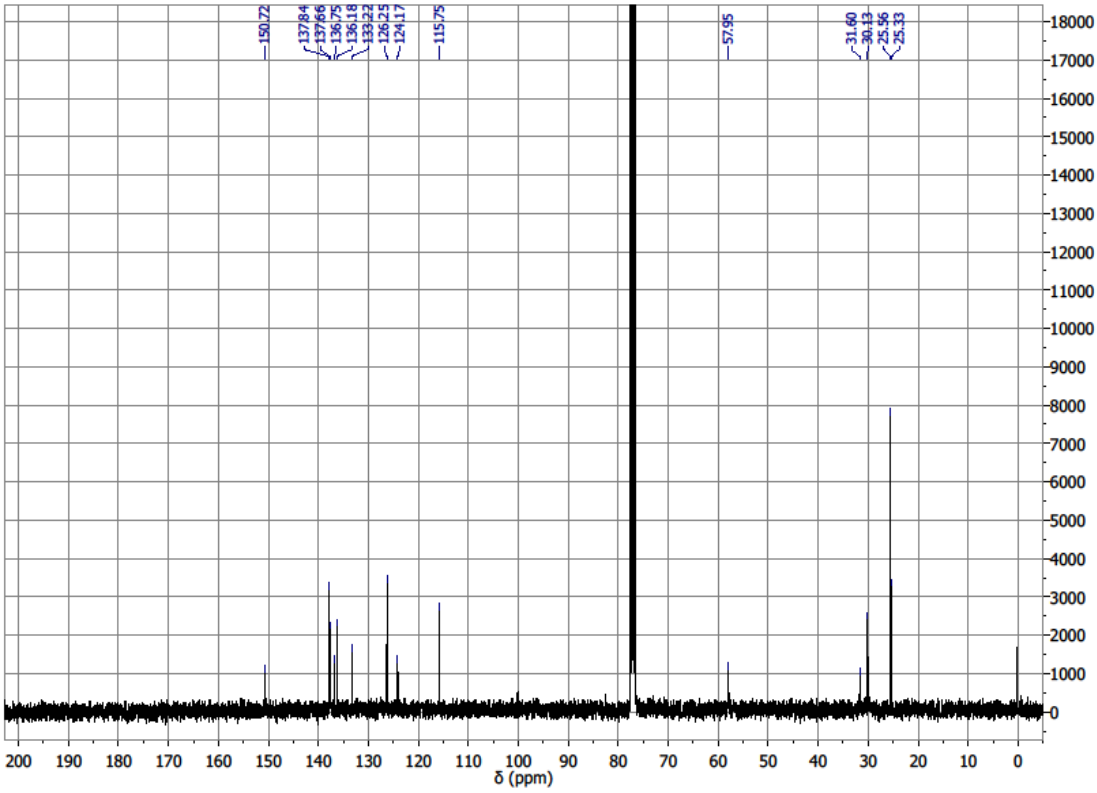

N-(pyridazin-3-yl)-4-(3-((5-(trifluoromethyl)pyridin-2-yl)oxy)benzylidene)piperidine-1-carboxamide PF04457845 (16)

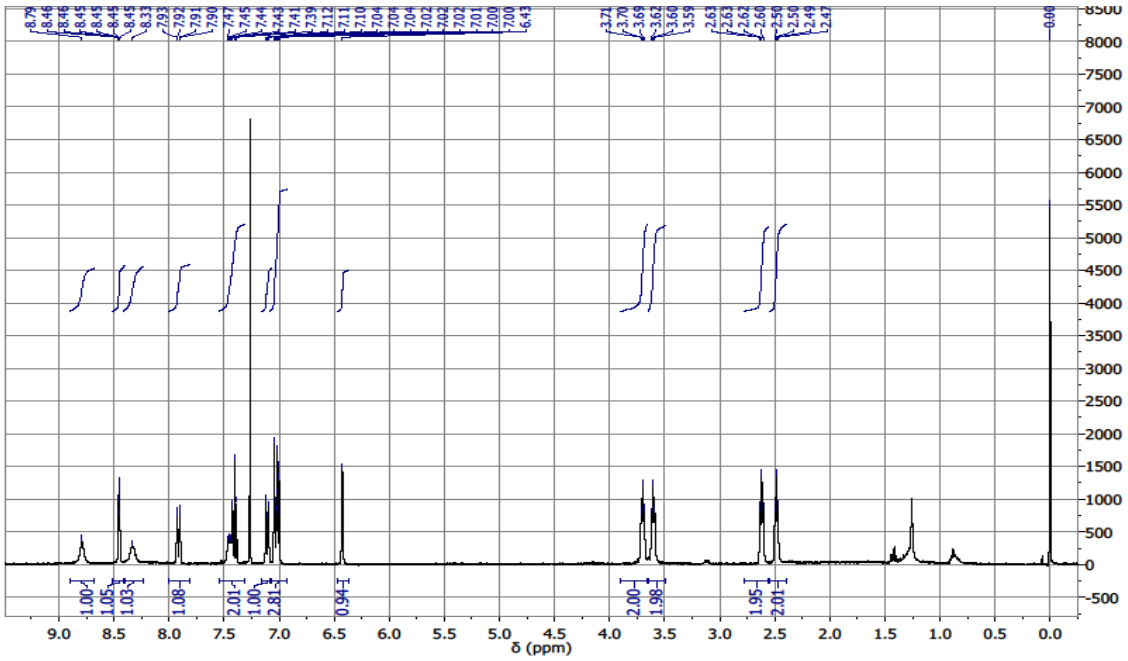

N-cyclohexyl-N-methyl-4-(pyridinyl)-1H-imidazole-1-carboxamide BIA 10-2639

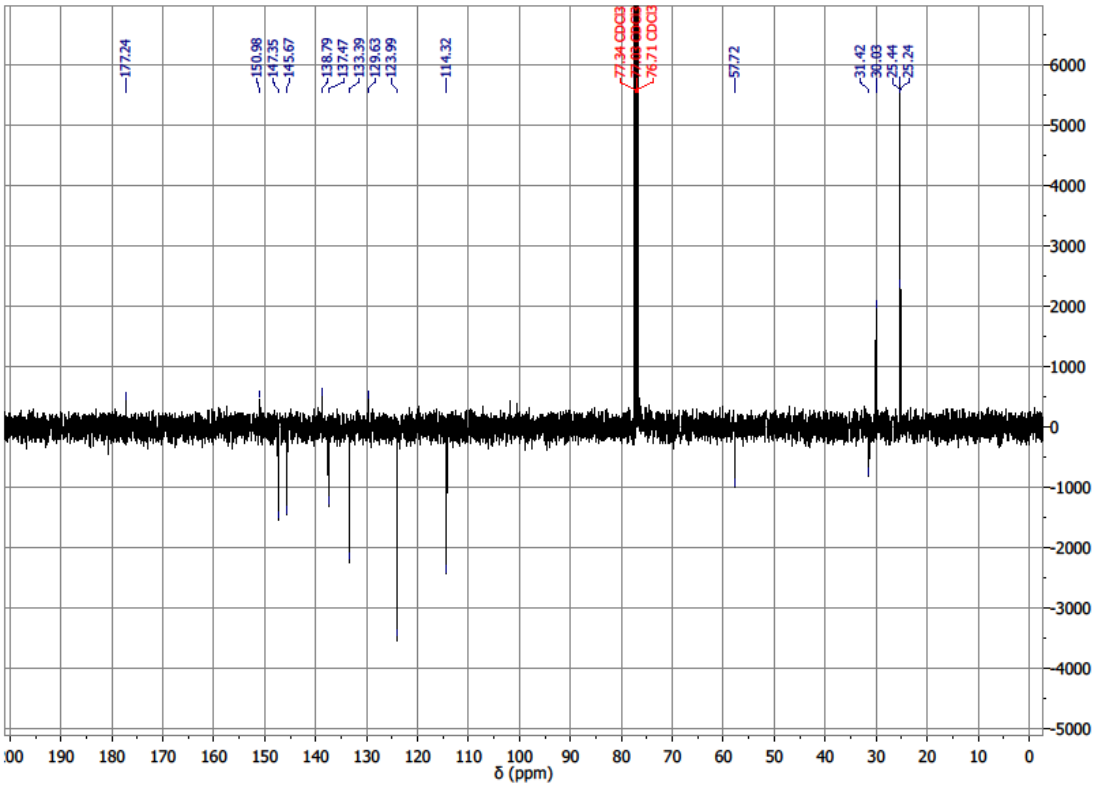

3-(1-(cyclohexyl(prop-2-yn-1-yl)carbamoyl)-1H-imidazol-4-yl)pyridine 1-oxide AJ167 (17)

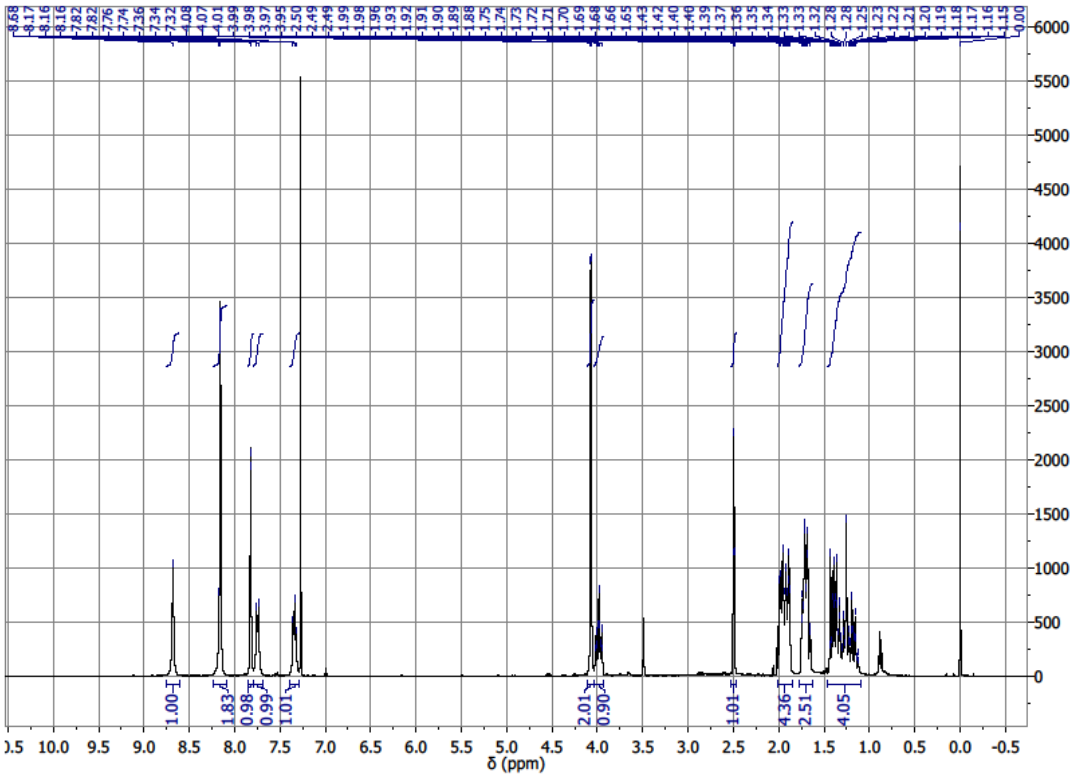

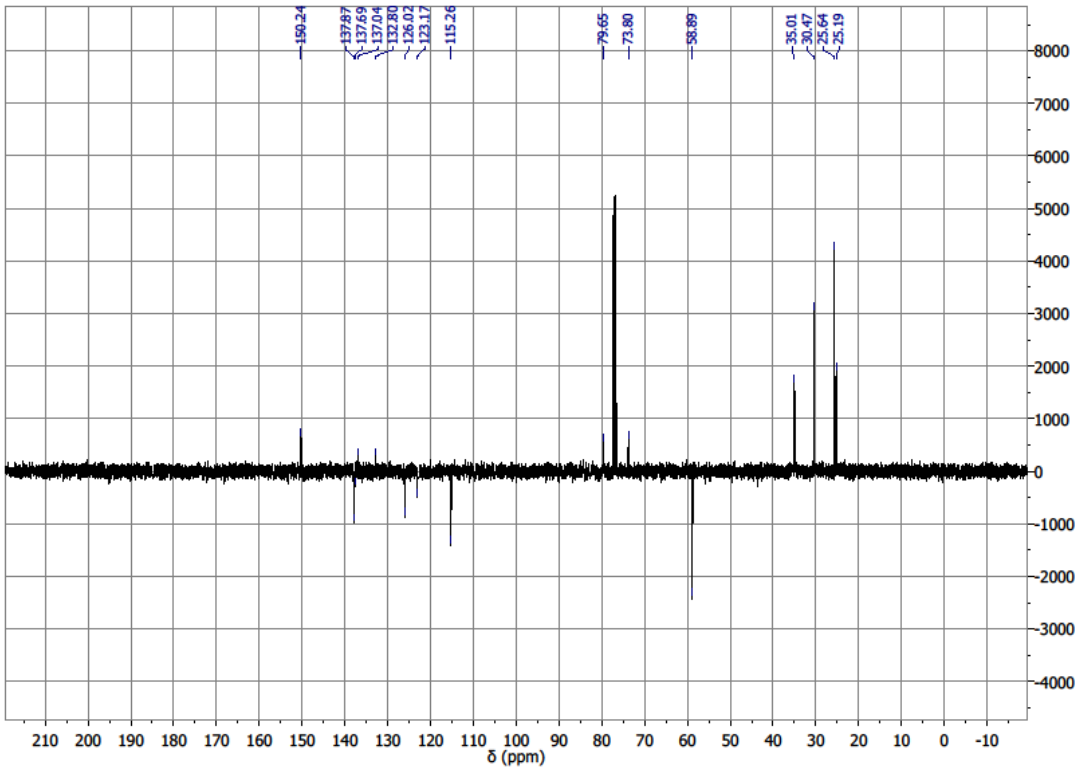

3-(1-((1-(hex-5-ynoyl)piperidin-4-yl)(methyl)carbamoyl)-1H-imidazol-4-yl)pyridine 1-oxide AJ179 (18)

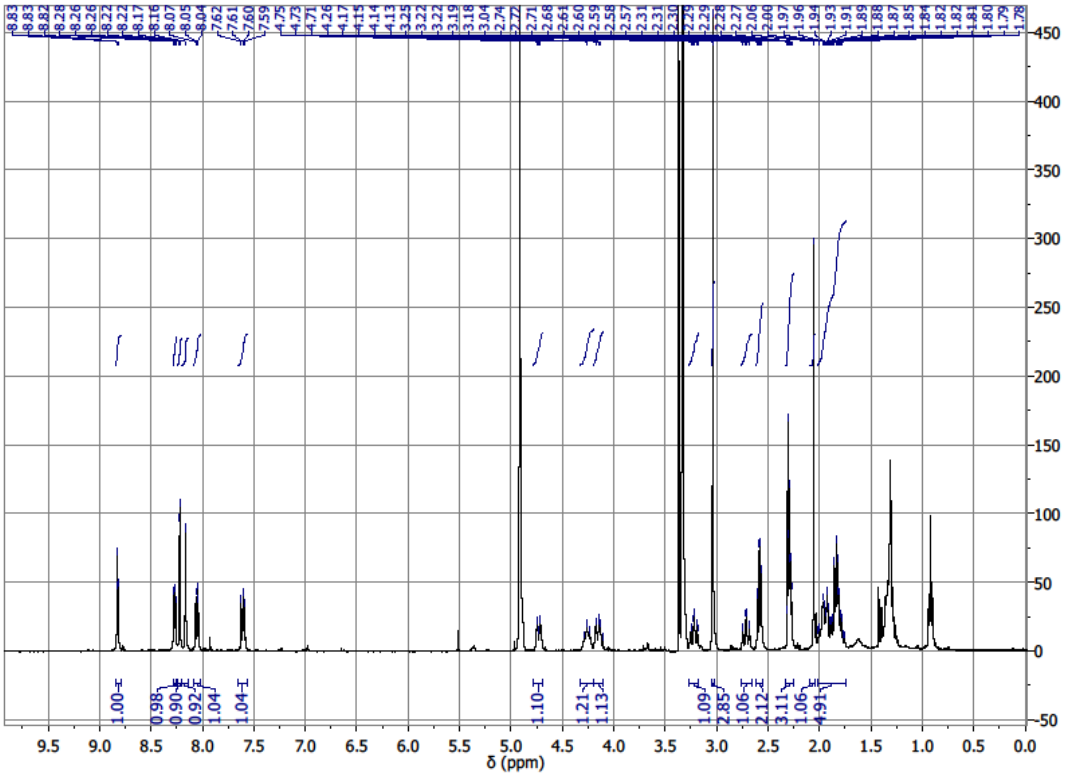

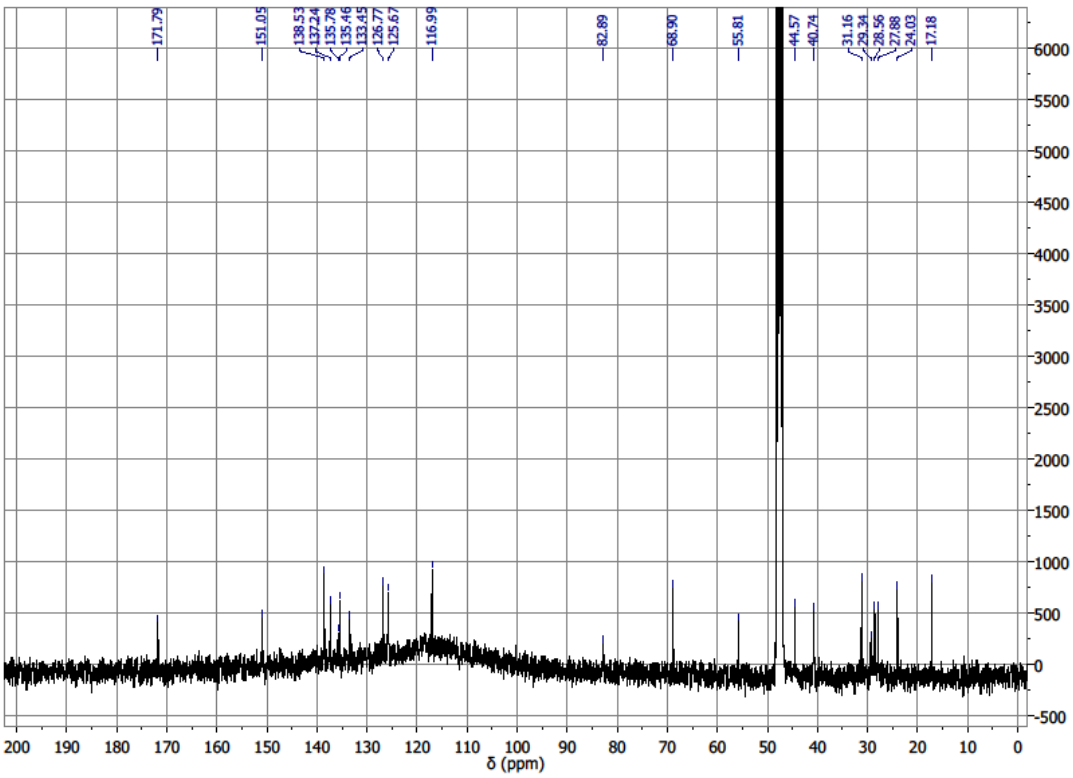

3-(1-(methyl(prop-2-yn-1-yl)carbamoyl)-1H-imidazol-4-yl)pyridine 1-oxide AJ198 (19)

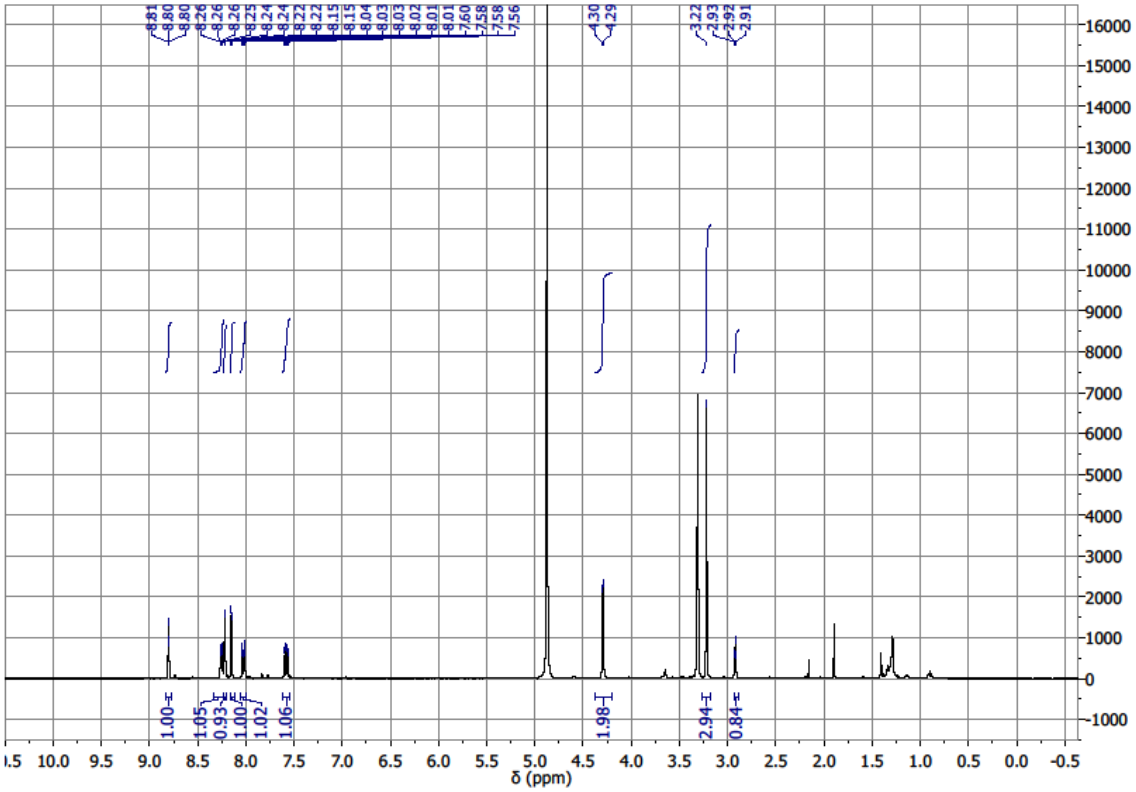

LC-traces of tested compounds

BIA 10-2474

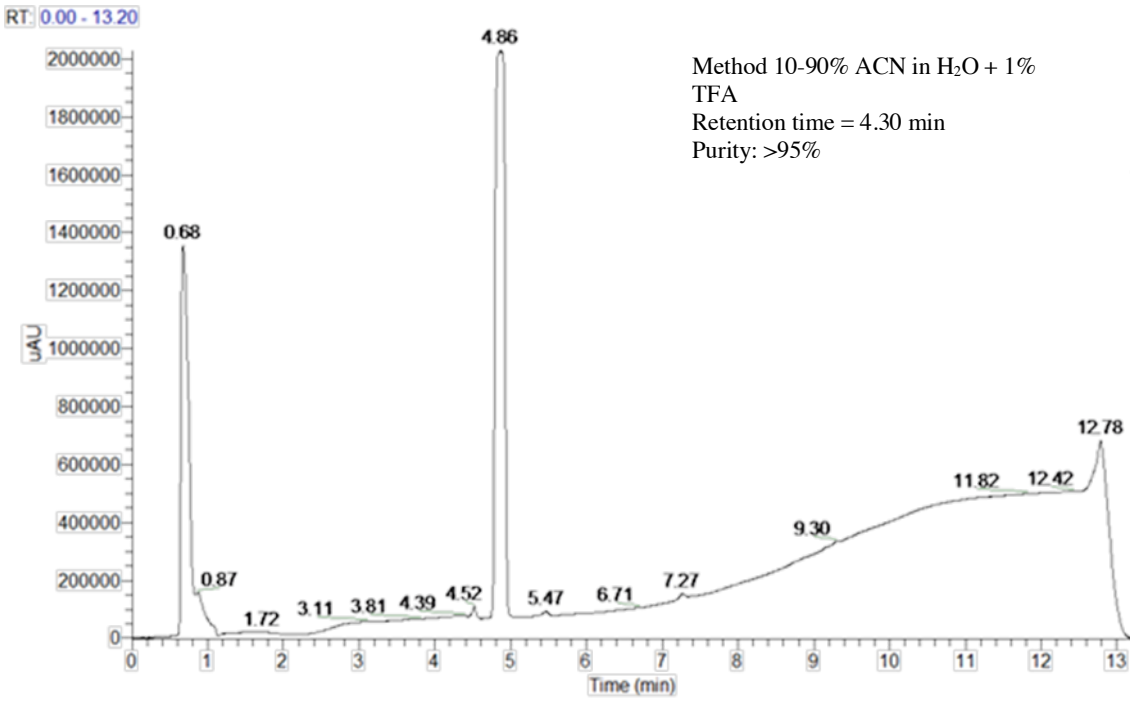

Method 10-90% ACN in H_2O + 1% TFA
Retention time = 4.30 min
Purity: >95%

PF04457845

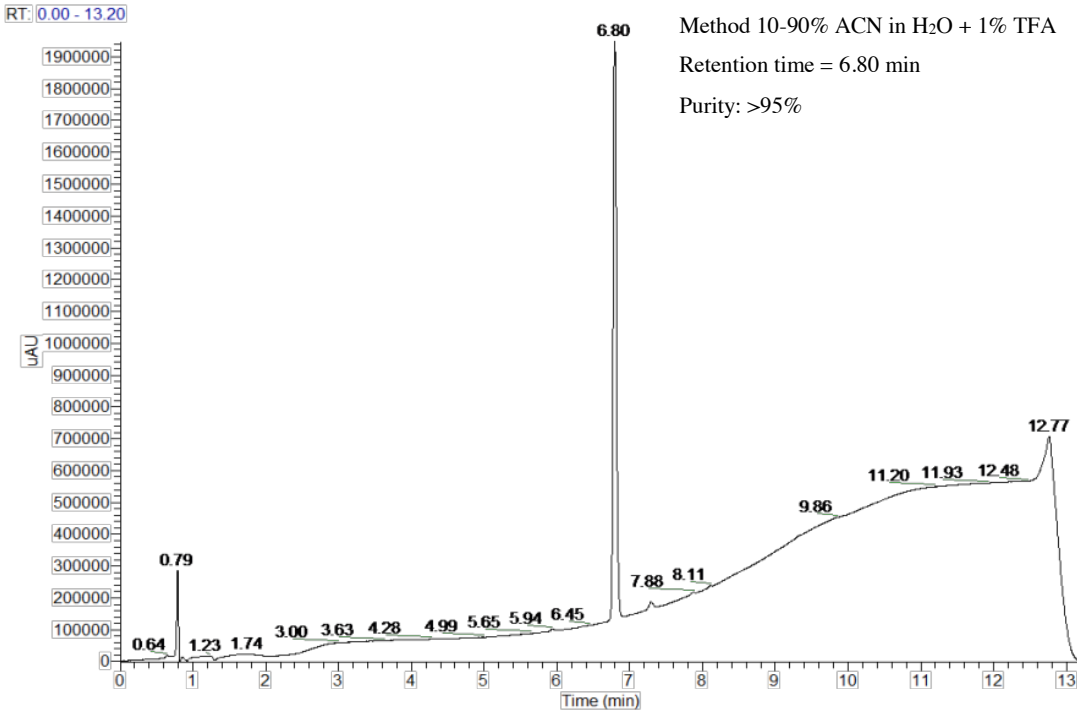

Method 10-90% ACN in H_2O + 1% TFA

Retention time = 6.80 min

Purity: >95%

BIA 10-2639

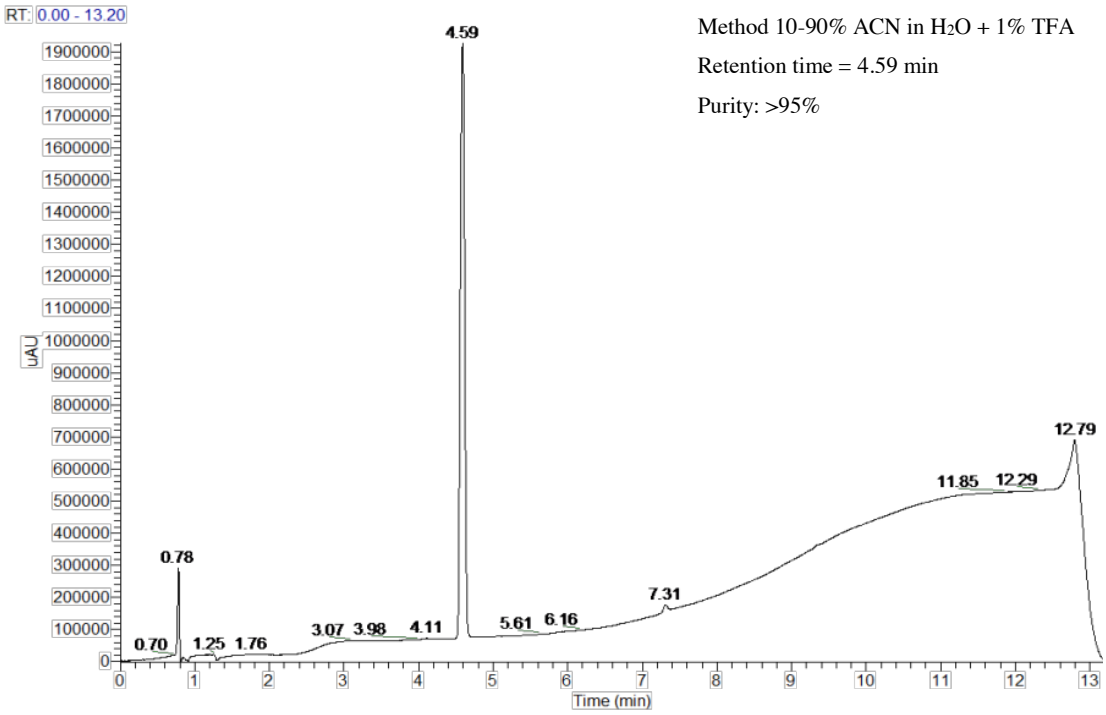

Method 10-90% ACN in H_2O + 1% TFA

Retention time = 4.59 min

Purity: >95%

AJ167

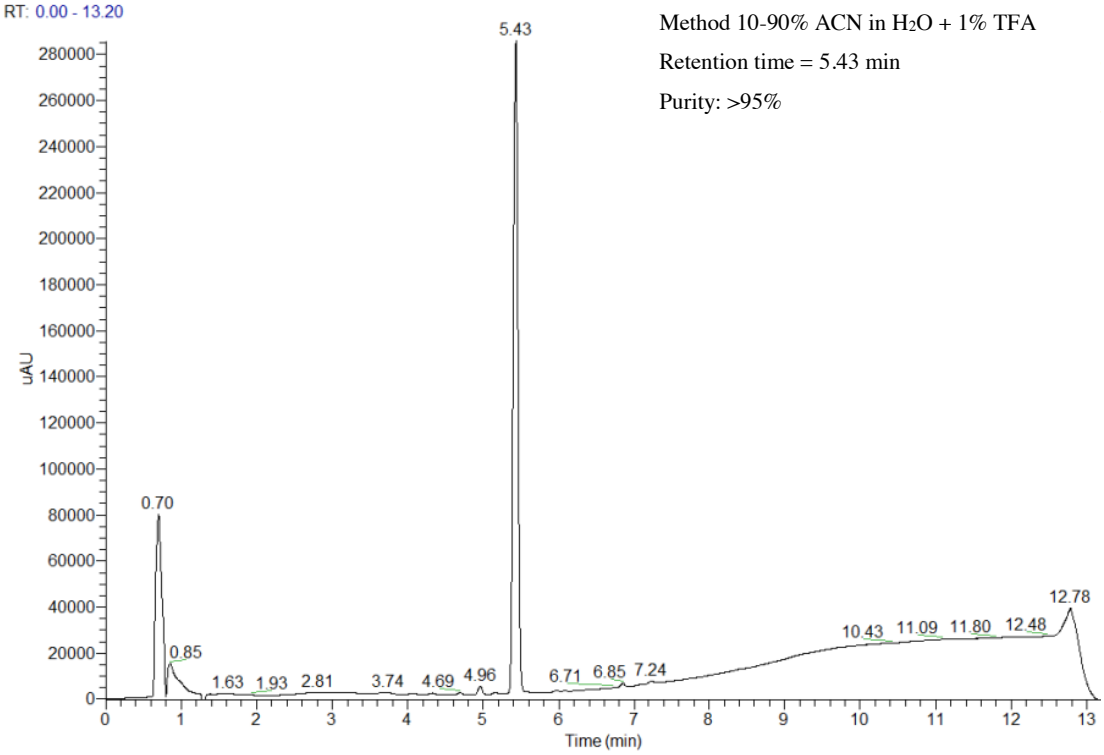

Method 10-90% ACN in H_2O + 1% TFA

Retention time = 5.43 min

Purity: >95%

AJ179

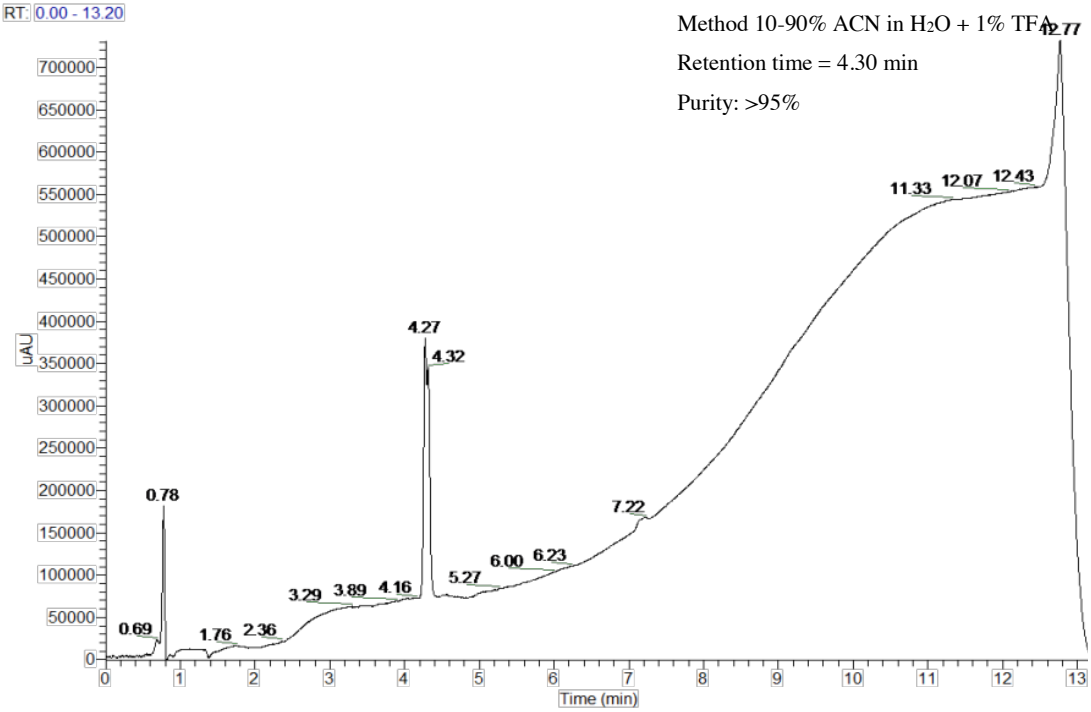

Method 10-90% ACN in H_2O + 1% TFA

Retention time = 4.30 min

Purity: >95%

AJ198

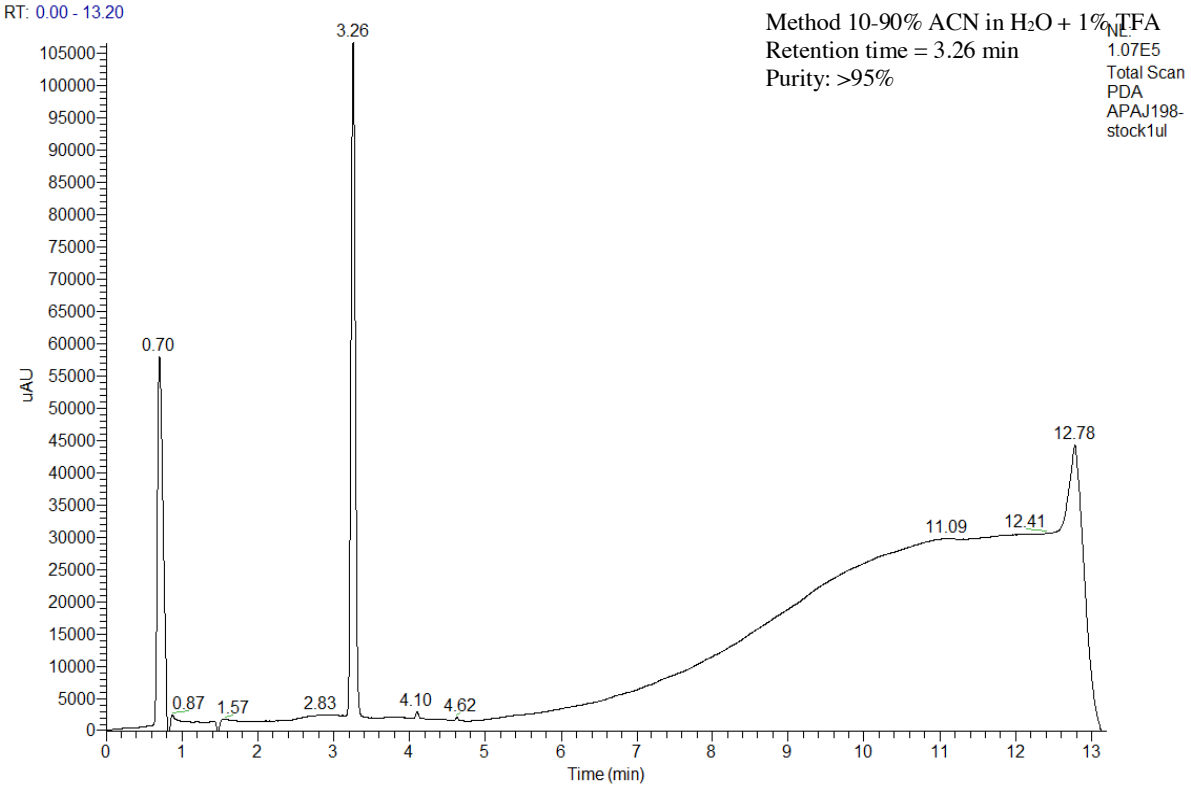
RT: 0.00 - 13.20
Method 10-90% ACN in H2O + 1% TFA
Retention time = 3.26 min
Purity: >95%
NL:
1.07E5
Total Scan
PDA
APAJ198-
stock1ul
uAU
Time (min)
0.70
0.87
1.57
2.83
3.26
4.10
4.62
11.09
12.41
12.78

References

1. M. Eddleston, A. F. Cohen, D. J. Webb, Implications of the BIA-102474-101 study for review of first-into-human clinical trials. *Br. J. Clin. Pharmacol.* **81**, 582–586 (2016).
2. D. Butler, E. Callaway, Scientists in the dark after French clinical trial proves fatal. *Nature*. **529**, 263–264 (2016).
3. A. Kerbrat *et al.*, Acute Neurologic Disorder from an Inhibitor of Fatty Acid Amide Hydrolase. *N. Engl. J. Med.* **375**, 1717–1725 (2016).
4. B. Bégaud *et al.*, Report by the Temporary Specialist Scientific Committee (TSSC), "FAAH (Fatty Acid Amide Hydrolase)", on the causes of the accident during a Phase 1 clinical trial, 1–28 (2016).
5. B. F. Cravatt *et al.*, Molecular characterization of an enzyme that degrades neuromodulatory fatty-acid amides. *Nature*. **384**, 83–87 (1996).
6. S. Kathuria *et al.*, Modulation of anxiety through blockade of anandamide hydrolysis. *Nat. Med.* **9**, 76–81 (2002).
7. W. Devane *et al.*, Isolation and structure of a brain constituent that binds to the cannabinoid receptor. *Science (80-.).* **258**, 1946–1949 (1992).
8. J. Z. Long *et al.*, Dual blockade of FAAH and MAGL identifies behavioral processes regulated by endocannabinoid crosstalk in vivo. *Proc Natl Acad Sci U S A*. **106**, 20270–20275 (2009).
9. M. van der Stelt *et al.*, Anandamide acts as an intracellular messenger amplifying Ca2+ influx via TRPV1 channels. *EMBO J.* **24**, 3026–3037 (2005).
10. A. J. Hampson *et al.*, Dual effects of anandamide on NMDA receptor-mediated responses and neurotransmission. *J. Neurochem.* **70**, 671–676 (1998).
11. J. P. Huggins, T. S. Smart, S. Langman, L. Taylor, T. Young, An efficient randomised, placebo-controlled clinical trial with the irreversible fatty acid amide hydrolase-1 inhibitor PF-04457845, which modulates endocannabinoids but fails to induce effective analgesia in patients with pain due to osteoarthritis of th. *Pain*. **153**, 1837–1846 (2012).
12. G. L. Li *et al.*, Assessment of the pharmacology and tolerability of PF-04457845, an irreversible inhibitor of fatty acid amide hydrolase-1, in healthy subjects. *Br. J. Clin. Pharmacol.* **73**, 706–716 (2012).
13. M. J. Niphakis, B. F. Cravatt, Enzyme Inhibitor Discovery by Activity-Based Protein Profiling. *Annu. Rev. Biochem.* **83**, 341–377 (2014).
14. M. P. Baggelaar *et al.*, Highly Selective, Reversible Inhibitor Identified by Comparative Chemoproteomics Modulates Diacylglycerol Lipase Activity in Neurons. *J. Am. Chem. Soc.* **137**, 8851–8857 (2015).
15. Y. Liu, M. P. Patricelli, B. F. Cravatt, Activity-based protein profiling: The serine hydrolases. *Proc. Natl. Acad. Sci.* **96**, 14694–14699 (1999).
16. K. Ahn *et al.*, Mechanistic and Pharmacological Characterization of PF-04457845: A Highly Potent and Selective Fatty Acid Amide Hydrolase Inhibitor That Reduces Inflammatory and Noninflammatory Pain. *J. Pharmacol. Exp. Ther.* **338**, 114–124 (2011).
17. L. E. Kiss *et al.*, Pharmaceutical Compounds (2010), WO 2010074588 A2.
18. V. V. Rostovtsev, L. G. Green, V. V. Fokin, K. B. Sharpless, A Stepwise Huisgen Cycloaddition Process: Copper(I)-Catalyzed Regioselective "Ligation" of Azides and Terminal Alkynes. *Angew. Chemie Int. Ed.* **41**, 2596–2599 (2002).
19. B. R. Lanning *et al.*, A road map to evaluate the proteome-wide selectivity of covalent kinase inhibitors. *Nat. Chem. Biol.* **10**, 760–767 (2014).
20. G. Thomas *et al.*, The serine hydrolase ABHD6 Is a critical regulator of the metabolic syndrome. *Cell Rep.* **5**, 508–520 (2013).

21. P.-A. Chang, Y.-J. Wu, Neuropathy target esterase: An essential enzyme for neural development and axonal maintenance. *Int. J. Biochem. Cell Biol.* **42**, 573–575 (2010).
22. A. Patat, in *Safety & Regulation in Early Clinical Drug Development* (Ghent, Belgium, 2016; http://www.bapu.be/autres/86_the_bial_10-2474.pdf).
23. R. J. Richardson, N. D. Hein, S. J. Wijeyesakere, J. K. Fink, G. F. Makhaeva, Neuropathy target esterase (NTE): overview and future. *Chem. Biol. Interact.* **203**, 238–44 (2013).
24. D. J. Read, Y. Li, M. V Chao, J. B. Cavanagh, P. Glynn, Neuropathy target esterase is required for adult vertebrate axon maintenance. *J. Neurosci.* **29**, 11594–600 (2009).
25. M. Moser *et al.*, Cloning and expression of the murine sws/NTE gene. *Mech. Dev.* **90**, 279–82 (2000).
26. R. B. Hufnagel *et al.*, Neuropathy target esterase impairments cause Oliver–McFarlane and Laurence–Moon syndromes. *J. Med. Genet.* **52**, 85–94 (2015).
27. A. K. Topaloglu *et al.*, Loss-of-function mutations in PNPLA6 encoding neuropathy target esterase underlie pubertal failure and neurological deficits in Gordon Holmes syndrome. *J. Clin. Endocrinol. Metab.* **99**, E2067-75 (2014).
28. D. Bertrand, S. Bertrand, E. Neveu, P. Fernandes, Molecular characterization of off-target activities of telithromycin: a potential role for nicotinic acetylcholine receptors. *Antimicrob. Agents Chemother.* **54**, 5399–402 (2010).
29. M. P. Baggelaar *et al.*, Development of an activity-based probe and in silico design reveal highly selective inhibitors for diacylglycerol lipase-α in brain. *Angew. Chem. Int. Ed. Engl.* **52**, 12081–5 (2013).
30. D. A. Bachovchin *et al.*, Superfamily-wide portrait of serine hydrolase inhibition achieved by library-versus-library screening. *Proc. Natl. Acad. Sci. U. S. A.* **107**, 20941–6 (2010).
31. A. B. Cognetta *et al.*, Selective N-Hydroxyhydantoin Carbamate Inhibitors of Mammalian Serine Hydrolases. *Chem. Biol.* **22**, 928–937 (2015).
32. J. M. Inloes *et al.*, The hereditary spastic paraplegia-related enzyme DDHD2 is a principal brain triglyceride lipase. *Proc. Natl. Acad. Sci. U. S. A.* **111**, 14924–9 (2014).
33. C. Hu *et al.*, RPLC-ion-trap-FTMS method for lipid profiling of plasma: method validation and application to p53 mutant mouse model. *J. Proteome Res.* **7**, 4982–91 (2008).
34. S. Gattinoni *et al.*, Enol carbamates as inhibitors of fatty acid amide hydrolase (FAAH) endowed with high selectivity for FAAH over the other targets of the endocannabinoid system. *ChemMedChem.* **5**, 357–360 (2010).
35. A. Ligresti *et al.*, Prostamide F2a receptor antagonism combined with inhibition of FAAH may block the pro-inflammatory mediators formed following selective FAAH inhibition. *Br. J. Pharmacol.* **171**, 1408–1419 (2014).
36. F. J. Janssen *et al.*, Discovery of Glycine Sulfonamides as Dual Inhibitors of sn-1-Diacylglycerol Lipase α and α/β-Hydrolase Domain 6. *J. Med. Chem.* **57**, 6610–22 (2014).
37. T. van der Wel *et al.*, A natural substrate-based fluorescence assay for inhibitor screening on diacylglycerol lipase α. *J. Lipid Res.* **56**, 927–935 (2015).
38. J. V Peppard, S. Mehdi, Z. Li, M. S. Duguid, Assay methods for identifying agents that modify the activity of nape-pld or abhd4 (2008).
39. P. Mukhopadhyay *et al.*, The novel, orally available and peripherally restricted selective cannabinoid CB 2 receptor agonist LEI-101 prevents cisplatin-induced nephrotoxicity. *Br. J. Pharmacol.* **173**, 446–458 (2016).
40. D. Ogasawara *et al.*, Rapid and profound rewiring of brain lipid signaling networks by acute diacylglycerol lipase inhibition. *Proc. Natl. Acad. Sci.* **113**, 26–33 (2016).

41. A. H. Sandtorv, H.-R. Bjørsvik, Fast Halogenation of Some N - Heterocycles by Means of N , N alpha -Dihalo-5,5-dimethylhydantoin. *Adv. Synth. Catal.* **355**, 499–507 (2013).
42. L. Roumen *et al.*, Synthesis, Biological Evaluation, and Molecular Modeling of 1-Benzyl-1 H -imidazoles as Selective Inhibitors of Aldosterone Synthase (CYP11B2). *J. Med. Chem.* **53**, 1712–1725 (2010).
43. S. A. Bial - Portela and Ca, D. Russo, J. B. R. Wahnon, W. Maton, T. Eszenyi, Process For The Synthesis Of Substituted Urea Compounds (2014), WO 2014017938 A2.
44. D. S. Johnson *et al.*, Discovery of PF-04457845: A Highly Potent, Orally Bioavailable, and Selective Urea FAAH Inhibitor. *ACS Med. Chem. Lett.* **2**, 91–96 (2011).

Acknowledgements

The human brain samples were obtained from The Netherlands Brain Bank (NBB), Netherlands Institute for Neuroscience, Amsterdam (open access: www.brainbank.nl). All material was collected from donors for whom, or from whom, the NBB had obtained written informed consent for a brain autopsy and the use of the material and clinical information for research purposes. We thank R. M. Suciu for assistance with the computational analysis of ABPP data. This work was supported by a Dutch Research Council– Chemical Sciences ECHO grant (to A.P.A.J. and M.v.d.S.); an ECHO-STIP Grant (to M.S. and M.v.d.S.) and Leiden University, Faculty of Science ("Profiling Programme: Endocannabinoids"; M.v.d.S., E.M., T.H., V.K.) grants from the Chinese Scholarship Council (to H.D.); the NIH (DA033760 to B.F.C.). ; Netherlands Organisation for Scientific Research (NWO 024.003.001 to S.A.K.). The work of F.F. and M.M. was partly supported by the Italian Ministry of Education, University and Research (competitive PRIN 2015 grant to M.M.). B.F.C. is a founder and advisor to Abide Therapeutics, a biotechnology company interested in developing serine hydrolase inhibitors as therapeutics. G.H. is founder of Toxys B.V., a company that performs cytotoxicity testing of compounds. The ToxTracker platform used for toxicological profiling is available for research purposes from Toxys B.V under a material transfer agreement.

Supplementary Materials

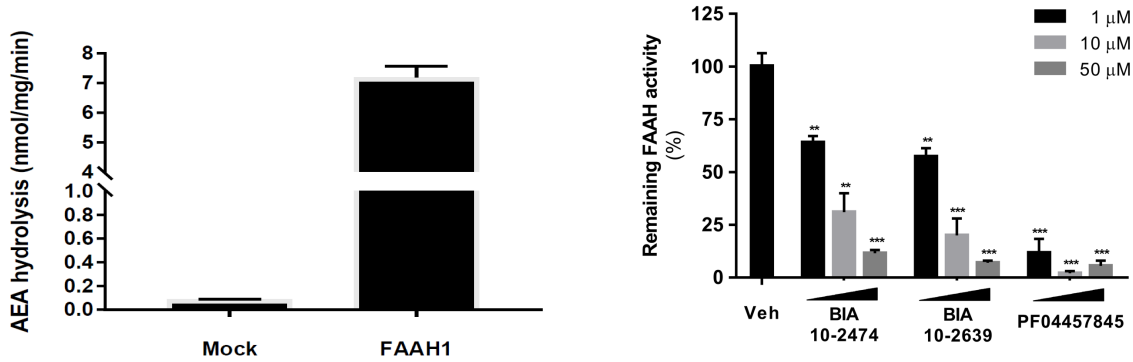

Figure S1: Anandamide (AEA) hydrolysis activity of mock- and human FAAH1-transfected HEK293T membrane cell lysate. (**A**) HEK293T lysates were incubated with AEA for 30 min at 37 °C. Arachidonic acid (hydrolysis product) was then quantified by LC/MS analysis. Data are presented as average values ± SD for two independent experiments per group. (**B**) hFAAH activities relative to control after incubation with 1, 10 and 50 µM of indicated inhibitors as measured in a radiometric [^{14}C]-anandamide assay on purified recombinant hFAAH enzyme. Activity is expressed as mean ± SEM (n=3) with *P<0.05, ** P<0.01, *** P<0.001 (two-tailed *t*-test).

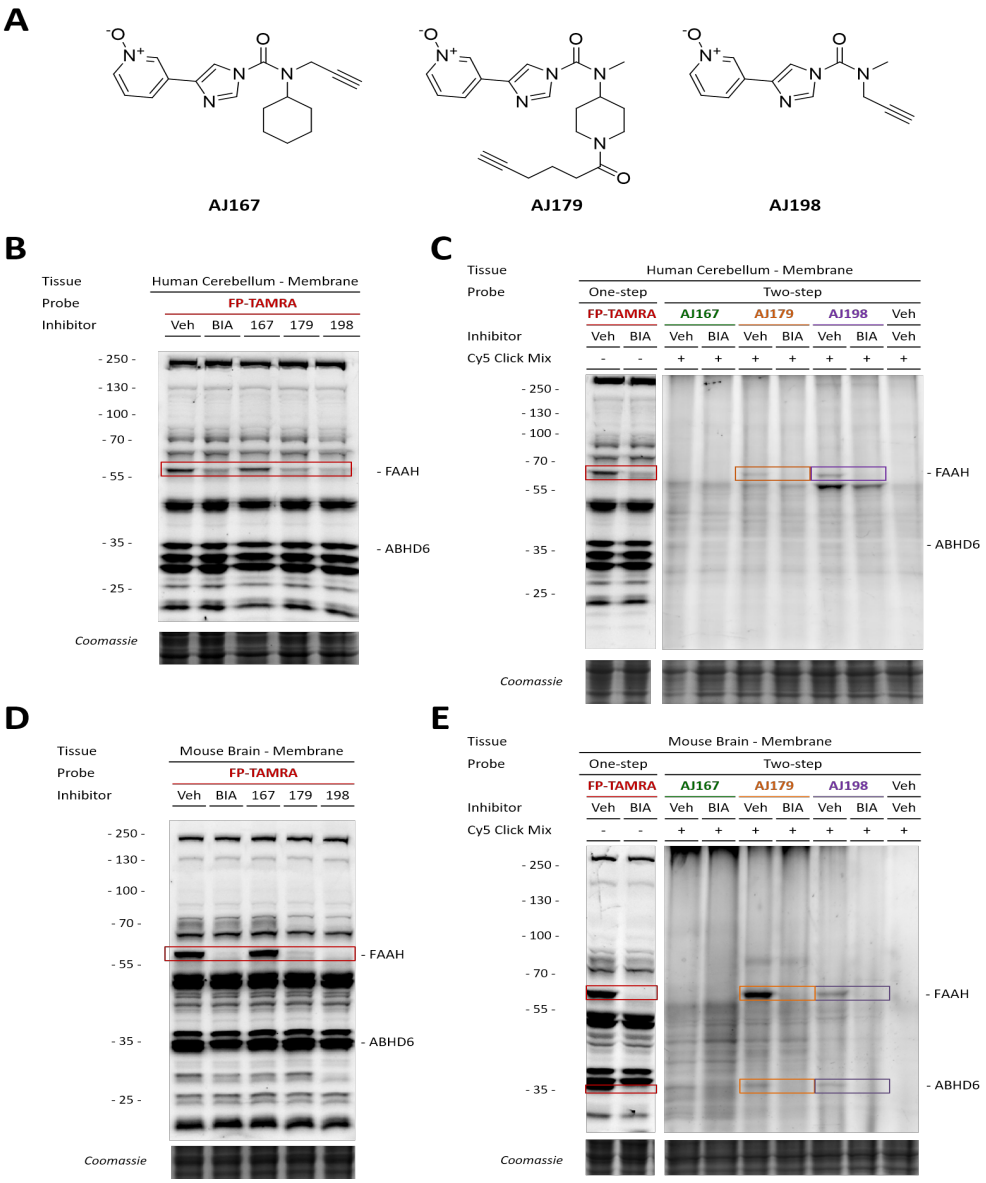

Figure S2: BIA 10-2474 interaction profiling by click chemistry-based profiling of human cerebellum and mouse brain proteomes. (**A**) Chemical structures of alkynylated BIA 10-2474-based probes AJ167, A179, and AJ198. **B**-**E**) Click chemistry-based ABPP with alkyne probes. **B**, **D**) Competitive ABPP with serine hydrolase-directed probes. Human cerebellum (**B**) and mouse brain (**D**) membrane proteome were incubated with BIA 10-2474 or the alkyne probes (50 µM, 30 min, 37 °C) and DMSO as vehicle. Subsequently, samples were incubated with FP-TAMRA (500 nM) (20 min, RT). (**C**, **E**) Click chemistry ABPP with alkyne probes. Human cerebellum (**C**) and mouse brain (**E**) membrane proteome were incubated with BIA 10-2474 (50 µM, 30 min, 37 °C), and DMSO as vehicle. Subsequently, samples were incubated with alkyne probes (AJ167, AJ179 or AJ198; 50 µM, 30 min, 37 °C), and DMSO as vehicle, followed by a click (copper-catalyzed azide-alkyne cycloaddition) reaction to Cy5-azide. Competitive ABPP of BIA 10-2474 with FP-TAMRA (as described for **B**, **D**) is shown as a reference.

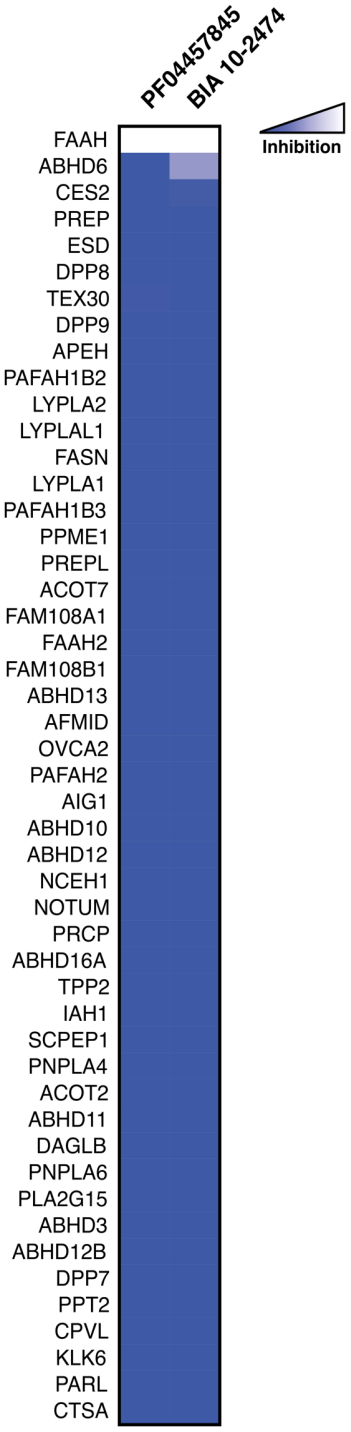

Figure S3: Quantitative proteomic analysis of serine hydrolase targets of BIA 10-2474 and PF04457845 tested at low concentrations (0.2 μM) in human cells. (MS)-based ABPP of serine hydrolase activities in SW620 cells treated in situ with PF04457845 or BIA 10-2474 (0.2 μM, 4 h, 37 °C) versus DMSO as vehicle. Data are expressed as median SILAC ratio values for all isotopic peptide pairs quantified per protein from one biological replicate.

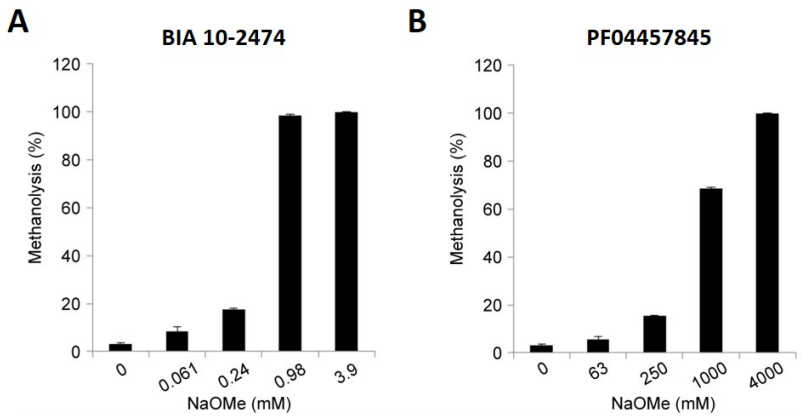

Figure S4: Methanolysis assay of BIA 10-2474 and PF04457845. Compounds (500 μM) were incubated with various concentrations of NaOMe in MeOH (24 h, 37 °C) and the reactions were quenched with AcOH. Methanolysis of the compounds was quantified by LC/UV-Vis monitoring. Percent methanolysis was calculated by product peak area/total peak area multiplied by 100. Data is expressed as mean ± SEM (n=3)

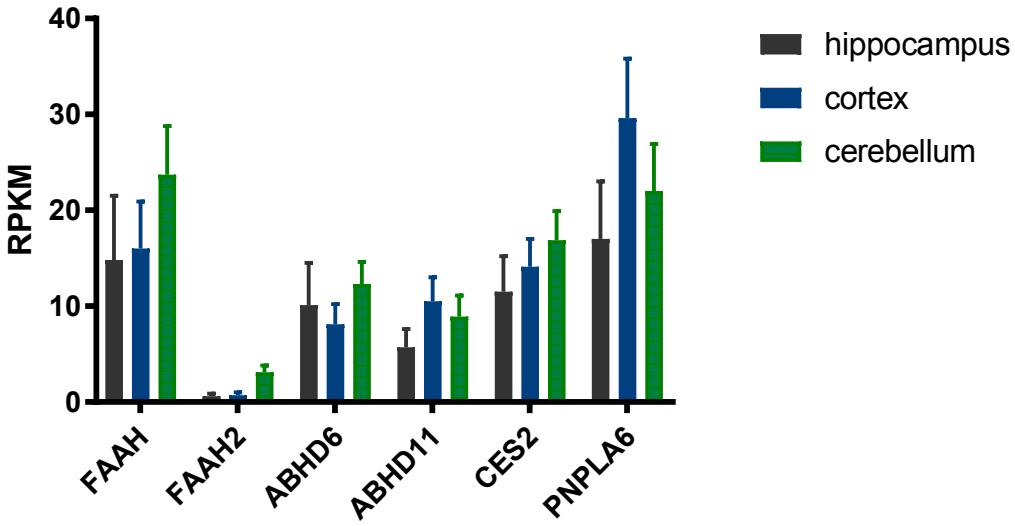

Figure S5: Expression of serine hydrolase targets of BIA 10-2474 in human brain regions. RNA sequencing-based mRNA measurements for the indicated enzymes in the indicated brain regions. Data were obtained from the GTEx Portal (https://gtexportal.org/home/) and expressed as median Reads Per Kilobase per Million (RPKM) ± SD.

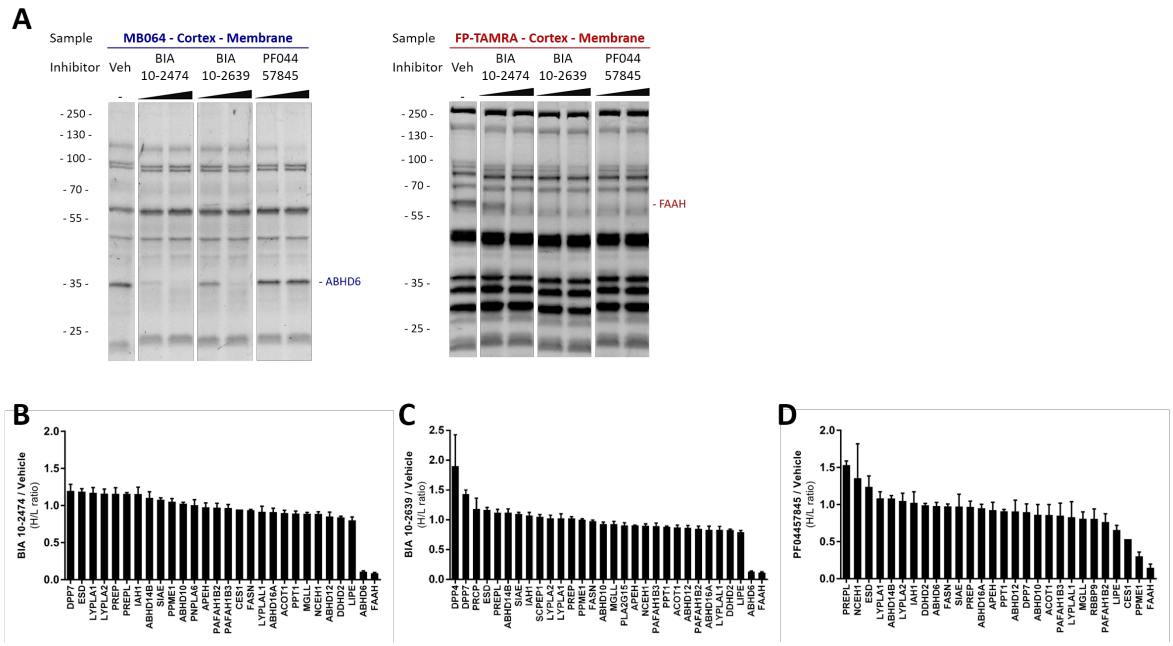

Figure S6: Identification of serine hydrolase targets of BIA 10-2474 and PF04457845 by quantitative MS-based ABPP of human cortex proteome. Human frontal cortex proteomes were treated with inhibitors BIA 10-2474, BIA 10-2639, and PF04457845 (50 μM, 30 min, 37 °C) or DMSO as a vehicle control and processed and analysed by gel-based (**A**) or quantitative MS-based (**B-D**) ABPP (see Experimental Methods for details). Data are expressed as mean values ± SEM (n=3 per group).

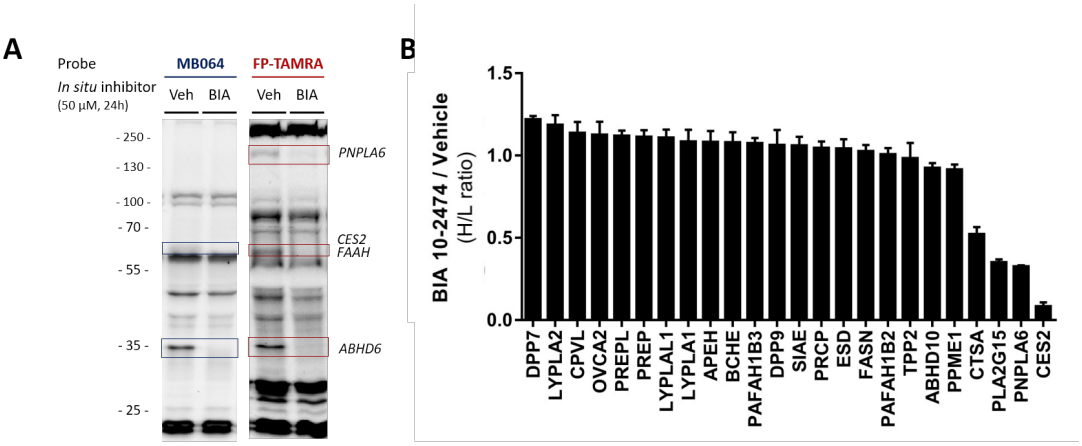

Figure S7: Quantitative MS-based ABPP of BIA 10-2474 *in situ*-treated human cortical neurons. (**A, B**) Cortical neurons were treated *in situ* with BIA 10-2474 (50 μM, **A**) or DMSO as vehicle (n=3) for 24 h at 37 °C. Cells were then processed and analysed by quantitative MS-based ABPP (**B**) (see Experimental Methods for details). Data are expressed as mean values ± SEM (n=3 per group).

Table S1: FAAH radiometric assay (rat brain membranes) with co-incubation and 20 min pre-incubation.

Compound	With co-incubation		With 20 min. pre-incubation	
	IC_{50} (μM)	Max Tested (μM) (% inhibition)	IC_{50} (μM)	Max Tested (μM) (% inhibition)
BIA 10-2474	3.1 ± 0.6	10 (95.4 ± 0.4)	1.0 ± 0.3	5 (95.4 ± 0.4)
PF04457845	0.06 ± 0.01	1 (90.7 ± 0.8)	0.01 ± 0.01	0.1 (98.5 ± 0.1)
BIA 10-2639	1.4 ± 0.30	10 (70.1 ± 1.1)	0.29 ± 0.01	1 (91.5 ± 1.5)

Table S2: Evaluating FAAH inhibitors against other endocannabinoid-related proteins.

		hDAGLα	mDAGLβ	hMAGL	hABHD6	hNAPE-PLD	hCB_1	hCB_2
Compound		Remaining activity (%) ± SD					Ra dioligand displacement (%) ± SEM	
BIA 10-2474	10 µM	102.7 ± 9.3	94.1 ± 4.3	117.9 ± 3.0	83.9 ± 8.2	96.9 ± 11.9	29.8 ± 1.5	6.0 ± 5.4
	30 µM	113.4 ± 4.0	102.9 ± 1.9	-	31.2 ± 13.2	-	-	-
	50 µM	-	-	-	-	95.9 ± 10.1	38.4 ± 2.3	16.7 ± 8.9
PF04457845	10 µM	99.2 ± 8.7	105.5 ± 0.5	-	108.3 ± 21.6	98.6 ± 6.7	59.9 ± 2.5	51.5 ± 4.6
	30 µM	83.0 ± 8.4	106.2 ± 1.5	-	97.5 ± 26.7	-	-	-
	50 µM	-	-	-	-	70.2 ± 6.8	103.8 ± 4.6	86.4 ± 1.3
BIA 10-2639	10 µM	107.6 ± 2.6	94.5 ± 1.7	-	111.2 ± 8.3	89.0 ± 7.2	36.8 ± 4.1	13.4 ± 8.0
	30 µM	110.2 ± 3.2	102.1 ± 4.2	-	90.3 ± 11.2	-	-	-
	50 µM	-	-	-	-	89.9 ± 2.6	44.0 ± 5.6	19.9 ± 5.4

DAGLα, DAGLβ, MAGL, ABHD6 and NAPE-PLD relative to DMSO as vehicle and [^{3}H]CP55940 displacement at overexpressing hCB1- and hCB2-receptor membranes.

Table S3. Evaluating FAAH inhibitors against for efficacy and affinity with TRPV-, TRPA1- and TRPM8-channels.

Compound	TRPV1		TRPV2		TRPV3	
	Efficacy (% ionomycin 4 μM)	IC_{50} (capsaicin 0.1 μM)	Efficacy (% ionomycin 4 μM)	IC_{50} (LPC 3 μM)	Efficacy (% ionomycin 4 μM)	IC_{50} (Thymol 100 μM)
BIA 10-2474	< 10	> 20 μM	< 10	> 20 μM	< 10	> 20 μM
PF04457845	< 10	> 20 μM	< 10	> 20 μM	< 10	> 20 μM
BIA 10-2639	< 10	> 20 μM	< 10	> 20 μM	< 10	> 20 μM
Compound	**TRPV4**		**TRPA1**		**TRPM8**	
	Efficacy (% ionomycin 4 μM)	IC_{50} (GSK 10 nM)	Efficacy (%AITC 100 μM)	IC_{50} (AITC 100 μM)	IC_{50} (icilin 0.25 μM)	
BIA 10-2474	< 10	> 20 μM	< 10	> 20 μM	> 20 μM	
PF04457845	< 10	> 20 μM	< 10	> 20 μM	> 20 μM	
BIA 10-2639	< 10	> 20 μM	< 10	> 20 μM	> 20 μM	

Table S4. *In situ* inhibitory potencies of BIA 10-2474, BIA 10-2639, and PF04457845 against FAAH and representative off-targets (human and mouse orthologues).

	IC_{50} (95% Confidence Interval) [μM] [1]		
Enzyme	**BIA 10-2474**	**BIA 10-2639**	**PF04457845**
hFAAH1	0.049 (0.043-0.056)	0.049 (0.034-0.071)	0.011 (0.0066-0.019)
hFAAH2	0.40 (0.28-0.55)	0.10 (0.080-0.13)	0.59 (0.40-0.88)
mABHD6	0.32 (0.22-0.46)	0.37 (0.28-0.51)	>10
hABHD6	0.081 (0.057-0.11)	0.079 (0.066-0.093)	>10
mCES2E	>10	>10	>10
hCES2	2.0 (1.3-3.0)	0.63 (0.46-0.84)	>10
mABHD11	>10	1.7 (1.5-2.0)	>10
hABHD11	>10	2.3 (1.8-2.9)	>10

[1] HEK 293T cells overexpressing off-target enzymes were treated for 4 h *in situ* with varying concentrations of inhibitors. Harvested cells were lysed and treated in vitro with TAMRA-FP (1 μM, 30 min, 37 °C) and human (h) and mouse (m) enzyme activities were then quantified by gel-based ABPP.

Table S5. Lipids significantly altered by in situ treatment of human cortical neurons with BIA 10-2474.

Lipid class	Metabolites identified as significant due to treatment	Effect
Phosphatidylcholines (PC)	C38:2, C38:6, C38:7, C40:6, C40:6, C40:7, C40:8	Increased
Lysophosphatidylcholines (LPC)	sn1&2: C14:0, C22:6, C16:0, C16:1, C18:0, C18:1, C18:2, C20:4	Increased
	sn1: C18:2, C20:1, C20:2 C20:4, C22:6, C20:3 (ω3ω6)	
	sn2: C14:0, C18:2, C20:4, C22:6, C20:3 (ω3ω6)	
Fatty acids	C20:4 (ω6), C20:5 (ω3), C22:4, C25:5 (ω3ω6)	Decreased
Plasmalogen phosphatidylcholines (pPC)	C36:4, C36:6, C38:4, C38:5, C38:7, C40:6	Decreased
Triglycerides	C46:1, C48:1, C48:2, C48:3, C50:1, C52:1, C54:1	Increased
N-Acylethanolamines	C20:4, C22:6, C18:1, C16:0, C16:1, C18:0	Increased
Mono&di-acylglycerols	sn1:C18:1, C18:2 & sn2: C18:1, C18:2	Increased
Sphingomyelins	C18:1/24:1	Increased

Lipids identified as significant based on t-test with a post-hoc false discovery rate (FDR) correction applied using Benjamini–Hochberg procedure. All lipids had an FDR rate less than 25%.

Chapter 6

Pharmacokinetic Modeling of Paracetamol Uptake and Clearance in Zebrafish Larvae: Expanding the Allometric Scale in Vertebrates with Five Orders of Magnitude

Vasudev Kantae*, Elke H.J. Krekels*, Anita Ordas*, Oskar González, Rob C. van Wijk, Amy C. Harms, Peter I. Racz, Piet H. van der Graaf*, Herman P. Spaink*, Thomas Hankemeier*

** Authors contributed equally*

Zebrafish. 2016; 13(6): 504-510

Abstract

Zebrafish larvae (*Danio rerio*) are increasingly used to translate findings regarding drug efficacy and safety from in vitro-based assays to vertebrate species, including humans. However, the limited understanding of drug exposure in this species hampers its implementation in translational research. Using paracetamol as a paradigm compound, we present a novel method to characterize pharmacokinetic processes in zebrafish larvae, by combining sensitive bioanalytical methods and nonlinear mixed effects modeling. The developed method allowed quantification of paracetamol and its two major metabolites, paracetamol-sulfate and paracetamol-glucuronide in pooled samples of five lysed zebrafish larvae of 3 days post-fertilization. Paracetamol drug uptake was quantified to be 0.289 pmole/min and paracetamol clearance was quantified to be 1.7% of the total value of the larvae. With an average volume determined to be 0.290 μL, this yields an absolute clearance of 2.96×10^{7} L/h, which scales reasonably well with clearance rates in higher vertebrates. The developed methodology will improve the success rate of drug screens in zebrafish larvae and the translation potential of findings, by allowing the establishment of accurate exposure profiles and thereby also the establishment of concentration–effect relationships.

Introduction

Zebrafish and zebrafish larvae (*Danio rerio*) are increasingly used as a complementary vertebrate model at various stages of drug discovery and development, ranging from disease modeling and target validation, to drug safety, toxicology, and efficacy screenings [1–6]. This is due to 1) their similarity to humans in terms of morphological, molecular, genetic, and pathological features; 2) their small size; 3) their easy and inexpensive maintenance; 4) the availability of a large set of genetic tools; 5) the limited ethical issues involved; and 6) the rapid development of optically transparent larvae, allowing high-throughput imaging-based phenotypic screening.

Although the zebrafish larva is a well-established vertebrate model for toxicity and safety purposes, its utilization has been limited due to the gaps in our understanding of basic pharmacokinetic (PK) processes like absorption, distribution, and clearance, that drive the exposure to drugs and drug metabolites [1,3]. Although, expression patterns of enzymes that drive drug metabolism have been characterized in zebrafish [7–10], to date metabolism and excretion of drug or drug metabolites have never been quantified in zebrafish larvae.

The aim of this study was to develop a new methodology to characterize drug elimination processes in 3-day-old zebrafish larvae, using paracetamol, also known as acetaminophen, as a paradigm compound. A highly sensitive liquid chromatography-mass spectrometry based method was developed to accurately measure concentrations of paracetamol and its metabolites in zebrafish larvae. The obtained data were subsequently analyzed with non-linear mixed effects modeling techniques.

Materials and Methods

Study design

To characterize the PK of paracetamol in zebrafish larvae, two experiments were performed. At day 3 post fertilization (dpf), hatched larvae were transferred to 24-well plates, with each well containing 5 larvae in 2 ml of embryo medium (pH = 7.9) with 1 mM paracetamol. In experiment 1, 150 zebrafish larvae were used to determine the absorption of paracetamol by continuous drug exposure and in experiment 2, 60 zebrafish larvae were used to study the elimination of paracetamol after the larvae were transferred from drug-containing to drug-free medium. All measurements in the experiments were carried out in triplicates, and the measured drug and drug metabolite amounts are expressed per larva, but represent mean values obtained from 5 larvae simultaneously.

Zebrafish larvae were handled in compliance with the local animal welfare regulations and maintained according to standard protocols (zfin.org). Embryos were collected from family crosses of AB/TL wild-type strain and grown at 28°C in embryo medium (60 g/ml Instant Ocean sea salts; Sera Marin) in the dark.

Experiment 1

Zebrafish larvae were exposed to the drug-containing medium for 10, 20, 30, 40, 50, 60, 80, 100, 120, or 180 min. At the time of the measurement three replicates of five larvae were collected, and washed twice with 80/20 (v/v) water/methanol solution, after which excessive medium was removed. The samples were subsequently prepared for analysis as described below. Additionally, samples from the incubation medium were collected to study the excreted amounts of the metabolites. Larvae in control groups were exposed to the drug solution for a few seconds and to determine drug adherence to the skin [11].

Experiment 2

Larvae were exposed to the drug-containing medium for 1hr, washed with fresh medium to remove the residual drug solution, and then transferred to a drug-free medium. After 0, 1, 2 and 3h of incubation, three replicates of five larvae were collected and washed two times in 80/20 (v/v) water/methanol solution after which excessive medium was removed and the samples were subsequently prepared for analysis as described below. Samples from the incubation medium were also collected at each time point.

This experiment was repeated a second time with three washing steps before transferal to drug-free medium, as the first time unchanged drug and metabolites seemed to have been transferred to the fresh medium. The second time, the duration of this experiment was also extended with sample collection up to 4h after transfer to the drug-free medium. Data on paracetamol, paracetamol-sulphate, and paracetamol-glucuronide concentrations in the incubation medium from the first time the experiment was performed were excluded from the analysis as contamination was suspected.

Sample preparation

The 5 zebrafish larvae of 3 dpf from a single well were added to 100 μl lysis buffer containing 90/10 (v/v) methanol/water solution with 45 ng/ml paracetamol-D_4 internal standard (Sigma-Aldrich Chemie B.V., Zwijndrecht, Netherlands). Lysis was performed by snap-freezing each sample in liquid nitrogen followed by 2-3 minutes sonication. This procedure was repeated until all larvae were lysed and the sample was homogenous. The lysed samples were centrifuged for 10 minutes at 16000 g at 4°C. 90 μl of supernatant was collected in a micro-centrifuge tube, after which 72 μl water was added, yielding a sample of 50/50 methanol/water solution which was injected to the Liquid Chromatography-Mass Spectrometer (LC-MS/MS) system directly.

The medium samples (2 ml) from each well were collected in new eppendorf tubes and concentrated by speedvac. After reconstitution in 150 μl of 50/50 methanol/water solution, samples were injected to the LC-MS/MS system directly.

Calibration curve

Paracetamol, paracetamol-sulphate, paracetamol-glucuronide was purchased from Sigma-Aldrich Chemie B.V., Zwijndrecht, Netherlands. Individual stock solutions at 1 mg/ml were prepared using methanol. Standard working solutions of 1000 ng/ml were prepared for these three compounds as well as for the paracetamol-D_4 internal standard. On the day of analysis, the standard working solutions were further diluted to five additional calibration points and mixed with the internal standard solution to final concentrations of 9, 18, 45, 90, 180, and 270 ng/ml for paracetamol and its metabolites and 45 ng/ml for the internal standard. All calibration points were prepared in a composition similar to the lysis buffer (90/10 methanol/water). For constructing a matrix-matched calibration curve, 100 μl of each

calibration point was spiked into a sample of 5 zebrafish larvae of 3 dpf and followed similar extraction procedure as described for the sample preparation above.

Quantification of paracetamol and metabolites

Analyses were performed on an Ultra Performance Liquid Chromatography (UPLC) system (Acquity, Waters, Milford, MA, USA) coupled to a Quadrupole – time of Flight (QTOF) mass spectrometer (MS) (Synapt G2S, Waters, Wilmslow, UK) with an electrospray ionization (ESI) source. Positive ionization mode was used for the analysis of paracetamol and negative mode for the analysis of the paracetamol-sulphate and paracetamol-glucuronide metabolites.

Chromatography was performed at 40°C on a Waters Acquity UPLC HSS T3 column (1.8 μm, 2.1 x 50 mm) using as aqueous mobile phase a 0.01% formic acid solution (A) and acetonitrile (B) as organic modifier at a flow rate of 0.4 mL/min. The run time was 5min, with the gradient at 100% A for the first 0.3 min, then B was linearly increased to 100% for the next 3min and held for 0.5 min and finally the system was equilibrated to the initial conditions for 1.2min. Injection volume was 5 μL and autosampler temperature was set to 10°C.

The MS method operated in both positive and negative polarities with separate injections in each polarity includes a MS scan function with a scan time of 0.2 sec operated at a trap cell collision energy of 4 eV and a transfer cell collision energy of 2 eV. ESI voltage was set at 0.9 kV both for positive and negative modes. Cone voltage was set at 30 V and source offset at 80 V. The source temperature was set at 150°C with desolvation temperature at 500°C. Nitrogen was used for the cone, desolvation and nebuliser gases with settings of 50 L/h, 1000 L/h and 6 bar, respectively. Data was collected in continuum mode with a scan range of 50-850 m/z using the QTOF detector in high-resolution mode (approximately 20000 full width half maximum (FWHM)). 0.1 mg/L Leucine enkephalin solution (acetonitrile: water 50:50 with 0.1% v/v formic acid) infused at a constant flow of 10 μl/min was used as the lock mass, a single point scan was collected every 10 sec and averaged over 3 scans to perform mass correction (556.2771 m/z). The instrument was calibrated for both positive and negative polarities before analysis using sodium formate.

Masslynx 4.1 SCN916 (Waters, Wilmslow, UK) was used to acquire all the data and Targetlynx application to perform the quantitative analysis. The quantification of paracetamol and its metabolites was achieved by correcting the peak area response of paracetamol and its

metabolites by the peak area response of the internal standard. The quantified values are expressed in terms of amount/larva. The developed method was sensitive with limits of quantification as low as 0.02 pmole/larva for paracetamol, 0.008 pmole/larva for paracetamol-sulphate, and 0.05 pmole/larva for paracetamol-glucuronide.

Non-linear mixed effects modeling

The non-linear mixed effects modeling of paracetamol was performed using NONMEM 7.3 software (ICON Development Solutions, Ellicott City, MD, USA) [12], facilitated with Pirana [13] and PsN [14,15]. The First Order Conditional Estimation method was used in NONMEM. R 3.0.0 was used for graphical analysis and model diagnostics.

In a pooled analysis of the paracetamol concentrations in the larvae, a 0-order absorption rate was estimated to quantify the uptake of paracetamol from the incubation medium. A 1st-order clearance rate was estimated to quantify the elimination of paracetamol from the larvae. Both 1 and 2-compartment models were tested to describe the distribution of paracetamol within the larvae. For both distribution models, the total distribution volume was fixed to 1, which meant for the 2-compartment model that both compartments were expressed as fraction of the total volume of one larva. To quantify the residual variability an additive and a proportional error were tested, as well as a combination of both. Due to the destructive nature of the measurements, inter-individual variability in the PK processes could not be quantified.

The likelihood ratio test, based on the objective function value (OFV) in NONMEM was used for model selection. Assuming a χ^2-distribution, a decrease in OFV of more than 3.84 points, corresponding to a significance level of $p<0.05$ with one degree of freedom, was considered to be statistically significant. Precision of parameter estimates was evaluated based on standard errors obtained from the NONMEM output tables. Furthermore the model fit was assessed by visual inspection of goodness-of-fit plots, these included plots of predicted *versus* observed paracetamol amounts in the zebrafish larvae, and of conditional weighted residuals [16] *versus* time after start of the experiment and conditional weighted residuals *versus* predicted paracetamol amounts.

Volume of zebrafish larvae

To enable the expression of paracetamol clearance in zebrafish larvae in absolute rather than relative terms, the average volume of the larvae was determined. For this, samples of 10, 20, 30, 40, 50, 100 larvae at 3 dpf were placed onto parafilm M(R) (Bemis NA) with a transfer pipette after which the excessive water was removed with variable volume pipettes and filter paper. Subsequently the weight of each sample was measured with a Mettler AE240 analytical balance. The average wet weight of the zebrafish larvae was determined using linear regression. To derive the average volume of the larvae, their density was assumed to be equal to the density of water at 25°C (0.997 g/ml).

Comparing paracetamol clearance in vertebrate species

A search was performed in PUBMED using 'paracetamol' OR 'acetaminophen' AND 'clearance'. Total paracetamol clearance values reported over the past 10 years in various vertebrate species were collected together with mean bodyweights of the individuals included in a study. When detailed information on bodyweight was not provided, average bodyweight values from the species were obtained from literature. Data from disease models, combined drug formulation, or obese individuals were excluded. Distinctions were made between data collected in mature or immature individuals of a species.

All obtained clearance values (CL) were plotted *versus* bodyweight (BW) on a double log scale. A linear model was fitted through the logarithm of the clearance values *versus* the logarithm of the bodyweight in R (version 3.3.1) to obtain the parameters in the allometric equation below that describes the relationship between bodyweight and paracetamol clearance (equation 1).

$$CL = a \cdot BW^{exp} \qquad \text{equation (1)}$$

The fit was based only on clearance values from the higher vertebrates, excluding the zebrafish larvae.

Results

Quantification of paracetamol and metabolites

Figure.1A shows the time-course of the amount of paracetamol and its two major metabolites in the zebrafish larvae at 3 dpf, obtained after continuous exposure for various durations in medium with 1 mM paracetamol. The amount of paracetamol in the zebrafish larvae reached a plateau within two hours, indicating that after two hours the amount of paracetamol taken up by the larvae and the amounts metabolized and excreted by the larvae are in equilibrium. Paracetamol-sulphate and paracetamol-glucuronide amounts in zebrafish larvae could be detected after 10 and 30 minutes, respectively. These metabolites reached equilibrium between formation and excretion within 2 hours as well

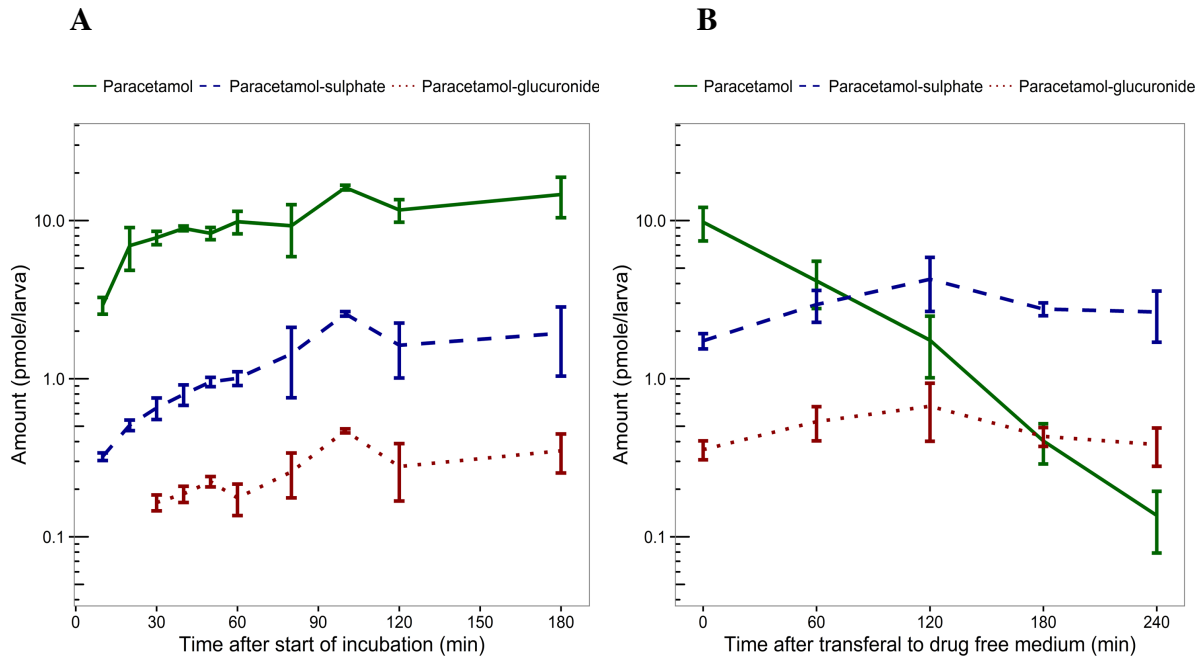

Figure 1: Time course of amounts of paracetamol and its major metabolites in zebrafish larvae. Depicted are mean values –1 standard deviations of paracetamol (green solid line), paracetamol-sulfate (blue dashed line), and paracetamol- glucuronide (red dotted line) amounts, after **(A)** continuous incubation in medium with 1 mM paracetamol (experiment 1), and **(B)** 1-h incubation in medium with 1 mM paracetamol and subsequent transferal to drug-free medium (experiment 2).

Figure.1B describes amounts of paracetamol and its major metabolites in the zebrafish larvae at 3 dpf following transferal to drug-free medium after one-hour incubation in drug-containing medium. After transfer to drug-free medium, paracetamol amounts in the zebrafish larvae decreased over time. The amounts of the paracetamol metabolites in the

larvae increased initially, indicating that per time unit larger amounts are formed than excreted. After 2 hours in drug-free medium the elimination of the metabolites started to exceed the formation, resulting in peak amounts followed by a decline.

In both experiments, the amount of excreted paracetamol-glucuronide in the incubation medium was below the lower limit of quantification (0.5 pmole excreted per larva) throughout the experiment. In the first experiment, excreted sulphate metabolite was detected after 3 hours of continuous exposure, but the level remained close to the limit of quantification (0.4 pmole excreted per larva). For the second experiment, excreted amounts of the sulphate metabolite that were close to the limit of quantification were detected in the medium 3 hours after the larvae were transferred from the drug-containing medium, to the drug-free medium. The excreted amounts are relatively low compared to the total amount of paracetamol and metabolites measured in the larvae, from which it can be concluded that a significant portion of the elimination of paracetamol is covered by measuring the sulphate and glucuronide metabolite in the larvae. Moreover, control experiments confirmed that paracetamol does not adhere to the skin of the zebrafish larvae, ratifying that paracetamol amounts quantified in the zebrafish larvae samples at 3 dpf indeed represent drug amounts taken up by the larvae.

Table 1. Pharmacokinetic model parameter estimates obtained with the population PK model

Parameter	Unit	Parameter estimate	Relative Standard Error of Estimate
Absorption rate constant (k_a)	pmole / min	0.289	5.0%
Distribution volume (V_1)	larva	1 FIX	-
Clearance (CL)	Proportion of larva volume / min	0.017	5.0%
Residual error (variance)		9.73	19%

Non-linear mixed effects model

The time-course of paracetamol amounts in zebrafish larvae at 3 dpf was best described by a standard one-compartment distribution model, with 0-order absorption, and linear 1st-order elimination. It was found that the zebrafish larvae in a medium with a 1 mM paracetamol concentration take up 0.289 pmole paracetamol per minute. Every minute, the amount of

paracetamol in 1.70% of the volume of the zebrafish larvae was cleared; this includes both metabolism and excretion of the unchanged drug. The obtained parameter values including the relative standard error of these estimates are provided in **Table. 1**.

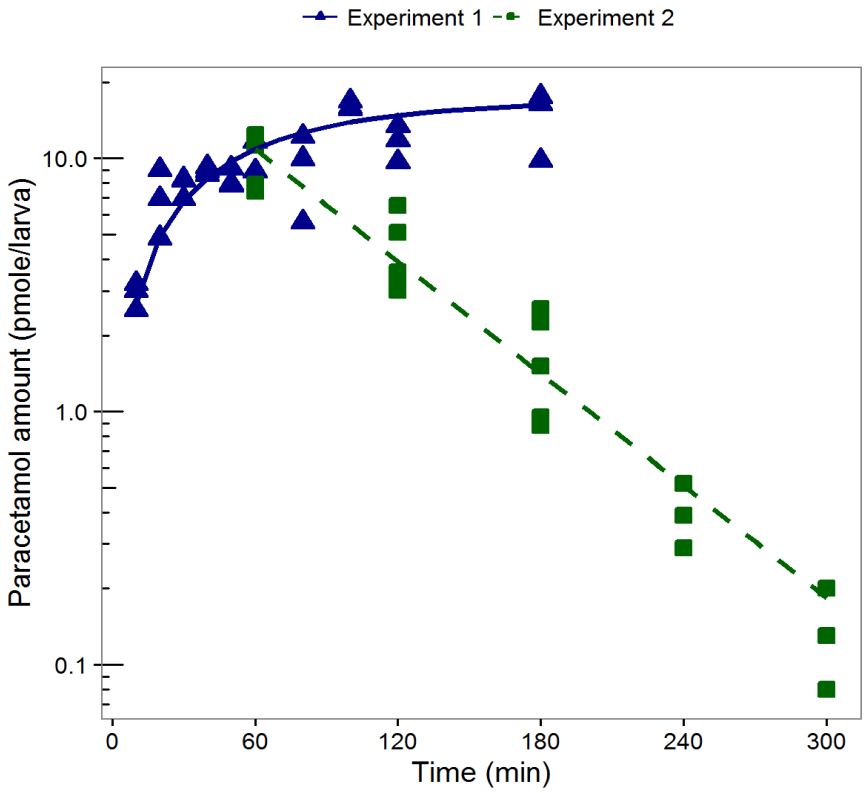

Figure 2: Observed and model predicted paracetamol amounts in zebrafish larvae. Observed (symbols) and model predicted (lines) paracetamol amounts in zebrafish larvae over time after continuous incubation in medium with 1mM para- cetamol (experiment 1, blue solid line and triangles) and after 1 h incubation in medium with 1 mM paracetamol and sub- sequent transfer to drug-free medium (experiment 2, green dotted line and squares).

The relative standard errors in the obtained model parameter estimates were below 20%, indicating good precision of the parameter estimates. **Figure. 2** shows how paracetamol amounts change over time in experiments 1 and 2 according to the obtained non-linear mixed effects PK model, as well as the amounts that were observed during the experiments. Goodness-of-fit plots are provided in the **Fig. S1**.

Paracetamol clearance in zebrafish larvae

The average wet weight of the zebrafish larvae at 3 dpf was found to be 0.291 mg, and from this an average volume of 0.290 μl was derived. This yields absolute paracetamol clearance in zebrafish larvae at 3 dpf of 2.96·10-7 l/h.

Comparing paracetamol clearance in vertebrate species

Paracetamol clearance values reported over the past 10 year in vertebrate species, including humans of different ages, were obtained from literature. Supplementary Table S1, provides an overview of the obtained values. **Figure. 3** show a plot of these clearance *versus* the bodyweight of each species.

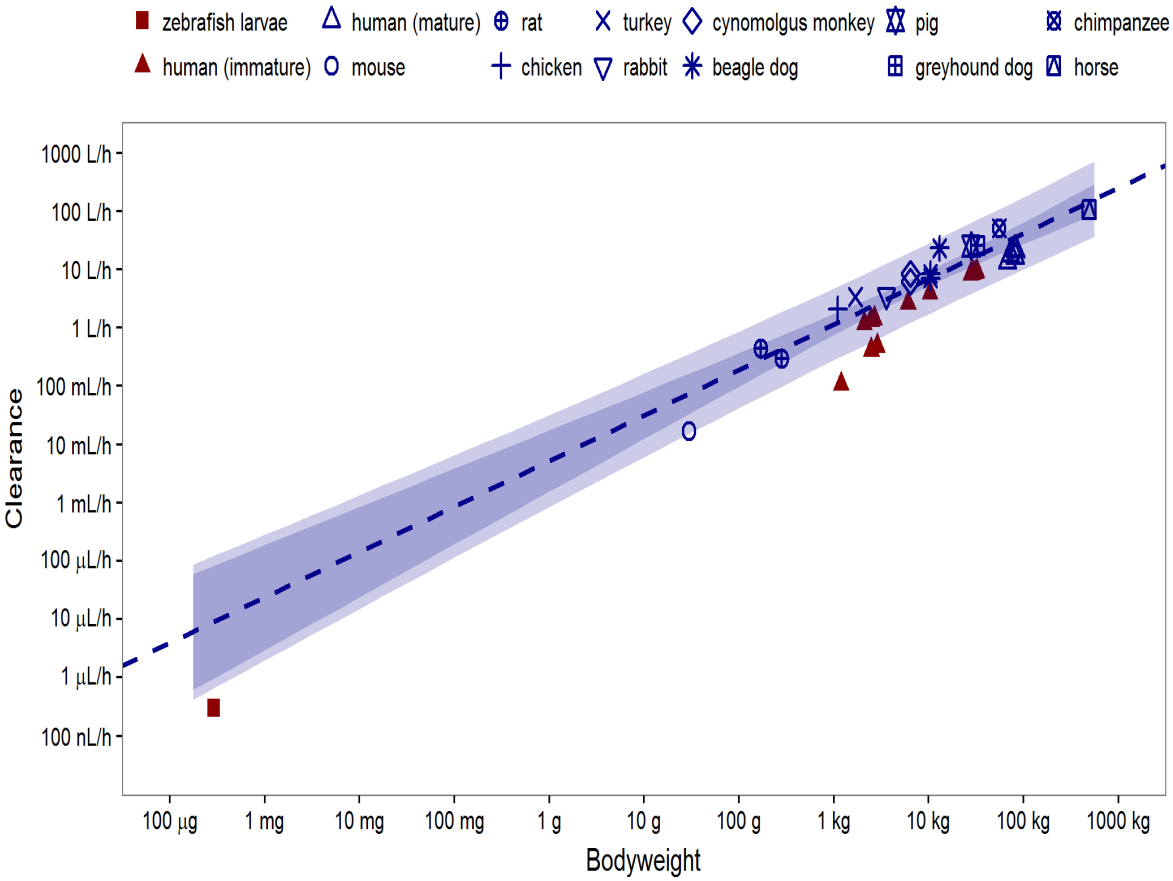

Figure 3: Paracetamol clearance across vertebrate species. Reported paracetamol clearances (points) and estimated allometric relationship (dashed line) between paracetamol clearance and bodyweight for mature individuals of various vertebrate species, including its 95% confidence (darker shaded) and prediction (lighter shaded) interval. Data from mature

individuals of species are depicted in blue, from immature including the zebrafish larvae in red.

The allometric equation that was fit to the data of mature individuals of the different species had an estimated exponent of 0.781 (r^2=0.902). The obtained relationship is depicted in Figure. 3 as well, including 95% confidence and prediction intervals and shows an over-prediction of the paracetamol clearance of the zebrafish larvae of 3 dpf. Interestingly however, this relationship also over-predicts the reported paracetamol clearances in human newborns and children. When including both the mature and the immature individuals of all species except the zebrafish larvae, the exponent was estimated to be 0.838 (r^2=0.835). **Fig. S2** depicts this relationship and shows that the clearance value for paracetamol in zebrafish larvae obtained in the current study does fall within the 95% confidence and prediction interval of this fit.

Discussion

Analytical methods that can accurately measure concentrations of paracetamol and its metabolites in low volumes are a prerequisite for characterizing the PK of this drug in zebrafish larvae. We have developed an analytical method based on ultra-performance liquid chromatography followed by mass spectrometric detection to separate and reliably quantify paracetamol and its major metabolite concentrations in samples of lysed zebrafish larvae at 3 dpf. The data obtained with this technique enabled the quantification of PK processes in this species with a non-linear mixed effects modeling approach, proving for the first time the feasibility of studies on drug PK and metabolism in zebrafish larvae.

Quantification of PK processes in zebrafish larvae will be invaluable for drug screening procedures in drug discovery and early drug development. This is because whereas it has been recognized in higher species and humans that drug concentrations rather than drug doses, are driving drug effects, screening studies in zebrafish larvae generally ignore drug PK, or if these aspects are considered, drug concentrations are measured at a single time-point, ignoring the full time-course of drug and/or metabolite exposure [3,17]. Combining information on full PK profiles with information on drug effects, is absolutely essential for the establishment of concentration-effect relationships, which are needed in translational pharmacology to scale drug effects between (vertebrate) species. Given that 70% of human genes have at least one obvious zebrafish orthologue [18] the potential for a strong resemblance between humans and zebrafish larvae regarding disease manifestation and drug response is high. The zebrafish larvae has for instance already been proven useful in studying drug effects in diseases like tuberculosis [17] and cancer [2].

In addition to improving the translation potential of drug effects from zebrafish larvae to higher vertebrate species, it was investigated to what extent PK studies in zebrafish larvae could serve as a convenient translational platform for studies on drug metabolism as well. The comparison of our findings on paracetamol clearance in zebrafish larvae at 3 dpf and reported clearance values in higher vertebrates in Figure. 3, shows that the clearance of paracetamol in the zebrafish larvae is lower than can be expected based on clearance values obtained in mature individuals of higher vertebrates, but that this value correlates well to values obtained in higher vertebrates when also values of immature individual are considered.

Zebrafish expresses phase II metabolizing genes similar to mammalian uridine glucuronosyltransferases (UGTs) and sulfotransferases (SULTs) isoforms throughout early development [19–21]. Previous studies using different probes in zebrafish larvae, also suggest

quantitative similarities in metabolite formation between zebrafish larvae and humans [22–24]. Our quantitative results on the metabolism of paracetamol in zebrafish larvae at 3 dpf do however not closely resemble observed metabolic profiles in adult humans. As the graphs in Fig.1 show, paracetamol-sulphate concentrations are about five to six times higher than the concentrations of the glucuronide metabolite, which is contrary to findings in humans, in which the glucuronide is the predominantly formed metabolite for paracetamol. This could possibly be attributed to the immaturity of the enzymes in zebrafish larvae at 3 dpf. In human newborns, glucuronidation capacity is for instance known to be limited, resulting in an increased relative contribution of sulphation in the metabolism of paracetamol, causing the sulphate metabolite to be formed 3.5 to 8 times more than the glucuronide metabolites in this immature human population [25–27]**.** Our experiments in the zebrafish larvae of 3 dpf were also performed before maturity in this species is reached. Although the dissimilarities in metabolic profiles between human adults and zebrafish larvae do not limit the applicability of our developed methodology in characterizing drug PK and determining accurate drug exposure in these larvae, it would be of interest to investigate if older larvae resemble metabolic profiles of human adults more closely. This is part of future investigations, as well as investigations on the clearance rates of other compounds in the zebrafish larvae.

In conclusion, we have successfully developed a feasible methodology for PK studies in zebrafish larvae at 3 dpf. The quantification of PK processes in these larvae by using a combination of ultra-sensitive liquid chromatography- mass spectrometry based analytical methods and non-linear mixed effects modeling, will allow for the extraction of more information from experiments in zebrafish larvae during drug discovery and early drug development, which may yield advantages regarding the inter-species translation potential of findings on drug effects in these experiments.

References

1. Fleming, A. & Alderton, W. K. Zebrafish in pharmaceutical industry research: finding the best fit. *Drug Discov. Today Dis. Model.* **10,** e43–e50 (2013).
2. Zon, L. I. & Peterson, R. T. In vivo drug discovery in the zebrafish. *Nat. Rev. Drug Discov.* **4,** 35–44 (2005).
3. Diekmann, H. & Hill, A. ADMETox in zebrafish. *Drug Discov. Today Dis. Model.* **10,** e31–e35 (2013).
4. Barros, T. P., Alderton, W. K., Reynolds, H. M., Roach, A. G. & Berghmans, S. Zebrafish: an emerging technology for in vivo pharmacological assessment to identify potential safety liabilities in early drug discovery. *Br. J. Pharmacol.* **154,** 1400–13 (2008).
5. Lieschke, G. J. & Currie, P. D. Animal models of human disease: zebrafish swim into view. *Nat. Rev. Genet.* **8,** 353–67 (2007).
6. MacRae, C. A. & Peterson, R. T. Zebrafish as tools for drug discovery. *Nat. Rev. Drug Discov.* **14,** 721–31 (2015).
7. Vliegenthart, A. D. B., Tucker, C. S., Del Pozo, J. & Dear, J. W. Zebrafish as model organisms for studying drug-induced liver injury. *Br. J. Clin. Pharmacol.* **78,** 1217–27 (2014).
8. Goldstone, J. V *et al.* Identification and developmental expression of the full complement of Cytochrome P450 genes in Zebrafish. *BMC Genomics* **11,** 643 (2010).
9. Alderton, W. *et al.* Accumulation and metabolism of drugs and CYP probe substrates in zebrafish larvae. *Xenobiotica.* **40,** 547–57 (2010).
10. Santoro, M. M. Zebrafish as a model to explore cell metabolism. *Trends Endocrinol. Metab.* **25,** 546–554 (2014).
11. Raterink, R.-J. *et al.* Rapid metabolic screening of early zebrafish embryogenesis based on direct infusion-nanoESI-FTMS. *Metabolomics* **9,** 864–873 (2013).
12. Beal SL, Sheiner LB, B. A. J. *NONMEM users guide (1989–2006). Icon Development Solutions: Ellicott City, MD; (eds)* (ICON Development Solutions,).
13. Keizer, R. J., van Benten, M., Beijnen, J. H., Schellens, J. H. M. & Huitema, A. D. R. Piraña and PCluster: a modeling environment and cluster infrastructure for NONMEM. *Comput. Methods Programs Biomed.* **101,** 72–9 (2011).
14. Lindbom, L., Pihlgren, P., Jonsson, E. N. & Jonsson, N. PsN-Toolkit--a collection of computer intensive statistical methods for non-linear mixed effect modeling using NONMEM. *Comput. Methods Programs Biomed.* **79,** 241–57 (2005).
15. Keizer, R. J., Karlsson, M. O. & Hooker, A. Modeling and Simulation Workbench for NONMEM: Tutorial on Pirana, PsN, and Xpose. *CPT pharmacometrics Syst. Pharmacol.* **2,** e50 (2013).
16. Hooker, A. C., Staatz, C. E. & Karlsson, M. O. Conditional weighted residuals (CWRES): a model diagnostic for the FOCE method. *Pharm. Res.* **24,** 2187–97 (2007).
17. Ordas, A. *et al.* Testing tuberculosis drug efficacy in a zebrafish high-throughput translational medicine screen. *Antimicrob. Agents Chemother.* **59,** 753–62 (2015).
18. Howe, K. *et al.* The zebrafish reference genome sequence and its relationship to the human genome. *Nature* **496,** 498–503 (2013).
19. Huang, H. & Wu, Q. Cloning and comparative analyses of the zebrafish Ugt repertoire reveal its evolutionary diversity. *PLoS One* **5,** e9144 (2010).
20. Yasuda, S. *et al.* A novel hydroxysteroid-sulfating cytosolic sulfotransferase, SULT3 ST3, from zebrafish: identification, characterization, and ontogenic study. *Drug Metab. Lett.* **3,** 217–27 (2009).

21. Liu, T.-A. *et al*. Zebrafish as a model for the study of the phase II cytosolic sulfotransferases. *Curr. Drug Metab*. **11,** 538–46 (2010).
22. Hu, G. *et al*. Metabolism of calycosin, an isoflavone from Astragali Radix, in zebrafish larvae. *Xenobiotica*. **42,** 294–303 (2012).
23. Li, Z. H. *et al*. Combined in vivo imaging and omics approaches reveal metabolism of icaritin and its glycosides in zebrafish larvae. *Mol. Biosyst*. **7,** 2128–38 (2011).
24. Chng, H. T., Ho, H. K., Yap, C. W., Lam, S. H. & Chan, E. C. Y. An investigation of the bioactivation potential and metabolism profile of Zebrafish versus human. *J. Biomol. Screen*. **17,** 974–86 (2012).
25. van Lingen, R. A. *et al*. Pharmacokinetics and metabolism of rectally administered paracetamol in preterm neonates. *Arch. Dis. Child. Fetal Neonatal Ed*. **80,** F59-63 (1999).
26. Allegaert, K. *et al*. Intra- and interindividual variability of glucuronidation of paracetamol during repeated administration of propacetamol in neonates. *Acta Paediatr*. **94,** 1273–9 (2005).
27. Krekels, E. H. J. *et al*. Developmental changes rather than repeated administration drive paracetamol glucuronidation in neonates and infants. *Eur. J. Clin. Pharmacol*. (2015). doi:10.1007/s00228-015-1887-y

Acknowledgements

This study was financially supported by the VIRGO consortium, which is funded by the Netherlands Genomics Initiative and by the Dutch Government (FES0908).

Supplementary materials

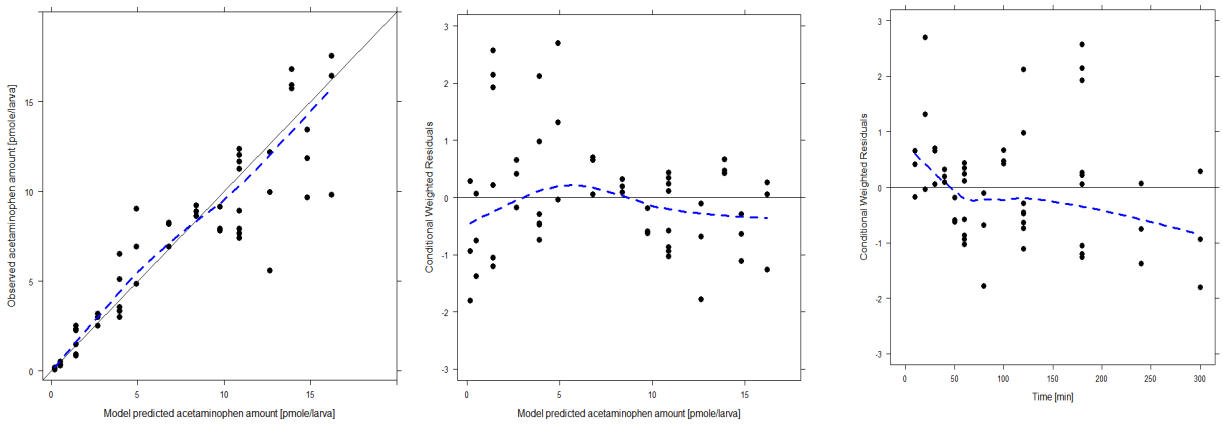

Figure S1: Basic goodness-of-fit plots with loess curves. Blue dotted lines for the population pharmacokinetic model of acetaminophen in zebrafish larvae, including observed *versus* predicted acetaminophen amounts (left), conditional weighted residuals *versus* time (middle), and conditional weighted residuals *versus* predicted concentration (right).

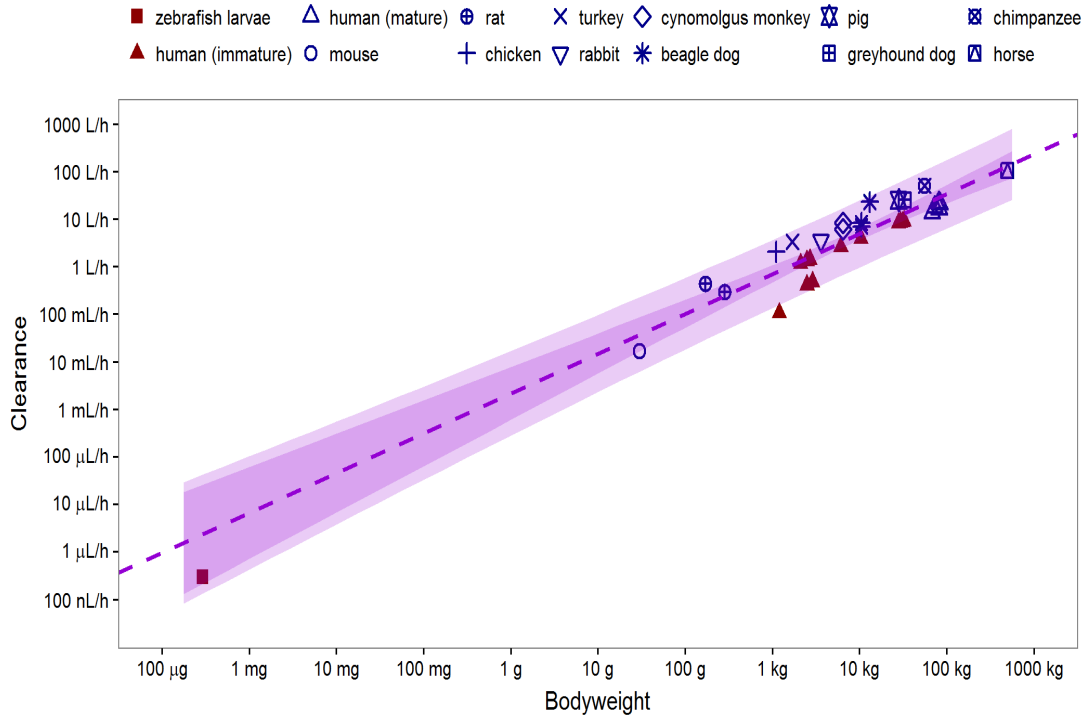

Figure S2. Paracetamol clearance across mature and immature vertebrate species. Reported paracetamol clearances (points) and estimated allometric relationship (dashed line) between paracetamol clearance and bodyweight for both mature and immature individuals of various vertebrate species, including its 95% confidence (darker shaded) and prediction (lighter shaded) interval. Data from mature individuals of species are depicted in blue, from immature including the zebrafish larvae in red**.**

Species	Weight [kg]	Reported CL [unit]	CL [L/h]	Reference
Mouse	0.030	0.28 [mL/min]	0.0168	28,29
Rat	0.17	2.53 [L/h/kg]	0.430	29,30
Rat	0.285	1.03 [L/h/kg]	0.294	31
Chicken	1.1	1.89 [L/h/kg]	2.08	32
Turkey	1.7	1.95 [L/h/kg]	3.32	32
Rabbit	3.61	3.52 [L/h]	3.52	33
Cynomolgus monkey	6.5	21.1 [ml/min/kg]	8.23	34,35
Cynomolgus monkey	6.5	15.7 [ml/min/kg]	6.12	34,35
Beagle dog	13.1	1.74 [L/h/kg]	22.8	32
Beagle dog	10.5	13.2 [ml/min/kg]	8.32	34
Beagle dog	10.5	11.1 [ml/min/kg]	6.99	34
Pig	28.1	0.88 [L/h/kg]	24.7	32
Greyhound dog	33	12.7 [ml/min/kg]	25.0	36
Greyhound dog	34	17.7 [ml/min/kg]	36.1	37
Chimpanzee	55.6	0.91 [L/h/kg]	50.6	38
Human (newborn)	1.2	0.0894 [L/h/kg]	0.107	39
Human (newborn)	2.1	16.3 [L/h/70kg$^{0.75}$]	1.17	40
Human (newborn)	2.3	0.348 [L/h]	0.348	41
Human (newborn)	2.5	5 [L/h/70kg$^{0.75}$]	0.411	42
Human (newborn)	2.5	16.3 [L/h/70kg$^{0.75}$]	1.34	40
Human (newborn)	2.7	16.3 [L/h/70kg$^{0.75}$]	1.42	40
Human (newborn)	2.9	5.24 [L/h/70kg$^{0.75}$]	0.481	43
Human (child)	6.1	16.3 [L/h/70kg$^{0.75}$]	2.61	40
Human (child)	10.4	16.3 [L/h/70kg$^{0.75}$]	3.90	40
Human (child)	27.9	16.3 [L/h/70kg$^{0.75}$]	8.18	40
Human (child)	29.3	16.5 [L/h/70kg$^{0.75}$]	8.59	44
Human (child)	30.9	16.3 [L/h/70kg$^{0.75}$]	8.83	40
Human (child)	32.3	16.3 [L/h/70kg$^{0.75}$]	9.13	40
Human (adult)	68	3.3 [ml/min/kg]	13.5	45
Human (adult)	73	17.4 [L/h/70kg$^{0.75}$]	18.0	46
Human (adult)	81	4.6 [ml/min/kg]	22.4	45
Human (adult)	83	4.2 [ml/min/kg]	20.9	45
Human (adult)	83	3.3 [ml/min/kg]	16.2	45
Horse	495	0.21 [L/h/kg]	104	32

Table S1: Overview of acetaminophen clearance values reported over the past 10 years in various higher vertebrates

Supplementary References

28. Saini, S. P. S. *et al*. Activation of liver X receptor increases acetaminophen clearance and prevents its toxicity in mice. *Hepatology* **54,** 2208–17 (2011).
29. Van Zutphen LFM, Baumans VBA: Handboek proef- dierkunde, 2rd ed. Elsevier gezondheidszorg, Maarssen, 2001
30. Yamasaki, I., Uotsu, N., Yamaguchi, K., Takayanagi, R. & Yamada, Y. Effects of kale ingestion on pharmacokinetics of acetaminophen in rats. *Biomed. Res.* **32,** 357–62 (2011).
31. Lee, S. H., An, J. H., Lee, H. J. & Jung, B. H. Evaluation of pharmacokinetic differences of acetaminophen in pseudo germ-free rats. *Biopharm. Drug Dispos.* **33,** 292–303 (2012).
32. Neirinckx, E. *et al*. Species comparison of oral bioavailability, first-pass metabolism and pharmacokinetics of acetaminophen. *Res. Vet. Sci.* **89,** 113–9 (2010).
33. Bienert, A. *et al*. Pharmacokinetics and ocular disposition of paracetamol and paracetamol glucuronide in rabbits with diabetes mellitus induced by alloxan. *Pharmacol. Rep.* **64,** 421–7 (2012).
34. Koyanagi, T., Yamaura, Y., Yano, K., Kim, S. & Yamazaki, H. Age-related pharmacokinetic changes of acetaminophen, antipyrine, diazepam, diphenhydramine, and ofloxacin in male cynomolgus monkeys and beagle dogs. *Xenobiotica* **44,** 893–901 (2014).
35. Cawthon Lang, K. Primate Factsheets: Long-tailed macaque (Macaca fascicularis) Taxonomy, Morphology, & Ecology. (2006). at <http://pin.primate.wisc.edu/factsheets/entry/long-tailed_macaque>
36. KuKanich, B. Pharmacokinetics of acetaminophen, codeine, and the codeine metabolites morphine and codeine-6-glucuronide in healthy Greyhound dogs. *J. Vet. Pharmacol. Ther.* **33,** 15–21 (2010).
37. KuKanich, B. Pharmacokinetics and pharmacodynamics of oral acetaminophen in combination with codeine in healthy Greyhound dogs. *J. Vet. Pharmacol. Ther.* **39,** 514–517 (2016).
38. Wong, H. *et al*. Glucuronidation in the chimpanzee (Pan troglodytes): studies with acetaminophen, oestradiol and morphine. *Xenobiotica*. **36,** 1178–90 (2006).
39. van Ganzewinkel, C. *et al*. Multiple intravenous doses of paracetamol result in a predictable pharmacokinetic profile in very preterm infants. *Acta Paediatr.* **103,** 612–7 (2014).
40. Anderson, B. J., Pons, G., Autret-Leca, E., Allegaert, K. & Boccard, E. Pediatric intravenous paracetamol (propacetamol) pharmacokinetics: a population analysis. *Paediatr. Anaesth.* **15,** 282–92 (2005).
41. Cook, S. F. *et al*. Population Pharmacokinetics of Intravenous Paracetamol (Acetaminophen) in Preterm and Term Neonates: Model Development and External Evaluation. *Clin. Pharmacokinet.* **55,** 107–19 (2016).
42. Allegaert, K., Palmer, G. M. & Anderson, B. J. The pharmacokinetics of intravenous paracetamol in neonates: size matters most. *Arch. Dis. Child.* **96,** 575–80 (2011).
43. Palmer, G. M. *et al*. I.V. acetaminophen pharmacokinetics in neonates after multiple doses. *Br. J. Anaesth.* **101,** 523–30 (2008).
44. Mohammed, B. S. *et al*. Population pharmacokinetics of single-dose intravenous paracetamol in children. *Br. J. Anaesth.* **108,** 823–9 (2012).
45. Liukas, A. *et al*. Pharmacokinetics of intravenous paracetamol in elderly patients. *Clin. Pharmacokinet.* **50,** 121–9 (2011).
46. Allegaert, K. *et al*. Covariates of intravenous paracetamol pharmacokinetics in adults. *BMC Anesthesiol.* **14,** 77 (2014).

Chapter 7

Systems pharmacology of an endocannabinoid system modulator in zebrafish larva

Vasudev Kantae, Annelot C. M. van Esbroeck, Floor Stevens, Rob C. van Wijk, Floris Luchtenburg, Amy C Harms, Marcel Schaaf, Piet H. Van der Graaf, Mario van der Stelt, Thomas Hankemeier

Manuscript in preparation

Abstract

The zebrafish is increasingly being used as an alternative pre-clinical *in vivo* model in drug research, but the pharmacological aspects of this model still need to be established. Recently we quantified the pharmacokinetics of paracetamol in zebrafish larvae. Here, we used Fatty acid amide hydrolase (FAAH) inhibitor PF-04457845 as a model drug compound to study the dynamic effects of the drug on 5 day post fertilization (dpf) zebrafish larvae. PF-04457845 treatment showed a concentration-dependent increase of endogenous anandamide (AEA) levels, a substrate of FAAH which belongs to the class of N-acylethanolamines (NAEs). The increase in AEA was observed at a dose of 0.1μM PF-04457845 added in the swimming medium. Next, the serine hydrolase interaction profile of PF-04457845 was evaluated using MS-based activity-based protein profiling (ABPP). Through chemoproteomics, 55 serine hydrolases were identified in vehicle treated zebrafish larvae. We observed that *in vivo* exposure to PF-04457845 completely inhibited FAAH2 activity without cross-reacting with the other detected serine hydrolases. In addition, the effect of the drug on the lipid network in zebrafish was evaluated. Using LC-MS based lipidomics, 235 lipids from 15 different classes were identified in vehicle treated zebrafish. Upon PF-04457845 treatment, NAE levels were increased, consistent with drug engagement with FAAH. The levels of other lipid species were not altered, demonstrating the absence of off-target effects with regards to lipid metabolism. Overall these results indicate that zebrafish is an attractive pre-clinical vertebrate model to study the pharmacology of drugs. We could prove target engagement of the drug and the absence of off-target effects with regards to a part of the protein landscape and lipid metabolism in zebrafish larvae.

Introduction

Zebrafish (*Danio rerio*) is increasingly used as an alternative pre-clinical vertebrate model during drug discovery and development [1,2]. Due to their high genetic homology with higher vertebrates and their advantages of their transparent bodies in early development, their cost-effective usage, the possibilities in genetic manipulation, and their fast development make them as an attractive model in translational science [3,4]. Although this model is extensively used in toxicological studies [5,6], the pharmacological aspects of this model needs more attention in order to draw accurate conclusions. Recently, we showed that internal drug exposure is an important parameter to consider when studying drug pharmacology in zebrafish larvae and we characterized the pharmacokinetic processes in zebrafish larvae using paracetamol as a model compound [7]. Another important parameter is to generate drug concentration-effect relationship (Pharmacodynamics, PD) in zebrafish larvae. So far, PD properties in this model organism was not well established. To improve the translational potential, determining Pharmacokinetics/Pharmacodynamics (PK/PD) relationship in this species can help to understand how drug exposure drives the drug effect and then use that to predict PK/PD in humans to determine optimal dose and clinical outcome. Here, we used an endocannabinoid system modulator as an example drug compound to demonstrate that zebrafish can be an attractive model to study the drug effects.

PF-04457845, a clinically proven irreversible inhibitor for FAAH (Fatty acid amide hydrolase) which has entered phase II clinical trials [8], was used as an example drug compound. Pharmacological blockade of FAAH is an attractive strategy to maintain increased endocannabinoid (ECB) tone and to retain the beneficial effects of cannabinoid receptors activation (decrease stress-associated behavioral responses and inflammatory pain), while avoiding the undesirable effects of direct CB1 agonists [9,10]. FAAH, a membrane-bound serine hydrolase is primarily responsible for the hydrolysis of anandamide (AEA) to arachidonic acid and ethanolamine. Another form of FAAH, FAAH-2 is also identified in mammals responsible for the hydrolyses AEA but with weak hydrolytic activity and it contribute to the degradation of monounsaturated lipid amides *in vivo* [11].

AEA is one of two well-studied endocannabinoids identified in mammals that activates the cannabinoid receptors CB1 and CB2. 2-AG is another well-studied endocannabinoid and studies showed FAAH can also metabolizes 2-AG [12] . AEA belongs to a family of bioactive N-acylethanolamines (NAEs), which include N-linoleoylethanolamine (LEA), N-palmitoylethanolamine (PEA), N-oleoylethanolamine (OEA) and N-stearoylethanolamine

(SEA), N-docosatetraenylethanolamide (DHEA). FAAH also hydrolyzes PEA, OEA, LEA, SEA and DHEA. The receptors, ligands (endocannabinoids) and the enzymes responsible for synthesis and hydrolysis of the endocannabinoids together constitutes the endocannabinoid system. The endocannabinoid system is used as an promising therapeutic drug target due to its regulatory and functional role in plethora of physiological and pathological conditions[13,14].

It was shown in previous studies that the endocannabinoid system, including receptors and enzymes including homologues of FAAH2, are highly conserved between zebrafish and humans, which leverages zebrafish to be used as an attractive pre-clinical model to study endocannabinoid system functionalities [11,15–17]. Recently, it was shown FAAH2a attenuates locomotor responses and is an important mediator of stress repose in zebrafish larvae [18]. Furthermore, genetic functional studies have confirmed the endocannabinoid systems in zebrafish and mammals have similar functions. Several studies have already been performed to study the role of the endocannabinoid system in many pathophysiological conditions using zebrafish as a model organism: functional vision and locomotion [19], learning and memory [20], addiction [21], anxiety [22], development [23], lipid metabolism studies [24].

Activity based protein profiling (ABPP) is a chemoproteomics method that uses active site-directed chemical probes (e.g., fluorophosphonate (FP), or b-lactones for serine hydrolases) to assess the functional state of entire enzyme classes directly in native biological systems [25,26]. ABPP is unique in its ability to rapidly identify inhibitor interactions and selectivity within large enzyme families in complex proteome samples either by analysis on SDS–polyacrylamide gel electrophoresis (SDS-PAGE) using fluorescent probes or by mass spectrometry (MS)–based analysis for target identification using biotinylated probes. As the enzymes of the endocannabinoid system in zebrafish larvae are well conserved [27], ABPP could serve as a powerful profiling technique to investigate the protein interaction landscape of newly developed drugs. It has been recently shown that most of the essential lipid classes in humans are present in zebrafish larvae [28], which allows us to study the interaction profile of the drug molecules on the lipid metabolism in zebrafish larvae. Taken together, ABPP and lipidomics are powerful phenotypic tools to assess the target engagement and off-target effects of small molecule drugs developed during early pre-clinical phases. For example, using ABPP and lipidomics, the off-target effect of BIA 10-2474 drug, which failed in phase I clinical trial, was elucidated in iPSC-derived cortical neurons [29].

Here, we quantified the pharmacodynamic processes in zebrafish larvae using FAAH inhibitor PF-04457845 as a model drug compound. We also studied the effect of FAAH inhibitor on the zebrafish behavior. In addition, we investigated the on-target engagement effects and off-target effects of PF-04457845 drug on part of protein landscape and lipid networks in zebrafish larvae.

Materials and methods

Zebrafish husbandry

Zebrafish larvae were handled in compliance with the local animal welfare regulations and maintained according to standard protocols (zfin.org). Embryos were collected from family crosses of AB/TL wild-type strain and grown at 28°C in embryo medium (60 μg/mL Instant Ocean sea salts; Sera Marin) in the dark. All embryos were raised in an incubator at 28.5°C with a 14/10-hour light/dark cycle until they were 5-day old post fertilization (dpf). At 5-dpf, 20 larvae were collected in a 1.5ml safe-lock Eppendorf tube to quantify endogenous endocannabinoid levels.

Drug solutions

PF-04457845 was purchased form Sigma-Aldrich, the Netherlands. Stocks are prepared in DMSO. For zebrafish experiments, the drug stocks were diluted using egg medium and prepared in way that the end solution has 0.05% of DMSO.

Time-response curve

5dpf zebrafish larvae were treated with drug PF-04457845 at 1μM for 30min, 1h, 2h, 4h, 8h and 24h. At each time, three replicates of 20 larvae each were collected and washed three times with 80/20 (V/V) egg medium/methanol, after which excessive medium was removed. The samples were subsequently frozen in liquid N2 and extracted endocannabinoids as described below.

Dose in medium to response curve

5dpf larvae were treated with drug PF-04457845 at different concentrations (DMSO, 0.1, 0.5, 1, 5, 10 μM) for 8hrs. At each time, three replicates of 20 larvae each were collected and washed three times with 80/20 (V/V) egg medium/methanol, after which excessive medium was removed. The samples were subsequently frozen in liquid N2 and extracted endocannabinoids as described below.

Endocannabinoid analysis

Sample extraction

Endocannabinoids and their congeners were quantified using LC-MS/MS analysis. The sample extraction was performed on ice. In brief, 20 zebrafish larvae at 5dpf were transferred to 1.5 mL Eppendorf tubes, spiked with 10 μL of deuterated labeled internal standard mix for endocannabinoids (N-arachidonoyl ethanolamine (AEA)-d8, N-arachidonoyldopamine (NADA)-d8, N docosahexaenoylethanolamide (DHEA)-d4, 2-arachidonoylglycerol (2-AG)-d8, N-stearoylethanolamine (SEA)-d3, N-palmitoylethanolamine(PEA)-d4, N-linoleoylethanolamine (LEA)-d3 and N oleoylethanolamine (OEA)-d4, followed by the addition of ammonium acetate buffer (100 μL, 0.1 M, pH 4). After extraction with methyl tert-butyl ether (800 μL), the tubes were thoroughly sonicated until the sample is homogenous. The samples were mixed for 6 min using a bullet blender at medium speed (Next Advance, Inc., Averill park, NY, USA), followed by a centrifugation step (5000 g, 12 min, 4°C). Then 750 µL of the upper layer methyl tert-butyl ether was transferred into clean 1.5 mL Eppendorf tubes. Samples were dried in a speed-vac followed by reconstitution in acetonitrile/water (30 µL, 90/10, v/v). The reconstituted samples were centrifuged (14000 g, 3 min, 4˚C) before transferring into LC-MS vials. 5 μL of sample was injected for LC-MS analysis.

LC-MS/MS analysis

A targeted analysis of 21 endocannabinoids and related NAEs (*N*-acylethanolamines) were measured using an Acquity UPLC I class Binary solvent manager pump (Waters, Milford, USA) in conjugation with AB SCIEX 6500 quadrupole-ion trap (QTRAP) (AB Sciex, Massachusetts, USA). Separation was performed with Acquity HSS T3 column (1.2 x 100 mm, 1.8 μm) maintained at 45 °C. The aqueous mobile phase A consisted of 2 mM ammonium formate and 10 mM formic acid, and the organic mobile phase B was acetonitrile. The flow rate was set to 0.4 ml/min; initial gradient conditions were 55% B held for 2 min and linearly ramped to 100% B over 6 minutes and held for 2min; after 10 secs, the system returned to initial conditions and held 2 min before next injection. Electrospray ionization-MS was operated in positive mode for measurement of 21 endocannabinoids and NAEs, and a selective Multiple Reaction Mode (sMRM) was used for quantification. Peak area integration was performed with MultiQuant (AB Sciex, Version 3.0.2) data analysis software. The obtained peak areas of targets were corrected by appropriate internal standards. Calculated response

ratios, determined as the peak area ratios of the target analyte to the respective internal standard, were used to obtain absolute concentrations from their respective calibration curves.

The validation parameters and the absolute concentrations for endocannabinoids in 5dpf zebrafish larvae are shown in **Table. S1**.

Activity based protein profiling (ABPP)

Gel based ABPP

Zebrafish larvae (5dpf) were treated with inhibitor PF-0445785 (1 μM) or vehicle (DMSO) for 8 hours. The treated larvae were pelleted and stored at -80 ˚C (n=4, ~60 larvae per pellet). Each pellet was resuspended in lysis buffer (250 mM Sucrose, 20 mM Hepes pH 7.2, 2 mM DTT, 1 mM $MgCl_2$, 10 U/mL Benzonase) and homogenized with a pestle. Clear lysate was obtained after two slow speed centrifugation steps (5 min, 1000 *g*, 4 ˚C). The total protein concentration of the clear lysate was determined with a Bradford Assay and the samples were diluted to a final concentration of 1.25 mg/mL in lysis buffer. ABPP was performed by incubating the samples with probes synthesized in-house, MB064 (2 μM, 20 min, 28.5˚C) or FP-TAMRA (500 nM, 20 min, 28.5˚C). The reaction was quenched with Laemlli sample buffer (15 min, 50 ˚C) and 12.5 μg sample was resolved by SDS-PAGE (10% acrylamide gel, 75 min, 180 V). In-gel fluorescence was measured in the Cy3 and Cy5 channel on a Chemidoc Imaging system (BioRad) and was analysed using Image Lab software (BioRad). Coomassie staining was used as a protein loading control. Probe labelling is expressed as the percentage fluorescence as compared to the fluorescence in the corresponding band of the vehicle treated sample.

Label free proteomics

Zebrafish larvae (5dpf) were treated with inhibitor PF-0445785 (1 μM, final concentration) or vehicle (DMSO) for 8 hours. The treated larvae were pelleted and stored at -80 ˚C (n=3, ~60 larvae per pellet). Each pellet was resuspended in lysis buffer (250 mM Sucrose, 20 mM Hepes pH 7.2, 2 mM DTT, 1 mM $MgCl_2$, 10 U/mL Benzonase) and homogenized with a pestle. Clear lysate was obtained after two slow speed centrifugation steps (5 min, 1000 g, 4 ˚C). The total protein concentration of the clear lysate was determined with a Bradford Assay and the samples were diluted to a final concentration of 2.0 mg/mL in buffer (20 mM Hepes pH 7.2, 2 mM DTT). ABPP was performed by incubating the samples (150 μL, 300 μg protein) with probe cocktail (MB108 and FP-Biotin, 10μM each, 30 minutes, 28˚C, 300 rpm). Heat-inactivated

samples (1% SDS, 100 ˚C, 5 min) of vehicle, BIA 10-2474 and PZ04457845 were used as control (n=1, each). Pull-down and labelfree proteomics proceeded according to the protocol described by Van Rooden et al. [30], with adjustments that beads were washed twice with PBS/SDS and samples were reconstituted in 25μL LC-MS solution (10 min, RT).

Lipidomics analysis

Sample extraction

Zebrafish larvae (5dpf) were treated with inhibitor PF-0445785 (1 μM) or vehicle (DMSO) for 8 hours. Briefly, 20 zebrafish larvae as were used and the endocannabinoid extraction protocol was followed. In addition to the above internal standards, 10 μL non-endogenous lipid internal standards were added (lysophosphatidylcholine (LPC)17:0, phosphatidylethanolamine (PE)17:0/17:0, phosphatidylcholine (PC)17:0/17:0, sphingomyelin (SM) d18:1/17:0, triglyceride (TG) 17:0/17:0/17:0, ceramide (Cer) d18:1/17:0) and fatty acid (FA)17:0-d33). Each sample was injected on three different lipidomics platforms: endocannabinoids (5 μL), positive lipids (2 μL) and negative lipids (8 μL).

LC-MS/MS analysis

The endocannabinoid analysis was followed as described above. Both lipidomics methods (positive and negative lipids) are adapted and modified from previously published work [29]. Briefly, these methods are measured on an Acquity UPLC Binary solvent manager pump (Waters) coupled to an Synapt G2 electrospray ionization quadrupole time-of-flight (ESI-Q-TOF, Waters, Wilmslow, United Kingdom) high resolution mass spectrometer using reference mass correction. The chromatographic separation was achieved on an Acquity HSS T3 column (1.2 x 100 mm, 1.8 μm) maintained at 40°C for both methods. The positive lipid run includes targets from different lipid classes including (lyso)phosphatidylcholines, triglycerides, ceramides. (lyso)phosphatidylethanolamines and sphingomyelins were separated using a flow of 0.4 mL/min over a 16 min gradient. In positive mode, the mobile phase A consisted of 60:40 (v/v) acetonitrile: H2O with 10 mM ammonium formate, and the mobile phase B consisted of 10:90 (v/v) acetonitrile: isopropanol with 10 mM Ammonium formate.

The negative lipids constitute mainly free fatty acids and (lyso)phosphatidylcholines were separated with a flow of 0.4 mL/min over 15 min gradient. In negative mode, the aqueous mobile phase A consisted of 5:95 (v/v) acetonitrile: H2O with 10 mM ammonium formate, and

the organic mobile phase B consisted of 99% (v/v) methanol with 10 mM Ammonium formate. The targets in both lipid methods were detected full scan (100-1000 m/z) in their respective ion charge mode.

PF-04457845 quantification

Sample extraction

Zebrafish larvae (5dpf) were treated with inhibitor PF-0445785 at 1 μM for 8 hours. PF - 04457845 molecule was quantified using LC-MS/MS analysis in blood samples pooled from 20-25 zebrafish larvae at 5dpf, roughly 83 nL. The blood sample was collected from anatomical locations of the larval circulation using a pulled needle (borosilicate glass capillary, original diameter: 0.5 mm. Sutter Instruments) in a micromanipulator, connected to a manual CellTram pump (Eppendorf) under 20x microscopic magnification (Leica). For determination of sample volume, an image was taken of each sample's blood content within the needle. To prevent coagulation, different strategies were tested, including heparin coating of needle and collection tube. The sample extraction was performed on ice. In brief, 200 μL of acetonitrile was added to the blood samples. The samples were vortexed and then centrifuged at 13000 xg for 10min. 150 μL of supernatant was evaporated to dryness using speedvac and reconstituted in 10 μL of acetonitrile.

LC-MS/MS analysis

PF-04457845 was measured using an Acquity UPLC I class Binary solvent manager pump (Waters, Milford, USA) in conjugation with AB SCIEX 6500 quadrupole-ion trap (QTRAP) (AB Sciex, Massachusetts, USA). Separation was performed with Acquity HSS T3 column (1.2 x 100 mm, 1.8 μm) maintained at 45 °C. The aqueous mobile phase A consisted of 2 mM ammonium formate and 10 mM formic acid, and the organic mobile phase B was acetonitrile. The flow rate was set to 0.5 ml/min; initial gradient conditions were 60% B held for 0.5 min and linearly ramped to 100% B over 2.5 minutes and held for 0.5 min; after 10 sec the system returned to initial conditions and held 1.5 min before next injection. Electrospray ionization-MS was operated in positive mode for measurement of PF-04457845 and a selective Multiple Reaction Mode (sMRM) was used for quantification. The ion masses monitored were Q1/Q3 456/335 (m/z). Peak area integration was performed with MultiQuant (AB Sciex, Version

3.0.2) data analysis software. The limits of detection (LOD) was 1pM and the linear range used was from 1 to 1000 pM.

Behavioral study

Embryos (0 day) were put individually in a 96 well plate (Costar 3599, Corning Inc., NY, USA) with 250 µL egg water and left until 5 dpf. All analyses were performed between 10:00 and 19:00. After addition of the drug compounds PF-04457845 at 1µM and DMSO for controls, the 96 well plate was immediately transferred to the recording apparatus (Daniovision, Noldus, the Netherlands). After starting of the recording, the fish were first allowed to acclimatize for 4 min with the lights on. This was followed by an alternating 4 min dark and 2 h light cycle and continued to record for 8h. These 4 min dark pulses induce anxiety-like behavior, which allows for analyzing potential anxiolytic effects of our compounds. Basal behavior could be derived from the 2h light periods. Recordings were analyzed using EthoVision 12 (Noldus, the Netherlands). Each experiment was performed three times with a different clutch of eggs for each experiment. Data shown are means of all larvae ± standard error of the mean (SEM).

Results

Pharmacological response of PF-04457845

a. Time-response profiles

We investigated if endogenous endocannabinoid system of zebrafish larvae can be modulated by an exogenous drug molecule. When treated with FAAH inhibitor PF-04457845 at 1μM in zebrafish swimming medium, anandamide levels followed an increasing trend with continuous exposure **(Fig. 1a)**. Of note, no effect of FAAH inhibitor was observed on 2-AG levels **(Fig. 1b)**. Next, we assessed the drug incubation time required to achieve maximum inhibition. Although we observed decrease in FAAH activity at 1hr of drug incubation, after from 5hrs FAAH activity is completely inhibited and reached steady state condition.

b. Dose in the medium to response profiles

Next, we assessed the amount of dose required to achieve maximal inhibition of FAAH activity. Anandamide levels increase started at 0.1μM (swimming medium) of PF-04457845 and followed an increasing trend with increase in drug dose **(Fig. 1c)**. Of note, no effect of FAAH inhibitor was observed on 2-AG levels even at high concentrations **(Fig. 1d).**

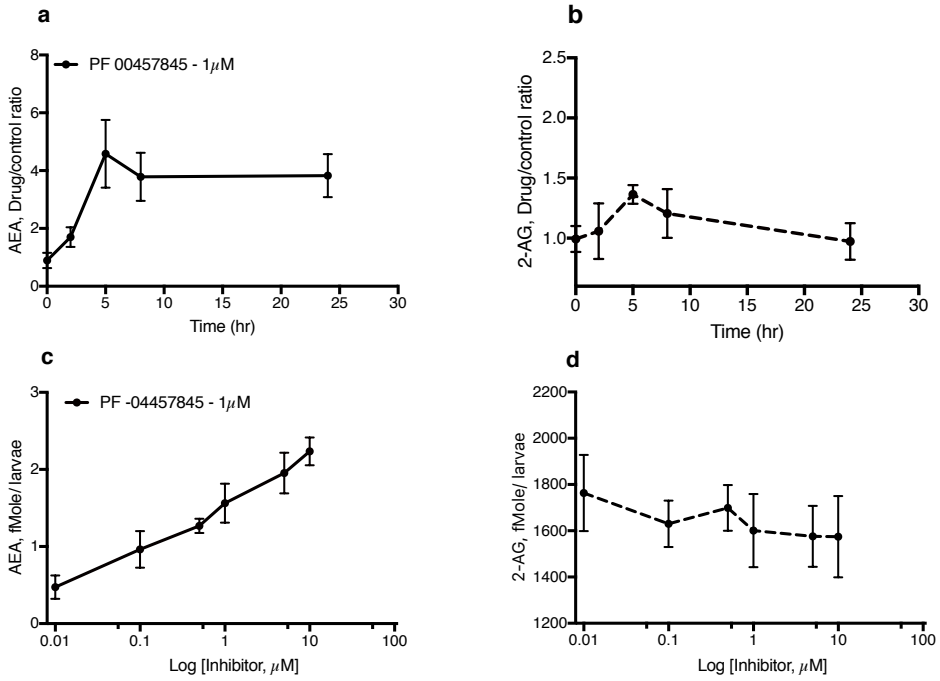

Figure 1: Pharmacological response of PF-04457845. Time-response curve and dose in medium to response curves of PF-04457845 for AEA (solid line **a, c**) and 2-AG (dashed line **b, d**) levels in zebrafish larvae.

c. Drug concentration in blood samples of zebrafish larvae

Blood samples from drug treated zebrafish larvae were drawn to assess if the drug actually entered the circulatory system of zebrafish larvae. Using LC-MS/MS analysis, PF-04457845 was quantified to be at 0.5 μM after 8h (n=1) of drug incubation.

Gel and proteomics based ABPP revealed selective FAAH2 inhibition by PF-04457845

To investigate the selectivity of PF-04457845 in zebrafish larvae we performed competitive ABPP using broad spectrum probe TAMRA-FP which targets serine hydrolases and a tailored lipase probeMB064 which targets serine hydrolases part of endocannabinoid system, as well as their biotinylated counterparts FP-Biotin and MB108 respectively. First, we used gel based ABPP to assess the PF-04457845 protein interaction profile in 5 dpf zebrafish larvae. The results revealed a clean profile under *in vivo* conditions (**Fig. 2a-c**).

It is worth mentioning that FAAH was not labelled in gel-based ABPP due to lack of sensitivity in this assay. To identify the serine hydrolases, including FAAH and PF-04457845 targets in these zebrafish larvae, we performed chemoproteomics, an MS-based approach of ABPP. We identified 55differnt serine hydrolases (**Fig. 2d**). Here, we confirmed that PF-04457845 at 1 μM fully inhibited FAAH2. The proteomics data demonstrates the drug is very selective towards FAAH and do not cross-reacts with other serine hydrolases (**Fig. 2a**). Of note, we investigated whether longer incubation (24h) of PF-04457845 effects the zebrafish protein interaction landscape. The results showed a similar protein profiles even with longer incubation times (data not shown).

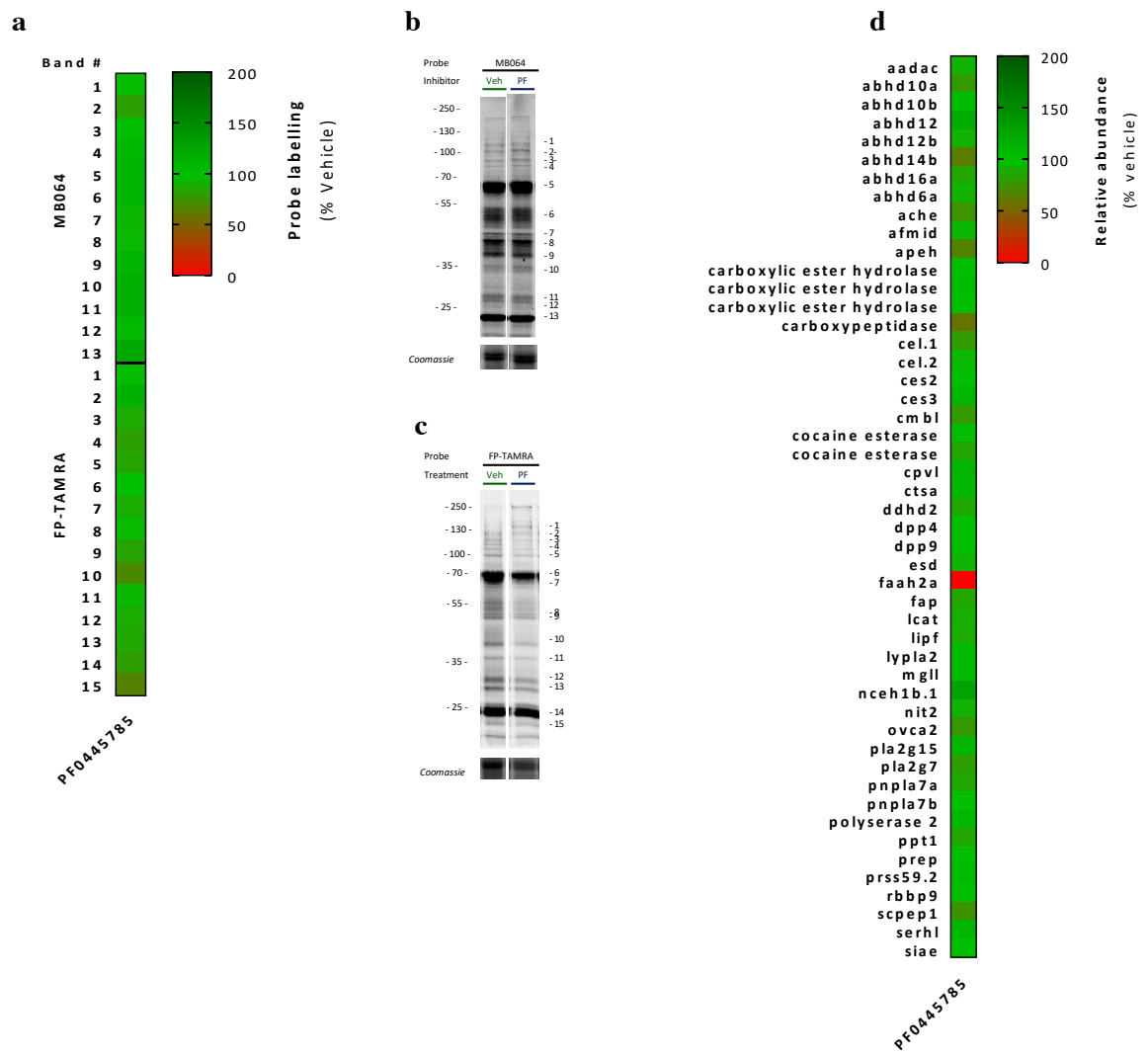

Figure 2: Activity based profiling of serine hydrolase targets of FAAH inhibitors in Zebrafish larvae (5dpf). a) Heat-map summary of gel-based ABPP, probe labelling (% vehicle) for MB064 (targeting serine hydrolases part of ECS) and FP-TAMRA (targeting boarder serine hydrolases) (n=4). Color scale indicates inhibition by inhibitor (red = full inhibition, bright green = no inhibition, blank = not detected in all samples, including vehicle). Numbers correspond to those indicated in panel **(b-c). b-c)** Representative probe labelling pattern of treated zebrafish (8h) labelled with MB064 (2 μM, 20 min, 28.5˚C) (c) or FP-TAMRA (500 nM, 20 min, 28.5˚C) **d)** Heat-map summary of activity based protein profiling data, showing relative abundance (% vehicle) for MB108 and THL-Biotin (n=3).

PF-04457845 altered FAAH substrate levels in zebrafish larvae

Next, we investigated whether PF-04457845 engages with FAAH and alters its substrates and other lipid network in zebrafish larvae. Initially, a semi-targeted lipidomics was performed to confirm the presence of 235 known lipids falling under 15 different lipid classes in 5dpf

zebrafish larvae (**Fig. 3a).** Zebrafish larvae were exposed to vehicle (DMSO) or PF-04457845 (1 μM). Drug treatment did not alter the lipid species, except NAE's, the FAAH substrates (**Fig. 3b**). Of note, we investigated if longer incubation (24h) alters the zebrafish lipid metabolism. The results showed similar profiles even with longer incubation times (data not shown).

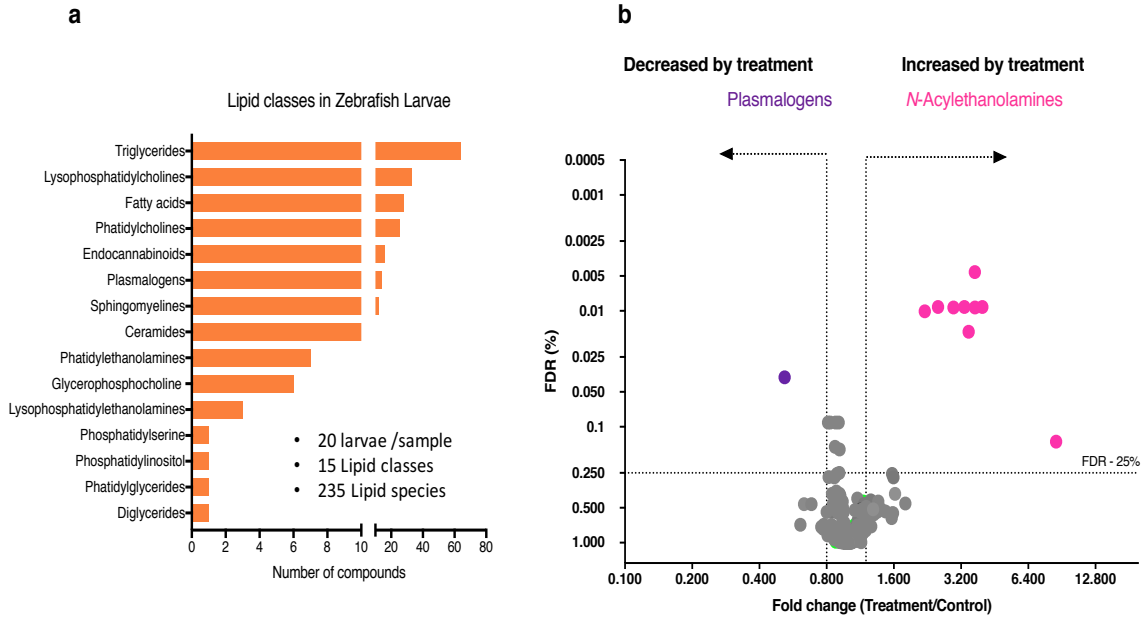

Figure 3: LC-MS/MS based lipidomics of FAAH inhibitorPF-04457845 in zebrafish larvae. a) Total lipid species detected in zebrafish larvae. **b)** Zebrafish larvae treated with DMSO or PF-04457845 **(1** μM) for 8 hours. The x-axis shows the fold change of lipid species in the inhibitor-treated versus DMSO-treated cells. Lipidomic data are presented as a volcano plot, and lipids with a fold-change threshold of ≥1.20 or ≤0.80 and a Benjamini-Hochberg false-discovery rate (FDR) ≤25% are represented by colored circles indicating lipid class.

Behavioral assay

It was shown in a previous study that the CB1 receptor agonist has an effect on zebrafish behavior [31]. So, we investigated if FAAH inhibitor PF-04457845 at 1 μM incubated for 8h, has an effect on zebrafish behavior. The activity of each larva was automatically recorded and analyzed in the ZebraBox recording apparatus equipped with VideoTrack software (both from Viewpoint S.A.). The experimental recording consists of two steps. First, larvae were acclimated to the behavioral setup with lights on for 4 min. This period was necessary and sufficient to ensure a low and stable behavioral activity. Once basal levels of the locomotor activity were stabilized following the acclimatizing period, the basal swimming activity was

recorded during 2 h with lights on. This period is referred to as the ‘‘basal phase.’’ Immediately following the basal phase recording, the lights were suddenly turned off for 4 min. The behavioral activity in the dark was also automatically recorded during this period. This period is referred to as the ‘‘dark challenge phase.’’

We observed no change in the zebrafish behavior (**Fig. 4**). The variation of behavior in the first and second light (L) and dark (D) phase is due to the adaption of the zebrafish. Additionally, there is a decreasing trend observed in the distance moved in the light cycle (L), which is due to the circadian rhythm in zebrafish.

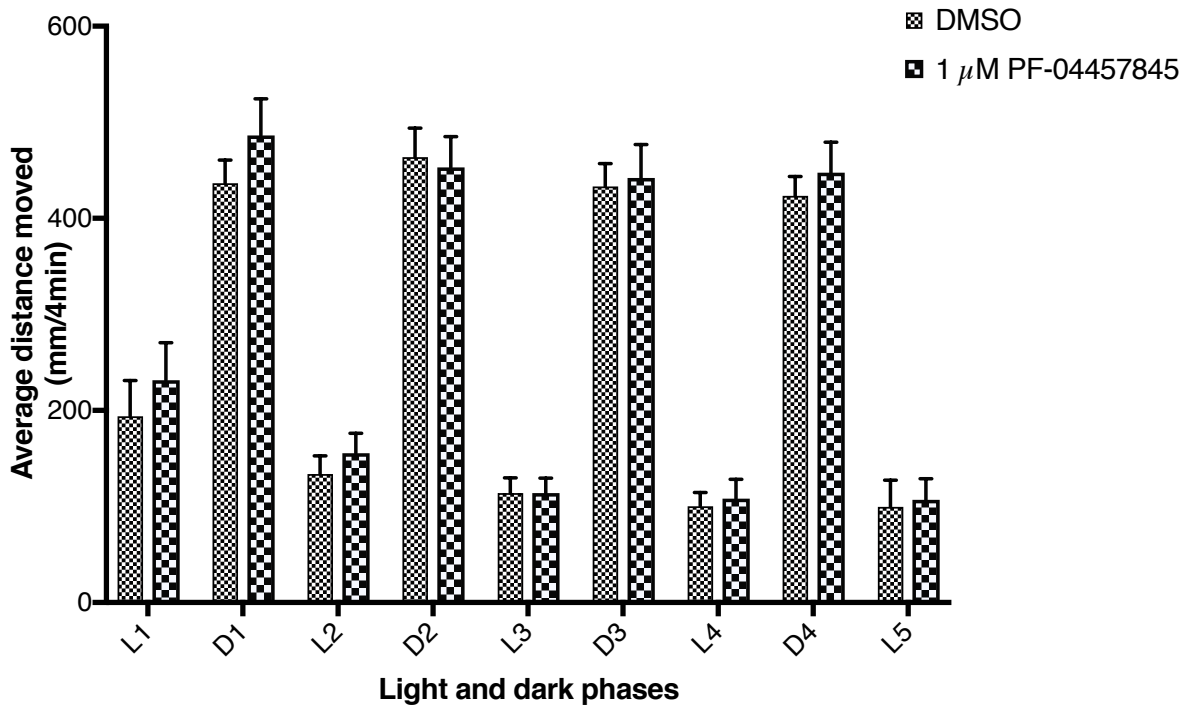

Figure 4: Behavioral study of zebrafish larvae treated with FAAH inhibitor PF-04457845(1 μM) or DMSO and recorded for 8 hours. The x-axis represents the zebrafish behavior recorded in light and dark phases. After the fish were first allowed to acclimatize for 4 min with the lights on. This was followed by an alternating 4 min dark and 2 hours light cycle. The y-axis shows the average distance moved per 4 mins.

Discussion

The inter-species translation potential of the zebrafish model to study the drug effects during discovery and early drug development phases is gaining more interest. Recently, we have successfully quantified the PK processes in zebrafish larvae and showed that they can be translated to humasn[7].However the pharmacodynamics aspects in zebrafish remains to be elucidated. In the present study, we aimed to quantify the pharmacodynamic(PD) processes in zebrafish larvae, which further strengthens the translational potential of this model during early drug development studies. In that context, we sought to expand the applicability of using zebrafish model to investigate the on-target engagement of newly synthesized drug molecules, including the drug effect on zebrafish behavior.

We assessed the effect of the exogenous FAAH inhibitor PF-04457845 on the endogenous endocannabinoid system in zebrafish larvae. The pharmacological characterization of cannabinoid-binding sites in zebrafish brain showed that the zebrafish cannabinoid system might not significantly differ from cannabinoid system in higher vertebrates [32]. Our UPLC-MS/MS based endocannabinoid analysis in zebrafish larvae confirmed that PF-044574845 inhibited FAAH activity. PF-04457845 treatment showed a concentration-dependent increase of the endogenous anandamide levels similar to what has been observed in higher vertebrates [8,33]. Furthermore, internal exposure of PF-04457845 was assessed by taking a blood sample of the zebrafish larvae and quantified using LC-MS/MS analysis.

As it has been recognized that the drug concentrations rather than the drug doses are driving drug effects in any pharmacological systems, quantification of full pharmacokinetic processes of the FAAH inhibitor PF-04457845 will be invaluable for drawing accurate conclusions. Although we have developed a methodology to quantify the pharmacokinetics studies in 3dpf zebrafish larvae [7], we cannot apply this method to the current drug due to its lipophilic nature, hence strongly binding to the skin of the larvae and cannot be removed with washing (data not shown).

We next investigated the target engagement of the FAAH inhibitor PF-04457845 on the protein landscape of zebrafish larvae. To the best of our knowledge, for the first time, we identified 55 different serine hydrolases proteins in the zebrafish larvae using MS-based proteomics, depicting the power of this technique. Gel-based and MS-based ABPP revealed that the drug engages with FAAH2. Furthermore, lipidomics data demonstrated that the drug changes with FAAH activity as the levels FAAH substrates *N*-acylethanolamines increased

with drug treatment. It should be noted that the PF-04457845 treatment did not cross-react with other serine hydrolases or did not alter lipid network. The results depict only the engagement of PF-04457845 towards the target and showed no interaction with other serine hydrolases measured in the current assay[29]. Our drug target engagement of PF-04457845 results are in line with the studies performed in mice and humans where they showed target engagement with FAAH activity, depicting the translational potential of zebrafish larvae [33]. It is worth mentioning that FAAH2 is obscured to some extent as rodent models have one gene encoding FAAH while many non-rodent vertebrates, including humans and zebrafish, have FAAH2 [11], which gives advantage of using zebrafish model. Previous reports investigated the role of FAAH2 in modulating anxiety in humans [34] stimulating the use of zebrafish model to study the role of FAAH2 in anxiety compared to rodent models which lack this enzyme.

Furthermore, we investigated the impact of FAAH inhibitor PF-04457845 on zebrafish behavior. It was previously observed that cannabinoids have behavioral effects in zebrafish larvae that are comparable to mammals. The authors reported that zebrafish larvae when treated CB1 agonist (D9-THC or WIN 55,212-2) show a biphasic response (increasing hyperactivity succeeded by suppression of activity with higher doses) while CB1 antagonist (AM2451) attenuates the increased locomotor activity induced by CB1 agonist [31]. We hypothesized that FAAH inhibition leads to increase in the levels of AEA, an endogenous agonist for CB1 receptor, which can potentially effect zebrafish behavior. Unfortunately, FAAH inhibitor did not affect zebrafish behavior at our experimental conditions. A possible explanation for not observing behavior effect could be that the anandamide level increase upon FAAH inhibitor treatment is not sufficient to cause a behavior effect.

The strength of this study is that we have investigated different pharmacological aspects in zebrafish larvae which allows us to reliably employ this model during drug discovery and early drug development phases. Taking into account the advantages of using zebrafish larvae [6], this model fits in the well-established pre-clinical animal model testing applied in drug research [35]. In modern drug discovery and development, there is an increase in the high attrition rate due to lack of proper balance between drug efficacy and potential adverse effects and only few compounds make the transition to clinical trial drug candidates [36]. Furthermore, during clinical trials, some drugs fail due to undesirable off-target activity which cannot be easily screened out from the mode of action of the target. Therefore, we need proper *invivo* models to prevent drugs with undesirable effects before entering or during clinical trials. Here we used zebrafish as an appropriate model to study the pharmacological properties, like PD to assess

the systemic drug effects. Additionally, we showed ABPP and lipidomics as powerful profiling platforms to investigate the target engagement of the drug developed in early pre-clinical stages.

A limitation of this study is that with the current experimental conditions, we cannot study the localized drug effect, for example in specific tissues, as it will be difficult to isolate tissue samples from a large number of larvae and to get sufficient signal with the current profiling platforms. This could be overcome by developing miniaturized analytical platforms to detect the low concentrations of drugs using limited number biological matrix. Secondly, the pharmacokinetic processes could not be quantified for the lyophilic drugs due to their sticking to the skin of the larvae. However, this problem could be addressed either by orally dosing the zebrafish larvae using nano-particles [37] rather than adding the drug in the swimming medium or by sampling blood samples from zebrafish larvae, which we measured for a single point in this study but require further optimization to make it practically feasible for collecting samples at more time points.

In summary, these results indicate that zebrafish is an attractive pre-clinical vertebrate model for pharmacology studies of drugs. We could prove target engagement of the drug, and the absence of off-target effects with regards to a part of the protein landscape and lipid metabolism in zebrafish larvae. Overall, this study expanded the applicability of zebrafish larvae as an attractive pre-clinical model in drug discovery and early drug development, also demonstrating the inter-species translational potential.

References

1. MacRae, C. A. & Peterson, R. T. Zebrafish as tools for drug discovery. *Nat. Rev. Drug Discov.* **14,** 721–31 (2015).
2. Diekmann, H. & Hill, A. ADMETox in zebrafish. *Drug Discov. Today Dis. Model.* **10,** e31–e35 (2013).
3. Lieschke, G. J. & Currie, P. D. Animal models of human disease: zebrafish swim into view. *Nat. Rev. Genet.* **8,** 353–67 (2007).
4. Blackburn, P. R., Campbell, J. M., Clark, K. J. & Ekker, S. C. The CRISPR System—Keeping Zebrafish Gene Targeting Fresh. *Zebrafish* **10,** 116–118 (2013).
5. Alderton, W. *et al.* Accumulation and metabolism of drugs and CYP probe substrates in zebrafish larvae. *Xenobiotica.* **40,** 547–57 (2010).
6. Rubinstein, A. L. Zebrafish assays for drug toxicity screening. *Expert Opin. Drug Metab. Toxicol.* **2,** 231–40 (2006).
7. Kantae, V. *et al.* Pharmacokinetic Modeling of Paracetamol Uptake and Clearance in Zebrafish Larvae: Expanding the Allometric Scale in Vertebrates with Five Orders of Magnitude. *Zebrafish* **13,** 504–510 (2016).
8. Ahn, K. *et al.* Mechanistic and Pharmacological Characterization of PF-04457845: A Highly Potent and Selective Fatty Acid Amide Hydrolase Inhibitor That Reduces Inflammatory and Noninflammatory Pain. *J. Pharmacol. Exp. Ther.* **338,** 114–124 (2011).
9. Ahn, K., Johnson, D. S. & Cravatt, B. F. Fatty acid amide hydrolase as a potential therapeutic target for the treatment of pain and CNS disorders. *Expert Opin. Drug Discov.* **4,** 763–784 (2009).
10. Cravatt, B. F. *et al.* Supersensitivity to anandamide and enhanced endogenous cannabinoid signaling in mice lacking fatty acid amide hydrolase. *Proc. Natl. Acad. Sci.* **98,** 9371–9376 (2001).
11. Wei, B. Q., Mikkelsen, T. S., McKinney, M. K., Lander, E. S. & Cravatt, B. F. A Second Fatty Acid Amide Hydrolase with Variable Distribution among Placental Mammals. *J. Biol. Chem.* **281,** 36569–36578 (2006).
12. Basavarajappa, B. S. Critical enzymes involved in endocannabinoid metabolism. *Protein Pept. Lett.* **14,** 237–46 (2007).
13. Di Marzo, V. Targeting the endocannabinoid system: to enhance or reduce? *Nat. Rev. Drug Discov.* **7,** 438–55 (2008).
14. Piomelli, D., Giuffrida, A., Calignano, A. & Rodríguez de Fonseca, F. The endocannabinoid system as a target for therapeutic drugs. *Trends Pharmacol. Sci.* **21,** 218–24 (2000).
15. McPartland, J. M., Glass, M., Matias, I., Norris, R. W. & Kilpatrick, C. W. A shifted repertoire of endocannabinoid genes in the zebrafish (Danio rerio). *Mol. Genet. Genomics* **277,** 555–570 (2007).
16. Klee, E. W. *et al.* Zebrafish: a model for the study of addiction genetics. *Hum. Genet.* **131,** 977–1008 (2012).
17. Krug, R. G. & Clark, K. J. Elucidating cannabinoid biology in zebrafish (Danio rerio). *Gene* **570,** 168–79 (2015).
18. Krug, R. G. *et al.* The endocannabinoid gene faah2a modulates stress-associated behavior in zebrafish. *PLoS One* **13,** e0190897 (2018).
19. Martella, A. *et al.* Important role of endocannabinoid signaling in the development of functional vision and locomotion in zebrafish. *FASEB J.* (2016).
20. Ruhl, T., Moesbauer, K., Oellers, N. & von der Emde, G. The endocannabinoid system and associative learning and memory in zebrafish. *Behav. Brain Res.* **290,** 61–69

(2015).
21. Braida, D. *et al*. Hallucinatory and rewarding effect of salvinorin A in zebrafish: κ-opioid and CB1-cannabinoid receptor involvement. *Psychopharmacology (Berl)*. **190,** 441–448 (2007).
22. Stewart, A. M. & Kalueff, A. V. The behavioral effects of acute Δ9-tetrahydrocannabinol and heroin (diacetylmorphine) exposure in adult zebrafish. *Brain Res*. **1543,** 109–119 (2014).
23. Migliarini, B. & Carnevali, O. A novel role for the endocannabinoid system during zebrafish development. *Mol. Cell. Endocrinol*. **299,** 172–177 (2009).
24. Nishio, S.-I. *et al*. Fasting Induces CART Down-Regulation in the Zebrafish Nervous System in a Cannabinoid Receptor 1-Dependent Manner. *Mol. Endocrinol*. **26,** 1316–1326 (2012).
25. Niphakis, M. J. & Cravatt, B. F. Enzyme Inhibitor Discovery by Activity-Based Protein Profiling. *Annu. Rev. Biochem*. **83,** 341–377 (2014).
26. Baggelaar, M. P. *et al*. Highly Selective, Reversible Inhibitor Identified by Comparative Chemoproteomics Modulates Diacylglycerol Lipase Activity in Neurons. *J. Am. Chem. Soc*. **137,** 8851–8857 (2015).
27. Oltrabella, F., Melgoza, A., Nguyen, B. & Guo, S. Role of the endocannabinoid system in vertebrates: Emphasis on the zebrafish model. *Dev. Growth Differ*. **59,** 194–210 (2017).
28. Fraher, D. *et al*. Zebrafish Embryonic Lipidomic Analysis Reveals that the Yolk Cell Is Metabolically Active in Processing Lipid. *Cell Rep*. **14,** 1317–1329 (2016).
29. Van Esbroeck, A. C. M. *et al*. Activity-based protein profiling reveals off-target proteins of the FAAH inhibitor BIA 10-2474. *Science (80-.)*. **356,** (2017).
30. van Rooden, E. J. *et al*. Mapping in vivo target interaction profiles of covalent inhibitors using chemical proteomics with label-free quantification. *Nat. Protoc*. **13,** 752–767 (2018).
31. Akhtar, M. T. *et al*. Developmental effects of cannabinoids on zebrafish larvae. *Zebrafish* **10,** 283–93 (2013).
32. Rodriguez-Martin, I., de Velasco, E. M. F. & Rodriguez, R. E. Characterization of cannabinoid-binding sites in zebrafish brain. *Neurosci. Lett*. **413,** 249–254 (2007).
33. Li, G. L. *et al*. Assessment of the pharmacology and tolerability of PF-04457845, an irreversible inhibitor of fatty acid amide hydrolase-1, in healthy subjects. *Br. J. Clin. Pharmacol*. **73,** 706–716 (2012).
34. Sirrs, S. *et al*. Defects in fatty acid amide hydrolase 2 in a male with neurologic and psychiatric symptoms. *Orphanet J. Rare Dis*. **10,** 38 (2015).
35. Zon, L. I. & Peterson, R. T. In vivo drug discovery in the zebrafish. *Nat. Rev. Drug Discov*. **4,** 35–44 (2005).
36. Bowes, J. *et al*. Reducing safety-related drug attrition: the use of in vitro pharmacological profiling. *Nat. Rev. Drug Discov*. **11,** 909–922 (2012).
37. Fenaroli, F. *et al*. Nanoparticles as Drug Delivery System against Tuberculosis in Zebrafish Embryos: Direct Visualization and Treatment. **8,** 7014–7026 (2014).

Supplementary Table 1: Target list and validation parameters

S. No	ID	Metabolite Name	PE (%)	R^2	Precision (%RSD)	Mean ± SEM fM/larvae
1	2&1AG (20:4)	Arachidonoylglycerol	78	0.998	5	2269.6±59.3
2	AEA (20:4)	Anandamide	85	0.999	12	0.5±0.02
3	DHEA (22:6)	*N*-Docosahexaenoyl ethanolamide	49	0.999	4	42.4±1.6
4	LEA (18:2)	*N*-Linoleoylethanolamide	79	0.999	3	0.38±0.11
5	OEA (18:1)	*N*-Oleoylethanolamide	84	0.999	6	1.2±0.3
6	PEA (16:0)	*N*-Palmitoylethanolamide	87	0.999	3	21.6±0.91
7	SEA (18:0)	*N*-Stearoylethanolamide	91	0.999	2	11.7±0.60
9	DEA (22:4)	*N*-Docosatetraenoyl ethanolamide	48	0.998	19	0.4±0.02
10	DGLEA (18:3)	Dihomo-γ-Linolenoyl Ethanolamide	65	0.999	35	0.1±0.01
11	2-LG (18:2)	2-Linoleoyl Glycerol	63	0.999	8	6153.6±493.7
12	1-LG (18:2)	1-Linoleoyl Glycerol	74	0.981	7	773.4±65.8
13	2-OG (18:1)	2-Oleoyl Glycerol	73	0.999	3	17999.4±1740.0
14	1-OG (18:1)	1-Oleoyl Glycerol	N/A	0.986	3	2563.7±191.45
15	EPEA (20:5)	*N*-Eicosapentaenoyl ethanolamide	65	0.999	5	7.3±0.44
16	POEA (16:1)	*N*-Palmitoleoylethanolamide	99	0.999	4	0.8±0.04
17	PDEA (15:0)	*N*-Pentadecanoylethanolamide	82	0.999	7	0.2±0.01
18	AA (20:4)	Arachidonic Acid	122	0.998	7	80167.4±5529.8

The target list includes endocannabinoids and *N*-acylethanolamines (NAEs). The compound ID is the abbreviation of metabolite name. R^2= correlation coefficient. The method is validated in terms of linearity, sensitivity (LOQ), process efficiency, PE (matrix effect with recovery) and precision (RSD: Relative standard deviation). Endogenous concentrations are denoted as mean ± SEM

Chapter 8

Endocannabinoid tone is higher in healthy lean South Asian than white Caucasian men

Vasudev Kantae*, Kimberly J. Nahon*, Maaike E. Straat, Leontine E.H. Bakker, Amy C. Harms, Mario van der Stelt, Thomas Hankemeier, Ingrid M. Jazet, Mariëtte R. Boon, Patrick C.N. Rensen

**Authors contributed equally*

Scientific Reports. 2017; 7(1): 7558.

Abstract

South Asians have a higher risk to develop obesity and related disorders compared to white Caucasians. This is likely in part due to their lower resting energy expenditure (REE) as related with less energy-combusting brown adipose tissue (BAT). Since overactivation of the endocannabinoid system is associated with obesity and low BAT activity, we hypothesized that South Asians have a higher endocannabinoid tone. Healthy lean white Caucasian (n=10) and South Asian (n=10) men were cold-exposed to activate BAT. Before and after cooling, REE was assessed and plasma was collected for analysis of endocannabinoids and lipids. At thermoneutrality, South Asians had higher plasma levels of 2-arachidonoylglycerol (2-AG; 11.36 vs 8.19 pmol/mL, $p<0.05$), N-arachidonylethanolamine (AEA; 1.04 vs 0.89 pmol/mL, $p=0.05$) and arachidonic acid (AA; 23.24 vs 18.22 nmol/mL, $p<0.001$). After pooling of both ethnicities, plasma 2-AG but not AEA positively correlated with triglycerides ($R^2=0.32$, $p<0.05$) and body fat percentage ($R^2=0.18$, $p<0.05$). Interestingly, AA negative correlated with REE ($R^2=0.46$, $p<0.001$) and positively with body fat percentage ($R^2=0.33$, $p<0.01$). Cooling increased endocannabinoids. In conclusion, South Asian compared to white Caucasian men have higher endocannabinoid tone. This suggests that endocannabinoids may, at least in part, underlie the disadvantageous metabolic phenotype of South Asians later in life.

Introduction

South Asians originally descend from the sub-Indian continent and comprise about 24% of the world population. This population is at higher risk for developing a disadvantageous metabolic phenotype consisting of obesity, dyslipidemia and insulin resistance compared to white Caucasians, making them more prone to develop type 2 diabetes (T2D) at a younger age and lower body mass index (BMI) [1]. The underlying mechanism of the increased predisposition for this unfavorable metabolic profile in South Asians is not well understood, but might be related to a disturbed energy metabolism [2].

The endocannabinoid system (ECS) is known to play an important role in energy metabolism by regulating appetite, lipolysis and energy expenditure [3]. The ECS is composed of endogenous lipid messengers (endocannabinoids), two distinct G-protein-coupled receptors, i.e. type 1 and type 2 cannabinoid (CB_1 and CB_2) receptors, and enzymes responsible for the synthesis and inactivation of the endocannabinoids. *N*-arachidonylethanolamine (anandamide; AEA) and 2-arachidonoylglycerol (2-AG) are the best-studied endocannabinoids. They are synthesized on demand from the membrane lipid precursors *N*-acylphosphatidylethanoamines and diacylglycerides, respectively. Furthermore, there are endogenous bioactive lipids called *N*-acylethanolamines (NAEs), such as *N*-linoleoylethanolamine (LEA), *N*-palmitoylethanolamine (PEA), *N*-oleoylethanolamine (OEA) and *N*-stearoylethanolamine (SEA), which are produced through the same biosynthetic pathway as AEA. NAEs are able to indirectly modulate cannabinoid receptor activity by interfering with endocannabinoid metabolism. In addition, OEA modulates satiety through its interaction with PPARα [4,5]. The ECS is present in both central and peripheral tissues that are involved in maintaining energy balance. These include the hypothalamus, liver, pancreas, skeletal muscle, white adipose tissue (WAT) and brown adipose tissue (BAT)[6].

High ECS activity has been associated with human obesity [7,8]. More specifically, elevated circulating AEA and 2-AG levels have been reported in obese individuals [8–10] and circulating 2-AG levels are positively correlated with different measures of adiposity, including BMI and body fat percentage [8], supporting a causal role of the ECS in energy metabolism. Indeed, reduction in 2-AG formation has been associated with reduced food intake in fasted mice [11,12] and chronic systemic blockade of the CB_1 receptor with the inverse agonist rimonabant leads to long-term maintained weight loss and reduction of dyslipidemia in obese rodents [13,14] and humans [15–17].

Mouse studies have shown that the beneficial metabolic effects of CB_1 receptor blockade are, at least in part, mediated via activation of energy-combusting BAT[18]. Moreover, cold mediated BAT activation leads to a tissue-specific upregulation of endocannabinoids in BAT via CB_1 receptors, thereby possibly controlling BAT activity by negative feed-back mechanisms [19]. BAT is present and active in human adults and dissipates triglyceride (TG)-derived fatty acids towards heat, thereby contributing to energy expenditure [20–23]. Cold acclimatization, the most important physiological activator of BAT, has been shown to recruit and activate BAT in obese humans [24]. The precise role of the ECS in human BAT activation remains to be determined. Interestingly, we have previously shown that South Asian individuals have lower BAT volume and activity, as measured with [^{18}F]fluorodeoxyglucose ([^{18}F]FDG) PET-CT scanning, compared to white Caucasians, which might, at least in part, contribute to their high susceptibility to develop obesity and T2D [25]. The underlying cause of the decreased BAT volume in South Asians is still a question that remains.

The main aim of this study was to investigate if healthy lean South Asians men who have not yet developed a disadvantageous metabolic phenotype have a higher endocannabinoid tone as compared to white Caucasians. Furthermore, we investigated whether cold mediated BAT activation leads to upregulation of endocannabinoid levels in humans. In addition, we aimed to assess whether plasma endocannabinoid levels correlate with BAT function, energy expenditure and serum lipid levels.

Materials and Methods

Ethics

Venous blood samples were collected as part of a previously conducted observational study aimed at investigating BAT activity and volume in Dutch South Asian and white Caucasian individuals[25]. This study was approved by the Medical Ethical Committee of the Leiden University Medical Center (LUMC) and undertaken in accordance with the principles of the revised Declaration of Helsinki. All volunteers provided written informed consent. Trial registration number and date: Netherlands Trial Register 2473 and 13-08-2010.

Participants and study design

We enrolled twenty-four Dutch healthy lean men, between 18-28 years of age, with a BMI 18-25 kg/m^2. Twelve men were of Dutch South Asian descent and twelve of Dutch white Caucasian descent [25]. This study was conducted at the Alrijne Hospital, Leiderdorp (the Netherlands) between March 2013 and June 2013 [25]. In short, subjects underwent medical screening including their medical history, a physical examination, blood chemistry tests and an oral glucose tolerance test to exclude individuals with type 2 diabetes according to the American Diabetes Association 2010 criteria. Other exclusion criteria were rigorous exercise, smoking and recent body weight change up to 3 months prior to the start of the study.

Study procedures

Subjects were studied after overnight fasting and 24 hours without heavy exercise. We determined body composition using a Dual Energy X-ray Absorptiometry (DEXA) scan (iDXA, GE healthcare, UK). Next, an intravenous cannula was inserted in the antecubital vein for blood collection and injection of [^{18}F]FDG. To assess BAT volume and activity, subjects were exposed to an individualized water cooling protocol to maximally activate BAT. In short, subjects were cooled for approximately 2 hours until just above shivering temperature, to ensure maximum non-shivering thermogenesis, followed by an [^{18}F]FDG PET-CT scan (Gemini TF PET-CT, Philips Healthcare, Best, the Netherlands). For the individual cooling protocol, subjects lay between two water perfused cooling mattresses (Blanketrol III, Cincinnati Sub-Zero Products, Cincinnati, OH, USA). After 60 minutes at 32°C (thermoneutral temperature), the temperature of the mattresses were gradually decreased with 5°C every 10 minutes until shivering occurred. At this point, the temperature

was raised by 3°C and the official cooling period of 2 hours was started. After 1 hour of cooling, 2 MBq/kg [^{18}F]FDG was administrated intravenously. Both in thermoneutral and cold-induced condition, indirect calorimetry was performed with a ventilated hood (Oxycon Pro™ , CareFusion, Heidelberg, Germany). Venous blood samples were collected in a fasted state at the end of the thermoneutral period and at the end of the cooling period. After 2 hours of cooling, an [^{18}F]FDG PET-CT scan was acquired starting with a low-dose CT scan followed by PET scanning.

Brown adipose tissue measurements and energy expenditure

BAT volume (in mL) and BAT activity (in standardized uptake value (SUV)) in the region of interest were determined from the [^{18}F]FDG PET-CT scans (Gemini TF PET CT, Philips, Best, the Netherlands) by a blinded nuclear physician and a researcher. Resting energy expenditure (REE), respiratory quotient and rates of lipid and glucose oxidation were measured with indirect calorimetry using a ventilated hood system (Oxycon Pro, CareFusion, Heidelberg, Germany).

Serum lipid measurements

Serum TG and free fatty acid concentrations were determined in the blood samples with the use of commercially available enzymatic kits 11488872 and 91096 (Roche Molecular Biochemicals, Indianapolis, USA) as described previously [25].

Endocannabinoid measurements

Plasma sample of only 20 subjects could be studied since four subjects were excluded due to insufficient volume of plasma sample left available for the analysis in 2 individuals of each ethnicity. In total, endocannabinoids and their congeners were quantified in 40 plasma samples using liquid chromatography coupled with tandem mass spectrometry (LC-MS/MS). From the pool of individual study samples, quality controls (QCs) were used to generate calibration curves. Additionally, all samples were randomized and each batch included calibration samples and an even distribution of QC samples and blanks.

Sample extraction

Endocannabinoid extraction was performed on ice. Briefly, 50 μL of plasma was transferred into 1.5 mL Eppendorf tubes, spiked with 10 μL of deuterated internal standard mix (**Table S1**) followed by addition of 50 μL of 0.1 M ammonium acetate buffer (pH 4). After two times extraction with 400 μL of methyl tert-butyl ether (MTBE) (443808, Sigma Aldrich, Zwijndrecht, the Netherlands), the tubes were thoroughly mixed for 4 min using a bullet blender (Next Advance, Inc., Averill park, NY, USA) at medium speed, followed by a centrifugation step (4°C, 5,000 g, 12 min). Then 750 µL (combined from two extractions) of the upper MTBE layer was transferred into clean 1.5 mL Eppendorf tubes. Samples were dried in a speed vac followed by reconstitution with 50 µL of acetonitrile/water (90/10, v/v). The reconstituted samples were centrifuged (4°C, 14,000 g, 3 min) before transferring into LC-MS vials. 5 μL of each sample was injected into the LC-MS/MS system.

LC-MS/MS Analysis

A targeted analysis of 22 compounds, including endocannabinoids and related *N*-acylethanolamines (NAEs) along with their precursor molecule and metabolite arachidonic acid (AA) (**Table S1**), was measured using an Acquity UPLC I class Binary solvent manager pump (Waters, Milford, USA) in conjugation with AB SCIEX 6500 quadrupole-ion trap (QTRAP) (AB Sciex, Massachusetts, USA). The separation was performed with an Acquity HSS T3 column (1.2x100 mm, 1.8 μm) maintained at 45°C. The aqueous mobile phase A consisted of 2 mM ammonium formate and 10 mM formic acid, and the organic mobile phase B was acetonitrile. The flow rate was set to 0.4 mL/min; initial gradient conditions were 55% B held for 2 minutes and linearly ramped to 100% B over 6 minutes and held for 2 minutes; after 10 seconds the system returned to initial conditions and held 2 minutes before next injection. Electrospray ionization-MS and a selective Multiple Reaction Mode (MRM) was used for endocannabinoid quantification. Individually optimized MRM transitions using their synthetic standards for target compounds and internal standards are described in **Table. S1**. Relative standard deviations (RSD) of QC samples were calculated to monitor the data quality and RSD less than 15% was observed for 90% the target compounds. Peak area integration was performed with MultiQuant (AB Sciex, Version 3.0.2) data analysis software. The obtained peak areas of targets were corrected by appropriate internal standards. Calculated response ratios, determined as the peak area ratios of the target analyte to the

respective internal standard, were used to obtain absolute concentrations from their respective calibration curves. The response ratios were further corrected using in-house QC tool [26].

Statistical analysis

As previously mentioned, four participants (2 white Caucasians and 2 South Asians) were excluded from the analyses due to insufficient sample for the endocannabinoid measurements. Data were collected and analysed using IBM SPSS statistics version 23.0. Baseline characteristics were compared using unpaired student t-tests. Differences in plasma endocannabinoid levels in (between) groups were analysed using two tailed paired (unpaired) t-tests. Furthermore, linear regression analysis computed by Pearson's correlation was used to determine correlations between plasma endocannabinoid levels and different metabolic parameters. Regression analysis was performed both with and without correction for the effect of ethnicity, by respectively including/excluding ethnicity as a covariate. P values < 0.05 were considered as statistical significant. Data are presented as mean ± SEM.

Results

Clinical characteristics

The characteristics of the participants are partly previously described in ref 25. Twenty-four healthy lean men were included, however, sufficient plasma to analyse the endocannabinoids of only twenty participants (10 white Caucasians and 10 South Asians) was available. In this cohort of 20 participants, mean age was comparable between South Asians and white Caucasians (23.7 vs 25.2 years, respectively) as was BMI (21.4 vs 22.3 kg/m^2), body fat percentage (23.4 vs 19.4%) and serum TG concentration (0.91 vs 0.82 mmol/L). South Asians had lower REE during thermoneutral conditions (1304 vs 1671 kcal/day, p<0.01) and cold conditions (1480 vs 2063 kcal/day, p<0.01), also after correction for lean body mass. Cold exposure increased REE significantly only in white Caucasians (+23.4%, p<0.01). Furthermore, BAT volume was lower in South Asians as compared to white Caucasians (185 mL vs 303 mL), which was borderline significant (p=0.052) while the difference was significant in the original study [25] due to larger sample size.

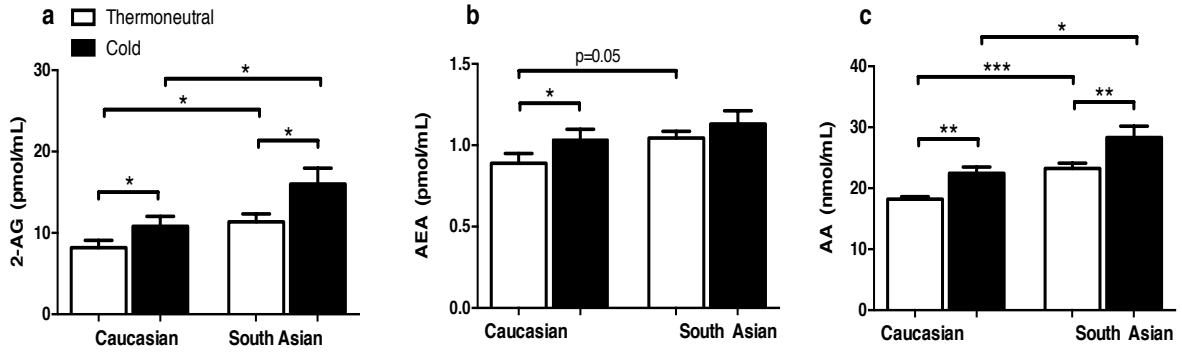

Figure 1: Circulating endocannabinoid levels are higher in South Asians and increased after short-term cooling. Blood was collected from healthy young South Asian (n=10) and matched white Caucasian (n=10) individuals before (thermoneutral) and after short-term mild cooling (Cold). Liquid chromatography coupled with tandem mass spectrometry (LC-MS/MS) was used to measure plasma concentrations of 2-AG **(a)**, AEA **(b)**, and AA **(c)** concentrations. Values are mean ± SEM. *P<0.05, **P<0.01, ***P<0.001. P-values are based on paired t-tests (effect of cold) or unpaired t-tests (effect of ethnicity).

Circulating endocannabinoid levels are higher in South Asians and are increased after cooling

At thermoneutrality, South Asians had higher mean levels of plasma 2-AG compared to white Caucasians (11.36 vs 8.19 pmol/mL, p<0.05) (**Fig. 1a**). In addition, there was a trend towards higher mean levels of AEA in South Asians (1.04 vs 0.89 pmol/mL, p=0.05) (**Fig 1b**). Levels of AA were also higher in South Asians (23.24 vs 18.22 nmol/mL, p<0.001) (**Fig. 1c**). No significant differences were observed for other NAEs and mono- and di-acyl glycerols measured, except LEA (*N*-linoleoylethanolamide), of which mean plasma levels were higher in South Asians compared to white Caucasians (5.88 vs 3.99 pmol/mL, p<0.005) (**Table S1**). Collectively, these results suggest that circulating endocannabinoid levels (2-AG and AEA) are higher in lean healthy male South Asians as compared to white Caucasians. We next assessed the endocannabinoid levels in plasma samples collected after short-term mild cold exposure. Interestingly, after cooling circulating levels of 2-AG were higher in South Asians (+41%, p<0.05) as well as white Caucasians (+32%, p<0.05) (**Fig. 1a**). Furthermore, AEA levels were significantly elevated after mild cold exposure in white Caucasians only (+16%, p<0.05) (**Fig. 1b**). Plasma AA significantly increased after cold exposure in both ethnic groups (South Asians (+22%, p<0.01) and white Caucasians (+23%, p<0.01) (**Fig. 1c**). The relative increases in endocannabinoid levels upon cooling were not significantly different between the two ethnicities.

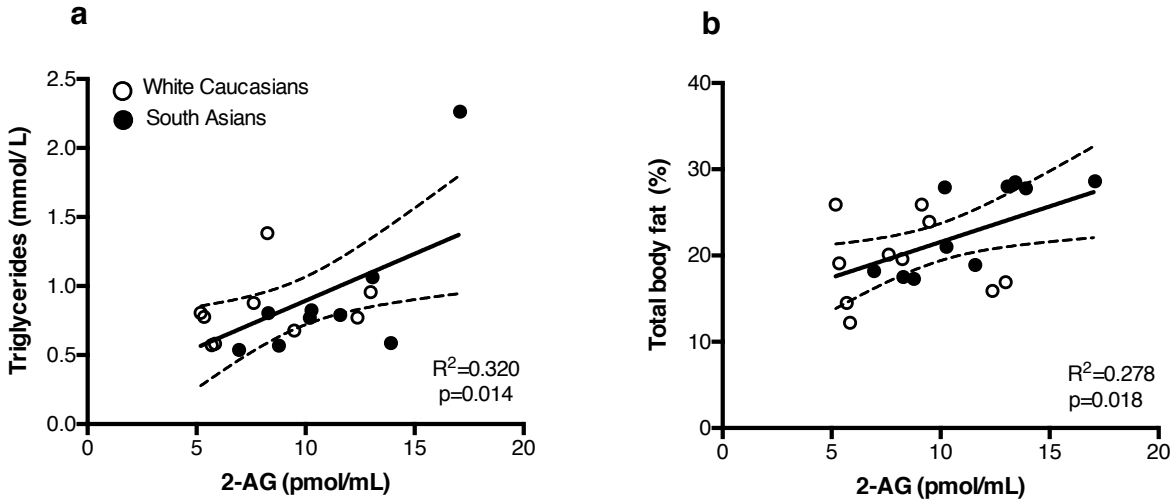

Figure 2: Thermoneutral plasma 2-AG levels positively correlate with serum triglyceride levels and total body fat percentage. Scatterplot of the correlations between 2-AG levels and serum TG **(a)** or total body fat percentage **(b)**. Correlations are shown for the total group combined (n=20), white circles are white Caucasian individuals (n=10) and black circles are South Asian individuals (n=10), with 95% confidence limits. Correlations were analysed using linear regression analysis.

Circulating endocannabinoid levels correlate with serum triglycerides and body fat

As the ECS is known to play an important role in energy metabolism, we investigated whether circulating endocannabinoid levels correlated with different metabolic parameters in our study cohort. For these analyses, we used combined data of South Asians and white Caucasians. Thermoneutral 2-AG levels positively correlated with TG levels (R^2=0.32, p<0.05) (**Fig. 2a**) and total body fat percentage (R^2=0.27, p<0.05) (**Fig. 2b**), but not with visceral fat percentage (data not shown). In contrast, AEA levels did not correlate with any of these metabolic parameters (data not shown).

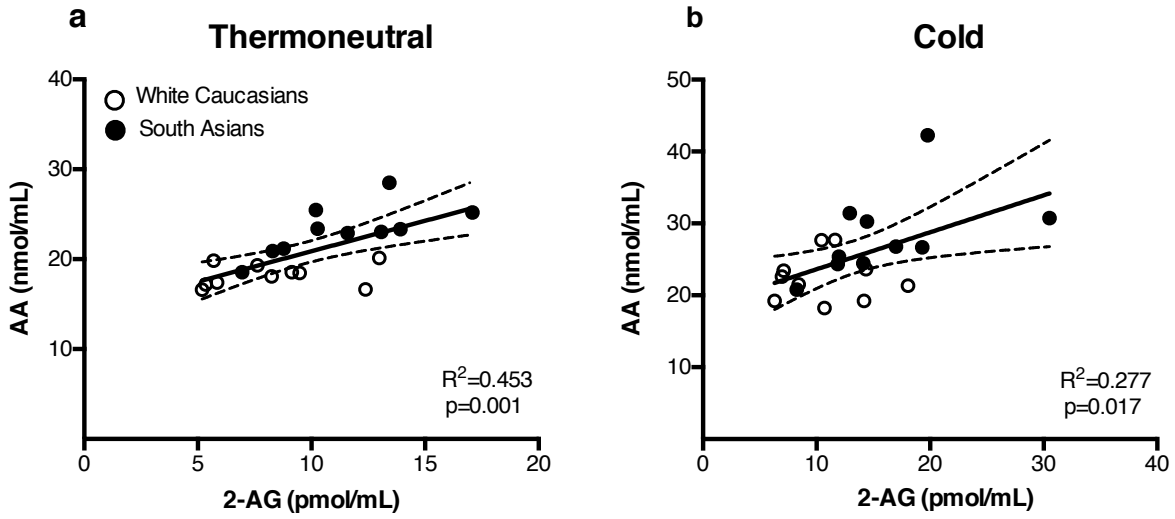

Figure 3: Plasma 2-AG levels correlate with plasma AA levels. Scatterplot of the correlations between plasma 2-AG and AA in both Caucasian and South Asian individuals (n=40). Correlation is shown for the total group combined under thermoneutral **(a)** and cold conditions **(b),** black circles are South Asian individuals and white circles are white Caucasian individuals, with 95% confidence limits. Correlations were analysed using linear regression analysis.

Additionally, 2-AG positively correlated with AA under thermoneutral (R^2=0.45, p=0.001) and cold conditions (R^2=0.28 p<0.05) (**Fig. 3**). AA also positively correlated with body fat percentage (R^2=0.34, p<0.01) (**Fig. 4a**). Interestingly, a strong negative correlation was observed with AA and REE (R^2=0.46, p<0.001) (**Fig. 4b**), with AA levels being higher in South Asians compared to white Caucasians (23.24 vs 18.22 nmol/mL, p<0.001). AA did not correlate with either fat or glucose oxidation (data not shown). We found no significant correlations between circulating endocannabinoids and other metabolic parameters, including

(systolic and diastolic) blood pressure, heart rate, fasting serum glucose or C-reactive protein (CRP) levels (data not shown). After cold exposure, there was no correlation between circulating endocannabinoids and REE (data not shown). Both thermoneutral and cold-induced REE positively correlated with BAT volume, but not activity (data not shown) [25]. To further understand the inter-relationship between endocannabinoids and BAT metabolism, we performed several regression analyses. Notably, no correlation was found between circulating endocannabinoid levels and BAT volume (2-AG: R^2=0.016, p=0.611; AEA: R^2=0.024, p=0.531; and AA: R^2=0.066, p=0.288) or activity (2-AG: R^2=0.008, p=0.714; AEA: R^2=0.132, p=0.126; and AA: R^2=0.031, p=0.473), nor was there a correlation between cold-induced or delta (cold minus thermoneutral) endocannabinoid levels upon cooling and BAT activity or volume (data not shown). To test whether the effects could be attributed to ethnicity, we also performed the regression analysis including ethnicity as covariate. Correcting for the effect of ethnicity, plasma 2-AG levels still correlated with serum TG levels ($p<0.05$) and tended to correlate with body fat percentage (p=0.08). In addition, thermoneutral 2-AG levels still correlated with thermoneutral AA levels ($p<0.05$), but not under cold conditions (p=0.12). Also, after correction for ethnicity the negative correlation between AA and REE was not significant anymore (p=0.41).

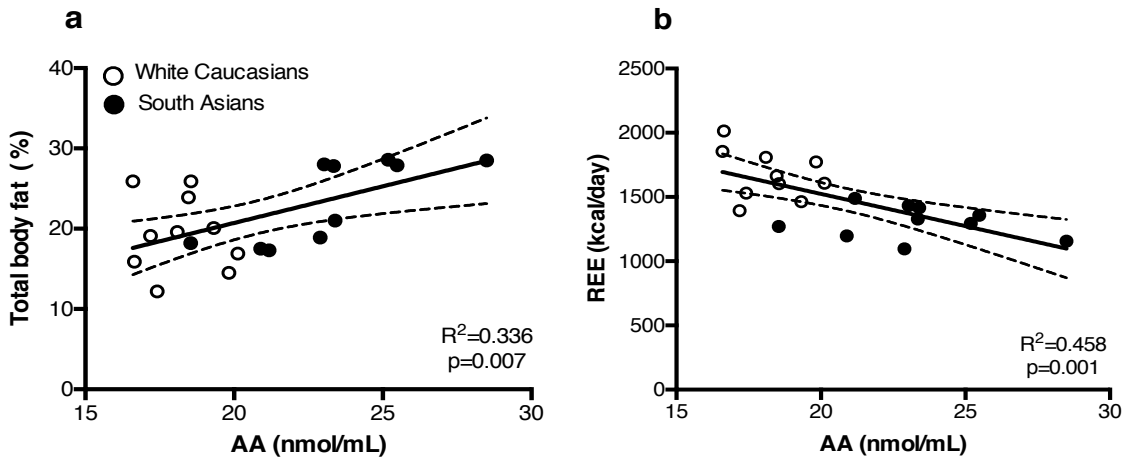

Figure. 4: Thermoneutral plasma AA levels positively correlate with body fat percentage and negatively correlate with resting energy expenditure. Scatterplot of the correlations between plasma AA levels measured at thermoneutrality and total body fat percentage **(a)** or thermoneutral resting energy expenditure (REE) **(b)** (n=20). Correlations are shown for the total group combined, black circles are South Asian individuals and white circles are white Caucasian individuals, with 95% confidence limits. Correlations were analysed using linear regression analysis.

Discussion

The contribution of the ECS in energy metabolism has been well established in humans and research has focused on manipulating this system for the treatment of metabolic disease, such as obesity and T2D. The South Asian population is very prone to develop metabolic disease; however, the underlying mechanism remains to be elusive. In the present study, we showed that healthy lean South Asian men without an apparent disadvantageous metabolic phenotype have higher circulating levels of endocannabinoids (2-AG and AEA) and their metabolite AA compared to matched white Caucasian men. In addition, plasma 2-AG levels positively correlate with serum TG and body fat percentage, and AA levels negatively correlate with REE and positively with body fat percentage.

To the best of our knowledge, this is the first study that shows higher plasma 2-AG, AEA and AA levels in healthy South Asians compared to white Caucasians. Jumpertz et al. [27] previously showed higher 2-AG levels in cerebrospinal fluid (CSF) of American Indians compared to white Caucasians. However, they did not observe differences in 2-AG or AEA levels in plasma of these individuals. This might be due to differences in the study population or a difference in the sensitivity of the assay. For example, Jumpertz et al. included young (±29 year), overweight individuals, while in the current study young (±24 year), healthy individuals were included. Furthermore, in South Asians we found higher levels of AA, the breakdown product of endocannabinoids. Although AA can also be synthesized independent of endocannabinoids, these data support the notion that the endocannabinoid tone is higher in healthy young male individuals of South Asian compared to white Caucasian origin.

High circulating endocannabinoid levels in South Asians can result in overstimulation of cannabinoid receptors on tissues such as liver, WAT, skeletal muscle and pancreas. This in turn can lead to several disadvantageous metabolic effects. In mice, a high endocannabinoid tone in the liver, for example, contributes to the development of fatty liver disease [28–30]. In addition, in WAT CB_1 receptor activation promotes adipogenesis, lipogenesis and energy storage instead of combustion[3]. Moreover, CB receptor stimulation in WAT and skeletal muscle has shown to disrupt insulin signaling thereby promoting insulin resistance, which in combination with reduced insulin secretion from the pancreas (also induced by CB receptor stimulation on pancreatic islet cells) might promote development of T2D [3,31]. Taken together this indicates that overall high endocannabinoid tone can deteriorate/ induce metabolic disease. As South Asians have already been shown to have more hepatic steatosis [32], adipocyte hypertrophy[32] disturbed muscle insulin signaling [2] and lower REE [25] (i.e. high

endocannabinoid tone reduces REE [18] and high plasma AA levels negatively correlate with REE (**Fig. 4b**) compared to white Caucasians, they are possibly at even greater risk for the negative metabolic effects of high endocannabinoid tone.

In addition, we observed positive correlations between plasma 2-AG and serum TG and body fat percentage, albeit the correlation with TG was enforced by a biological outlier. These results are in line with results from Bluher et al.[8] who showed positive correlations between circulating 2-AG levels and both body fat percentage and serum TG in lean and obese individuals. However, they also showed positive correlations between 2-AG and BMI and free fatty acids which could not be reproduced in our study population [8]. Jumper et al. [27] showed positive correlations between AEA, but not 2-AG, and BMI and body fat percentage. However, they studied overweight individuals whereas we studied healthy lean individuals. Consistent with our data, they also found no correlation between plasma 2-AG or AEA levels and REE [27].

Furthermore, we found that plasma 2-AG and AA levels in both ethnicities are increased after short-term mild cooling, the physiological stimulator of BAT[33]. This observation is consistent with a study in mice showing that BAT activation increases expression and protein levels of endocannabinoids in BAT [19]. The authors hypothesized that increase in endocannabinoids in BAT represents a negative feedback mechanism, as they could locally act on the presynaptic nerve terminal to inhibit noradrenalin release, thereby preventing excessive activation of BAT [19]. Possibly, also in humans the increase in 2-AG and AEA could be derived from BAT, however in our observational study the contribution of other tissues to the plasma endocannabinoid levels could not be excluded. Another explanation for the increased endocannabinoid levels upon cooling could be a higher availability of biosynthetic precursors such as diacylglycerols (DAGs) or *N*-acyl-phosphatidyl-ethanolamines (NAPEs), which are generated during lipolysis of WAT and/or BAT during cooling [19]. In addition, it has been shown that cold exposure reduces the mRNA expression of the breakdown enzyme *FAAH* in BAT, which might also in part explain higher plasma endocannabinoid levels upon cooling [19]. Alternative explanations can also not be excluded at present. For example, 2-AG has a circadian rhythm in humans with the lowest plasma concentration peak around 5:00 am and the highest peak concentration around 13:00 pm [34]. Since the blood samples in the current study were withdrawn around 9:30 (thermoneutrality) and 12:30 (cold), a small increase, of approx. 15%, in plasma 2-AG could already be expected from its circadian rhythm. However, we found a larger 37% average

increase in 2-AG when combining the South Asians and white Caucasians. In addition, cooling elicits a stress response in the body, and stress, via glucocorticoids, has been shown to increase the peripheral ECS tone [35,36].

Previous mouse studies showed that global blockade of the CB_1 receptor by rimonabant activates BAT, markedly enhances energy expenditure and leads to a tissue-specific upregulation of endocannabinoids [18,19]. In fact, human studies showed that taranabant, another inverse agonist of the CB_1 receptor also reduced food intake, induced weight loss and increased REE and fat oxidation in obese individuals [37]. Therefore, we hypothesized that these effects may have been due to BAT activation. However, in our study there was no significant correlation between plasma endocannabinoids and BAT volume/activity, fatty acid or glucose oxidation. Possibly our sample size was too small to reliably assess this, as the variation in BAT between subjects was rather large.

A strength of this study is that we investigate differences in circulating endocannabinoid levels in lean healthy South Asians and white Caucasians individuals before they develop metabolic diseases. This allowed us to investigate in more detail whether ethnic differences in endocannabinoid tone are already present before the onset of the disease rather than being a consequence of the metabolic disease. However, a limitation of our study is that we could only measure circulating endocannabinoid levels which do not necessarily reflect endocannabinoid signalling within peripheral organs and thus the endocannabinoid function. For future studies, it would be interesting to measure endocannabinoid levels and levels of endocannabinoid synthesis and breakdown enzymes in specific tissues, such as WAT and skeletal muscle. In addition, we cannot exclude that 'thermoneutrality' might have been experienced differently between the two ethnicities, which might have biased our results. Furthermore, the small sample size might have limited the number of correlations we could detect. However, despite this we were able to reproduce some correlations shown previously by others underscoring the robustness of these findings. Future studies in larger cohorts should verify the translational value of these results for the general population.

In conclusion, our data demonstrate that healthy lean South Asian men have a higher endocannabinoid tone compared to white Caucasian men. Provided that our cohort is representative for the general population, this might, at least in part, contribute to the development of a disadvantageous metabolic phenotype later in life. These results are in line with the hypothesis that the ECS functions as a negative feedback system on BAT. Future research should focus on elucidating the underlying cause of the high endocannabinoid tone

in this vulnerable population and verify potential causal relationships. This knowledge might lead to the development of novel treatment strategies to combat metabolic disease.

Acknowledgement

The Blanketrol III cooling device was kindly provided by FMH Medical (Veenendaal, Netherlands).

This study is supported by 'the Netherlands CardioVascular Research Initiative: the Dutch Heart Foundation, Dutch Federation of University Medical Centers, the Netherlands Organisation for Health Research and Development and the Royal Netherlands Academy of Sciences' for the GENIUS project 'Generating the best evidence-based pharmaceutical targets for atherosclerosis' (CVON2011-9). M.R. Boon is supported by an NWO-Rubicon grant (grant 825.13.021) and by a Dutch Diabetes Research Foundation Fellowship (grant 2015.81.1808). P.C.N. Rensen is an Established Investigator of the Netherlands Heart Foundation (grant 2009T038). This project received support from the Faculty of Science ("Profiling programme: Endocannabinoids"), Leiden University (VK, MvdS, TH).

References

1. Chiu, M., Austin, P. C., Manuel, D. G., Shah, B. R. & Tu, J. V. Deriving ethnic-specific BMI cutoff points for assessing diabetes risk. *Diabetes Care* **34,** 1741–1748 (2011).
2. Hall, L. M. L. *et al*. Fat oxidation, fitness and skeletal muscle expression of oxidative/lipid metabolism genes in South Asians: Implications for insulin resistance? *PLoS One* **5,** e14197 (2010).
3. Silvestri, C., Ligresti, A. & Di Marzo, V. Peripheral effects of the endocannabinoid system in energy homeostasis: Adipose tissue, liver and skeletal muscle. *Rev. Endocr. Metab. Disord.* **12,** 153–162 (2011).
4. Rodríguez De Fonseca, F. *et al*. An anorexic lipid mediator regulated by feeding. *Nature* **414,** 209–212 (2001).
5. Fu, J. *et al*. Oleylethanolamide regulates feeding and body weight through activation of the nuclear receptor PPAR-α. *Nature* **425,** 90–93 (2003).
6. Matias, I. *et al*. Role and regulation of acylethanolamides in energy balance: Focus on adipocytes and ??-cells. *Br. J. Pharmacol.* **152,** 676–690 (2007).
7. Engeli, S. Dysregulation of the endocannabinoid system in obesity. *J. Neuroendocrinol.* **20,** 110–115 (2008).
8. Blüher, M. *et al*. Dysregulation of the peripheral and adipose tissue endocannabinoid system in human abdominal obesity. *Diabetes* **55,** 3053–3060 (2006).
9. Engeli, S. *et al*. Activation of the peripheral endocannabinoid system in human obesity. *Diabetes* **54,** 2838–2843 (2005).
10. Côté, M. *et al*. Circulating endocannabinoid levels, abdominal adiposity and related cardiometabolic risk factors in obese men. *Int. J. Obes.* **31,** 692–699 (2007).
11. Deng, H. *et al*. Triazole Ureas Act as Diacylglycerol Lipase Inhibitors and Prevent Fasting-Induced Refeeding. *J. Med. Chem.* **60,** 428–440 (2017).
12. Janssen, F. J. & van der Stelt, M. Inhibitors of diacylglycerol lipases in neurodegenerative and metabolic disorders. *Bioorganic Med. Chem. Lett.* **26,** 3831–3837 (2016).
13. Gary-Bobo, M. *et al*. Rimonabant reduces obesity-associated hepatic steatosis and features of metabolic syndrome in obese zucker fa/fa rats. *Hepatology* **46,** 122–129 (2007).
14. Ravinet Trillou, C. *et al*. Anti-obesity effect of SR141716, a CB1 receptor antagonist, in diet-induced obese mice. *Am. J. Physiol. - Regul. Integr. Comp. Physiol.* **284,** R345–R353 (2003).
15. Després, J.-P., Golay, A. & Sjöström, L. Effects of Rimonabant on Metabolic Risk Factors in Overweight Patients with Dyslipidemia. *N. Engl. J. Med.* **353,** 2121–2134 (2005).
16. Van Gaal, L. F., Rissanen, A. M., Scheen, A. J., Ziegler, O. & Rössner, S. Effects of the cannabinoid-1 receptor blocker rimonabant on weight reduction and cardiovascular risk factors in overweight patients: 1-Year experience from the RIO-Europe study. *Lancet* **365,** 1389–1397 (2005).
17. Després, J. P., Ross, R., Boka, G., Alméras, N. & Lemieux, I. Effect of rimonabant on the high-triglyceride/low-HDL-cholesterol dyslipidemia, intraabdominal adiposity, and liver fat the ADAGIO-lipids trial. *Arterioscler. Thromb. Vasc. Biol.* **29,** 416–423 (2009).
18. Boon, M. R. *et al*. Peripheral cannabinoid 1 receptor blockade activates brown adipose tissue and diminishes dyslipidemia and obesity. *FASEB J.* **28,** 5361–5375 (2014).
19. Krott, L. M. *et al*. Endocannabinoid regulation in white and brown adipose tissue

following thermogenic activation. *J. Lipid Res.* **57,** 464–473 (2016).
20. Cypess, A. M. *et al.* Identification and Importance of Brown Adipose Tissue in Adult Humans. *N. Engl. J. Med.* **360,** 1509–1517 (2009).
21. Virtanen, K. A. *et al.* Functional Brown Adipose Tissue in Healthy Adults. *N. Engl. J. Med.* **360,** 1518–1525 (2009).
22. van Marken Lichtenbelt, W. D. *et al.* Cold-Activated Brown Adipose Tissue in Healthy Men. *N. Engl. J. Med.* **360,** 1500–1508 (2009).
23. Boon, M. R. *et al.* [Brown adipose tissue: the body's own weapon against obesity?]. *Ned. Tijdschr. Geneeskd.* **157,** A5502 (2013).
24. Hanssen, M. J. W. *et al.* Short-term cold acclimation recruits brown adipose tissue in obese humans. *Diabetes* **65,** 1179–1189 (2016).
25. Bakker, L. E. H. *et al.* Brown adipose tissue volume in healthy lean south Asian adults compared with white Caucasians: A prospective, case-controlled observational study. *Lancet Diabetes Endocrinol.* **2,** 210–217 (2014).
26. Dane, A. D. *et al.* Integrating metabolomics profiling measurements across multiple biobanks. *Anal. Chem.* **86,** 4110–4114 (2014).
27. Jumpertz, R., Guijarro, A., Pratley, R. E., Piomelli, D. & Krakoff, J. Central and peripheral endocannabinoids and cognate acylethanolamides in humans: Association with race, adiposity, and energy expenditure. *J. Clin. Endocrinol. Metab.* **96,** 787–791 (2011).
28. Osei-Hyiaman, D. *et al.* Hepatic CB1 receptor is required for development of diet-induced steatosis, dyslipidemia, and insulin and leptin resistance in mice. *J. Clin. Invest.* **118,** 3160–3169 (2008).
29. Osei-Hyiaman, D. *et al.* Endocannabinoid activation at hepatic CB1 receptors stimulates fatty acid synthesis and contributes to diet-induced obesity. *J. Clin. Invest.* **115,** 1298–1305 (2005).
30. Jeong, W. il *et al.* Paracrine Activation of Hepatic CB1Receptors by Stellate Cell-Derived Endocannabinoids Mediates Alcoholic Fatty Liver. *Cell Metab.* **7,** 227–235 (2008).
31. Jourdan, T. *et al.* Activation of the Nlrp3 inflammasome in infiltrating macrophages by endocannabinoids mediates beta cell loss in type 2 diabetes. *Nat. Med.* **19,** 1132–1140 (2013).
32. Anand, S. S. *et al.* Adipocyte hypertrophy, fatty liver and metabolic risk factors in south asians: The molecular study of health and risk in ethnic groups (mol-SHARE). *PLoS One* **6,** e22112 (2011).
33. Van Der Lans, A. A. J. J. *et al.* Cold acclimation recruits human brown fat and increases nonshivering thermogenesis. *J. Clin. Invest.* **123,** 3395–3403 (2013).
34. Hanlon, E. C. *et al.* Circadian rhythm of circulating levels of the endocannabinoid 2-arachidonoylglycerol. *J. Clin. Endocrinol. Metab.* **100,** 220–226 (2015).
35. Dlugos, A., Childs, E., Stuhr, K. L., Hillard, C. J. & De Wit, H. Acute stress increases circulating anandamide and other n-acylethanolamines in healthy humans. *Neuropsychopharmacology* **37,** 2416–2427 (2012).
36. Bowles, N. P. *et al.* A peripheral endocannabinoid mechanism contributes to glucocorticoid-mediated metabolic syndrome. *Proc. Natl. Acad. Sci. U. S. A.* **112,** 285–90 (2015).
37. Addy, C. *et al.* The Acyclic CB1R Inverse Agonist Taranabant Mediates Weight Loss by Increasing Energy Expenditure and Decreasing Caloric Intake. *Cell Metab.* **7,** 68–78 (2008).

Supplementary information

Table S1: MRM (Multiple reaction monitoring) parameters and endogenous concentrations of the target list

S. No	ID	Metabolite Name	Q1	Q3	DP, CE	Concentration (pmol/mL)		
						Caucasians	South Asians	P-Value
1	1-1OG (18:1)	1-Oleoyl Glycerol	357	265	80, 20	1055±100	954±135	0.554
2	2-OG (18:1)	2-Oleoyl Glycerol	357	265	80, 20	97.6±7.2	83.0±9.9	0.247
3	1-LG (18:2)	1-Linoleoyl Glycerol	355	263	80, 15	338.0±39.4	436.4±54.3	0.160
4	2-LG (18:2)	2-Linoleoyl Glycerol	355	263	80, 20	59.6±8.1	74.5±9.3	0.244
5	2&1-AG (20:4)	2&1-Arachidonoylglycerol	379	287	56, 19	8.19±0.89	11.36±0.97	0.028*
6	2AGE (20:4)	2-Arachidonyl Glycerol ether	365	273	72, 25	ND	ND	-
7	PDEA (15:0)	*N*-Pentadecanoyl ethanolamide	286	62	80, 18	0.23±0.13	0.10±0.01	0.312
8	PEA (16:0)	*N*-Palmitoyl ethanolamide	300	62	78, 36	9.28±0.71	10.60±0.26	0.099
9	SEA (18:0)	*N*-Stearoyl ethanolamide	328	62	72, 31	7.24±0.33	7.41±0.19	0.677
10	POEA (16:1)	*N*-Palmitoleoyl ethanolamide	298	62	86, 32	1.03±0.15	1.02±0.12	0.990
11	OEA (18:1)	*N*-Oleoylethanolamide	326	62	72, 30	6.57±0.43	7.39±0.38	0.175
12	LEA (18:2)	*N*-Linoleoyl ethanolamide	324	62	74, 36	3.99±0.39	5.88±0.39	0.003*
13	Alpha-LEA (18:2)	*N*-α-Linolenyl ethanolamide	322	62	80, 20	0.01±0.01	0.01±0.01	0.408
14	DGLEA (18:3)	Dihomo-γ-Linolenoyl Ethanolamide	350	62	70, 20	0.21±0.02	0.20±0.02	0.796
15	ETAEA (20:3)	Eicosatrienoic Acid Ethanolamide	350	62	80, 46	ND	ND	-

16	AEA (20:4)	Anandamide	348	62	70, 42	0.89±0.06	1.04±0.04	0.050
17	O-AEA (20:4)	O-Arachidonoyl ethanolamine	348	62	70, 25	ND	ND	-
18	EPEA (20:5)	Eicosapentaenoyl Ethanolamide	346	62	80, 20	0.05±0.01	0.07±0.01	0.191
19	DEA (22:4)	*N*-Docosatetraenoyl ethanolamide	376	62	72, 20	0.27±0.02	0.28±0.03	0.916
20	DHEA (22:6)	*N*-Docosahexa enoylethanolamide	372	62	70, 25	5.14±0.44	5.61±0.55	0.522
21	NADA (28:4)	*N*-Arachidonoyl dopamine	440	137	75, 24	ND	ND	-
22	Arachado nic Acid (20:4)	5,8,11,14-Eicosatetraenoic acid	303	259	-80, -18	18223±401	23244±872	0.001** *
1	2-AG (20:4)-d8	2-Arachidonoyl glycerol-d8	387	294	56, 20	-	-	-
2	PEA (16:0)-d4	Palmitoyl ethanolamide-d4	304	62	78, 36	-	-	-
3	SEA (18:0)-d3	Stearoyl ethanolamide-d3	331	62	72, 31	-	-	-
4	OEA (18:1)-d4	Oleoyl Ethanolamide-d4	330	66	72, 30	-	-	-
5	LEA (18:2)-d4	Linoleoyl ethanolamide-d4	328	66	74, 36	-	-	-
6	AEA (20:4)-d8	Arachidonoyl Ethanolamide-d8	356	62	70, 42	-	-	-
7	DHEA (22:6)-d4	Docosahexaenoyl Ethanolamide-d4	376	66	70, 25	-	-	-
8	NADA (28:4)-d8	*N*-Arachidonoyl dopamine-d8	448	137	75, 34	-	-	-

The target list includes endocannabinoids and *N*-acylethanolamines (NAEs) and deuterated (d) labelled internal standards. The compound ID is the abbreviation of metabolite name along with number of carbon atoms and number of double bonds in the fatty acid chain of the molecule, respectively. All compounds are analysed in positive mode except arachidonic acid in negative mode. Q1 and Q3 are optimized precursor ion and product ion, expressed as *m/z*. DP and CE are declustering potential (volts) and collision energy (volts). All compounds are acquired in positive MRM mode except Arachidonic acid acquired in negative mode. Endogenous concentrations are denoted as mean ± SEM (standard error of mean). *P<0.05, ***P<0.001. P-values are based on unpaired t-tests. ND: Not detected in human plasma.

Chapter 9

Conclusions and Future Perspectives

Conclusions and future perspectives

Recent drug discovery and development processes have evolved from a specific targeted approach to a broader systems approach. This approach integrating different biochemical components (genes, proteins, metabolites) can generate system response profiles to study the system-state differences such as differences between healthy versus diseased or drug responders versus non-responders. In this thesis, we developed and applied a system pharmacology approach to understand and modulate the endocannabinoid system across different species and model systems (cells, zebrafish, mice and humans). We have chosen the endocannabinoid system as a pharmacological target due its ubiquitous nature throughout the body and its regulatory role in a huge number of physiological and pathological conditions. We studied the functional role of the endocannabinoid system in healthy and diseased states. In addition, we modulated the endocannabinoid system using new enzyme inhibitors to gain better understanding in different signaling pathway associated with endocannabinoids synthesis and degradation. Furthermore, we aimed to understand the drug pharmacology and whether such new compound inhibitors may modify the disease biochemistry; this includes the study of target engagement, downstream effects and the off-target effects of new compounds.

Chapter 2 introduces a system pharmacology approach integrating concepts of metabolomics with pharmacology (Pharmacokinetics-Pharmacodynamics, PK-PD) and discusses its potential to realize personalized medicine. Identification and quantification of predictors that account for inter-individual variability in drug response upon drug administrations is necessary to achieve personalized medicine. An interplay between many factors related both to drug pharmacology and a patients' (patho)physiology is responsible for the drug treatment outcome for a patient. Here we highlighted the potential of pharmacometabolomics, a discipline of metabolomics, in prospectively informing on the inter-individual differences in drug pharmacology, including PK-PD processes, and thereby guiding drug selection and drug dosing. In some cases, metabolite markers can be used to understand the disease biochemistry and drug biochemistry. In this regard, high sensitive analytical platforms are a pre-requisite to identify endogenous metabolite markers that can predict PK-PD.

All the personalized medicine strategies in the clinic require the use of decision-making processes based on biomarker-driven approaches. Although (pharmaco)metabolomic studies have identified a number of potential metabolite biomarkers that can describe and predict inter-individual variability in the PK and PD of drugs [1], the application of the obtained knowledge

in clinical practice remains relatively limited. These discovered metabolite biomarkers urgently need to be validated to prove their specificity, sensitivity, reproducibility and clinical relevance. In addition, studies to investigate the molecular interactions with the drug (target engagement) and their influence upon drug dose should be performed. Ideally, the usefulness of potential new biomarkers should be replicated in a randomized clinical trial. However, conducting these trials are rather expensive, time consuming and difficult to perform in academic settings. Alternatively, the discovered biomarkers can be first validated making use of previously completed clinical studies or in large epidemiological cohorts (for example the Rotterdam study) preferably including diverse cohorts which include samples which accounts for confounding factors such as diet, environment, race, and socio-economic factors. After validation, it will be more attractive to implement targeted metabolite assays in the clinical lab for clinical decision support on drug therapy. To implement these biomarkers in routine clinical lab services, cost-effective and time-effective analytical platforms should be developed, possibly using aptamers, miniaturized NMR or MS, or in chip-formats (like the lab-on-a-chip sensor to measure glucose [2]).

Chapter 3 describes the development and validation of a nano liquid-chromatography-mass spectrometry (nano LC-MS/MS) analytical method for the in-depth quantification of endocannabinoids and their congeners in human cerebrospinal fluid) (CSF). This miniaturized method was developed to quantify endocannabinoids in human CSF which are present at pico molar to femto molar range under normal physiological conditions. This method was applied to 45 healthy human CSF samples and demonstrated the potential age and gender effect on concentrations of endocannabinoids and NAEs.

In parallel, highly sensitive LC-MS/MS analytical methods using 2.1 mm ID analytical columns were developed and validated to quantify endocannabinoids and NAEs in various biological matrices, like cells, zebrafish larvae, mice plasma and human plasma. In addition, LC-MS based lipidomics platforms were further optimized to detect and semi-quantify different lipid species (polar and apolar lipids) in cells and zebrafish larvae. Overall, these analytical methods provided detailed snapshots of the endocannabinoid biochemistry and their interaction with associated lipid pathways. These developed methods were applied to answer various biological questions discussed in later chapters.

The LC-MS/MS based analytical platforms developed in this thesis target only endocannabinoids and their congeners, including arachidonic acid. However, the

endocannabinoids 2-Arachidonoylglycerol (2-AG) and N-arachidonoylethanolamide (Anandamide; AEA) are oxidized by several other enzymes such as cyclo-oxygenase-2 (COX-2), cytochrome P450 and lipoxygenase (LOX) enzymes. These enzymes convert endocannabinoids into a new range of oxygenated intermediates such as prostaglandin ethanolamides (called prostamides) and prostaglandin glycerol esters or the lipids can be lipooxegenated to many hydroxylated end-products [3,4]. Therefore, the current analytical methods need to be expanded to include the above mentioned related lipids of the endocannabinoid system to better understand the downstream endocannabinoid signaling and their cross-talk with related pathways (whole arachidonic acid pathway). In addition, current methods need to be miniaturized to handle small sample volumes (e.g. for use with 1000 cells in case of organ-on-a-chip model systems) and high-throughput to analyze hundreds of samples in a short time.

Furthermore, when employing targeted or semi-targeted metabolomic approaches reporting the identify of metabolites detected, for instance studying a particular pathway or to gain a quantitative understanding of cellular metabolism, reporting absolute endocannabinoid concentration levels provides more information than reporting only relative concentrations. For example, when studying the endocannabinoid system, the absolute concentration of AEA (1-5 nM) and 2-AG (10-500 nM) reported in serum of healthy individuals have a relatively wide range of values. Some of the likely factors that can affect the endogenous levels of endocannabinoids are stress, time of sample collection, exercise, inflammation, health state etc. [5] Analytical variability, due to lack of proper method validation, can also lead to differences in reported concentrations. Therefore, metabolic databases should be developed where absolute concentrations of metabolites of bio fluids, cells and tissues are deposited, and where the conditions of the human or cell system is well described; these values would allow to compare the absolute values across different studies [6]. Consortiums should be initiated to standardize metabolomics measurements by performing inter-laboratory experiments to control variation due to analytical methods. Additionally, these absolute metabolite concentrations can also be used to study thermodynamics of metabolic reactions, and are useful as input for dynamic modeling of metabolism and for conducting *in vitro* assays under physiological relevant conditions [7]. Furthermore, harmonization of data generation, reporting and data visualization in clinically accessible formats will be crucial to accelerate clinical implementations.

Chapter 4 describes research to investigate which isoform of diacylglycerol lipases (DAGL) - alpha or –beta (DAGL-α- and -β) is leading in the synthesis of 2-AG, a well-studied endocannabinoid pathway mediated via cannabinoid receptors. Modulating 2-AG signaling is a promising target for the treatment of obesity and neurodegenerative diseases. Activity based protein profiling (ABPP) was used to assess DAGL activity, and lipidomics was used to quantify downstream effects in Neuro2A cells using DH376, an *in vivo* potent DAGL inhibitor. Next, specific Neuro2A knockout populations (DAGL-α, DAGL-β and DAGL-α/ β) were generated using CRISPR-Cas9 technology and the loss of activity was confirmed using ABPP. Lipidomics, however, revealed no significant reduction of 2-AG levels in any of these DAGL KOs, whereas DH376 substantially suppressed 2-AG levels in these cells. These data suggest the presence of additional enzymes responsible for 2-AG synthesis, which can be targeted by DH376. Further investigations to identify these new targets are currently ongoing.

In another study, we applied ABPP along with lipidomics and identified a potent, highly selective and reversible DAGLs inhibitor LEI105. This inhibitor was applied to Neuro2A cells and we observed a concentration-dependent reduction in DAGL-labelling and endogenous 2-AG levels, while FAAH activity and the AEA levels were unaffected demonstrating the inhibitor selectivity. Although inhibitor treatment to mouse hippocampal slice model (*in vitro* treatment) showed a reduction in short-term synaptic plasticity, this inhibitor was not active *in vivo* [8]. Overall, these studies show the power of combining ABPP and lipidomics tools in identifying enzyme targeted by small molecule inhibitors and especially in identifying small molecule inhibitors.

Chapter 5 focused on unraveling the reason behind the failure of a recent phase I clinical trial of Fatty acid amide hydrolase (FAAH) inhibitor BIA 10-2474. FAAH is a serine hydrolase enzyme responsible for the hydrolysis of anandamide, another well-studied endocannabinoid mediated via cannabinoid receptors. This drug was developed to treat pain and inflammation. During the clinical trial, this drug led to the death of one volunteer and the hospitalization of four others. ABPP analysis was used to determine the protein interaction landscape of BIA 10-2474 and revealed that the drug inhibited several other lipases which were not inhibited using a highly selective and clinically tested FAAH inhibitor, PF-04457845. Furthermore, LC-MS based lipidomics showed that BIA 10-2474, but not PF-04457845, produced substantial alterations in the lipid networks in iPSC derived human cortical neurons. This study demonstrates the power of ABPP and lipidomics techniques not only for identifying drug on-

target engagement effects and associated downstream effects, but also for identifying drug off-target effects and drug effects on downstream lipid networks. Hence, we believe these techniques can be employed in early drug discovery and development pipelines to screen for on-target engagement and off-target effects of candidate drug molecule. We envision that metabolomics/lipidomics can serve as a powerful phenotypic approach to study molecular interactions of drugs within whole biological networks in an untargeted/unbiased fashion, while ABPP can be employed more in a targeted fashion to quantify drug on-target engagements and off-target effects by designing and choosing the ABPP probes to target the family of enzymes assumed to be (potentially) effected by the drug.

The quantification of endocannabinoid levels in the above described *in vitro* studies were performed either to understand the pathophysiology of the endocannabinoid system or to investigate the intracellular effects of drugs on the endocannabinoid system, but missed the information of the extracellular compartment. So far, the trafficking of the endocannabinoids is poorly understood: it is not fully clear for instance how these endocannabinoids traverse within the cell and how the cellar uptake from extracellular medium is regulated. Some of the possibilities reported include passive diffusion, endocytosis, membrane transporter proteins or a combination of these mechanisms [9,10]. Therefore, quantifying endocannabinoids in extracellular medium along with intracellular levels will give us a better understanding on the storage, release and transport of these endocannabinoids.

Better measurements of intracellular drug concentrations could improve the modeling of drug effects on the endocannabinoid system. Traditional dose-response curves (in the field of endocannabinoid related drugs) in *in vitro* studies are generated using the drug concentrations added to the cell medium. However, the amount of drug uptake to the cell is often not considered, which might lead to false positive results. Therefore, in these studies, the amount of drug uptake by the cells needs be quantified to evaluate the true effect caused by the drug.

Chapter 6 describes the method development to characterize the pharmacokinetic (PK) processes in zebrafish larvae. Using paracetamol as a paradigm compound, the PK parameters were determined by combining sensitive bioanalytical methods and nonlinear mixed effects modeling (NONMEM). The bioanalytical LC-MS/MS method allowed to quantify paracetamol and its two major metabolites, paracetamol-sulfate and paracetamol-glucuronide, in five zebrafish larvae of 3 days post-fertilization (dpf). The drug clearance value of zebrafish

scales reasonably well with the clearance values of higher vertebrates, including humans, and expanded the current allometric scale by 5-orders of magnitude. Although the zebrafish is a well-established model for drug toxicity and safety studies, this study filled gaps in our understanding of basic pharmacokinetic (PK) processes like absorption, distribution, and clearance in zebrafish larvae that determine the exposure of target (in specific organ) to drugs and drug metabolites in zebrafish larvae, and how these PK processes translate to humans. This method will improve the success rate of employing zebrafish larvae as an alternative pre-clinical model in early drug research and can yield advantages in translating studies on drug effects between species.

Chapter 7 described research to improve the applicability of zebrafish larvae in early drug research by quantifying pharmacodynamic (PD) processes. Here, we used an endocannabinoid system modulator PF-04457845 as an example drug compound to study the dynamic effects of the drug molecules on zebrafish larvae using a systems pharmacology approach. PF-04457845 treatment showed a concentration-dependent increase of endogenous anandamide (AEA) levels, a substrate of FAAH. Furthermore, ABPP and metabolomics/lipidomics were used to measure the target engagement and downstream effects of PF-04457845. We observed that *in vivo* exposure to PF-04457845 completely inhibited FAAH2 activity without cross-reacting with the other detected serine hydrolases and increased the endogenous levels of AEA and related N-acylethanolamines (NAEs) in zebrafish larvae. Overall these results indicate that zebrafish larvae are an attractive pre-clinical vertebrate model to study the system pharmacology of drugs. We could prove target engagement of the drug, on-target effects and the absence of off-target effects with regards to lipid metabolism and a part of the protein landscape in zebrafish larvae. In the future, similar to the translational aspects of PK properties from zebrafish larvae to humans demonstrated in Chapter 6, quantitative pharmacodynamic modelling should be performed in the zebrafish model as it has the potential to accurately translate the drug concentration-effect relationship to humans.

The above zebrafish studies provide proof-of-principle in employing zebrafish as an alternative animal model in drug research. However, there are still some limitations hampering the use of this model in the translation drug studies. One limitation is that in the above studies, drugs and their metabolites were analyzed in whole zebrafish larvae after lysis. This can hamper translation from zebrafish larvae to other animal models like mice and human, as PK and PD analysis using whole body data can only partly or not at all describe details such as

drug distribution between plasma and tissue (s). In addition, tissue specific drug effects cannot be studied when only analyzing whole larvae. Some of these limitations could be overcome by sampling blood from the zebrafish larva. We have demonstrated that this is feasible, but for more routine implementation a further optimization of sampling and improvement of the sensitivity to analyze such small samples of 75-200 nanolitres (pooled blood volume from 20-30 larvae) are necessary. In addition, isolating various tissue samples from larvae could provide information in the local effects of drugs; also for this, highly sensitive analytical platforms should be developed to quantify low quantities of drugs to allow the analysis of small tissue samples from zebrafish larvae. Another limitation is that pharmacokinetic processes could not be quantified for lyophilic drugs when drug exposure was by addition of the drug to the water in which the larvae are present as these drugs were sticking to the skin of the larvae. To overcome this problem of drug dosing, oral dosing to zebrafish larva could be employed, for example, by using nano-particles containing the drug at the required concentrations [11].

The endocannabinoid system can also be studied in mice models, and the analytical methods developed in this thesis have been applied in mice models, too. Although not included in this thesis, as short summary of the results is given here (Kuipers EN*, Kantae V*. et al., *Submitted* [12]). In this study, we aimed to investigate the rate of derailment of the endocannabinoid system and the metabolic organs involved during diet-induced obesity in mice. Plasma levels of endocannabinoids 2-AG and AEA levels increased upon high fat diet (HFD) induced obesity and the increase is accompanied by upregulating their synthetic enzymes in adipose tissue depots (white adipose tissue (WAT) and brown adipose tissue (BAT)). We speculate that this sequence of events attenuates sympathetic signaling in these tissues by CB1 receptor agonism by elevated endocannabinoids, thereby reducing thermogenesis and facilitating storage of excess lipids in white adipose tissue. Given the fact that strictly peripheral CB1R antagonism activates BAT and reduces adiposity in mice [13], we anticipate that strategies inhibiting CB1 receptor selectively on (brown) adipocytes or regulating endocannabinoid synthesis in adipocytes may be an alternative therapeutic strategies to combat obesity and associated metabolic disorders.

Chapter 8 focused on unravelling the molecular mechanism underlying high susceptibility in developing abdominal obesity and type 2 diabetes in individuals from South Asian descent when compared with White Caucasians. As individuals from South Asian

descent have lower energy expenditure, which results in developing disadvantageous metabolic profile, and since the endocannabinoid system dampens energy expenditure, we hypothesized that South Asians may have a higher endocannabinoid tonus. This study demonstrates that healthy lean South Asian men have a higher endocannabinoid tone compared to white Caucasians. This might, at least in part, contribute to the development of a disadvantageous metabolic phenotype later in life. However, in another study population, the high levels of endocannabinoid tone in circulation is not observed in overweight pre-diabetic South Asians when compared to White Caucasians. Here, gene expression levels showed that overweight South Asian men have lower expression of CB receptors and the endocannabinoid degradation enzyme FAAH2 in skeletal muscle compared to white Caucasians, which may reflect a prolonged high endocannabinoid tone. To this end, inhibitors for synthetic and hydrolytic enzymes to tune endocannabinoid levels in adipose tissue might be a novel treatment strategy to combat metabolic disease.

In another clinical study, the effect of prolonged very low-calorie diet (VLCD) restriction on endocannabinoids in relation to fat distribution and cardiac function was investigated on obese T2D patients with coronary artery disease (CAD) [14]. VLCD decreased circulation levels of AEA and related NAEs, which is paralleled by decreased lipid accumulation in adipose tissue, liver and heart, and improved cardiovascular function. Interestingly, baseline AEA levels strongly correlated with subcutaneous white adipose tissue (SAT) volume. We anticipate that dietary interventions are worthwhile strategies in advanced T2D, and that reduction in AEA may contribute to the improved cardio-metabolic phenotype induced by weight loss.

The above described clinical study outcomes are based on measurements from blood samples. While these outcomes suggested that South Asians are prone to develop disadvantageous metabolic profiles compared to White Caucasians, the speculated molecular mechanism in target tissues was only based on the circulatory endocannabinoid levels. Although we hypothesized that endocannabinoid signaling is dysregulated in adipose tissue depots, especially in BAT or SAT, this cannot be proven due to lack of adipose tissue samples from study participants. This limitation could be addressed either by using *in vivo* models like mice or zebrafish larvae or proof-of principal studies using *in vitro* cell models like human (brown) adipocytes or organ-on-chip model systems. The findings in clinical studies can be translated to these model systems in order to do mechanistic studies to obtain deeper insights into the molecular biochemistry. Furthermore, the effect of novel small molecules inhibitors

(inhibiting enzymes part of endocannabinoid system) using zebrafish or organ-on-chip model systems, can studied in disease models in more targeted fashion, i.e. focusing on certain cell types, tissues, or cell-cell interactions.

In this context, organ-on-a-chip platforms can serve as an alternative model system interface between conventional and 'simple' *in vitro* models and *in vivo* conditions to study the molecular biochemistry and drug biochemistry [15,16] in a more physiologically relevant context. These models are comprised of human cell cultures that are co-cultured in a relevant microenvironment, which provides an opportunity to screen for drugs in both healthy and diseased conditions. In a clinical setting, patient-derived cells can be cultured in an organ-on-a-chip platform and used to screen the efficacy of drugs to support the choice of the proper treatments. Read out of these experiments can be visualization using a microscope to study the physiological status of the cells, advanced imaging using staining and confocal microscopy, or the cells can be extracted to generate metabolite profiles (and other omics profiles).

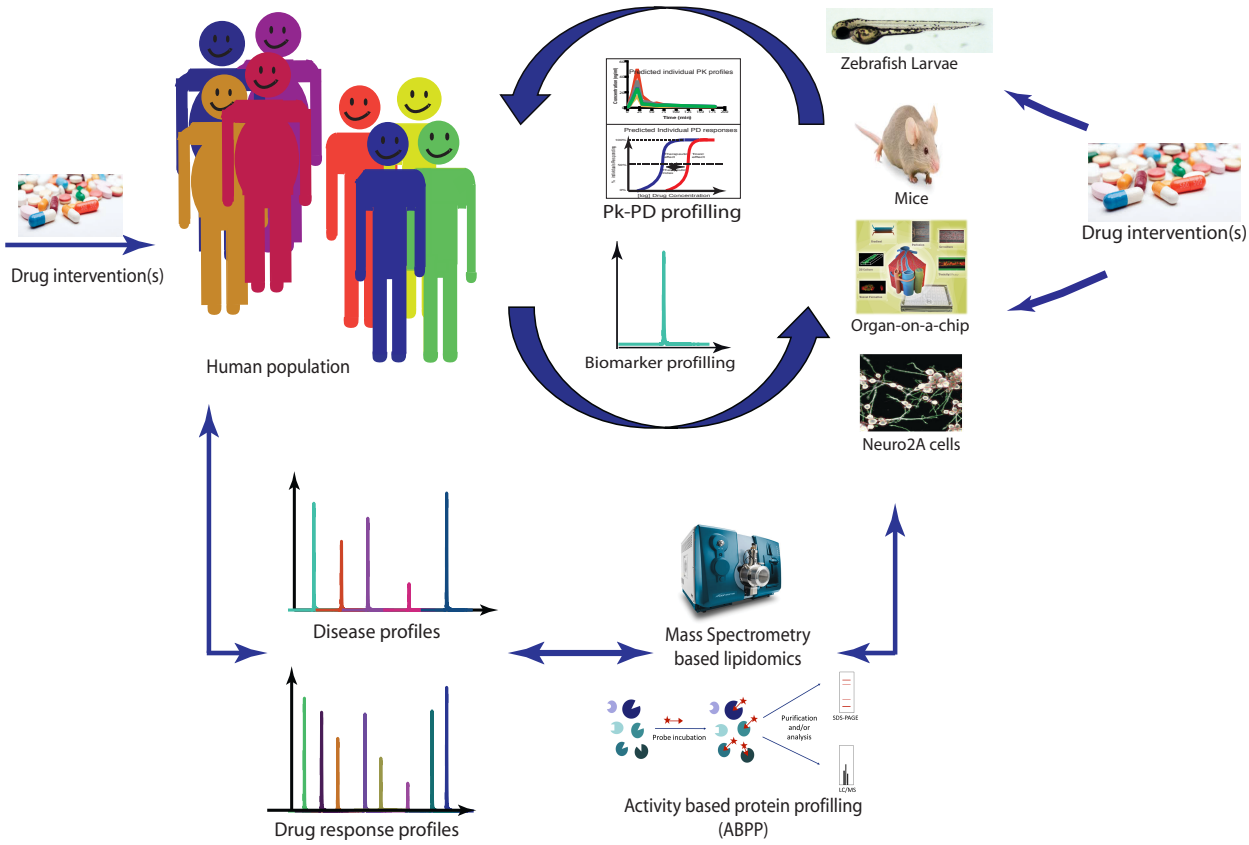

Figure 1: Future directions to realize a systems pharmacology approach

We envision that in the future observations and findings in clinical studies will be more often translated to *in vitro (organ-on-a-chip)* or *in vivo (zebrafish)* models to reveal the underlying molecular disease mechanisms and pharmacology (i.e. effect of drugs) in particular tissues. Integration of research fields such as metabolomics/lipidomics, proteomics, pharmacology (PK-PD), clinical trial design, biostatistics and computational modelling will enable to study pathophysiology of diseases and drug effects in a systems pharmacology perspective (**Fig. 1**). Metabolomics/lipidomics allow to study disease and drug effects, including target engagement and on/off-target effects, in a system wide, unbiased and hypothesis-free manner [17]. After identifying the effected metabolic pathways, chemoproteomic techniques like ABPP can be applied in a more targeted manner to investigate the drug on-target engagement and their downstream effects across the targeted enzyme family [18].

The above described approaches can not only be applied to drug research, but also in the clinic to provide patients with targeted and personalized interventions, in order to realize personalized medicine [19]. A systems approach, integrating metabolomics and other "omics" data to capture biological networks, will allow a contextual pathophysiological understanding of the disease for better diagnosis and treatment. In such a "systems biology" approach, phenotypes can be biochemically described at the functional level of genes (genomics), gene modifications (epigenomics), gene expression (transcriptomics), protein translation including PTM's (proteomics) and the metabolic network (metabolomics). Disease modeling based on these omics data can integrate biological knowledge, and powerful computational modelling can be used to interpret curated disease information across multi-dimensional and multi-level biological systems in translational and clinical research. Integrating the multi-dimensional data with clinical information (generating patient-centric models) can help to gain insights into patient-specific molecular mechanisms, and to translate them into personalized clinical treatments [20]. In the future, we envision that after performing proper biomarker validations and developing highly sensitive analytical platforms, sophisticated computational methods will facilitate omics analysis of multi-tissue and multi-organ data, thus enabling a real investigation of systemic effects [21–23].

These system biology approaches can be applied to study the complex endocannabinoid system which has a wide distribution of cannabinoid receptors in both periphery and central tissues: the methods developed in this thesis can help to study the interactions of the endocannabinoid system between organs and the impact of dysregulation in endocannabinoid signaling in one organ on another organ. Secondly, system approaches can help to build up a

computational biological network that represents the endocannabinoid complexity in several physiological and pathological processes. Additionally, it allows to evaluate the effect of drugs and compounds on the whole biological network which helps to identify the part of a biological network that is affected by the drug. For instance, we can evaluate the systemic effect of DH376, a DAGLs inhibitor, on different classes of networks to identify the affected metabolic network and their associated proteins along with their related genes or gene products (mRNAs).

Another emerging direction promising for systems pharmacology is to use single-cell analysis; especially single-cell metabolomics [24] can in principle provide information on the metabolome of a single cell and allow a quick readout of how cells react to environmental stimuli. Single cell investigations will reveal cell-to-cell variation (either cellular heterogeneity or different phenotypes among similar cells) within cellular population and achieve detailed understanding of cell functions and how individual cell reacts to a drug molecule. However, there are currently still serious challenges in single cell metabolomics, and further improvements in the sensitivity, targeting the right cell type, reproducible sampling and data normalization and analysis are required. One next step will be to integrate metabolomics with other omics levels in single-cell analysis to understand the response of a biological network to a pathological stimuli or to a drug [25]. For instance, this approach could be used to understand the cell-specific molecular composition and the regulation of endocannabinoid system at the synapses.

Finally, the findings observed in model systems should be translated back to the patients to develop models to predict clinical outcome of treatments. This is especially true for the endocannabinoid system, which is a complex and important signaling system involved in many physiological and pathological conditions: a system pharmacology approach can lead to develop novel therapeutic biomarkers to treat metabolic or neurological diseases. We are convinced that this will finally lead to realize more individualized drug treatments.

References

1. Kantae, V. *et al*. Integration of pharmacometabolomics with pharmacokinetics and pharmacodynamics: towards personalized drug therapy. *Metabolomics* **13,** 9 (2017).
2. Jung, D. G., Jung, D. & Kong, S. H. A Lab-on-a-Chip-Based Non-Invasive Optical Sensor for Measuring Glucose in Saliva. *Sensors (Basel)*. **17,** (2017).
3. Urquhart, P., Nicolaou, A. & Woodward, D. F. Endocannabinoids and their oxygenation by cyclo-oxygenases, lipoxygenases and other oxygenases. *Biochimica et Biophysica Acta - Molecular and Cell Biology of Lipids* **1851,** 366–376 (2015).
4. Rouzer, C. A. & Marnett, L. J. Endocannabinoid oxygenation by cyclooxygenases, lipoxygenases, and cytochromes P450: cross-talk between the eicosanoid and endocannabinoid signaling pathways. *Chem. Rev.* **111,** 5899–921 (2011).
5. Hillard, C. J. Circulating Endocannabinoids: From Whence Do They Come and Where are They Going? *Neuropsychopharmacology* **43,** 155–172 (2018).
6. Fiehn, O. *et al*. Establishing Reporting Standards for Metabolomic and Metabonomic Studies: A Call for Participation. *Omi. A J. Integr. Biol.* **10,** 158–163 (2006).
7. Park, J. O. *et al*. Metabolite concentrations, fluxes and free energies imply efficient enzyme usage. *Nat. Chem. Biol.* **12,** 482–9 (2016).
8. Baggelaar, M. P. *et al*. Highly Selective, Reversible Inhibitor Identified by Comparative Chemoproteomics Modulates Diacylglycerol Lipase Activity in Neurons. *J. Am. Chem. Soc.* **137,** (2015).
9. Nicolussi, S. & Gertsch, J. Endocannabinoid transport revisited. *Vitam. Horm.* **98,** 441–485 (2015).
10. Fowler, C. J. Transport of endocannabinoids across the plasma membrane and within the cell. *FEBS J.* **280,** 1895–1904 (2013).
11. Fenaroli, F. *et al*. Nanoparticles as Drug Delivery System against Tuberculosis in Zebrafish Embryos: Direct Visualization and Treatment. **8,** 7014–7026 (2014).
12. Kuipers, E. N. *et al*. Derailment of the endocannabinoid system by high fat diet starts in adipose tissue. *Submitted*
13. Boon, M. R. *et al*. Peripheral cannabinoid 1 receptor blockade activates brown adipose tissue and diminishes dyslipidemia and obesity. *FASEB J.* **28,** 5361–5375 (2014).
14. van Eyk, H. J. *et al*. Caloric restriction lowers endocannabinoid tonus and improves cardiac function in type 2 diabetes. *Nutr. Diabetes* **8,** 6 (2018).
15. van Duinen, V., Trietsch, S. J., Joore, J., Vulto, P. & Hankemeier, T. Microfluidic 3D cell culture: From tools to tissue models. *Curr. Opin. Biotechnol.* **35,** 118–126 (2015).
16. Trietsch, S. J. *et al*. Membrane-free culture and real-time barrier integrity assessment of perfused intestinal epithelium tubes. *Nat. Commun.* **8,** 262 (2017).
17. Kaddurah-Daouk, R., Kristal, B. S. & Weinshilboum, R. M. Metabolomics: a global biochemical approach to drug response and disease. *Annu. Rev. Pharmacol. Toxicol.* **48,** 653–83 (2008).
18. Trupp, M. *et al*. Metabolomics reveals amino acids contribute to variation in response to simvastatin treatment. *PLoS One* **7,** e38386 (2012).
19. Beger, R. D. *et al*. Metabolomics enables precision medicine: "A White Paper, Community Perspective". *Metabolomics* **12,** 149 (2016).
20. Benson, M. Clinical implications of omics and systems medicine: focus on predictive and individualized treatment. *J. Intern. Med.* **279,** 229–240 (2016).
21. Liu, W. *et al*. Topologically inferring pathway activity toward precise cancer classification via integrating genomic and metabolomic data: prostate cancer as a case. *Sci. Rep.* **5,** 13192 (2015).
22. Do, K. T. *et al*. Network-Based Approach for Analyzing Intra- and Interfluid Metabolite

Associations in Human Blood, Urine, and Saliva. *J. Proteome Res.* **14,** 1183–1194 (2015).
23. Tebani, A., Afonso, C., Marret, S. & Bekri, S. Omics-Based Strategies in Precision Medicine: Toward a Paradigm Shift in Inborn Errors of Metabolism Investigations. *Int. J. Mol. Sci.* **17,** (2016).
24. Zenobi, R. Single-cell metabolomics: analytical and biological perspectives. *Science* **342,** 1243259 (2013).
25. Wang, D. & Bodovitz, S. Single cell analysis: the new frontier in "omics." *Trends Biotechnol.* **28,** 281–290 (2010).

Appendix

Summary

Nederlandse Samenvatting

Dankwoord / Acknowledgements

Curriculum Vitae

List of publications

Summary

The main goal in current drug development is to discover a chemical molecule that specifically interacts with a single molecular target to re-instate the healthy state biochemistry and reduce the unwanted side effects. However in reality due to the complexity in biochemical networks and their cross-talks in whole organism, some of the drugs interact with the target that is not the central to the pathophysiology of the disease or in some instances interacts with other unanticipated targets (off-targets) which leads to unwanted side effects. Therefore, recent drug discovery and development processes have evolved from a specific targeted approach (studying molecules, cells and other components of living system in isolation) to a broader systems approach (studying in intact organism). This approach integrating different biochemical components (genes, proteins, metabolites) can generate molecular network descriptions to study the system-state differences such as differences between healthy versus diseased or drug responders versus non-responders. Systems pharmacology is a concept that attempts to characterize the molecular network changes due to a disease state and its changes due to a drug. In this thesis, we developed and applied this system pharmacology approach to understand and modulate the endocannabinoid system across different model systems (cells, zebrafish, mice and humans). The primary goal is to achieve deeper insights in the functional role of endocannabinoid system in healthy and diseased states. In addition, this research seeks to modulate the endocannabinoid system with new enzyme inhibitors to gain better understanding in different signaling pathway associated with endocannabinoids synthesis and degradation and to understand the drug pharmacology and whether such new inhibitor compounds may modify the disease biochemistry; this includes the study of target engagement, downstream effects and the off-target effects of new compounds. We have chosen the endocannabinoid system as a pharmacological target due its ubiquitous nature throughout the body and its regulatory role in a huge number of physiological and pathological conditions. The endocannabinoid system comprises with cannabinoid receptors (CB1 & CB2), their endogenous ligands, the endocannabinoids and the enzymes that synthesize and degrade the endocannabinoids.

Chapter 2 introduces the concept of system pharmacology: integrating metabolomics with pharmacology (Pharmacokinetics (what drug does to the body)-Pharmacodynamics (what body does to the drug), PK-PD) in order to support the development of personalized medicine. Metabolomics is the study of metabolites. Metabolites are the intermediate and end products of the different processes and chemical reactions that takes place in cells and between cells.

Identification and quantification of predictors/biomarkers that account for inter-individual variability in drug response upon drug administrations is necessary to achieve personalized medicine. Here we highlighted the potential of pharmacometabolomics, a discipline of metabolomics, in prospectively informing on the inter-individual differences in drug pharmacology, including PK-PD processes, and thereby guiding drug selection and drug dosing.

Similar to Metabolomics, the concept of studying set of lipids is called Lipidomics. To study endocannabinoids and their related lipids that under normal physiological conditions are present at very low concentrations (nanomole to picomole range) in various biological matrices, sensitivity is the key factor. **Chapter 3** describes the development and validation of a nano liquid-chromatography-mass spectrometry (nano LC-MS/MS) analytical method for the in-depth quantification of endocannabinoids and related lipids in human cerebrospinal fluid (CSF). In parallel, highly sensitive LC-MS/MS analytical methods were extended to other biological matrices, like cells, zebrafish larvae, plasma (mice and humans).

To understand the physiological role of endocannabinoids, especially of 2-Arachidonoylglycerol (2-AG) and N-arachidonoylethanolamide (Anandamide; AEA), selective small molecule inhibitors for their synthetic and hydrolytic enzymes are required. **Chapter 4** aims to investigate which isoform of diacylglycerol lipase (DAGL-α and -β) takes the lead in 2-AG biosynthesis using DH376, a potent *in vivo* active DAGL inhibitor. Activity based Protein Profiling (ABPP) technique was used to investigate the activity of the enzymes and lipidomics was used to measure the downstream effect of the enzyme. Effects of a DH376 treatment was investigated in wild type and generated DAGL knock-outs (alpha, beta and alpha/beta) Neuro2A cell populations. It was observed that DH376 treatment to knock-outs cells substantially reduced 2-AG levels. These data suggest the presence of additional enzymes responsible for 2-AG synthesis, which can be targeted by DH376. Further investigations to identify these new targets are currently ongoing.

Chapter 5 focused on unraveling the reason behind the failure of a recent phase I clinical trial of Fatty acid amide hydrolase (FAAH) inhibitor BIA 10-2474. FAAH is an enzyme responsible for the degradation of anandamide. This drug is developed to treat pain and inflammation. ABPP and lipidomics analysis of BIA-102474 treatment to human neurons reveled that this drug inhibits several other lipases (off-targets) other than its target enzyme and produced substantial changes in the lipid networks. This study demonstrates the power of ABPP and lipidomics techniques in not only identifying drug on-target engagement effects and

associated downstream effects but also in identifying drug off-target effects and drug effect on downstream lipid networks. Hence, we believe these techniques can be employed in early drug discovery and development pipelines to screen for on-target engagement and off-target effects of candidate drug molecule

In order to gain better understanding of the *in vivo* pharmacology of the endocannabinoid system, proper *in vivo* model systems are required and need to be properly validated. In this regard, zebrafish larvae were tested as an attractive pre-clinical model system in **chapter 6** which characterizes the pharmacokinetics of paracetamol as a model compound. The zebrafish drug clearance scales reasonably well with the clearance rates in higher vertebrates, including humans, and this study expanded the current allometric scale by 5 orders of magnitude. Although the zebrafish is a well-established model for drug toxicity and safety studies, this study filled gaps in our understanding of basic pharmacokinetic (PK) processes and how these PK processes translate to humans. This method will improve the success rate of employing zebrafish larvae as an alternative pre-clinical model in early drug research.

Chapter 7 described the efforts to improve the applicability of zebrafish larvae in early drug research by quantifying the pharmacodynamics (PD) processes using an FAAH inhibitor PF-04457845 as an example drug compound. ABPP and lipidomics tools were used to investigate the on-target engagement of PF04457845 on the protein landscape and its downstream effects on the lipid networks. The results show the *in vivo* exposure of PF04457845 completely inhibited FAAH2 and increased the levels of NAEs, substrates of FAAH, while no cross-reactivity was observed with other serine hydrolases or alterations in lipid networks. Overall these results indicate that zebrafish larvae are an attractive pre-clinical vertebrate model to study the system pharmacology of drugs.

To expand our findings from models to clinical studies, **Chapter 8** focused on unravelling the molecular mechanism underlying high susceptibility in developing abdominal obesity and type 2 diabetes (T2D) in individuals from South Asians descent when compared with White Caucasians. As individuals from South Asians descent have lower energy expenditure, and since endocannabinoid system dampens energy expenditure and is upregulated in obesity and T2D conditions, we hypothesized that South Asians may have a higher endocannabinoid tonus. Quantification of endocannabinoids in plasma showed that the healthy lean South Asian men have have a higher endocannabinoid tone compared to white Caucasians. This might, at least in part, contribute to the development of a disadvantageous metabolic phenotype later in life.

The above described clinical study outcomes are based on measurements from blood samples. While these readouts are very informative, it will rather be difficult to speculate about molecular mechanisms in target tissues only based on the circulatory endocannabinoid levels. Therefore, in the future, we envision that observations and findings in clinical studies will be more often translated to *ixn vitro (organ-on-a-chip)* or *in vivo (zebrafish)* models to reveal the underlying molecular disease mechanisms and pharmacology (i.e. effect of drugs) in particular tissues. Integration of research fields such as metabolomics/lipidomics, proteomics, pharmacology (PK-PD), clinical trial design, biostatistics and computational modelling will enable to study pathophysiology of diseases and drug effects in a systems pharmacology perspective. Metabolomics/lipidomics allow to study disease and drug effects, including target engagement and on/off-target effects, in a system wide, unbiased and hypothesis-free manner. After identifying the effected metabolic pathways, chemoproteomic techniques like ABPP can be applied in a more targeted manner to investigate the drug on-target engagement and their downstream effects across the targeted enzyme family. The approaches described above can not only be applied to drug research, but also in the clinic to provide patients with targeted and personalized interventions, in order to realize personalized medicine.

Overall, the findings observed in model systems should be translated back to the patients to develop models to predict clinical outcome of treatments. This is especially true for the endocannabinoid system, which is a complex and important signaling system involved in many physiological and pathological conditions: a system pharmacology approach can lead to develop novel therapeutic biomarkers to treat metabolic or neurological diseases. We are convinced that this will finally lead to realize more individualized drug treatments.

Samenvatting

Het voornaamste doel van hedendaags geneesmiddelenonderzoek is het zoeken naar nieuwe chemische verbindingen, die door middel van specifieke, doelgerichte interactie met een moleculair doelwit de verstoorde fysiologische gesteldheid naar een normale toestand herstelt en ongewenste bijwerkingen reduceert. In werkelijkheid, echter, kunnen geneesmiddelen door de complexiteit van biochemische netwerken en overspraak in organismen ook werken op delen die niet centraal staan in de pathofysiologie, of zelfs interactie aangaan met geheel onverwachte doelen ("off-target" effecten), met ongewenste bijwerkingen tot gevolg. Mede hierdoor zijn de processen in het geneesmiddelenonderzoek gegroeid van een specifieke, op één doel gerichte aanpak (ofwel het bestuderen van moleculen, cellen of andere geïsoleerde delen van organismen) naar een brede systeem-gerichte aanpak (het bestuderen van intacte organismen). Deze brede aanpak, die diverse biochemische componenten zoals genen, proteïnen en metabolieten integreert, kan worden gebruikt voor het beschrijven van moleculaire netwerken. Hiermee kunnen verschillen in de gezondheidsstaat van het systeem worden bestudeerd; zoals in gezonde of zieke staat, of het al of niet reageren op geneesmiddelen. Het zogeheten "Systems Pharmacology" (systeemfarmacologie) is een concept dat zich richt op het karakteriseren van veranderingen in deze moleculaire netwerken onder invloed van ziekte en geneesmiddelen. In deze thesis is een systeemfarmacologie gerichte aanpak ontwikkeld en toegepast om het endocannabinoïde systeem in diverse modelsystemen zoals cellen, zebravissen, muizen en mensen, te bestuderen, begrijpen en moduleren. Het primaire doel hierbij is om diepere inzichten te verkrijgen in de functionele rol die het endocannabinoïde systeem speelt bij gezondheid en ziekte. Daarnaast is het endocannabinoïde systeem gemoduleerd met nieuwe enzym-inhibitors ("remmers") om meer inzicht te krijgen in de diverse signalerende reactiepaden die geassocieerd zijn met de synthese en afbraak van endocannabinoïden, de farmacologie van de medicijnen te begrijpen, en te onderzoeken of deze inhibitors de biochemie van ziekte kunnen veranderen; onder andere door het bestuderen van doelgerichtheid, effecten stroomafwaarts in de reactiepaden, en off-targets van deze middelen. Het endocannabinoïde systeem is overal aanwezig in het lichaam en speelt een belangrijke regulaire rol in vele fysiologische en pathologische aandoeningen. Om deze redenen is het endocannabinoïde systeem gekozen als farmacologisch doelwit. Het systeem bestaat uit de cannabinoïde receptoren CB1 en CB2, hun endogene liganden, de endocannabinoïden, en de enzymen die verantwoordelijk zijn voor de synthese en afbraak van de endocannabinoïden.

In **Hoofdstuk 2** wordt allereerst het concept systeemfarmacologie geïntroduceerd: de integratie van metabolomics met farmacologie (dat is: farmaco-kinetic, wat geneesmiddelen doen met het lichaam, en farmaco-dynamiek: wat het lichaam doet met geneesmiddelen) om de ontwikkelen van geneesmiddelen-op-maat te bevorderen. "Metabolomics" is de studie van metabolieten; dit zijn tussen- of eindproducten van de diverse intra- en intercellulaire processen en chemische reacties. Het kunnen identificeren en kwantificeren van, al dan niet voorspellende, biomarkers, waarmee rekening kan worden gehouden met interindividuele variaties in de reactie op geneesmiddelen, is van cruciaal belang voor de ontwikkeling van gepersonaliseerde geneesmiddelen. In dit hoofdstuk wordt de mogelijke rol van farmaco-metabolomics, een discipline binnen metabolomics, toegelicht in het voorspellen van interindividuele variaties in farmacologie waaronder PK-PD, en bijbehorende de leidende rol in selectie van geneesmiddelen en afstemmen van de dosering.

Net als metabolomics is de naam lipidomics afgeleid van de studie van lipiden (vetachtige stoffen). Endocannabinoiden en de bijbehorende lipiden zijn onder normale fysiologische omstandigheden slechts in zeer lage concentraties aanwezig (nanomolair tot picomolair). Om ze te kunnen bestuderen in verschillende biologische matrices, zijn selectiviteit en detectie gevoeligheid van cruciaal belang. **Hoofdstuk 3** beschrijft de ontwikkeling en validatie van een nano vloeistofchromatografie – massa spectrometrie (nano LC-MS/MS) methode voor de kwantificatie van endocannabinoiden en bijbehorende lipiden, in humaan hersenvocht. Parallel hieraan zijn zeer gevoelige LC-MS/MS methodes verder uitgebreid voor het gebruik van andere biologische matrices zoals cellen, zebravis larven, en plasma van mensen en muizen.

Om de fysiologische rol van endocannabinoïden, in het bijzonder 2-Arachidonoylglycerol (2-AG) en N-arachidonoylethanolamide (Anandamide, AEA) beter te begrijpen zijn selectieve inhibitors nodig die richten op hun synthetische en hydrolytische enzymen. **Hoofdstuk 4** doet onderzoek naar welke iso-vormen van diacylglycerol lipase (DAGL-a en -B) de dominante rol spelen in de biosynthese van 2-AG met DH376, een potente *in vivo*-actieve DAGL inhibitor. De activiteit van de enzymen is gemeten met "activity-based protein profiling" (ABPP), en stroomafwaartse effecten zijn gemeten met lipidomics. Het effect van behandeling met DH376 is onderzocht in wild-type Neuro2A cellen, en Neuro2Acellen waarbij DAGL is uitgeschakeld (alpha, beta en alpha/beta). Bij de knock-out variant leidde behandeling met DH376 tot substantiële verlaging van het 2-AG niveau. Dit resultaat suggereert de aanwezigheid van een additioneel enzym, dat verantwoordelijk is voor de

synthese van 2-AG, en dat gericht kan worden geblokkeerd door DH376. Er zijn nadere studies gaande om deze nieuwe doelen te identificeren.

Hoofdstuk 5 besteedt aandacht aan het achterhalen van de redenen tot het mislukken van een recente Phase I trial van Fatty acid Amide Hydrolase (FAAH) inhibitor BIA 10-2474. Het enzym FAAH is verantwoordelijk voor de afbraak van anandamide, een geneesmiddel dat gebruikt wordt tegen pijn en ontstekingen. ABPP en lipidomics analyse van menselijke neuronen, behandeld met BIA-102474, heeft aangetoond dat dit geneesmiddel ook andere lipases inhibeert (off-target effect) dan het eigenlijke doelwit, en daarbij substantiële veranderingen in de lipide netwerken teweeg brengt. Deze studie laat ook de kracht van ABPP en lipidomics zien, niet enkel in het identificeren van doelgerichtied, alsook voor de identificatie van off-target en stroomafwaartse effecten. Deze technieken kunnen derhalve wordt ingezet in de processen voor ontdekking en ontwikkeling van geneesmiddelen in een vroeg stadium, om doelgerichtheid en off-target effecten van een potentieel geneesmiddel te onderzoeken.

Om meer inzicht te verkrijgen in de in vivo farmacologie van het endocannabinoid systeem, zijn goede en gevalideerde *in vivo* modelsysteem nodig. Zebavis larven zijn hiervoor als veelbelovend preklinisch model gebruikt in **Hoofdstuk 6**, waarin de farmaco-kinetica van paracetamol is gekarakteriseerd. De afbraak van geneesmiddelen schaalt tot op zekere hoogte met de afbraaksnelheid in grotere gewervelden, waaronder de mens. In deze studie is de huidige allometrische schaal met 5 ordegroottes uitgebreid. Ondanks dat zebravissen een wijdverspreid model zijn voor het testen van veiligheid en toxiciteit van geneesmiddelen, heeft deze studie bijgedragen tot vernieuwde inzichten omtrent de basis-farmacokinetische processen, en hoe deze zich laten vertalen naar mensen. Hiermee wordt de slagingskans van zebravis larven als alternatief pre-klinisch model, aanzienlijk vergroot.

In **Hoofdstuk 7** wordt beschreven hoe de toepasbaarheid van zebravis larven in vroege stadia van geneesmiddelenonderzoek kan worden verbeterd geïllustreerd door middel van het kwantificeren van de farmacodynamische processen met FAAH-inhibitor PF-04457845. Wederom zijn ABPP en lipidomics gebruikt om de doelgerichtheid van PF-04457845 op de enzymfunctie, respectievelijk de effecten op de lipide netwerken te meten. De resultaten hiervan tonen aan dat *in vivo* blootstelling aan PF-04457845 het FAAH2-complex volledig remt, en tegelijkertijd een toename in de concentratie NAE, substraten van FAA, zonder dat hierbij kruisreactiviteit met andere serine hydrolases is waargenomen, noch veranderingen in de lipide

netwerken. Deze resultaten laten zien dat de zebravis larve een veelbelovend model is voor studies naar de systeem farmacologie van geneesmiddelen in gewervelden.

In **Hoofdstuk 8** worden de voorgaande bevindingen verder uitgebreid en toegepast op klinische studies. Hierbij worden de moleculaire mechanismen onderzocht die ten grondslag liggen aan de verhoogde kans op het ontwikkelen van abdominale obesitas en Type 2 Diabetes in mensen van Zuid-Aziatische afkomst in vergelijking met individuen met Kaukasische achtergrond. Individuen van Zuid-Aziatische afkomst hebben een lager energieverbruik. Het endocannabinoide systeem vermindert het energieverbruik verder, en is verhoogd actief in Type 2 diabetes. Dit vormt de basis voor de hypothese dat Zuid-Aziatische individuen een verhoogde endocannabinoide tonus hebben. Uit kwantitatieve metingen van endocannabinoïden in plasma blijkt dat gezonde, slanke Zuid-Aziaten hogere endocannabinoïden niveaus hebben ten opzichte van Kaukasische individuen. Deze verhogingen dragen, ten minste gedeeltelijk, bij aan de ontwikkeling van een ongunstig metabolisch fenotype in een later stadium.

Bovenstaande resultaten van een klinische studie zijn gebaseerd op metingen in bloed. Hoewel de uitkomsten zeer informatief zijn, is de vertaling ervan beperkt. Zo is het moeilijk om op basis van concentraties in de circulaire bloedsomloop een uitspraak te kunnen doen over de moleculaire mechanismen in specifieke weefsels. Voor toekomstige studies zouden ondervindingen uit klinische studies kunnen worden vertaald naar *in vitro* (bijv. *organ-on-a-chip*) of *in vivo* (zebravis larven) modellen om de onderliggende moleculaire mechanismen van ziekte, alsmede de farmacologie, in specifieke weefsels te ontrafelen. Een volwaardige integratie van diverse onderzoeksgebieden zoals metabolomics/lipidomics, proteomoics, farmacologie (PK-PD), ontwerp van klinische studies, biostatistiek en computermodellen, maakt de weg vrij voor het bestuderen van pathofysiologie van ziektes en medicijnen in het perspectief van systeem farmacologie. Met metabolomics en lipidomics kunnen ziekte en de werking van medicijnen, waaronder doelgerichtheid en eventuele off-target effecten worden bestudeerd in een systeem-brede, objectieve en hypothese-vrije aanpak. Na identificatie van de metabole routes kunnen chemo-proteomics methodes zoals ABPP gericht worden ingezet om doelgerichtheid en de effecten stroomafwaarts in de gehele enzym-familie nader te bestuderen. Deze aanpak is niet alleen toepasbaar in onderzoek naar geneesmiddelen, maar kan ook in de kliniek worden gebruikt om gepersonaliseerde medicijnen voor patiënten te maken.

Uiteindelijk zullen de uitkomsten van deze modelsystemen terug moeten worden vertaald naar de patiënt, om daarmee modellen te ontwikkelen die het mogelijk maken de uitkomst van klinische proeven te voorspellen. Dit geldt in het bijzonder voor het

endocannabinoïde systeem, een zeer complex en belangrijk signaleringssysteem dat betrokken is bij vele fysiologische en pathologische aandoeningen. Met een systeem farmacologie-gerichte aanpak is het mogelijk om nieuwe therapeutische biomarkers te ontwikkelen, en metabole of neurologische ziekten beter te behandelen. Uiteindelijk is dit de weg naar verwezenlijking van op-maat-gemaakte geneesmiddelen.

Acknowledgements

I would like to express my sincere gratitude to all the people who contributed to the completion of this thesis.

I really enjoyed working with Prof. Thomas Hankemeier and I am impressed by the amount of support, encouragement and freedom I received from you. More importantly for transferring your enthusiasm and happiness, which gave me a huge impact on my daily work. I learned a lot form you (especially the leadership qualities). I also had great time working with Prof. Piet H van der Graaf who gave me continuous support and encouragement. I really appreciate the amount of help I received from Dr. Amy Harms and for your "any time" support you gave me throughout my PhD.

My sincere thanks to all my external collaborators, without you my PhD thesis would not have been successful. I specially thank Prof. Mario van der Stelt for continuously guiding me throughout my PhD. The help I received from you is significant and it was pleasure working with you. I would like to acknowledge Prof. Patrick Rensen from LUMC for believing in me and for providing your support through my PhD. Special thanks to Elke for your guidance and teaching me pharmacology aspects during our long endless discussion. My gratitude to all my external colleagues: Marc, Annelot, Floor, Juan, Elliot, Anthe, Kimberly, Mariette, Eline, Huub and in particular to Rob for all your help.

I am grateful to the past and present colleagues of Analytical Biosciences and the BMFL. I can only say thank you for everything and making this PhD period a long lasting memory. I really enjoyed my stay either be, coffee corner discussions (scientific, politics and what not), lab-day outs, parties and especially time spent at "borrels". I would like to acknowledge Loes for all your help and support from the beginning. Ivonne, I appreciate your help with regard to my PhD graduation. I would like to express my thanks to Nelus, Anne-Charlotte, Yuylia, Isabelle, Peter, Gerwin, Junzeng, Rosilene, Amar, Tom, Abidemi, Wei (M&F), Zheng Zheng, Simon, Michel, Alberto and Marian. Thanks guys for all your support and you all made my life more happier. Paul, I really appreciate your help in writing the Dutch summary. Rawi, thanks for all your support and for proof-reading the Dutch summary.

My sincere gratitude to Faisa for all the support, help and encouragement you gave me from the beginning till the end. You stood for me for everything. Thanks a lot. Many thanks to Can and Cornelius for all your help and support and all the extra fun we had together. My dear

friends: Poorna & Raji, Venkat & Sruthi, Swaroop, Meherji, Chakri and Karthik thanks for all your support and for everything.

My dear parents, grandparents, dear brother, uncle, sister-in-law and my in-laws, thank you all for giving me your support and encouragement. It is difficult for me to express my gratitude in words, but I believe my actions will make you proud and happy. Last but not least my love of my life, my wife, Madhuri: You left your career and moved to Netherlands and stood by me and offered your unfailing support and unconditional love in all my endeavors. Special mention to my little champ Chandra Teja, who was born in my final year and made my life more joyful and cheerful.

Curriculum Vitae

Vasudev Kantae was born on December 20th 1987 in the village of Vetlapalem, India. He obtained his high secondary education in Biology, Physics and Chemistry at Sri Chaitanya Institute, India in 2003. He studied Biotechnology at the SRM University, India, and obtained his B.Tech (Bachelors in Technology) degree in 2009, with grade 'Excellent'. During bachelors, he was a student representative for a batch 300 students and a key organizer of a bio-science national conference, 2009. After completion, he was enrolled in MSc program in Biotechnology at University of Helsinki, Finland (selected for a free education program), with a specialized track in cellular biotechnology and developmental and structural biology. During his summer internship and master graduation project at Institute of Molecular Medicine Finland (FIMM), Helsinki, Finland, he specialized to metabolomics using advanced analytical technologies including tandem mass spectrometry, high-resolution mass spectrometry, and ultra-performance liquid chromatography. In 2012, he obtained his MSc degree and from June 2012, he continued as a Research scientist at FIMM working in developing and validating the bioanalytical methods and serving both internal and external clients. During this period, he learned a great deal about the human metabolome, and the challenges of its characterization along with various analytical method developments, as well as about the opportunities offered by the applications of metabolomics to study human health and disease. In March 2014, he started as a systems pharmacology cluster PhD student at Systems Biomedicine and Pharmacology, LACDR, Leiden University. He is selected as a part of "Profiling program: Endocannabinoids", an inter-faculty program, initiated by Faculty of Science, Leiden University. This research was conducted under the supervision of Prof. dr. Thomas Hankemeier, Prof. dr. Piet H van der Graaf and Dr. Amy C. Harms.

During the course of his PhD, he had opportunity to present his research results as a poster at various national and internal conferences. Oral presentations were given at MSB conference (the Netherlands, 2017), NVMS (the Netherlands, 2017), Pharmaceutical Sciences World Congress (FIP), PSWC (Sweden, 2017), Metabolomics Symposium with SCIEX (the Netherlands, 2018), International cannabinoid research society (ICRS, the Netherlands, 2018).

List of Publications

1. **Kantae V***, Krekels EHJ*, Esdonk MJ Van, Lindenburg P, Harms AC, Knibbe CAJ, Van der Graaf PH, Hankemeier T. Integration of pharmacometabolomics with pharmacokinetics and pharmacodynamics: towards personalized drug therapy. *Metabolomics*. 13: 9, **2017**.

2. **Kantae V***, Ogino S*, Noga M, Harms AC, van Dongen RM, Onderwater GLJ, van den Maagdenberg AMJM, Terwindt GM, van der Stelt M, Ferrari MD, Hankemeier T. Quantitative profiling of endocannabinoids and related N -acylethanolamines in human CSF using nano LC-MS/MS. *J Lipid Res*. 58: 615–624, **2017**.

3. **Kantae V***, Van Esbroeck ACM*, Zohu J, Harms AC, Hankemeier T*, Van Der Stelt M*. Investigating the players of 2-arachidonyl glycerol biosynthesis in cellular system.
   Manuscript in preparation

4. Baggelaar MP, Chameau PJP, **Kantae V**, Hummel J, Hsu K-L, Janssen F, van der Wel T, Soethoudt M, Deng H, den Dulk H, Allarà M, Florea BI, Di Marzo V, Wadman WJ, Kruse CG, Overkleeft HS, Hankemeier T, Werkman TR, Cravatt BF, van der Stelt M. Highly Selective, Reversible Inhibitor Identified by Comparative Chemoproteomics Modulates Diacylglycerol Lipase Activity in Neurons. *J Am Chem Soc*. 137: 8851–8857, **2015**.

5. Van Esbroeck ACM*, Janssen APA*, Cognetta AB*, Ogasawara D*, Shpak G, Van Der Kroeg M, **Kantae V**, Baggelaar MP, De Vrij FMS, Deng H, Allarà M, Fezza F, Lin Z, Van Der Wel T, Soethoudt M, Mock ED, Den Dulk H, Baak IL, Florea BI, Hendriks G, De Petrocellis L, Overkleeft HS, Hankemeier T, De Zeeuw CI, Di Marzo V, Maccarrone M, Cravatt BF, Kushner SA, Van Der Stelt M. Activity-based protein profiling reveals off-target proteins of the FAAH inhibitor BIA 10-2474. *Science*. 356: 1084-1087, **2017**.

6. **Kantae V***, Krekels EHJ*, Ordas A*, González O, van Wijk RC, Harms AC, Racz PI, van der Graaf PH*, Spaink HP*, Hankemeier T*. Pharmacokinetic Modeling of Paracetamol Uptake and Clearance in Zebrafish Larvae: Expanding the Allometric Scale in Vertebrates with Five Orders of Magnitude. *Zebrafish*. 13: 504–510, **2016**.

7. **Kantae V**, Van Esbroeck ACM, Stevens F, van Wijk RC, Luchtenburg F, Harms AC, Schaaf M, van der Graaf PH, Van Der Stelt M, Hankemeier T. Systems pharmacology of an endocannabinoid system modulator in zebrafish larva.
   Manuscript in preparation

8. Kuipers, EN*, **Kantae V***, Eveleens Maarse, BC, van den Berg SM, van Eenige R, Nahon KJ, Reifel-Miller A, Coskun T, de Winther MPJ, Lutgens E, Kooijman S, Harms AC, Hankemeier T, Van Der Stelt M, Rensen PCN, Boon MR. Derailment of the endocannabinoid system by high fat diet starts in adipose tissue.

   *Manuscript Submitted, **2018***

9. **Kantae V***, Nahon KJ*, Straat ME, Bakker LEH, Harms AC, Van Der Stelt M, Hankemeier T, Jazet IM, Boon MR, Rensen PCN. Endocannabinoid tone is higher in healthy lean South Asian than white Caucasian men. *Sci Rep*. 7: 7558, **2017**.

10. Nahon KJ*, **Kantae V***, Haan RD, Hanssen MJW, Harms AC, Van Der Stelt M, Hankemeier T, Jazet IM, van Marken Lichtenbelt WD, Rensen PCN, Boon MR. Gene expression of endocannabinoid system components in skeletal muscle and adipose tissue of South Asians and White Caucasians with overweight. *Obesity, **2018**, doi: 10.1002/oby.22245*

11. Van Eyk HJ*, Van Schinkel LD*, **Kantae V***, Dronkers CEA, Westenberg JJM, De Roos A, LambHJ, Jukema JW, Harms AC, Hankemeier T, Van Der Stelt M, Jazet IM, Rensen PCN*, Smit JWA*. Caloric restriction lowers endocannabinoid tonus and improves cardiac function in type 2 diabetes. *Nutr Diabetes*. 8: 6, **2018**.

12. Zhou J, Mock ED, Martella A, **Kantae V**, Burggraaff L, Baggelaar MP, Al-Ayed K, Bakker A, Florea BI, Grimm S, den Dulk H, Overkleeft HS, Hankemeier T, van Westen GJP, van der Stelt M. Activity-based protein profiling identifies α-keto amides as inhibitors for Phospholipase A2 Group XVI.

    *Manuscript submitted, **2018***

13. van Wijk RC, Krekels EHJ, **Kantae V**, Harms AC, Hankemeier T, van der Graaf PH, Spaink HP. Impact of post-hatching maturation on the kinetics of exogenous compounds in zebrafish larvae.

    Manuscript in preparation

* *Authors contributed equally*